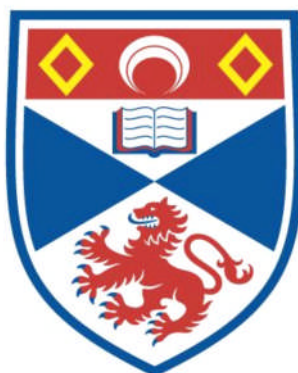


**A FULLY AUTOMATED MILLIMETRIC ROTARY POLARISER
QUASI-OPTICAL SYSTEM**

CHARLES PETER UNSWORTH

**A Thesis Submitted for the Degree of PhD
at the
University of St Andrews**



1997

**Full metadata for this item is available in
Research@StAndrews:FullText
at:**

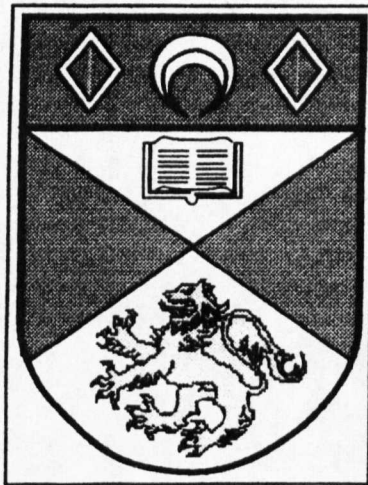
<http://research-repository.st-andrews.ac.uk/>

Please use this identifier to cite or link to this item:

<http://hdl.handle.net/10023/6504>

This item is protected by original copyright

A Fully Automated Millimetric Rotary Polariser Quasi-Optical System



A thesis presented by
Charles Peter Unsworth B.Sc. (Hons) M.Sc.
to the
University Of St. Andrews
in application for the degree of
Doctor of Philosophy

January 1997



Declaration

I, Charles Peter Unsworth, certify that this thesis has been composed by myself, that it is a record of my own work, and that it has not been accepted in partial or complete fulfilment of any other degree or professional qualification.

I was admitted to the Faculty of Science of the University of St. Andrews in October 1993 and as a candidate for the degree of Ph.D. in October 1994.

The research was carried out in the Physical Science Laboratory of St. Salvator's College, in the University of St. Andrews, under the supervision of Dr. J. C. G. Lesurf.

In submitting this thesis to the University of St. Andrews I understand that I am giving permission for it to be made available for use in accordance with the regulations of the University Library for the time being in force, subject to any copyright vested in the work not being affected thereby. I also understand that the title and abstract will be published, and that a copy of the work may be made and supplied to any *bona fide* research worker.

Charles P. Unsworth
January 1996

Certificate

I hereby certify that C. P. Unsworth has fulfilled the conditions of the Resolution and Regulations appropriate to the degree of Ph.D.

Jim C. G. Lesurf
January 1996

Acknowledgements

First and foremost, I wish to thank my supervisor, Jim Lesurf, for his help, guidance and kindness throughout my study. Thankyou very much for letting me pursue my own thoughts. I feel that the confidence that you have given me will help me greatly in my new career as a scientist.

I would also like to extend my thanks to Duncan Robertson who has helped me through difficult times with his knowledge and support and also for showing me that nobody can play 'Air Hammond' quite like he.

I wish to thank Graham Smith for his great insight into all areas of physics, for the debates that we have had of which I've won very few. Good luck with the E.S.R., man !

Thanks to George and Tom for helping me out more times than I can mention and to all my friends in the physics department who have made life here very memorable.

Cheers to George, Andy, Willie, Jim and all the crew in the mechanical workshop, whose skills in the manufacture of my system are much appreciated.

Finally I want to thank my family for the love and encouragement they have given me and to all my friends that I have made here in St. Andrews. Lastly to Sibylle who is the best friend I have.

*A Fully Automated, Millimetric
Rotary Polariser Quasi-Optical System*

To My Family
And In Memory Of
My Father.

Abstract

The thesis presents the design, construction, interfacing and performance of a "Fully Automated, Millimetric Rotary Polariser Quasi-Optical System".

The system demonstrates that linear, elliptical and circular polarised millimetric radiation can be identified uniquely and that a measure of the ellipticity can be made. Furthermore, the system can analyse the amount of Faraday Rotation and ellipticity that has been incurred upon a linear polarised beam on exit of a magnetic sample.

With the above mentioned features, the system was used to determine the suitability of new magnetic materials for use in Freespace Faraday Rotators. This was performed by the new method of 'Faraday Angle Resonance'. The method proved quick and accurate in comparison to a conventional Reflectance Method which is also documented.

In addition, the millimetric measurements served to give a further insight into the behaviour of the 'Faraday Angle Resonance' profile in the 'Frequency dependent' region of a magnetic material. This agreed with predictions and served to complement the original work performed by Raum.

Additional uses and experimental examples of the system are also highlighted. These includes gaining a further insight into the operation of 'Freespace Faraday Rotators' from direct measurement of the Faraday rotation and ellipticity. In addition, the successful characterisation of a quarter-wave plate, in the form of a 'Millimetric Fresnel Rhomb' was performed. Lastly, the location of the principle axes of a birefringent material was determined and a measurement of the ratio of the refractive indices of the principle axes was undertaken.

The system consisted of an 'Automated Oscillator Tuning System' which was developed to automatically tune and optimise the power output of a Gunn oscillator over W-band. A 'Rotary Polariser' was also designed to be used in conjunction with existing quasi-optics and could accurately rotate a polariser grid through discrete increments. The above three instruments together with a Freespace Powermeter, Lockin Amplifier, Boonton Powermeter and EIP frequency counter formed the final system design. All the devices were interfaced to a computer which was used for control and data acquisition.

Contents

Declaration	i
Certificate	i
Acknowledgements	ii
Dedication	iii
Abstract	iv
Contents	v
Chapter 1 (Millimeter Waves – An Overview)	1
Chapter 2 (Gaussian Beams & Lens Design)	6
Introduction	
(2.1) The Gaussian Beam $TEM_{0,0}$ Mode Solution	7
<i>(2.1.1) The time independent wave equation & the planar wave solution</i>	7
<i>(2.1.2) The mathematical representation of a $TEM_{0,0}$ mode Gaussian beam</i>	7
(2.2) A Physical Interpretation Of The $TEM_{0,0}$ Mode Solution	10
<i>(2.2.1) The first term of the $TEM_{0,0}$ mode solution</i>	10
<i>(2.2.2) The beamwidth parameter</i>	12
<i>(2.2.3) The Raleigh Range Parameter (z_R)</i>	14
<i>(2.2.4) The second term of the $TEM_{0,0}$ mode solution</i>	15
<i>(2.2.5) The third term of the $TEM_{0,0}$ mode solution</i>	15
<i>(2.2.6) The phasefront radius parameter $R(z)$</i>	16
(2.3) Modes & The General $TEM_{0,0}$ Solution	17
<i>(2.3.1) The $TEM_{m,n}$ acronym & modes</i>	18
<i>(2.3.2) The general $TEM_{m,n}$ mode solution</i>	19
<i>(2.3.2.1) The first weighting factor</i>	20
<i>(2.3.2.2) The 2nd weighting factor</i>	21
(2.4) Lens Design	22
<i>(2.4.1) Phase Transformation</i>	22
<i>(2.4.2) Determining the amount of phase retardation</i>	24

(2.4.3) <i>Phase retardation for a planar convex lens</i>	25
(2.4.4) <i>Lenses developed for the 'Rotary Polariser Quasi-Optical System'</i>	28
Chapter 3 (The Gunn Oscillator & The A.O.T.S.)	36
Introduction	
(3.1) The Gunn Effect	36
(3.1.1) <i>Types of diode available</i>	37
(3.2) The Transferred Electron Device	38
(3.2.1) <i>The band structure of GaAs & InP</i>	39
(3.2.2) <i>Application of an electric field</i>	40
(3.2.3) <i>The classical 'Domain Accumulation Mode' of operation</i>	40
(3.2.4) <i>The 'Limited Space Charge Accumulation Mode' of operation</i>	43
(3.2.5) <i>The Gunn diode package</i>	43
(3.3) Overview Of The Gunn Oscillator	44
(3.3.1) <i>Oscillator block construction</i>	45
(3.3.2) <i>The first section</i>	45
(3.3.3) <i>The second section</i>	46
(3.3.3.1) <i>The choke structure</i>	47
(3.3.4) <i>The cap & post structure</i>	49
(3.3.5) <i>The third section</i>	51
(3.4) 2nd Harmonic Generation & Millimeter Wave Production	52
(3.5) Characterisation Of The Gunn Oscillator	55
(3.6) The 'Automatic Oscillator Tuning System' (A.O.T.S)	57
(3.6.1) <i>A.O.T.S. system description</i>	58
(3.6.2) <i>Circuitry necessary for A.O.T.S. operation</i>	60
(3.6.3) <i>Housing of the circuitry</i>	63
(3.6.4) <i>Program Development</i>	64
(3.6.4.1) <i>Overview of the characterisation program - CharOsc</i>	64
(3.6.4.2) <i>'General Purpose Interface Bus' commands</i>	65
(3.6.4.3) <i>'Wildvision' commands</i>	69

(3.6.5) Results obtained from the automatic characterisation	73
Chapter 4 (Magnetic Behaviour)	75
Introduction	
(4.1) What Determines Whether A Material Is Paramagnetic, Ferromagnetic Or Antiferromagnetic ?	75
(4.2) Paramagnetism, The Bohr Magneton & Orbital-Spin Coupling	76
(4.3) Ferromagnetism, Antiferromagnetism & The 'Exchange Interaction'	80
(4.4) Itinerant Exchange	82
(4.5) Direct Exchange	82
(4.6) Indirect Exchange	82
(4.7) Superexchange	82
(4.8) Hund's Rules & The Electron Configuration Within An Atom	84
(4.9) Domain Formation	88
(4.10) Domain Boundary Displacement	90
(4.11) Domain Rotation	91
(4.12) Coherent Domain Rotation	91
(4.13) Magnetostatic Energy (E_{MSI})	92
(4.14) Anisotropy Energy (E_{AN})	95
(4.15) The Magnetoelastic Energy (E_{ME}) Or Magnetisation	97
(4.16) Exchange Energy (E_{EX}) & Bloch Walls	100
(4.17) Temperature Dependence Of A Magnetic Material & The Curie Point	102
Chapter 5 (The Faraday Effect & Faraday Rotator Design)	105
Introduction	
(5.1) The Faraday Effect	106
(5.1.1) The effect of an applied static magnetic field on (μ_s)	106
(5.2) The Effect Of A Propagating Beam Through A Magnetised Ferrite	110
(5.3) Frequency Dependent Interaction Of The (+ve) Circular State	114
(5.3.1) Electron spin states & electron spin resonance	115
(5.4) The Freespace Faraday Rotator	120

(5.5) The Freespace Quasi-Optical Isolator	121
(5.6) Suitable Materials	123
(5.6.1) <i>The 'Magnetisation' of the sample (M)</i>	125
(5.6.2) <i>The 'Demagnetisation Field' (H_D)</i>	125
(5.6.3) <i>The Anisotropy Field (H_A)</i>	126
(5.7) The Manufacturing Process	127
(5.7.1) <i>Manufacturing Terminology</i>	129
(5.8) Limiting Features Of BaM & SrM	130
(5.9) Experimental Methods Used To Determine Ferrite Material Parameters	130
(5.9.1) <i>The Reflectance/Transmission Method</i>	131
(5.9.2) <i>The Faraday Angle Resonance Method</i>	131
(5.10) Characterisation Of A Freespace Faraday Rotator & Isolator	135
Chapter 6 (Plastoferrite Investigation)	137
Introduction	
(6.1) Experimental Reflectance Setup	137
(6.2) Experiment Methodology	143
(6.3) Predicted Nature Of The 'Reflectance vs. Frequency' Curves	145
(6.4) Determination Of Refractive Index From Reflectance Measurements	149
(6.4.1) <i>Materials used in study</i>	154
(6.5) Anisotropic SrM Plastoferrite Reflectance vs. Frequency Curves	156
(6.6) Isotropic SrM Plastoferrite Reflectance vs. Frequency Curves	161
(6.7) Semi-Anisotropic SrM Plastoferrite Reflectance vs. Frequency Curves	166
(6.8) Predicted Nature Of The Refractive Index	168
(6.9) Computerfitted Curves Of The Refractive Index Results	172
(6.10) Interpretation Of The Refractive Index Results	175
(6.11) Calculated 'Ideal Thickness' Or 45° Rotation vs. Frequency	176
(6.12) Plastoferrite, Quasi-Optical Freespace Faraday Rotators	177
(6.12.1) <i>Construction of Faraday Rotators</i>	177
(6.12.1.1) <i>Faraday Rotators (IA1) & (IA2)</i>	177

(6.12.1.2) <i>Faraday Rotator (I9)</i>	178
(6.13) Experimental Setup Used To Determine Isolation & Insertion Loss	178
(6.14) Isolation & Insertion Loss Results For (IA1), (IA2) & (I9)	180
(6.14.1) <i>Results for (IA1)</i>	181
(6.14.2) <i>Results for (IA2)</i>	182
(6.14.3) <i>Results for (I9)</i>	183
(6.15) Results Analysis	183
(6.15.1) <i>Results analysis of (IA1)</i>	183
(6.15.2) <i>Results analysis of (IA2)</i>	184
(6.15.3) <i>Results analysis of (I9)</i>	184
(6.16) Conclusions & Final Remarks	185
Chapter 7 (Instrument Development Of The Rotary Polariser)	188
Introduction	
(7.1) Design Requirements	189
(7.1.1) <i>The size of the circular polariser</i>	189
(7.1.2) <i>The length of the cavity & disposal of transmitted power</i>	193
(7.2) The Inertia Of The System	196
(7.3) The Motor & Motor-Drive Requirements	198
(7.3.1) <i>The motor mechanism</i>	199
(7.3.2) <i>The motor-drive unit</i>	205
(7.3.3) <i>The indexer & non-volatile memory</i>	206
(7.3.4) <i>The translator</i>	207
(7.3.5) <i>The switch mode power supply</i>	207
(7.3.6) <i>Summary of the motor & motor-drive</i>	207
(7.4) Determination Of Torque Required To Move Load	208
(7.4.1) <i>The torque/speed plot</i>	208
(7.4.2) <i>The move profile</i>	209
(7.5) Interfacing & Control Of The Drive Unit	212
(7.5.1) <i>Interfacing drive to computer</i>	212

(7.5.2) <i>Establishing communications flow</i>	213
(7.5.3) <i>Transmitting commands & receiving a response</i>	213
(7.5.4) <i>Programs developed</i>	216
Chapter 8 (A Prototype Rotary Polariser Quasi-Optical System)	218
(8.1) Preliminary Tests & Measurements	218
(8.1.1) <i>Grid alignment experiment</i>	219
(8.1.2) <i>Offset determination of polariser wires from vertical</i>	220
(8.1.3) <i>Relationship between 'Seen angle' (χ) & 'Actual Angle' (θ)</i>	221
(8.2) Polarisation Classification	224
(8.2.1) <i>Case One : Linear polarisation</i>	224
(8.2.1.1) <i>Computer model for linear polarisation</i>	227
(8.2.1.2) <i>Interpretation of results for linear polarisation</i>	232
(8.2.2) <i>Case Two : Elliptical polarisation</i>	236
(8.3) Example - Predicted Rotation Of Isolator (IA1)	239
(8.4) The Computer Data Plotting Program	240
(8.5) Experimental Work Performed For The D.R.A.	242
(8.5.1) <i>The 26GHz Resonant Sample</i>	243
(8.5.2) <i>The 13GHz Resonant Sample</i>	243
(8.5.3) <i>The 4GHz Resonant Sample</i>	244
(8.5.4) <i>The 45GHz Resonant Sample</i>	244
(8.5.4.1) <i>45GHz Unmagnetised Results</i>	245
(8.5.4.2) <i>45GHz Magnetised Results</i>	245
Chapter 9 (A Fully Automated Millimetric Rotary Polariser Quasi-Optical System)	250
(9.1) The Thomas Keating (T.K.) Freespace Power Meter	251
(9.1.1) <i>Positioning of the T.K. power meter</i>	252
(9.1.2) <i>Amplitude modulation of the incident beam</i>	253
(9.1.3) <i>Interfacing of the T.K. to the computer</i>	253

(9.1.4) Computer procedures developed for the lockin amplifier	254
(9.1.5) Calibration of the T.K. power meter over W-band	259
(9.1.6) Method of calibration	260
(9.1.7) Computer program T_DLinReg developed for T.K. calibration	261
(9.1.8) Results obtained from program T_DLinreg	264
(9.1.9) Interpolation of datafiles for an arbitrary frequency	266
(9.1.10) Determination of power from the output voltage of the T.K.	269
(9.2) Reducing Experimental Time By Introducing 'PROTrack'	276
(9.2.1) Dissection Of Procedure 'PROTrack'	279
(9.3) Sources Of Noise	282
(9.3.1) Standing Waves	282
(9.3.2) Accurate prediction of Major & Minor Faraday Angles over thermal & acoustic/vibrational noise fluctuations	284
(9.3.2.1) The 'Least Squares Parabolic Fit'	285
(9.4) Experimental Results Using The Fully Automated System	292
(9.5) Faraday Angle Resonance Results	293
(9.5.1) Results for Sample 11	293
(9.5.1.1) Results analysis for Sample 11	294
(9.5.2) Results for Sample 32	297
(9.5.2.1) Results analysis for Sample 32	298
(9.6) Faraday Rotator Assessment	300
(9.6.1) Results for Faraday Rotator (19)	301
(9.7) Additional Functions Of The 'Rotary Polariser Quasi-Optical System'	305
(9.7.1) Design & testing of a millimetric Fresnel Rhomb	305
(9.7.1.1) Quarter-wave plates	306
(9.7.2) Location of the principle axes associated to a birefringent material	312
(9.8) Conclusions & Final Remarks	318
Chapter 10 (Final Summary & Scope For Further Work)	320
(10.1) Improving Design & Scope For Further Work	326
APPENDIX 1 (Computer Program - FarAngRes6)	327-346

Chapter 1

Millimeter Waves ~ An Overview

Millimeter waves occupy the 1mm-10mm wavelength region of the electromagnetic spectrum. This corresponds to the frequency region of 30-300GHz. This region exists between the two well established regions of microwaves and the infrared. Thus, the millimeter wave region can be described as the transition region from the electronic techniques used in microwave research to that of optical techniques employed in the infrared.

Since, we are dealing with wavelengths of 1mm-10mm, the small aperture sizes that are required of waveguide structures become increasingly difficult to manufacture. In addition, due to the 'Skin effect'¹ the attenuation of waveguide structures dramatically increases as one approaches these high frequencies. As an alternative, the millimetric radiation is propagated out into freespace where the attenuation is considerably less. The propagation of the radiation is via 'Gaussian Beams'. The Gaussian beams are channelled through a system by components that fall under the title of 'Quasi-Optics'. These consist of modular components such as wire grid polarising structures, dielectric lenses, corner cubes and mirrors² which can be easily used to direct, transform and efficiently couple the Gaussian beams through a quasi-optical system. The advantage of millimeter wave technology is that it gives one a choice in the techniques of either electronics, optics or both regimes in order to produce a 'Hybrid' quasi-optical system that suits the task in question.

¹ Microwaves 2nd Edition - An Introduction To Microwave Theory & Techniques, A.J. Baden Fuller, Pergamon Press, Section (6.6).

² Millimeter-wave Optics, Devices & Systems, J.C.G. Lesurf, Adam Hilgar Publishers, 1990, Chapter 2.

As will be highlighted shortly, the advantages of millimeter wave systems are their :

- Small Aperture Size & Compactness
- Narrow Beamwidth & Highly Directional Beams
- High Resolution
- Large Bandwidth
- Low Attenuation to smoke, fog, haze which is superior to that in the infrared and optical regions.

These features are fully exploited today and have applications in High Resolution Radar, Satellite Communications, Remote Sensing, Imaging and Astronomy.

A lot of the above mentioned applications exploit certain 'Atmospheric Windows' and 'Absorption Lines' that exist within the millimetric spectrum.

Atmospheric Windows exists at 35, 90, 140 and 220GHz and are frequencies that allow virtually attenuation free propagation of millimeter waves through the atmosphere. Furthermore, at 94GHz there is little attenuation to smoke.

Oxygen Resonance Absorption lines exist at 60 and 120GHz and there are Ozone absorption lines at 115 and 180GHz. As the name suggests, millimetric radiation at these frequencies is heavily attenuated.

There are a variety of military applications which are based at 94GHz in order to take advantage of the low attenuation characteristic of millimeter waves at this frequency to smoke. This is ideal for battlefield encounters and when coupled together with their low attenuation to fog, haze and cloud in comparison to the infrared and optical regions, they provide the opportunity to perform High Resolution Radar³. The forms of radar can be either

³ C.R. Seashore, J.Miley, B.Kearns, *Microwave Journal*, 22.(Aug), 1979, pgs.47-51

passive⁴ or active and usually employ Radiometric detection methods. Due to the large temperature difference that exists at these frequencies between warm bodies contrasted to that of cold sky reflections, high resolution can be achieved. In addition, the radar is less sensitive to burning debris in comparison to that of the infrared. Hence, a millimetric radar can avoid becoming dominated by saturation effects encountered in the infrared. At present I am involved in the development of a 'Passive Wave Millimetric Real Time Imager' at the DRA in Malvern. The system avoids detection by collecting the passive millimetric radiation that is emitted naturally from bodies at around 94GHz. The system hopes to be the first of its type which can demonstrate millimetric imaging in real time.

The small apertures that are required at millimeter wavelengths are responsible for the production of highly directional narrow main beams with a low sidelobe level. This in effect serves to reduce 'unwanted clutter' around a target by reducing the radiometric return in a reflected wavefront. Hence, an object's location can be monitored very accurately. This idea is exploited in missile guidance systems. In addition, the narrow beam makes intercept and jamming very difficult.

The Oxygen resonance absorption line provides high attenuation to millimetric radiation at 60GHz. This absorption feature can be used for covert communications. This allows a covert signal to be rapidly attenuated if it misses its target, hence avoiding detection. This technology is commonly employed in covert line of sight communication for fighter aircraft flying in formation.

Recently the DRA in collaboration with St. Andrews have put forward a prototype millimetric combat ID system. This will act as a 'Friend or Foe' system and will serve to reduce casualties as experienced in the Gulf War due to 'Friendly fire'.

Remote Sensing applications also employ millimetric techniques to provide imaging of the earth's surface. One example of this is

⁴ The Passive Millimeter-Wave Scenario, Microwave Journal, March 1996.

described by Vowinkel⁵. His work demonstrated that the atmospheric temperature could be monitored at 183GHz due to an atmospheric vapour transition. Also a survey at 93GHz provided information of the surface and lower atmospheric temperature. When cryogenic cooling was employed, temperatures of 0.01° K could be resolved.

The Earth's Ozone depletion due to CFC emission can also be monitored due to the absorption lines of (CO) at 115 and 180GHz.

In the area of biological imaging, Millimetric 'Thermography' has been developed for the detection of certain types of cancerous tumours⁶.

In Satellite Communications, the opportunity arises to take advantage of the compact physical size of a millimeter wave systems and the large bandwidth available that gives scope for more carrier frequencies. These facts together with the low attenuation, due to the Atmospheric window at 35GHz, provides satellite to ground communications⁷. By this method, powers as low as half a Watt have been used to broadcast distances of up to 40,000km. In addition, millimeter waves can permeate electron plasma. Spacecraft become surrounded by electron plasma upon re-entry of the earth's atmosphere. Hence, millimetric frequencies can be used to communicate with re-entering craft⁸.

My line of interest lies in the uses of magnetic materials in the millimeter waveband⁹ and in particular the area of High Performance Freespace Faraday Rotators¹⁰. They provide the

⁵ B. Vowinkel, J.K.Petonen, W.Reinert, IEEE MTT-S International Microwave Symposium Digest, Washington D.C., 1980, pgs. 21-23.

⁶ J.Robert, J.Edrich, P.Thouvenot, M.Gutherie, J.M.Escanye, Journal Of Microwave Power 14 (June), 1979, pgs. 131-134.

⁷ L.J. Pollito, Proceedings Of The IEEE, 59, pgs.189-205.

⁸ M.I. Skolnik, Symp. On Millimeter-Waves, Polytechnics Technical Press, (31st March-2nd April 1970), pg.9.

⁹ Ferrite Uses At Millimeter Wavelengths, C.Vittoria, Journal Of Magnetism & Magnetic Materials, 71, 1980, pgs.109-118.

¹⁰ Microwave, Millimeter Wave & Submillimeter Wave Freespace Faraday Rotators, G.M.Smith, S.Kang, C.Unsworth, E.Puplett, D.Franklin, J.C.G.Lesurf, IEEE MTT-S International Microwave Symposium Digest (Orlando), 1995.

opportunity to distinguish between incident and reflected transmissions and can be employed to redirect beams in various ways depending on their orientation and direction of travel of the beam¹¹. Here at St.Andrews, a number of quasi-optical, millimetric systems have been developed using these 'State of the Art' Faraday Rotators which provide low loss and high isolation. The work was initiated by Webb¹². Since, then a 'Quasi-Optical Cavity Dumping'¹³ system incorporated a Faraday Rotator to produce a novel quasi-optical switch. This provided nanosecond switching at millimeter wavelengths.

The frequency discrimination that occurs through the rotational change in a polarised output of a Faraday Rotator was exploited in a 'Millimetric Noise Measurement System'¹⁴. In this system, the non-reciprocal nature of the Faraday Rotator was used to stop unwanted reflections from destabilising a millimeter wave oscillator¹⁵.

Recently at St.Andrews, Faraday Rotators have been employed in the 'Millimetric Combat ID system', described earlier. Furthermore, a 'Highly Sensitive Millimetric Electron Spin Resonance Spectrometer' has been developed which has a 1000 times the sensitivity of a conventional system and is the most sensitive of its kind in the world.

¹¹ A Quasi-Optical Reflection Circulator, B.Lax, A.Weiss, IEEE Transactions On Microwave Theory & Techniques, Vol.41, No.12, December 1993.

¹² A Millimeter Wave Four Port Quasi-Optical Circulator, M.R.Webb, Int.Journal Of Infrared & Millimeter Waves, Vol.12, pgs.286-299, 1966.

¹³ Quasi-Optical Cavity Dumping At Millimeter Wave Frequencies, G.M.Smith, J.C.G.Lesurf, Y.Cui, M.Dunn, IEEE MTT Conf.Digest, Atlanta, June 1993.

¹⁴ A Highly Sensitive Noise Millimeter Wave Measurement Quasi-Optical FM Noise Measurement System, G.M.Smith, J.C.G.Lesurf, IEEE MTT Special Issue, December 1991.

¹⁵ Quasi-Optical Stabilisation Of Millimeter Wave Sources, G.M. Smith, J.C.G.Lesurf, IEEE MTT Conference Digest, Albuquerque, June 1992.

Chapter 2

Gaussian Beams & Lens Design

Introduction

The simplest way to visualise a gaussian beam is to initially picture a plane wave moving along its axis of propagation and to imagine that as the beam propagates, a divergence or spreading of the beam is occurring¹. This is the approach 'Gaussian Beam Mode' theory takes in order to mathematically describe a gaussian beam. I shall assume that the beam's axis of propagation is in the (z) direction.

Although the planar wave solution of the time-independent wave equation describes a planar wave completely by its amplitude and longitudinal phase, a solution for planar wave with an inclusive diffraction factor $\psi(x,y,z)$ is a lot more complex. The first part of the chapter will show that as well as having the amplitude and longitudinal phase terms possessed by a planar wave the gaussian solution also possesses an additional radial phase term together with new factors such as anomalous phase, beamwidth and phase-front radius. And that it is these additional terms and parameters that are necessary to completely describe a solution which defines a gaussian beam.

After explaining the essential attributes of gaussian beams the chapter will be concluded with a short discussion on how a lens can be designed to contain a gaussian beam within a quasioptical system by its intrinsic property of phase transformation. An explanation of how I designed planar/convex lenses for my quasioptical system together with the necessary calculations will be included.

¹ J.C.G. Lesurf , Millimeter Wave Optics, Devices & Systems, Adam Hilgar Publishers, 1990, Chapter 1.

(2.1) The Gaussian Beam TEM_{0,0} mode solution

As mentioned earlier a gaussian beam can be described as a plane wave in which some divergence of the beam is taking place as it progresses in (z). The best way to mathematically describe such a beam is to firstly look at the mathematical description of a planar wave and then introduce these 'spreading' effects to the solution. Hence, one can deduce the mathematical description for a gaussian beam.

(2.1.1) The 'Time-Independent Wave Equation' & Planar wave solution

As one can find in any textbook the scalar version of the time-independent wave equation can be expressed by equation (2.1)

$$\nabla^2 E + \frac{\omega^2 n^2}{c^2} E = 0 \quad \dots (2.1)$$

where, $k^2 = \frac{\omega^2 n^2}{c^2}$

The simplest solution of which is that of a plane parallel wave, described by equation (2.2).

$$E = |E_0| e^{-j(kz)} \quad \dots (2.2)$$

This represents a plane wave of amplitude $|E_0|$ and longitudinal phase of (kz) travelling in the (+z) direction.

(2.1.2) The Mathematical representation of a TEM_{0,0} mode Gaussian beam

Upon knowing the planar wave solution to the scalar time-independent wave equation, one can now introduce the divergence or 'spreading' of the beam as some scalar function described by $\psi(x,y,z)$. Introducing this term into equation (2.2) gives²

² Verdeyen. J.T. , Laser Electronics(2nd Ed.), Prentice Hall, Chapter 3

$$E = |E_0| \psi(x, y, z) e^{-j(kz)} \quad \dots (2.3)$$

By then reintroducing this back into equation (2.1), a new scalar representation for the wave equation can be written.

$$\nabla^2 \psi - j2k \frac{\partial \psi}{\partial z} + \frac{\partial^2 \psi}{\partial z^2} = 0 \quad \dots (2.4)$$

Since the first derivative is multiplied by a very large number, k , equation (2.4) can be simplified by allowing :

$$2k \frac{\partial \psi}{\partial z} \gg \frac{\partial^2 \psi}{\partial z^2} \Rightarrow \frac{\partial^2 \psi}{\partial z^2} = 0 \quad \dots (2.5)$$

$$\therefore \nabla^2 \psi - j2k \frac{\partial \psi}{\partial z} = 0 \quad \dots (2.6)$$

This is the version of the scalar wave equation used to describe a planar wave which suffers a divergence as it propagates. From this a variety of solutions exist which in turn describe a variety of gaussian beam modes. Since typical feedhorns and beam launchers are designed to produce gaussian beams which are very close to the fundamental freespace TEM_{0,0} mode³, I will discuss the TEM_{0,0} mode solution. This also happens to be the simplest of all the solutions for this new form of the wave equation. Furthermore, it is a lot easier to then move on and understand the general TEM_{m,n} solution for a gaussian beam after acquainting oneself with the simplest solution (instead of the other way around which is what most textbooks do !).

³ Modes will be discussed in section (2.3.1)

Therefore, the cylindrical TEM_{0,0} mode solution can be written as :

$$\begin{aligned}
 E &= |E_0| \times && \leftarrow \text{Amplitude at } z = r = 0 \\
 &\frac{\omega_0}{\omega(z)} \exp\left\{-\left(\frac{r}{\omega(z)}\right)^2\right\} \times && \leftarrow \text{Amplitude variation with radial distance (} \\
 &\exp\left\{-j\left(kz - \tan^{-1}\left(\frac{z}{z_R}\right)\right)\right\} \times && \leftarrow \text{Longitudinal Phase Term} \\
 &\exp\left\{-j\left(\frac{kr^2}{2R(z)}\right)\right\} && \leftarrow \text{Radial Phase Term} \quad \dots (2.7)
 \end{aligned}$$

where,

$$\omega(z) = \omega_0 \sqrt{1 + \left(\frac{z}{z_R}\right)^2} \quad \leftarrow \text{Beamwidth Radius} \quad \dots (2.8)$$

$$R(z) = z \sqrt{1 + \left(\frac{z_R}{z}\right)^2} \quad \leftarrow \text{Phasefront Radius} \quad \dots (2.9)$$

$$z_R = \frac{\pi n \omega_0^2}{\lambda} \quad \leftarrow \text{Rayleigh Range (Confocal Distance)} \quad \dots (2.10)$$

This is the form of the solution that one usually has to familiarise oneself with when designing quasi-optical systems. There are a variety of reasons behind why the TEM_{0,0} modes use is favoured over any other mode. The main reasons for this choice are as follows. Firstly the TEM_{0,0} is the only mode in which there is no cutoff frequency in freespace, hence it is sometimes referred to as the 'Fundamental Freespace Mode', and secondly it offers the least attenuation of all the modes for apertures that are of finite size. Couple these two main reasons with the fact that the TEM_{0,0} mode is both easy to produce and detect as well as offering great simplification of any calculations that have to be made; Then the Fundamental Freespace TEM_{0,0} mode is the best choice over any other mode to launch into freespace.

(2.2) Physical Interpretation of the TEM_{0,0} mode solution

What now follows is a discussion and physical interpretation of each of the terms of the TEM_{0,0} mode solution together with its parameters.

(2.2.1) The First term of the TEM_{0,0} mode solution

The first term of the solution describes how the amplitude of the gaussian beam varies radially as it propagates in (z). The term itself can be split into two parts, shown below:

$$\frac{\omega_0}{\omega(z)} \cdot \exp\left\{-\left(\frac{r}{\omega(z)}\right)^2\right\}$$

\uparrow
 Longitudinal Variation
of radial profile

\uparrow
 Radial Profile
of amplitude

The exponential part describes the radial variation of the amplitude for a particular (z), namely its cross-sectional profile. Any function of the general form $\exp\left\{-\left(\frac{\sqrt{x^2 + y^2}}{a}\right)^2\right\}$ is normal in its distribution. Therefore, one can say the radial amplitude profile of the beam is also normal distributed. With maximum amplitude at $r = 0$, which $\rightarrow 0$ as $r \rightarrow \infty$. See figure(2.1)

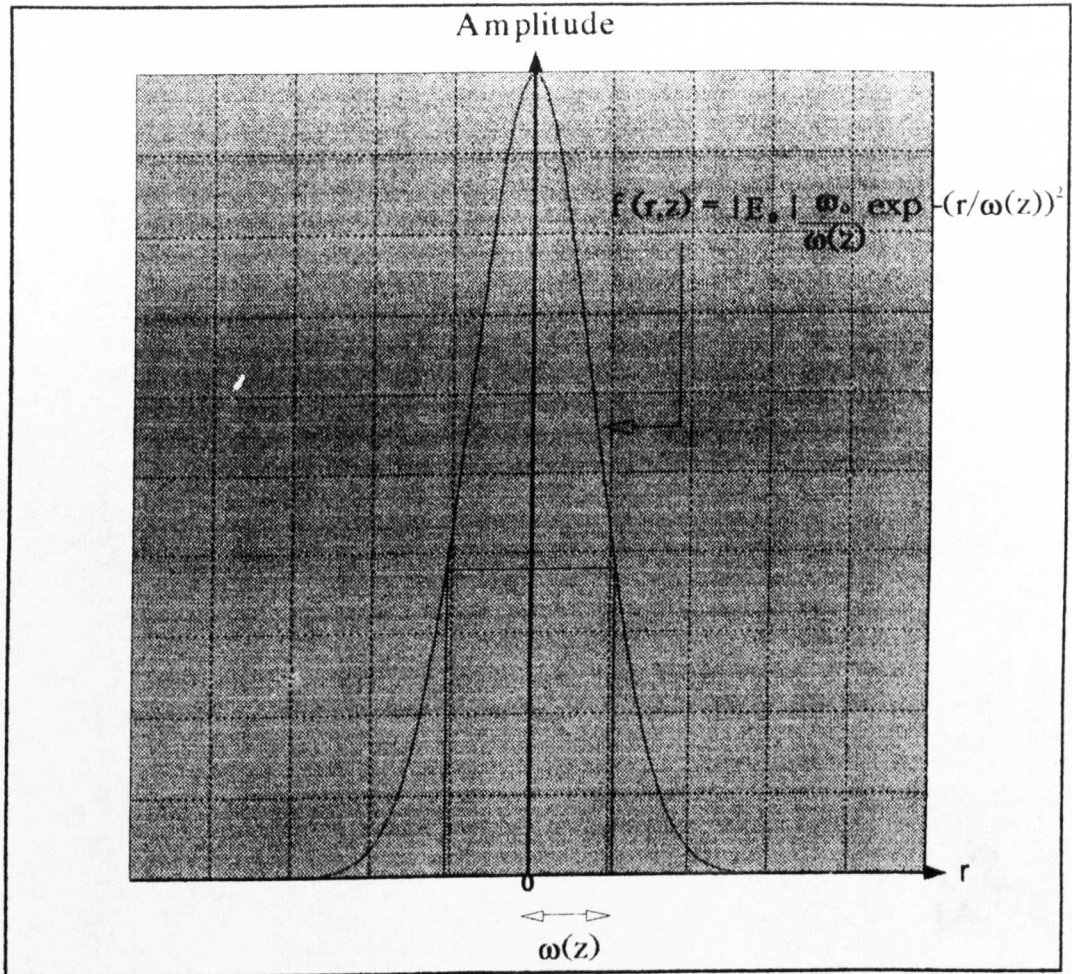


Figure (2.1)

By examining equation (2.8), one can see that for $r = z = 0$

$$\omega(z) = \omega_0 \sqrt{1 + \left(\frac{z}{z_R}\right)^2} \Rightarrow \omega_0 \quad \text{and} \quad \exp\left\{-\left(\frac{r}{\omega(z)}\right)^2\right\} \Rightarrow 1$$

Hence, $Amplitude = |E_0| \cdot \frac{\omega_0}{\omega_0} \cdot 1 = |E_0|$

The amplitude of the gaussian profile can be seen to tend to its maximum value of $|E_0|$. Continuing the argument for any arbitrary longitudinal distance (z) the amplitude varies as :

$$Amplitude = |E_0| \cdot \frac{\omega_0}{\omega(z)} \cdot 1 = \frac{\omega_0}{\omega(z)} \cdot |E_0|$$

Hence, at any arbitrary distance (z) the maximum amplitude value at $r = 0$, or the height of the normal profile, decreases with increasing (z). Where the $(\frac{\omega_0}{\omega(z)})$ part is responsible for modifying the maximum amplitude value and the exponential part describes the cross-sectional profile of the beam.

(2.2.2) The Beamwidth Parameter

Upon further investigation of equation (2.8) at $z = 0$ we get $\omega(0) \Rightarrow \omega_0$. Now the amplitude value at this radial distance $r = \omega_0$, $z = 0$ turns out to be :

$$Amplitude = |E_0| \cdot \frac{\omega_0}{\omega_0} \cdot \frac{1}{e} = \frac{|E_0|}{e} \quad \dots (2.11)$$

Hence, the amplitude drops down one e'th of that at its maximum $r = z = 0$ central value.

Continuing the argument for some arbitrary (z) distance, equation (2.8) shows :

$$\omega(z) = \omega_0 \sqrt{1 + \left(\frac{z}{z_R}\right)^2} > \omega_0$$

Hence for :

$$\exp\left\{-\left(\frac{r}{\omega(z)}\right)^2\right\} = \frac{1}{e}, \quad r > \omega_0$$

Therefore, one can deduce that as the beam progresses in (z) the e'th value occurs at larger radial distances (r) as compared to the $z = 0$ position.

It is this $(\frac{|E_0|}{e})$ radius value which is used to define the the spot size, or beamwidth, of the gaussian beam. The beamwidth is more

accurately referred to as the $(\frac{1}{e^2})$ radius⁴ in which the intensity of the beam has fallen to $(\frac{1}{e^2})$ of that at its central $r=0$ value. As described earlier the beamwidth has a minimum value (ω_0) which is commonly referred to as the beamwaist location. A plot of the changing beamwidths can be shown to vary hyperbolically with (z) , shown in figure (2.2). In the same plot one can also see that the amplitude at $r=0$ falls from it's maximum value at the beamwaist $z=0$ as the beam progresses in (z) .

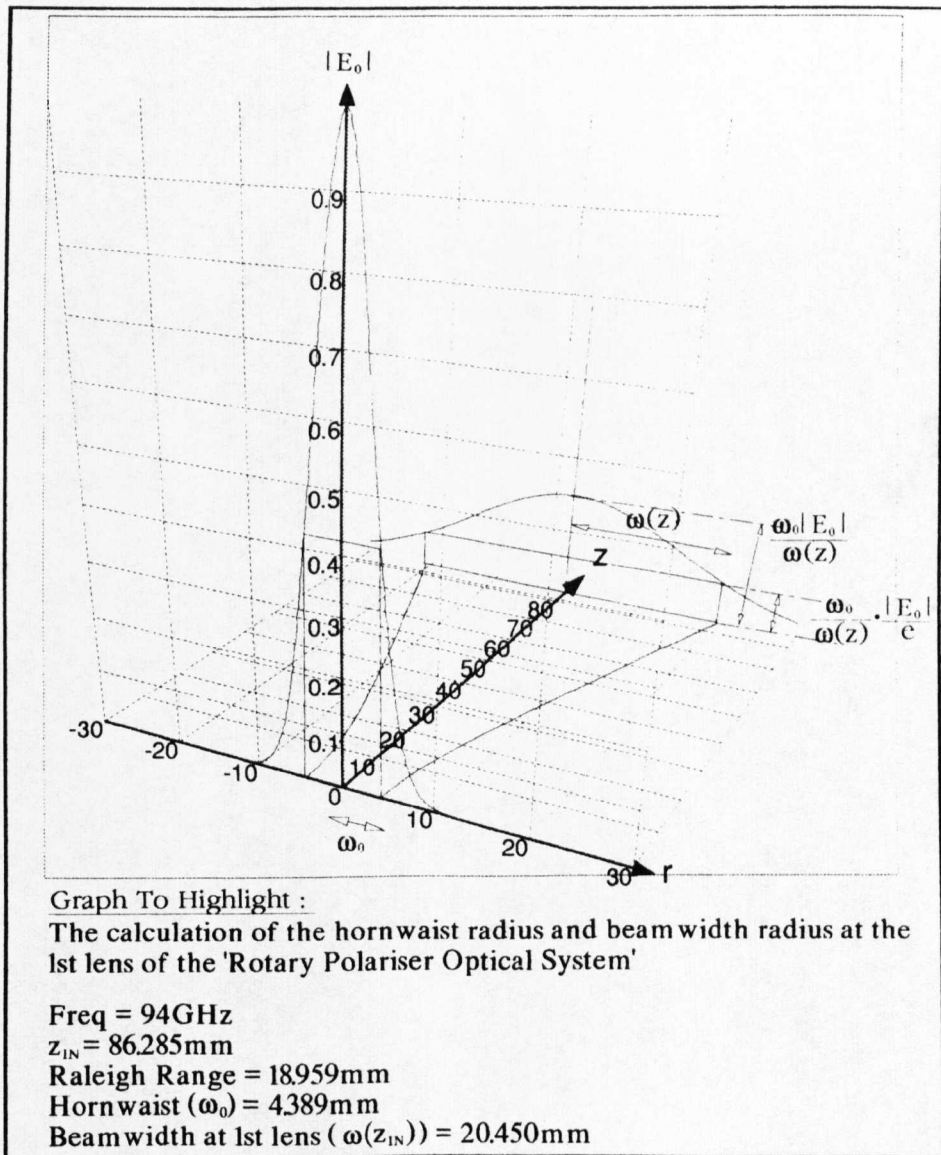


Figure (2.2)

⁴ Dickson, L.D., Characteristics of a propagating gaussian beam, Applied Optics Vol 9(8), Aug 1970, pp1840-1861

(2.2.3) The Raleigh Range Parameter (z_R)

The Raleigh range is a very important and useful parameter. It defines the distance which marks the transition region between the near and far field regions.

$$Raleigh\ Range = \frac{\pi n \omega_0^2}{\lambda} \quad \dots (2.12)$$

It is sometimes referred to as the 'Confocal Distance'. It also marks where the beamwidth is $\omega(z) = \sqrt{2}\omega_0$ and also where the radius of curvature of the beam is minimal at $2\omega_0$.⁵ See figure (2.3)

At $z < z_R$, The Near field region. One can assume the beam has a constant beamwidth $\approx \omega_0$.

And at $z > z_R$, The Far field region the beamwidth can be said to vary linearly with the expansion angle. Where the expansion angle ($\frac{\theta}{2}$) is defined as the angle between the (z) axis and the asymptote to which the expansion curves traced out by the beamwidth locations tend to as $z \Rightarrow \infty$.

$$Expansion\ Angle = \frac{\theta}{2} = \frac{\omega_0}{z_R} \quad \dots (2.13)$$

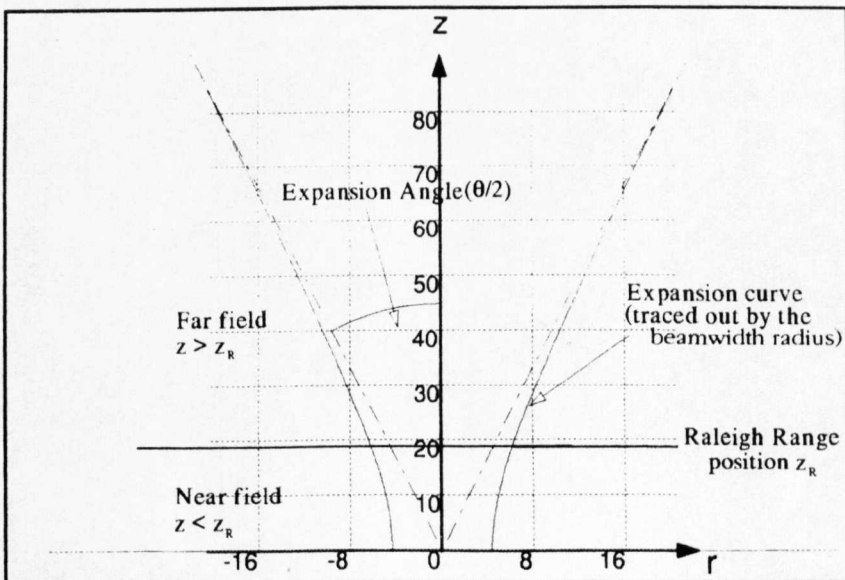


Figure (2.3)

⁵ Goldsmith P.F., Infrared & Millimeter waves, Vol 6, pgs 278-282

(2.2.4) The Second Term of the TEM_{0,0} mode solution

The second term of the solution describes the longitudinal phase of the gaussian beam.

$$\begin{array}{ccc}
 kz & - & \tan^{-1}\left(\frac{z}{z_R}\right) \\
 \uparrow & & \uparrow \\
 \text{Planar phase} & & \text{Anomalous phase}
 \end{array}$$

The (kz) part describes the phase of the beam as if it were planar. The arctangent part of the term is the additional phase the beam possesses due to its gaussian nature. This is sometimes referred to as the 'anomalous phase'. The deviation of the longitudinal phase of the gaussian beam in comparison with that of a planar beam can be seen in figure(2.4)

(2.2.5) The Third term of the TEM_{0,0} mode solution

The third term of the TEM_{0,0} mode solution describes the 'planeness' of the gaussian beam.

$$\exp\left\{-j\left(\frac{kr^2}{2R(z)}\right)\right\}$$

Its effect is to alter the longitudinal phase radially of a wavefront for a particular (z). When the gaussian beam is left to propagate naturally, this term tends to impose a curvature to the wavefront. This causes a relative lagging of wavefront's phase from that at the central r=0 position. The amount of curvature imposed on the wavefront is called the 'Phasefront Radius' R(z) of the beam and will now be described.

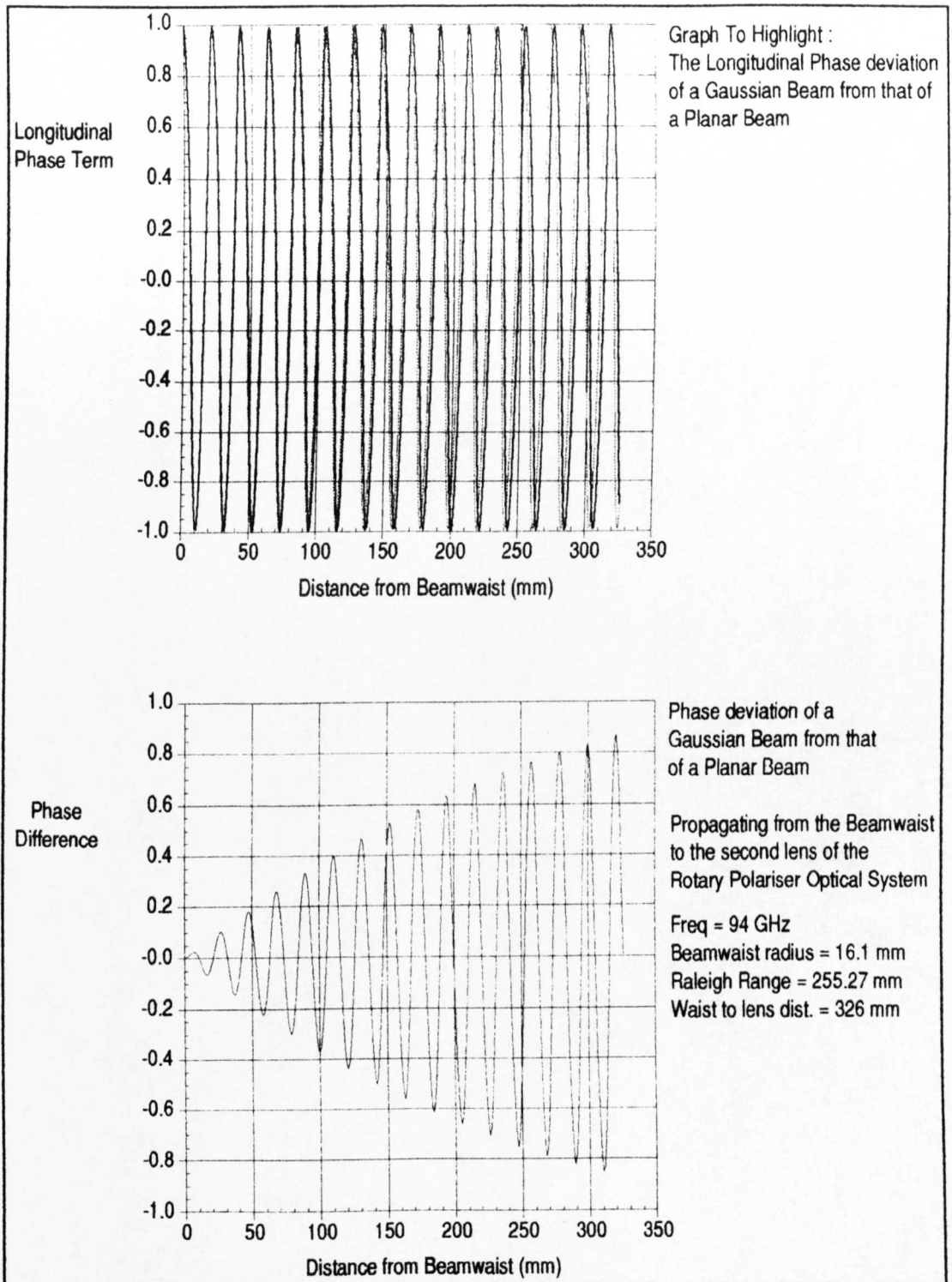


Figure (2.4)

(2.2.6) The Phasefront Radius Parameter $R(z)$

The parameter $R(z)$ describes the amount of curvature of the

wavefront for a particular (z).

$$R(z) = z\sqrt{1 + \left(\frac{z_R}{z}\right)^2}$$

As one can see at the beamwaist $z=0$ the phasefront radius $R(z) \Rightarrow \infty$ which corresponds to a wavefront that is plane. As (z) increases from the beamwaist, the wavefront starts to curve in a convex fashion. The curvature is such that the wavefront is orthogonal to expansion curves traced out by the beamwidth locations shown in figure (2.5). Beyond the Raleigh range location the phasefront radius has its centre at the beamwaist position. This is because the beamwidth varies linearly with the expansion angle for $z > z_R$, as described in section(2.2.3).

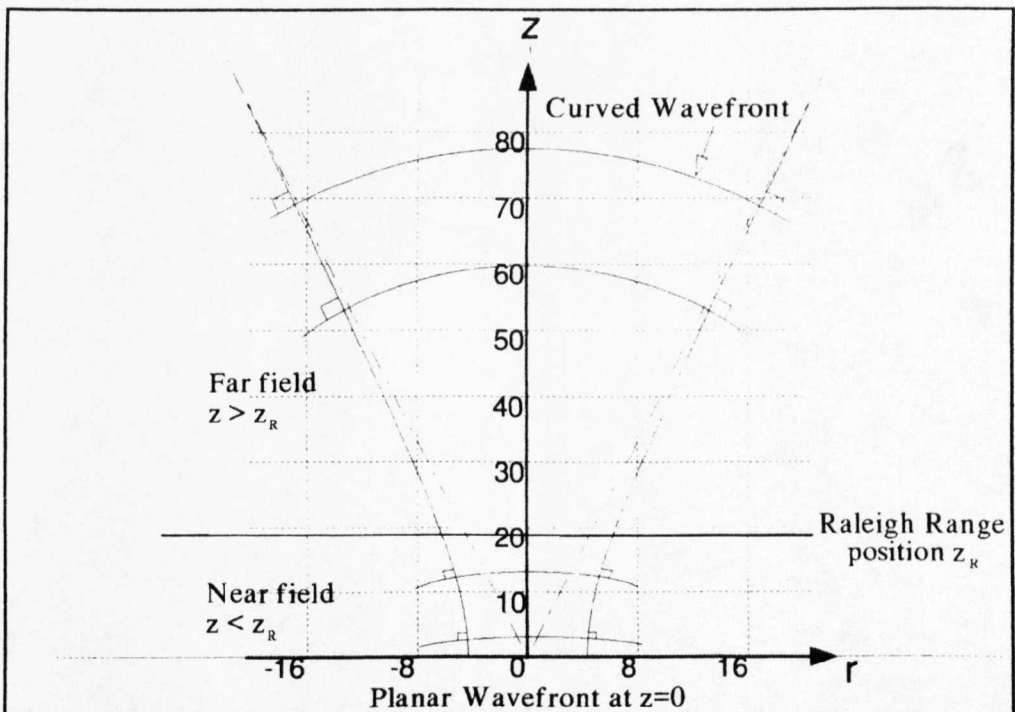


Figure (2.5)

(2.3) Modes and the General $TEM_{m,n}$ solution

After understanding the basic terms and parameters of the simplest and most widely used solution of the gaussian beam, it is a lot

easier to understand the general $TEM_{m,n}$ solution of the time-independent wave equation. Before going on to describe the general solution, I will firstly highlight the concept of modes.

(2.3.1) The $TEM_{m,n}$ acronym and Modes

Usually when talking about particular solutions to the time-independent wave equation for a gaussian beam, one usually refers to a particular $TEM_{m,n}$ mode. The $TEM_{m,n}$ acronym which stands for 'Transverse Electric Magnetic' describes the orientation of the electric and magnetic fields of the gaussian beam in respect to its direction of propagation vector. The transverse nature of the fields means that that the electric and magnetic fields are orthogonal to their direction of travel and to one another.⁶

The $TEM_{m,n}$ m,n values correspond to the electric and magnetic mode numbers respectively. The mode number describes how many times the corresponding electric or magnetic field is forced to zero other than at infinity. In its fundamental form where $m=n=0$ we have a normal profile for both the electric and magnetic fields. The resultant of both profiles define $(m+1) \times (n+1)$ number of power maxima, or spots, encountered in the (x) and (y) directions respectively, as shown in figure (2.6)⁷.

⁶ There are also other modes such as $TE_{m,n}$ and $TM_{m,n}$ which describe the electric field or the magnetic field as just being transverse to the direction of propagation . The complementary field being at some arbitrary orientation to the transverse field and its direction of propagation. Furthermore, $HE_{m,n}$ or $HM_{m,n}$ modes exist. These are known as highly symmetric Hybrid modes which are made up of usually one $TE_{m,n}$ and one $TM_{m,n}$ mode which are commonly employed in feedhorn design (See Smith G.M., Thesis, Transferred Electron Oscillators At Millimeter Wave Frequencies & Their Characterisation Using Quasioptical Techniques, section 8.3).

⁷ Figure taken from : Kogelnik H., Li T., Laser Beams & Resonators, Proceedings of the IEEE, Vol. 54, No.10, Oct 1996 - Gives an some excellent examples of visible $TEM_{m,n}$ modes.

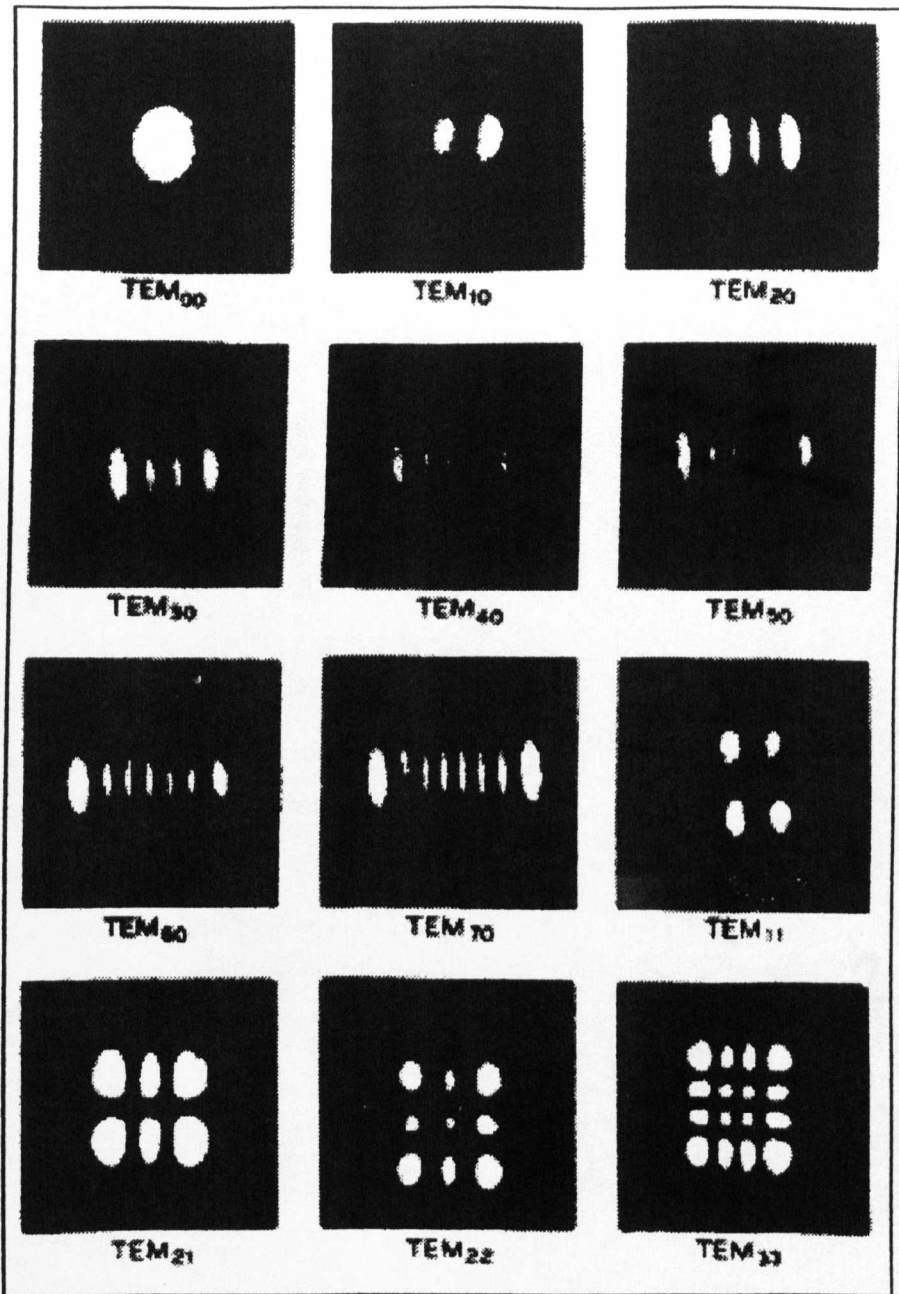


Figure (2.6)

(2.3.2) The General TEM_{m,n} mode solution

The general TEM_{m,n} mode solution at first glance can look quite bewildering.

$$\begin{aligned}
 E = | E_0 | \times & \\
 H_m \left[\frac{\sqrt{2}x}{\omega(z)} \right] \cdot H_n \left[\frac{\sqrt{2}y}{\omega(z)} \right] \cdot \frac{\omega_0}{\omega(z)} \exp \left\{ - \left(\frac{r}{\omega(z)} \right)^2 \right\} & \times \\
 \exp \left\{ - j \left(kz - (1 + m + n) \tan^{-1} \left(\frac{z}{z_R} \right) \right) \right\} & \times \\
 \exp \left\{ - j \left(\frac{kr^2}{2R(z)} \right) \right\} & \dots (2.14)
 \end{aligned}$$

where, $r^2 = x^2 + y^2$

However upon understanding the TEM_{0,0} mode solution one can easily spot that the TEM_{m,n} solution is identical to the TEM_{0,0} solution except for two additional factors. The two additional factors are very apparent. The first weighting factor affects the amplitude of the original TEM_{0,0} mode solution and the second weighting factor affects the longitudinal phase.

(2.3.2.1) The First weighting factor

The first weighting factor for a cartesian coordinate system consists of two Hermite polynomials of order (m) and (n). If in a cylindrical coordinate system a Laguerre polynomial pair would be used. It is these polynomials that are responsible for forcing the electric and magnetic fields to zero for specific m's and n's, as described in section (2.3.1).

$$H_m \left[\frac{\sqrt{2}x}{\omega(z)} \right] \cdot H_n \left[\frac{\sqrt{2}y}{\omega(z)} \right]$$

The Hermite polynomial for a particular function of variable (u) in the cartesian coordinate system is described by :

$$H_m [u] = (-1)^m e^{u^2} \cdot \frac{d^m (e^{-u^2})}{du^m} \dots (2.15)$$

For the first few low order Hermites one finds :

$$\begin{aligned} H_0[u] &\Rightarrow 1 \\ H_1[u] &= 2(u) \Rightarrow u \\ H_2[u] &= 2(2u^2 - 1) \Rightarrow 2u^2 - 1 \quad \dots (2.16) \end{aligned}$$

As one can see for the TEM_{0,0} mode $H_0[u] \Rightarrow 1$. Hence the weighting factor vanishes as expected for the fundamental mode.

(2.3.2.2) The Second weighting factor

The other factor affects the anomalous phase factor of the Longitudinal phase term.

$$(1 + m + n) \tan^{-1} \left(\frac{z}{z_R} \right)$$

Which implies that different TEM_{m,n} modes have different longitudinal phases. Although it might appear that there is nothing to worry about with the previous statement there is actually one important consequence of it. Under close scrutiny the factor (1+m+n) implies that multimode quasioptical systems are not desirable, as described by Harvey⁸. The reason why an quasioptical system should not employ more than one mode is because of the following. If two modes were present in a system they would, due to the (1+m+n) factor, have two different anomalous phase factors and hence have two different Longitudinal phase terms. The two modes could well couple efficiently through a quasioptical system to a detector for one particular frequency. However, for other frequencies interference would occur and the system would be said to suffer 'frequency dependent throughput'.

⁸ Harvey A.R., (Thesis) A Millimeter wave quasioptical complex impedance bridge. Chapter.3, pg.22

(2.4) Lens Design

Now one understands the nature of how quasi-optical beams propagate, it is quite obvious that one needs some means of constraining the gaussian beam to propagate through a quasioptical system. Without some means of constraint the gaussian beam would rapidly diverge and become unusable. The employment of mirrors and lenses within a system can be used to transform a rapidly diverging beam to that of one which converges to a beamwaist and then re-diverges out to another mirror or lens. Hence the process repeats and the wave can be guided in freespace to the desired location. At St.Andrews we design and manufacture dielectric planar/convex lenses for this purpose. In the following section, I will outline the theory and methods I used in order to design suitable lenses for use in the 'Rotary Polariser Quasi-Optical System'. I will also include the relevant calculations necessary to predict the beamwidths at the lenses and the locations and size of beamwaists after the lenses.

Other common laboratory quasioptics include feedhorns, mirrors, corner-cubes, wiregrid polarisers. These are all used to produce and manipulate gaussian beams in a variety of manners within a quasioptical circuit. A full discussion of the interactions of the gaussian beam with these structures can be found in Goldsmith⁹ and Lesurf¹⁰.

(2.4.1) Phase Transformation

The reason a lenses can cause a diverging gaussian beam to converge upon propagation through itself is because the lens acts as a radial phase transformer. Hence, adjusting the radial phase of the diverging wavefront into one which converges. As will be explained this radial phase transformation is an intrinsic property of a dielectric

⁹ *Infrared & Millimeter Waves (Vol 6)*, P.F. Goldsmith, Academic Press, 1982, Chapter 2.

¹⁰ *Millimeter-Wave Optics, Devices & Systems*, J.C.G.Lesurf, Adam Hilgar Publishers, 1990, Chapter 2 & 9.

and its shape.

The simplest of lens can be described as a dielectric slab¹¹ of thickness (d) and refractive index (n).

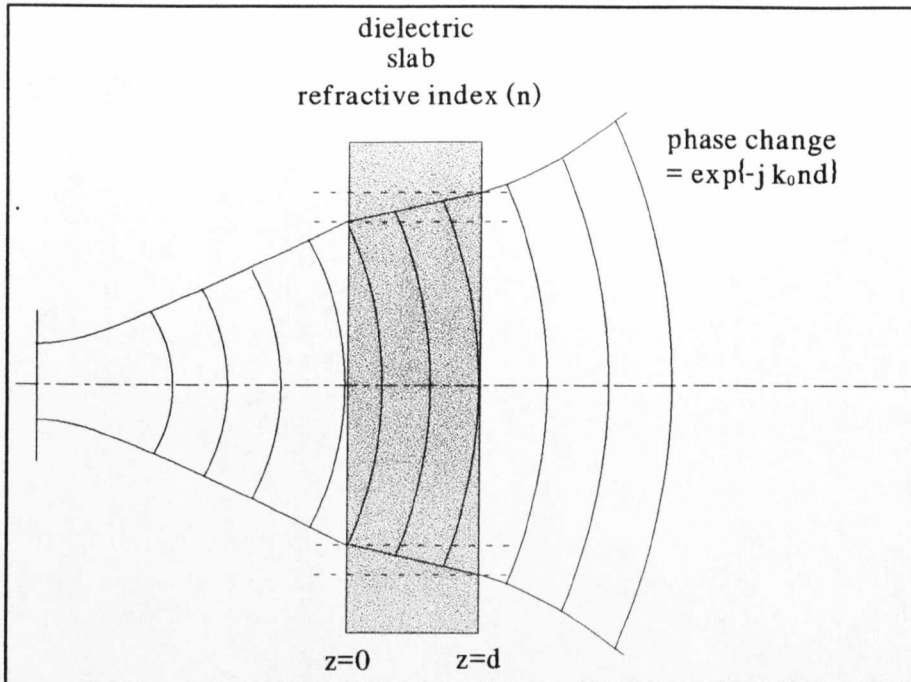


Figure (2.7)

One can see from figure (2.7) as the wavefront penetrates the dielectric slab it is slowed down since the refractive index of the dielectric is greater than that in freespace. This serves to phase retard the wavefront. The more dielectric passed through the more phase retardation incurred. The dielectric slab would make a useless lens since every part of the wavefront has travelled through the same amount of dielectric and hence the phase is retarded by the same amount. Therefore, the wavefront would still diverge on exit of the slab. However, if one acknowledges the fact that the axial part ($r=0$) of the gaussian beam is ahead in phase from the rest of its wavefront, one can arrange to retard the central ($r=0$) part of the wavefront more than the rest of the wavefront by simply forcing it to pass through a larger amount of dielectric. Similarly, the edges of the wavefront which are lagging most from the central ($r=0$) value

¹¹ Syms R., Cozens J., Optical Guided Waves and Devices, M^c Graw Hill, Chapter 4, Sect. 4.3

should be allowed to pass through the least amount of dielectric. Therefore, it follows by designing the dielectric to be thickest at its central point and then to taper the thickness radially to zero one can create a lens that produces a gaussian beam with least divergence, namely an almost plane parallel beam. See figure (2.8).

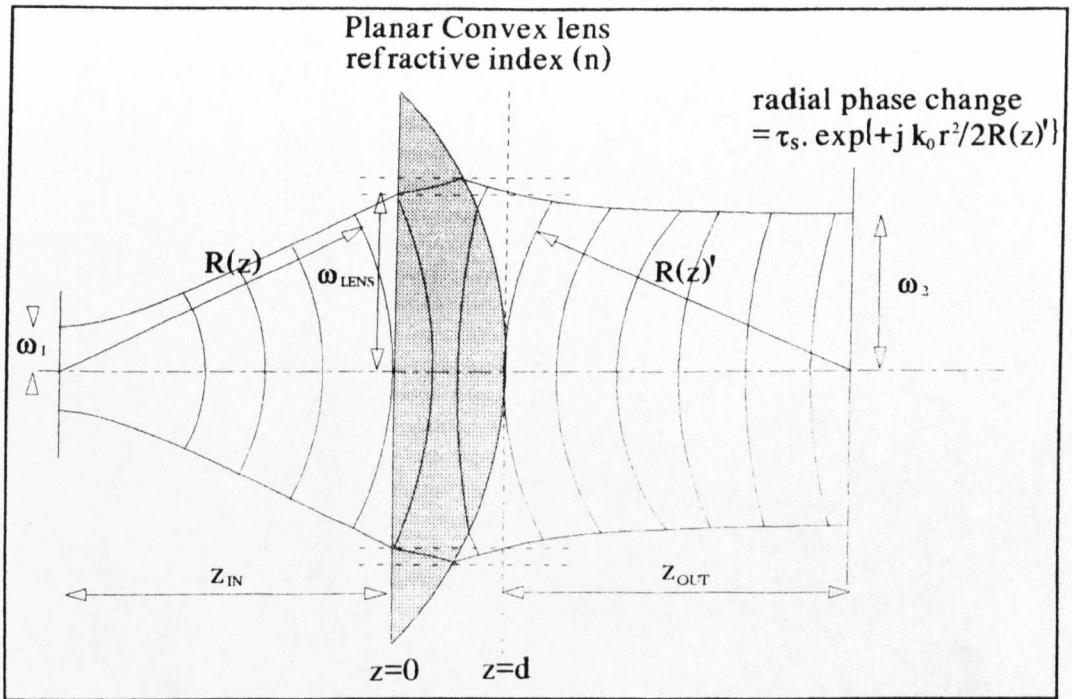


Figure (2.8)

Another advantage for designing the lens to give an almost plane parallel beam is that it tends to reduce the thickness of the lens. This can help to reduce any anomalous phase distortions which can sometimes occur in the manufacture of thicker lenses.

(2.4.2) Determining the amount of phase retardation

The amount of phase retardation incurred upon a wavefront by a dielectric of refractive index (n) is defined by the 'transparency function' (τ). The solution to the time-independent wave equation as described by equation (2.2) can be re-expressed for a medium of refractive index (n):

$$|E_0| = |E_0| e^{-j(kz)} = |E_0| e^{-j(k_0 n z)} \quad \dots (2.17)$$

where $k_0 = \frac{\omega n_0}{c} = \frac{\omega}{c}$

If the wavefront passes through a dielectric slab of thickness (d) the resultant wavefront will be :

$$|E_0| = |E_0| e^{-j(k_0 n(0) + k_0 n d)} = |E_0| e^{-j(k_0 n d)} \quad \dots (2.18)$$

The phase retardation caused by the slab is :

$$\tau_{SLAB} = \exp\{-jk_0 n d\} \quad \dots (2.19)$$

where, $\delta = nd =$ optical thickness

Hence, the phase shift depends on the optical thickness of the material.

The resultant amplitude of the beam can also be expressed as :

$$|E_{OUT}| = \tau_s |E_0| \quad \dots (2.20)$$

(2.4.3) Phase Retardation for a Planar/Convex Lens

The thickness (t) of a general shaped lens at any radial distance (r) can be expressed as :

$$t = d - \left(\frac{r^2}{2}\right) \left(\frac{1}{r_1} + \frac{1}{r_2}\right) \quad \dots (2.21)$$

where, (r_1) and (r_2) are the radius of curvature and (d) is the maximum thickness of the lens.

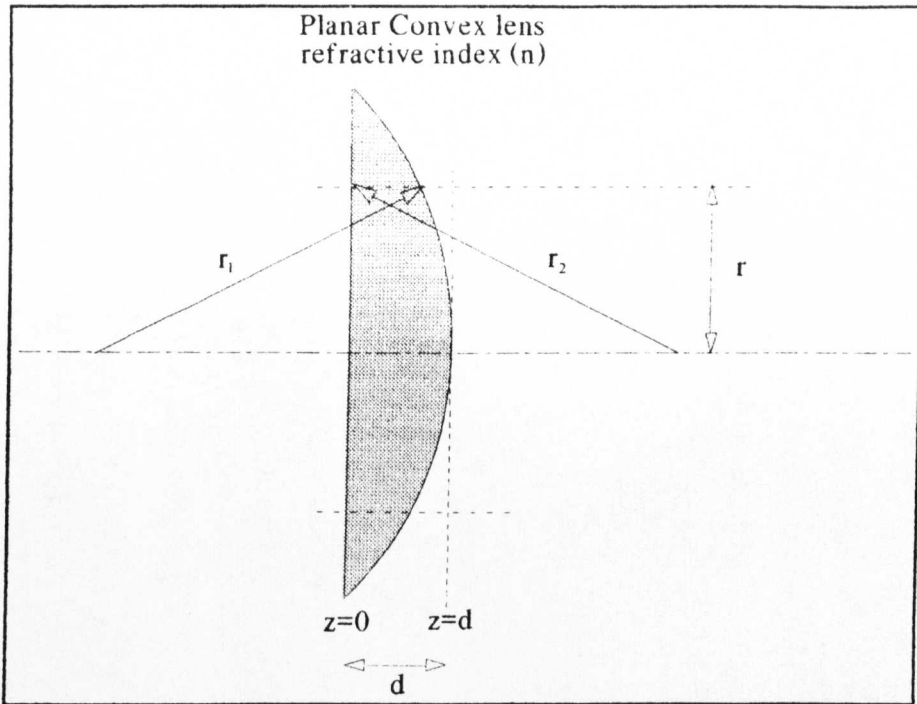


Figure (2.9)

Now for planar/convex lens one of the radii of curvature is infinite ($r_2 = \infty$) due to its planar nature. See figure (2.9) and the distance traversed through the dielectric becomes :

$$\therefore t = d - \left(\frac{r^2}{2}\right)\left(\frac{1}{r_1}\right) = d - \left(\frac{r^2}{2r_1}\right) \quad \dots (2.22)$$

Similarly the distance traversed in freespace between $z=0$ and $z=d$ is (t_0) such that :

$$t_0 = n_0(d - t) = (d - t) \quad \dots (2.23)$$

Now the distance traversed by the wavefront through the lens is described by the optical thickness (δ) such that :

$$\delta = n(t + t_0) = nt + (d - t) \approx nd - (n - 1)\left(\frac{r^2}{2r_1}\right) \quad \dots (2.24)$$

The 'transparency function' for planar/convex lens can be written as:

$$\begin{aligned}
 \tau_{PLANAR/CONVEX} &= \exp\left\{-jk_0\left(nd - (n-1)\left(\frac{r^2}{2r_1}\right)\right)\right\} \\
 &= \exp\{-jk_0nd\} \cdot \exp\left\{+j(n-1)\left(\frac{r^2}{2r_1}\right)\right\} \\
 &\quad \uparrow \qquad \qquad \qquad \uparrow \\
 &\quad \tau_{SLAB} \qquad \qquad \qquad \text{Due to lens curvature} \\
 &= \tau_{SLAB} \cdot \exp\left\{+j(n-1)\left(\frac{r^2}{2r_1}\right)\right\}
 \end{aligned}$$

Now the 'Lens makers equation' states that :

$$\frac{1}{f} = (n-1)\left(\frac{1}{r_1} + \frac{1}{r_2}\right) \Rightarrow (n-1)\left(\frac{1}{r_1}\right) \quad \text{for a planar/convex.... (2.25)}$$

where (f) is the focal length of the lens.

Hence, the 'transparency function' for a planar/convex lens is given by :

$$\tau_{PLANAR/CONVEX} = \tau_S \cdot \exp\left\{+j\left(\frac{k_0 r^2}{2f}\right)\right\} \quad \dots (2.26)$$

This is the radial change in phase that is incurred upon a gaussian beam after it has passed through a planar/convex lens.

One can now proceed to determine how this will affect the radial phase of a diverging gaussian beam. The radial phase term is given by :

$$\exp\left\{-j\left(\frac{kr^2}{2R(z)}\right)\right\}$$

Upon propagating through the planar/convex lens the radial phase term becomes :

$$\exp\left\{-j\left(\frac{kr^2}{2R(z)}\right)\right\} \cdot \tau_s \cdot \exp\left\{+j\left(\frac{k_0r^2}{2f}\right)\right\}$$

Quoting the 'Thin lens equation' :

$$\frac{1}{f} = \frac{1}{R(z)} + \frac{1}{R(z)'} \quad \dots (2.27)$$

Where $R(z)$ represents the radius of curvature on the left side of the lens and $R(z)'$ represents that on the right. Hence the new radial phase term becomes :

$$= \tau_s \cdot \exp\left\{+j\left(\frac{kr^2}{2R(z)'}\right)\right\} \quad \dots (2.28)$$

The most important aspect of the new transformed radial phase term is the sign. The sign is positive which represents a gaussian beam diverging in the (-z) direction or conversely that of a gaussian beam converging in the (+z) direction.

(2.4.4) Lenses Designed For The 'Rotary Polariser Quasi-Optical System'

A lens design program was developed by Smith¹² which takes the λ , z_{IN} and w_{LENS} values specified by the user and computes the best planar convex lens to optimise the throw of the beam. The beamwidth I required at the lens was set to a radius of 24mm. This beamwidth was chosen due to the dimensions of the 'Quasioptical Fresnel Rhomb'¹³ that I developed and was a safe figure to allow good coupling through the device.

¹² Smith G.M., Thesis, Transferred Electron Oscillators at millimeter wave frequencies & their characterisation using quasioptical techniques. pgs. 178-182

¹³ As described in section (9.7.1).

The computer program generated a lens with a :

- A maximum throw of 526mm ($\cong 4.38$ half cubes)
- Effective focal length of 77.178mm
- A Maximum Thickness of 25.917mm

This throw was sufficient to use the lenses for both a 'Fresnel Rhomb Transmission System' and the 'Rotary Polariser Quasi-Optical System'.

Upon knowing the focal length (f) of the lens one can take the 'Thin Lens Formula', equation (2.27) and combine this with the phasefront radius, equation (2.9) to get :

$$\frac{1}{f} = \frac{1}{R(z)} + \frac{1}{R(z)'} \\ = \frac{1}{z_{IN}(1 + (z_{R1}/z_{IN})^2)} + \frac{1}{z_{OUT}(1 + (z_{R2}/z_{OUT})^2)} \quad \dots (2.29)$$

We can also say that for a gaussian beam that has been transformed by a lens, that the beamwidth at the lens (ω_{LENS}) will be the same as for the gaussian beam projected from waist (ω_1) as it will from (ω_2).

Referring to diagram (2.7) and using equation (2.8) we also get :

$$\omega_{LENS} = \omega_1 \sqrt{1 + \left(\frac{z_{IN}}{z_{R1}}\right)^2} \quad \& \quad \omega_{LENS} = \omega_2 \sqrt{1 + \left(\frac{z_{OUT}}{z_{R2}}\right)^2} \\ \therefore \omega_1 \sqrt{1 + \left(\frac{z_{IN}}{z_{R1}}\right)^2} = \omega_2 \sqrt{1 + \left(\frac{z_{OUT}}{z_{R2}}\right)^2} \quad \dots (2.30)$$

Solving equations (2.29) and (2.30) one gets¹⁴ :

¹⁴Goldsmith P.F., Infrared & Millimeter waves, Vol. 6, Chapter 5(c), Focussing of Gaussian Beams

$$\omega_2 = \omega_1 \sqrt{\frac{1}{((z_{IN}/f) - 1)^2 + (z_{R_1}/f)^2}} \quad \dots (2.31)$$

$$z_{OUT} = f \left\{ 1 + \frac{(z_{IN}/f) - 1}{[(z_{IN}/f) - 1]^2 + (z_{R_1}/f)^2} \right\} \quad \dots (2.32)$$

Hence, one can completely describe the sizes of the beamwaists and their locations by just knowing λ , the z_{IN} distance and the focal length of the lens used.

I designed the lenses to work over a 78-110GHz Bandwidth. The maximum beamwidth would occur at 78GHz and would have a radius of 24mm, as mentioned earlier. In order to achieve this beamwidth the (z_{IN}) distance to the lens would have to be fixed to 86.2mm. Fixing the (z_{IN}) and (z_{OUT}) distances one can calculate the beamwidths at the lenses in the system and beamwaist radius' and their locations, as shown in figure (2.10) below:

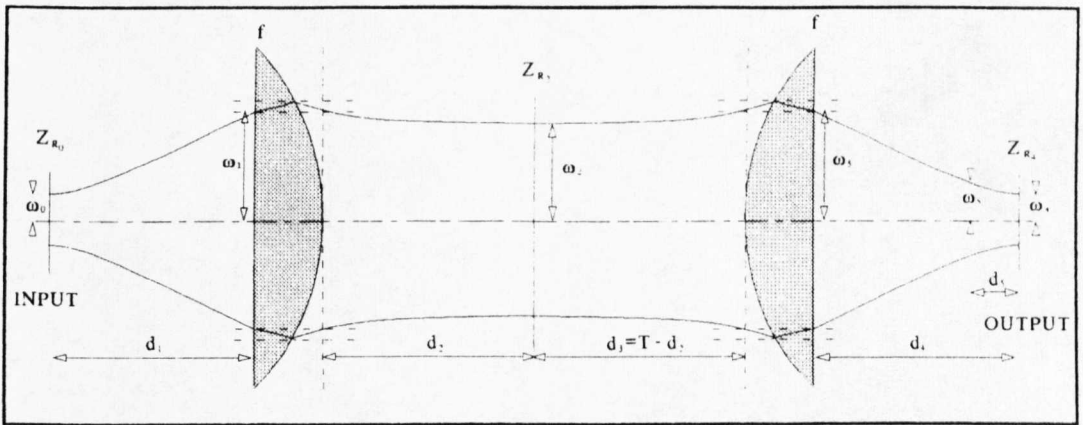


Figure (2.10)

$$\omega_1 = \omega_0 \sqrt{1 + \left(\frac{d_1}{z_{R_0}}\right)^2} \quad \& \quad z_{R_0} = \frac{\pi \omega_0^2}{\lambda}$$

$$\omega_2 = \omega_0 \sqrt{\frac{1}{((d_1/f) - 1)^2 + (z_{R_0}/f)^2}}$$

$$d_2 = f \left\{ 1 + \frac{(d_1/f) - 1}{[(d_1/f) - 1]^2 + (z_{R_0}/f)^2} \right\}$$

$$d_3 = T - d_2$$

$$\omega_3 \approx \omega_2 \sqrt{1 + \left(\frac{d_3}{z_{R_2}} \right)^2} \quad \& \quad z_{R_2} = \frac{\pi \omega_2^2}{\lambda}$$

$$\omega_4 = \omega_3 \sqrt{\frac{1}{((d_3/f) - 1)^2 + (z_{R_2}/f)^2}}$$

$$d_4 = f \left\{ 1 + \frac{(d_3/f) - 1}{[(d_3/f) - 1]^2 + (z_{R_2}/f)^2} \right\}$$

The plots of the predicted hornwaists, beamwidths at the lenses and the beamwaist sizes and their locations, for this quasioptical arrangement, can be seen in figures (2.11 - 2.15).

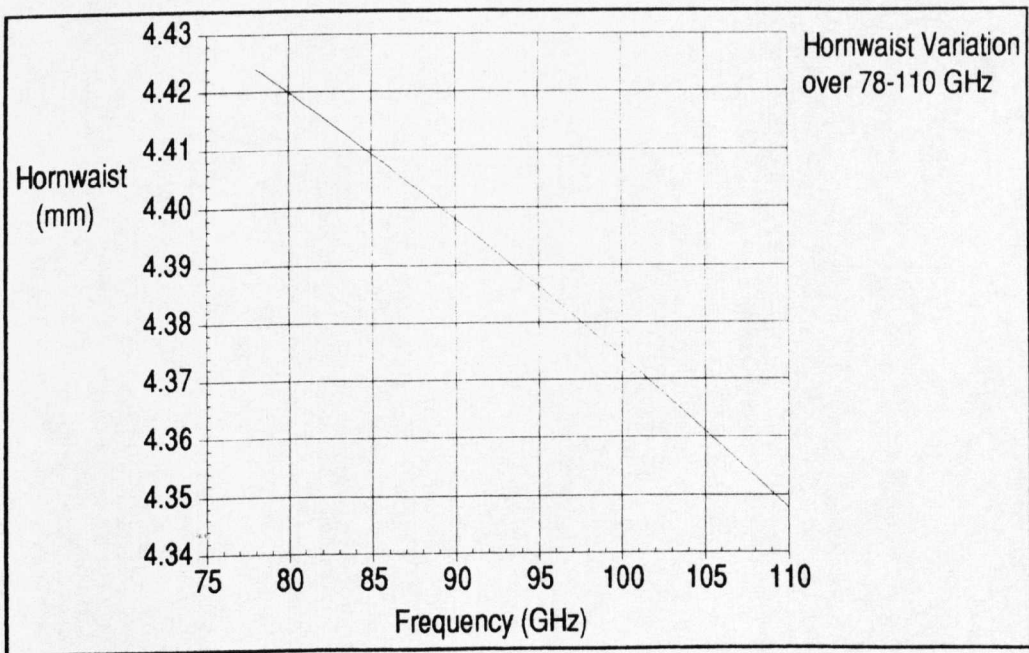


Figure (2.11)

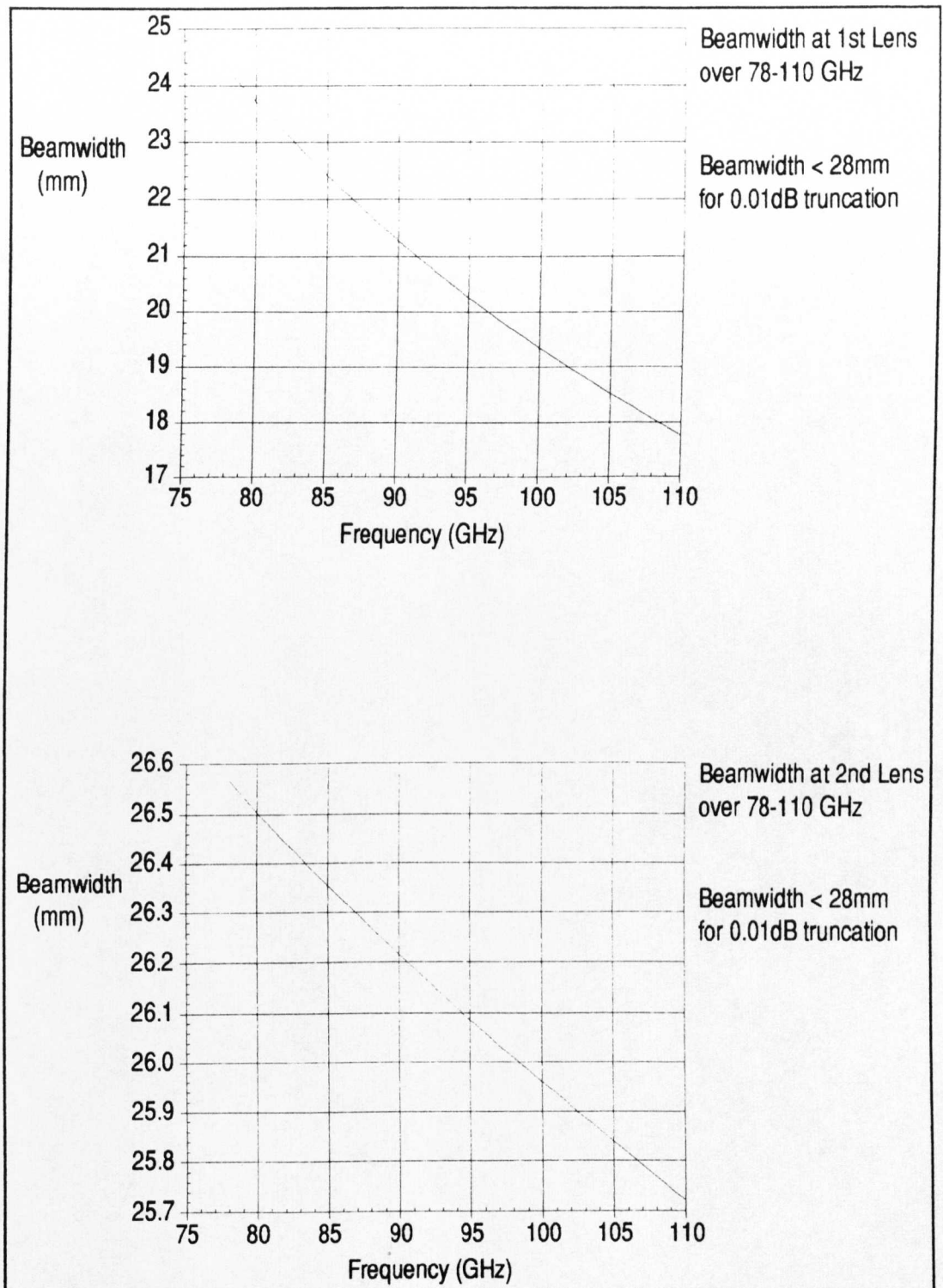


Figure (2.12)

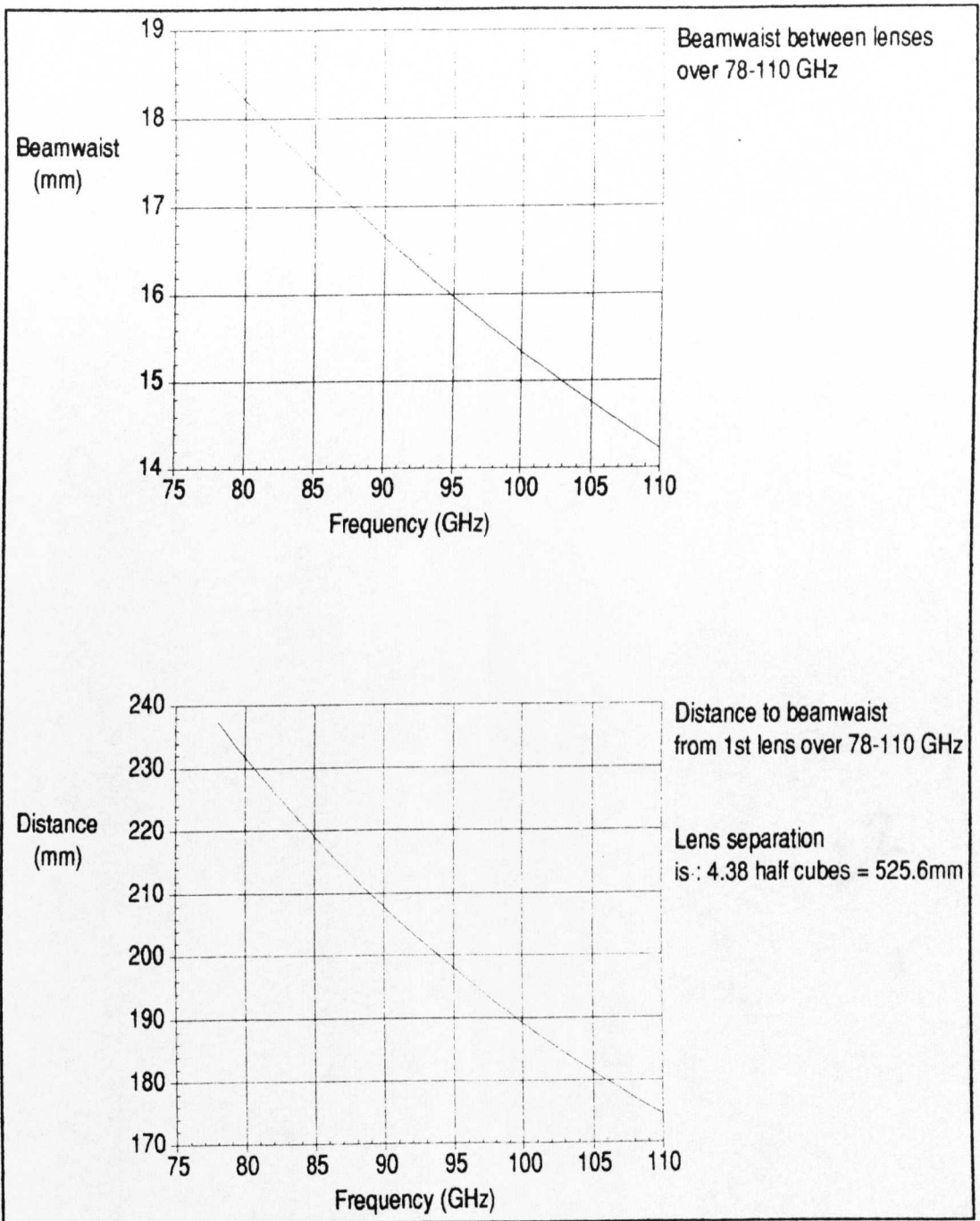


Figure (2.13)

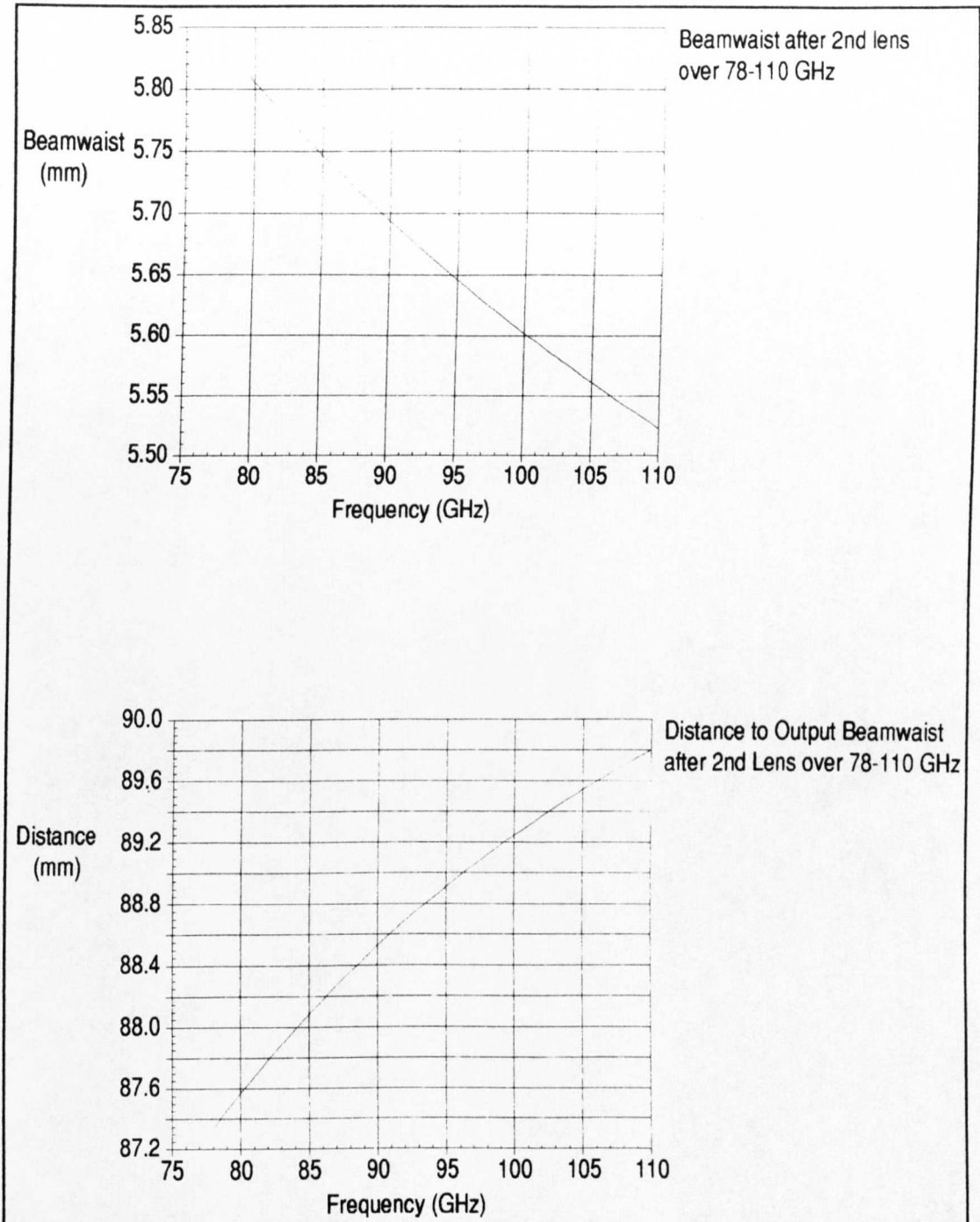


Figure (2.14)

After determining the distance from the second lens to the final beamwaist over the 78-110GHz band, it was decided to position the T.K. detector at 87.3mm which would give a beamwidth of no greater than 5.8 mm over the whole specified frequency range. This beamwidth would couple easily into the T.K. detector as it has a

detection sensitive area of 30×30mm.

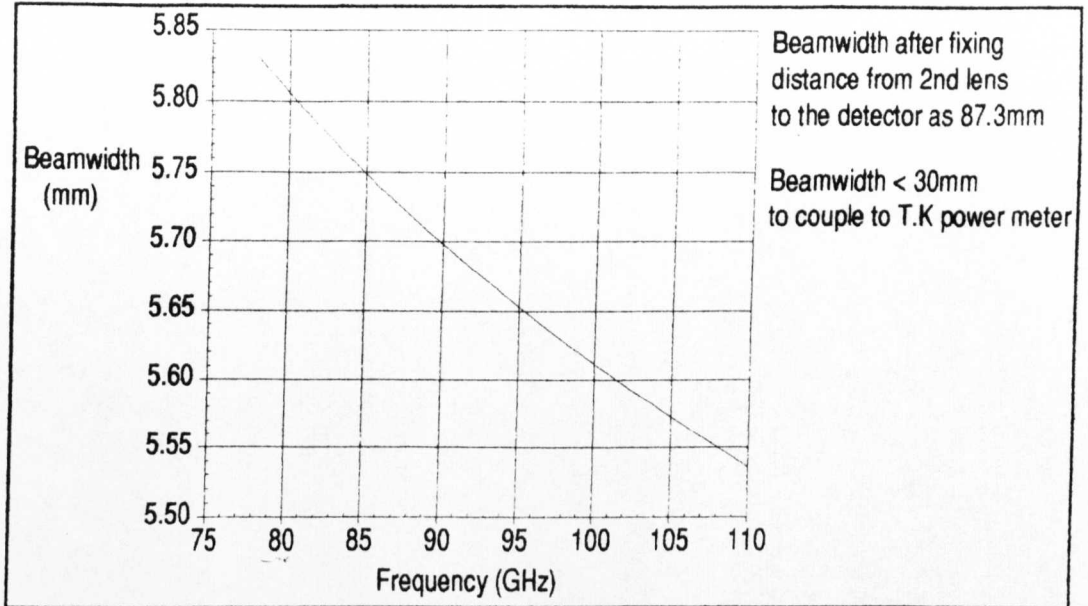


Figure (2.15)

Finally the dielectric Planar/Convex lenses were manufactured from High Density Polyethylene (H.D.P.E) which is virtually transparent at microwave and millimetric wavelengths and has a refractive index of 1.55. In order to avoid any unwanted surface reflections the dielectric lenses were blazed by cutting concentric grooves of depth $(\frac{\lambda}{4\sqrt{n}})$ mm and 0.04mm width with a mark/space ratio of 1:1.

Chapter 3

The Gunn Oscillator & The A.O.T.S

Introduction

The Gunn oscillator is the fundamental millimetric source of radiation we employ here at St.Andrews. I intend in the first part of the chapter, to present a full understanding of how the Gunn oscillator operates and is constructed. This will cover theoretical areas such as the Gunn Effect, the Gunn diode and its band structure, engineering areas such as harnessing certain modes of operation in the oscillator design and construction to experimental areas of Gunn oscillator characterisation. The second part of the chapter will discuss the design and development of a fully Automated Oscillator Tuning System (AOTS). Its sections will detail how the system was designed to mechanically adjust the micrometer tuners of a conventional Gunn oscillator via a small electronics package interfaced to a computer. Furthermore, it will be shown that by the development of appropriate control programs, the system can be used to drive the oscillator's micrometer tuners in any way the user so desires. This is finally demonstrated in the control program 'CharOsc' which was developed to automatically characterise a Gunn oscillator.

(3.1) The Gunn Effect

J.B Gunn was the first person to report the phenomena of the 'Gunn Effect'¹ to which he was to give his name. His discovery was that of

¹ Gunn J.B., Microwave oscillations of current in III-V semi-conductors, Solid state communications, Vol 1., pgs.88-91, 1963.

a new type of high frequency current oscillations which appeared in n-type GaAs and InP, III-V semiconductors, when an applied electric field exceeded some critical or threshold value. Gunn rejected the postulate by Ridley and Watkins² of the 'transferred electron effect' which suggested the idea of a bulk negative differential resistance occurring within a semi-conductor for high fields. Ironically, this was later accepted as the mechanism which produced the phenomena Gunn had originally observed¹, as published in a manuscript by Kroemer³. By exploitation of this effect the Gunn diode was born. When the device is harnessed in an appropriate resonant circuit, the diode acts as a low noise, wide band millimetric to sub-millimetric local oscillator. The following sections will give a detailed explanation of the Gunn Effect and operation of the Gunn diode. Furthermore, the sections will explain how an appropriate oscillator can be configured to achieve millimetric frequencies.

(3.1.1) Types Of Diode Available

There are two main types of diode that are on the market. These are the Gunn diode which exploits the Gunn effect for its operation and the IMPATT, or 'Impact Avalanche Transit Time' diode. Both types corner different areas of the market. The IMPATT is employed for high power applications. The Gunn diode is a low power device and has low noise operation in comparison to the IMPATT. This is due to the difference in the mechanisms employed for operation, as detailed by Brookbanks⁴. When placed in an appropriate circuit the Gunn diode can also exhibit wideband performance. For these reasons its area of the market is that of the local oscillator.

There are two types of semi-conductor which are commercially used

² Ridley B.K., Watkins T.B., The possibility of negative resistance effects in semi-conductors, Proc.Phys.Soc, 78, pgs 293-304, 1962.

³ Kroemer H., Theory of the Gunn effect, Proc.IEEE, 52, 12, pg. 1736, 1964.

⁴ Brookbanks D.M., Millimeter Wave Solid State Sources, Allen Clark Research Centre, Annual Review, 1981.

in the manufacture of the Gunn diode. These are Gallium Arsenide (GaAs) and Indium Phosphide (InP). The GaAs operates up to 115GHz and the InP Gunn diode operates around 70-140GHz. The InP Gunn diode typically has a greater input to output efficiency, sometimes referred to as its peak to valley ratio, and a higher output power than GaAs. The Gunn diodes that we employ here at St.Andrews are of the GaAs type.

(3.2) The Transferred Electron Device

The transferred electron device (T.E.D.) or Gunn Diode consists of a piece of n-type III-V semi-conductor, known as the 'Active region', with two ohmic contacts on either end. Although various III-V semi-conductors exhibit this phenomena it is the Gallium Arsenide (GaAs) and Indium Phosphide (InP) types which are commercially available as diode packages. It is for this reason, their characteristics will be focussed upon during this discussion. They are also categorized as 'Bulk effect' devices. This is because the phenomena occurs as an intrinsic bulk property of the semi-conductor. Furthermore, they come under another heading of 'Transit-Time' devices which implies their frequency of operation is proportional to the reciprocal of the carrier time across the active region, as depicted in figure(3.1).

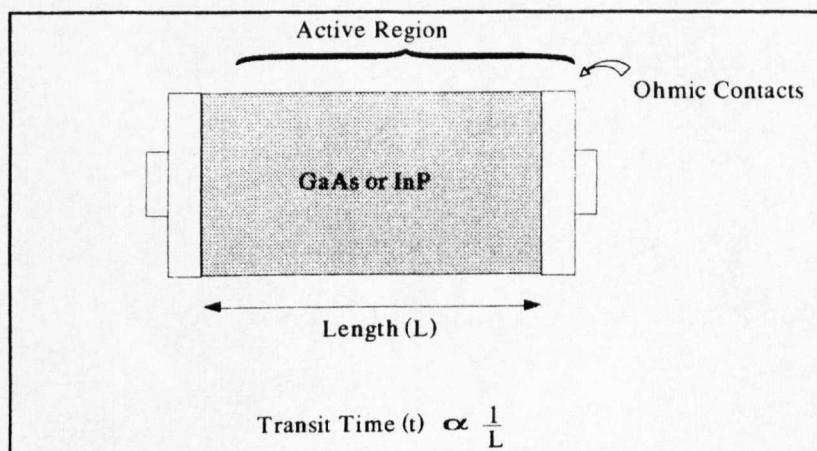


Figure (3.1)

(3.2.1) The Band Structure Of GaAs & InP

The common feature of these devices is their band structure. The band structures for GaAs and InP are shown in figure(3.2)

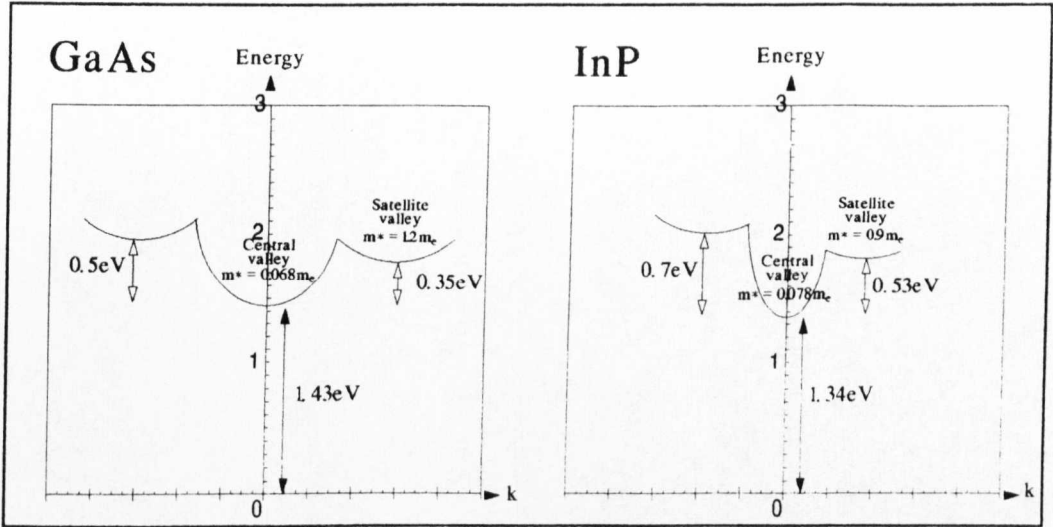


Figure (3.2)

The two important features to note about the band structure are the central valley region and the satellite valley region. As will be disclosed shortly it is the variation in the population of charge carriers in the band structure due to increasing field that is responsible for the Gunn effect phenomena.

In thermal equilibrium the electrons of the semi-conductor lie in the central valley region. The electrons in this region are in the lowest energy conduction band. They also have a low effective mass (m^*) which is 0.068 of that of a free electron (m_e) for GaAs and 0.078 m_e for InP. This low effective mass implies that the electrons can move with a high effective velocity, making them highly energetic and implying a high mobility.

The satellite region is the region where electrons have high energies $>0.35\text{eV}$ for GaAs and $>0.55\text{eV}$ for InP. The electrons here have a high effective mass which is ≈ 20 times greater than that in the central valley region for GaAs and ≈ 10 times greater than that in the central valley region for InP. This implies that the electrons have a

low effective velocity and therefore a low mobility.

(3.2.2) Application of an Electric Field

When in thermal equilibrium the electrons of the semi-conductor lie in the central valley region. Upon application of a low electric field, such that the field is below a critical value known as the 'Threshold Field', the electrons gain energy. As discussed in the previous section, these electrons with low effective mass are extremely energetic and their only mechanism to lose the energy is to interact with the lattice. This results in a lattice vibrations or phonons.

At moderate fields below the threshold field, the electrons begin to possess energy in excess of what they can lose to the lattice. Therefore, their momentum increases and they race up the sides of the central valley. However, they are still not energetic enough to overcome the potential of the central valley and are constrained to this region.

When strong electric fields are applied which are greater than the threshold field, namely at 0.35eV for GaAs and 0.53eV for InP, the electrons start to migrate to the satellite region. Since the effective mass of the electrons in the satellite region is high, $1.2m_e$ for GaAs and $0.9m_e$ for InP, the electrons slow down and their mobility decreases. Now electrons that migrate later start to catch up with the initial migrating electrons since their mobility is higher. This causes an accumulation of charge carriers in the satellite region. There are two main ways the charge carriers accumulate which affect the way the device operates. This depends on the length of the active region as will now be explained.

(3.2.3) The Classical Domain Accumulation mode of operation

When the active region is long the device will operate in this classical domain accumulation mode. Furthermore, having a long active length means the device will operate at low frequencies. Therefore, the classical domain mode is associated with low

frequency operation. Since the electrons in the central valley region are essential playing 'catch up' with those that have just migrated to the satellite region an accumulation region is formed. As the electrons at the front of the accumulation zone move toward the anode of the device they create a depletion region between themselves and the transitional electrons behind them. If the density of electrons contained in the central valley and satellite regions is given by (n_c) and (n_s) respectively and the mobility of the electrons in the central valley and satellite regions is (μ_c) and (μ_s) respectively. The current density (J) arising in both the central and satellite valley regions due to the applied electric field (E) can be expressed by the equation(3.1).

$$J = \sigma E = (n_c e \mu_c + n_s e \mu_s) E \quad \dots (3.1)$$

Where, (e) is the electronic charge of the carriers.

One can see from the equation, as more electrons migrate to the satellite region, the central valley region is depopulated whilst the satellite region's population increases. Hence, the electron density (n_c) decreases and (n_s) increases. This tends to make the bracketed term decrease and hence reduce the current density of the device. The creation of the depletion region also produces a 'High Field Dipole Domain'. This serves to lower the electric field in the sample below the critical threshold field, hence no more domains form. The domain then travels to the anode at what is termed as the saturated drift velocity ($\approx 1 \times 10^7$ cm/sec).

This results in the current oscillations that Gunn observed. Such a transfer results in a field vs. velocity profile, like that shown in figure(3.3).

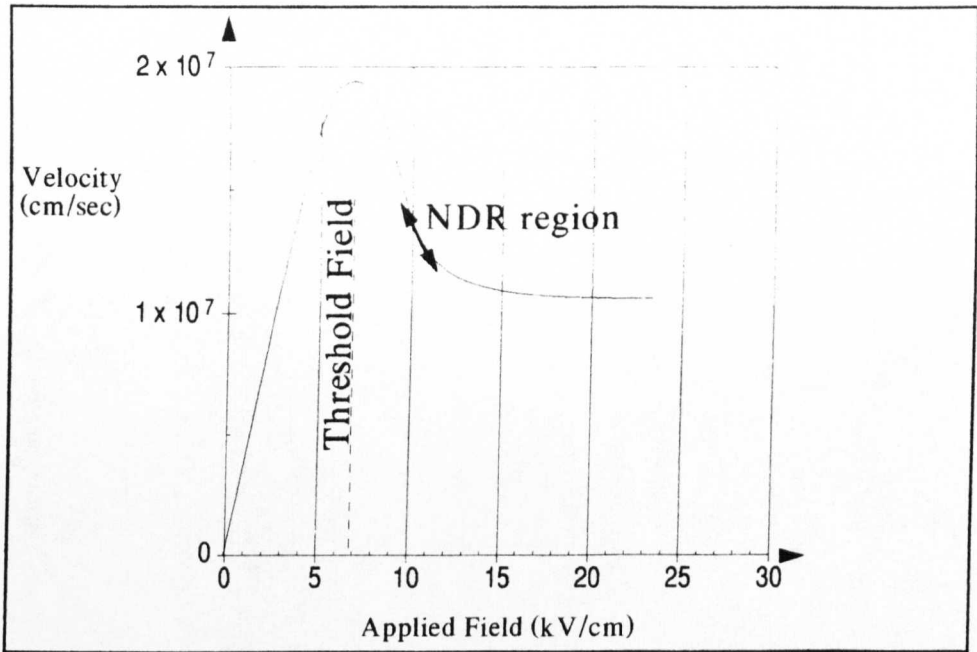


Figure (3.3)

As can be seen at around 10keV the device exhibits a 'Negative Differential Resistance' and the current oscillations occur. Thus by D.C. biasing the device to sit within this region the desired oscillations can be produced.

A 'dead time' exists between achieving enough carriers in the satellite region and reducing the electric field in the sample so a current oscillation can be produced. This 'dead time' can be expressed as such⁵ :

$$t_{DEAD} = \sqrt{\frac{2m \cdot \Delta\epsilon}{eE^2}} \quad \dots (3.2)$$

Where, ($\Delta\epsilon$) represents the energy transfer and (E) is the applied electric field. As one can see from the band structure of GaAs and InP in figure(3.2). Although, the carriers in InP have to attain more energy than those in GaAs, with their threshold field being greater than GaAs they do so relatively more quickly. Therefore, the dead time period of InP is somewhat higher than that of GaAs. This gives

⁵ Lesurf J.C.G., Millimeter wave Optics, Devices & Systems, Chapt.11, pgs.202-203.

InP a potentially higher efficiency of operation over GaAs. This measure of efficiency is known as the 'peak-to-valley' ratio. A higher peak to valley ratio implies a higher conversion of bias power to oscillations. For GaAs this is ≈ 2.2 and for InP this is ≈ 3.5 .

(3.2.4) The Limited Space-charge Accumulation mode of operation

The second operational mode occurs when the length of the active region is short (\approx few microns). This mode is associated with high frequency oscillation as documented by Copeland⁶. Since the length of the active region is so small, the value of the electric field rises so quickly across the sample, that the depletion region and high field dipole domain do not have time to form. Instead the accumulation of charge carriers appears at the cathode of the device and the field over most of the device is in the negative resistance range. In this mode a greater proportion of the electrons are in the satellite region which gives an increase in efficiency over the classical domain mode.

(3.2.5) The Gunn Diode Package

The Gunn diode package consists of the diode which is encircled by a ceramic annulus and topped by a gold lid. It sits on a gold plated screw cap which acts as a base and a heat sink for the diode. Small metal tapes run from the top of the diode to the gold lid. Therefore, by applying a potential difference to the gold lid, the diode can be biased appropriately. A more detailed explanation of the package can be found by reference to Robertson⁷. The package can be seen in figure(3.9)

⁶ Copeland J.A., A New Mode of Operation for Bulk Negative Resistance Oscillators, Proc.IEEE, 54, pgs.1479-1480, 1966.

⁷ Robertson M.R., (Thesis) Novel Solid-State Millimeter-Wave Devices, pgs.15-17.

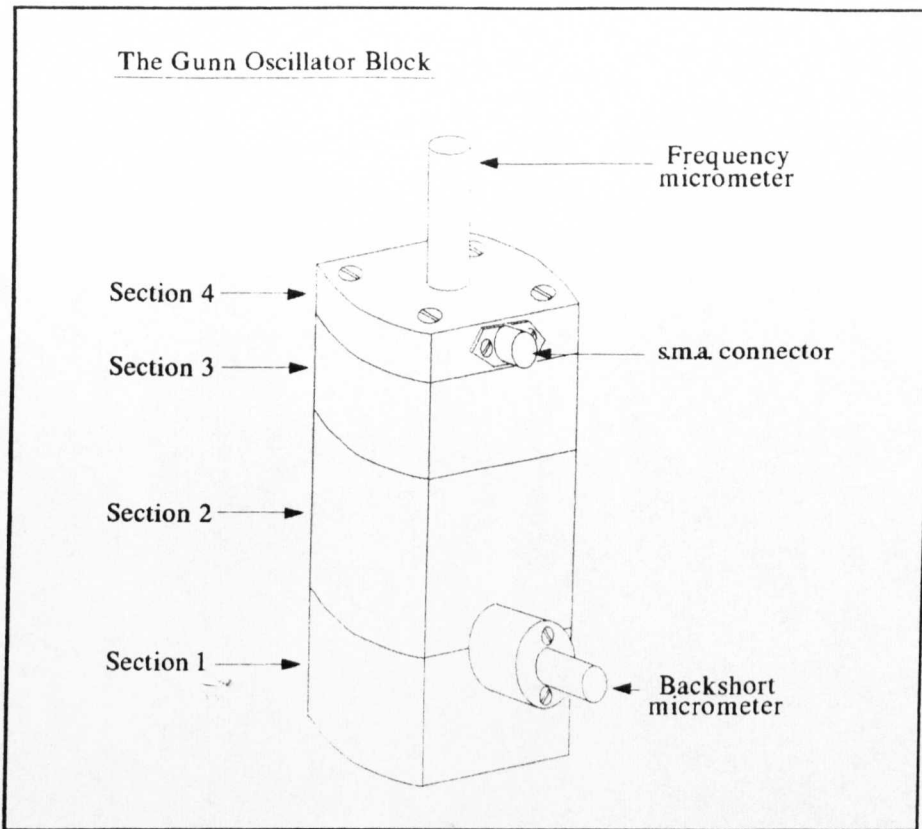


Figure (3.4)

(3.3) Overview of the Gunn Oscillator

The Gunn oscillator is the millimeter wave source used here at St.Andrews. The oscillators are constructed to the specifications of a coaxial cavity, resonant cap design which was developed by Smith.⁸ They are designed to perform over the W-band region centred around 94GHz using 2nd harmonic mode generation. The oscillator block which houses the above mentioned design consists of four sections, as shown in figure(3.4).

Two micrometers are located on the outside of the block. The first of the micrometers is situated on the top of the block and is used to tune the frequency of the oscillations. The second micrometer is used to optimise the power output and is located on the side of the block, between sections one and two. Located on the outside of section two is an S.M.A. connector. By applying a p.d across the

⁸ Smith G.M., (Thesis) Transferred Electron Oscillators at millimeter wave frequencies and their characterisation using quasi-optical techniques.

connector, current is drawn through it. The current firstly passes through a safety circuit housed within the second section. This electrical circuit then continues within an insulated choke structure finally to a cap and post structure that is in contact with the Gunn diode package. The cap and post structure together with the Gunn diode form a resonator which is responsible for the millimetric radiation produced. The oscillator blocks are manufactured here in the physics workshop department⁹, the Gunn diodes are bought commercially and they are constructed by the members of the millimeter wave laboratory. Whilst here at St.Andrews I have constructed several oscillator blocks, the construction of which I will now describe.

(3.3.1) Oscillator Block construction

As mentioned in the overview, there are four separate sections that make up the oscillator block. The fourth section is quite simple and requires no further explanation than that it just locates the frequency micrometer. The other sections starting with the bottom section will now be explained.

(3.3.2) The First Section

There are three main features to the first section of the oscillator block. The first section of the block is shown in figure(3.5).

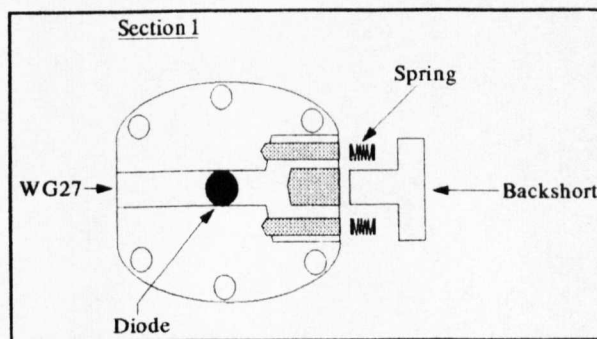


Figure (3.5)

⁹ The Millimeter Wave lab are indebted to George Radley and Bill Smith for their skilful manufacture of the oscillator blocks.

Located across its length are the rectangular dimensions which represent that of waveguide 27 for W-band. This waveguide structure is responsible for coupling the 2nd harmonic oscillations produced by the diode and resonant cap into freespace. The diode itself is located in the central threaded hole within the waveguide structure of the section. The commercial available GaAs diodes are supplied mounted on a small screw thread base. This can easily be positioned in place, such that the base is flush with the waveguide surface. The shaded areas in the diagram represent three recesses in the section. The top and bottom recesses hold two springs. A small T-shaped backshort presses against the springs such that the 'nose' of the backshort protrudes into the left side of the waveguide. The central recess accommodates the backshort micrometer which in turn presses against the back of the backshort. Together the springs and the micrometer serve to position the nose of the backshort within the waveguide.

As described by Haydl¹⁰, due to the fundamental frequency of the diode lying below the waveguide cutoff the oscillator frequency is independent of position of the backshort and serves to optimise the power output. However, in practice a frequency pulling of few megahertz is usually observed. The optimum position of the backshort from the diode for maximum power output is $x=\lambda/4$.

(3.3.3) The Second Section

The second section of the block houses the main body of the oscillator design which is shown as a cross-section in figure(3.6).

¹⁰ Haydl, W.H., Fundamental & Harmonic Operation of mm-wave Gunn diodes. IEEE transactions on microwave techniques. Vol. MTL 31, No.11, Nov. 1983.

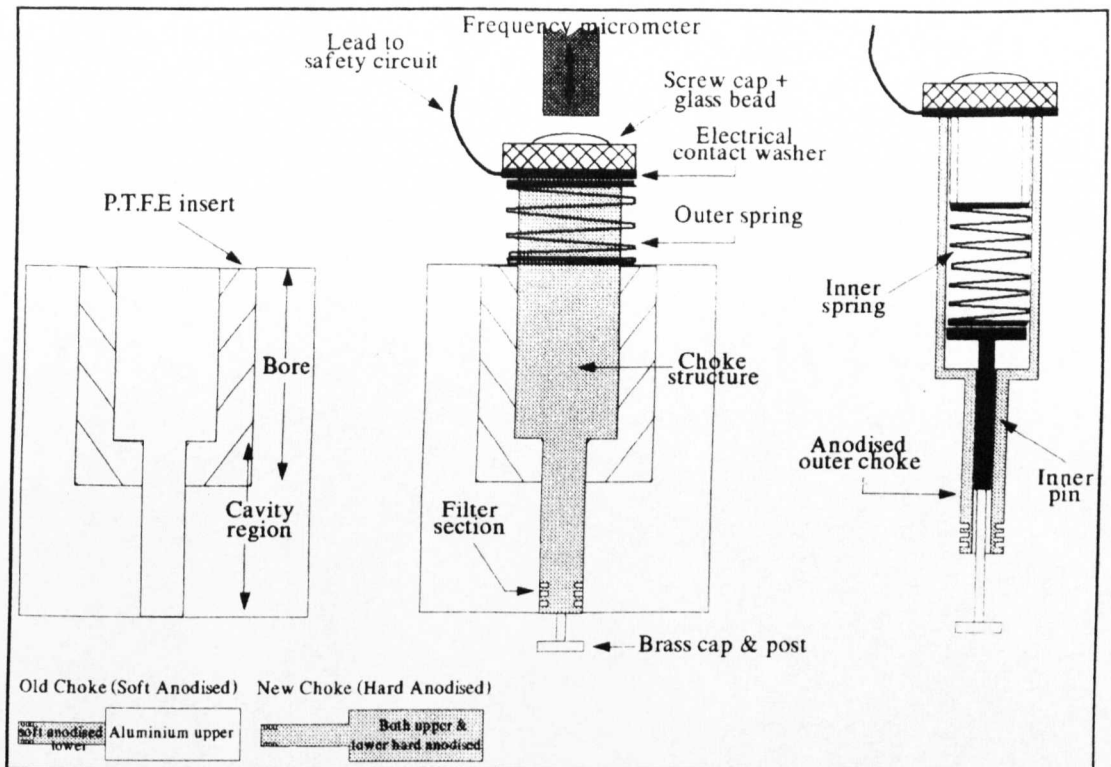


Figure (3.6)

The bare structure of the second section consists of an cylindrical aluminium cavity region which is approximately the same size in diameter of the output waveguide structure ($\approx 3\text{mm}$). Above the cavity region a larger cylindrical bore exists into which fits a P.T.F.E insert, whose function as well as to provide a smooth travel for the choke structure will be disclosed shortly. Together the cavity region and P.T.F.E insert provide a perfect housing for the choke structure which will now be described.

(3.3.3.1) The Choke Structure

As mentioned above, the choke is designed to fit flush with the bare structure of the second section such that a centimetre or so of the upper part of the choke protrudes out of the top of the section. The choke structure is hollow in its design and insulated on its outer side. It has two main functions which will now be described. Firstly, its outer part serves to alter the size of the cavity region by moving up and down its length which is achieved by the following. An

aluminium screw cap with a glass bead affixed on top is screwed into the top of the upper part of the choke structure. Between the screw cap and the top of the section is placed an outer spring. The frequency micrometer from the fourth section presses down on top of the glass bead. The micrometer and outer spring together serve to position the choke in the vertical, hence altering the cavity length.

The second function of the choke lies in its hollow design. Its inner parts provide an insulated electrical pathway to the cap and post and finally to the diode. A small electrical contact washer lies between the upper part of the choke and the aluminium screw cap, as described earlier. The contact washer has a small insulated lead that connects to the safety circuit which will be described in section(3.3.5). The bottom of the screw cap is also in contact with an inner spring which in turn is in contact with an aluminium pin. It is this aluminium pin that presses on top of the post structure of the brass cap and post which is located on top of the diode. One can now get a picture of what happens as the choke is moved down the cavity by the frequency micrometer. When this happens, more of the post, of the cap and post structure, moves into the inner region of the choke. These inner workings ensure the cap and post structure always remain in physical and therefore good electrical contact with the diode, whatever the position of the choke in the cavity.

As well as remaining in good electrical contact, the electrical circuit also has to be insulated from the rest of the aluminium block. This is the reason for the P.T.F.E insert, an insulated anodised outer choke and the glass bead. Together these three things completely insulate the inner parts of the choke from the rest of the aluminium block and hence prevent any earthing problems.

Until recently the lower part of the aluminium choke would be insulated by the process of 'soft anodising'. It is for this reason that the P.T.F.E. insert is present as it serves to insulate the upper part of the unanodised choke from the block. However, the 'soft anodising'

could easily be scratched off when assembling the block, hence resulting in earthing problems. Block (D4) for the first time had its choke hardanodised. The hard anodising was performed by 'Letchworth Polishing and Plating Ltd.'. For best results, the choke should be made from Aluminium Type (HE30 TE) and a radial allowance for the outer change in dimension should be 18-22 μ m. The hard anodising was found to be extremely robust and also seemed to help increase power output. This could be due to the fact that the hard anodising also permeates into the aluminium increasing the insulation more so than the soft anodising.

Finally, at the lower part of the choke structure is a filter section. This consists of several small cylindrical grooves which are roughly of a width size $\lambda/8 - 3\lambda/8$ mm. These act to combat any low frequency oscillations (10-100MHz) of the diode with the bias supply and also provide a stopband at both the fundamental and harmonic frequencies (30-300GHz).

(3.3.4) The Cap and Post Structure

This is one of the most important components of the oscillator. The dimensions of the structure are critical to ensure good performance of the oscillator. The cap and post has a dual role. It acts as an impedance transformer for the diode (\approx a few negative ohms, due to the negative resistance) to that of the waveguide (\approx a few hundred ohms). The other role is to act as a resonator for the diode.

The cap and post is machined on a lathe from a single piece of brass. See figure(3.7). The post is constructed in three sections.

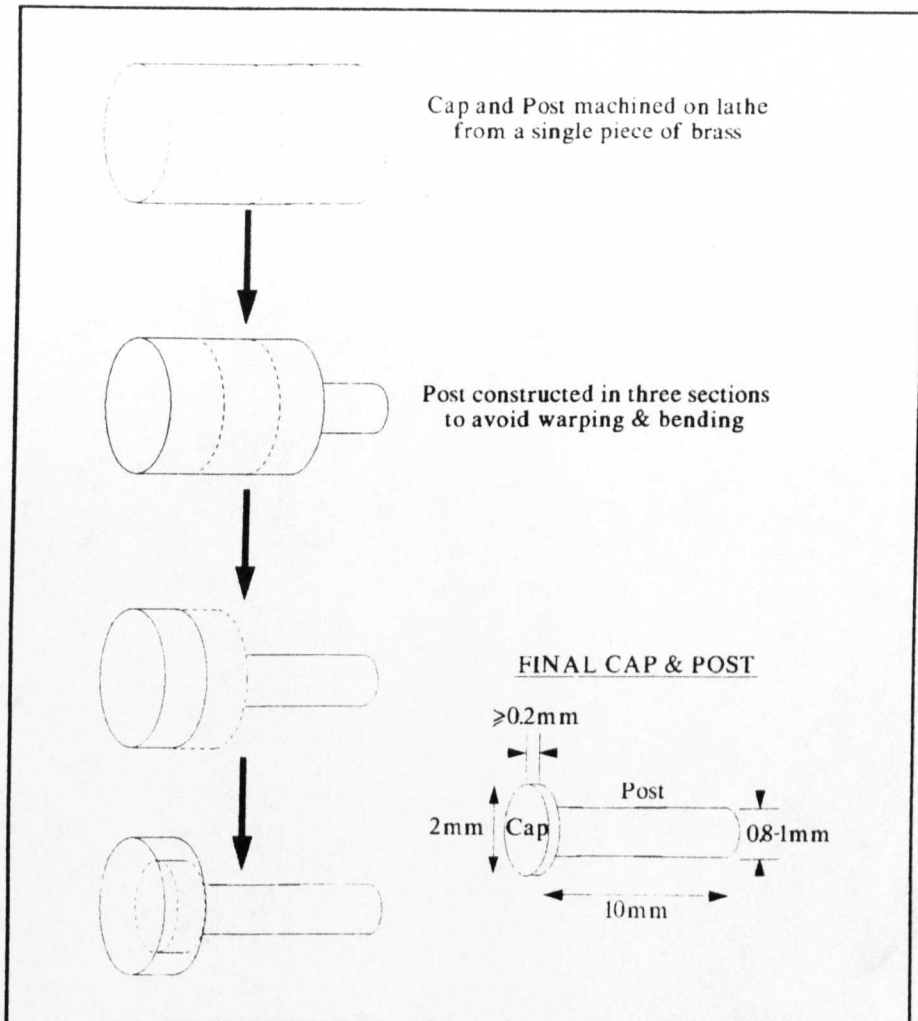


Figure (3.7)

This is due to the likelihood of warping or bending if constructed in one piece. I usually machine the post to give the closest fit to the inner cavity of the choke structure which varies from block to block. The size of the cap can be altered to give a better power output. However, caution should be taken in making the cap too thin, as this will result in a more fragile component. The dimensions of the cap and post are critical. Increasing any of the post's dimensions increases the inductance of the the oscillator circuit¹¹ and tends to decrease the fundamental frequency and hence lower the operation frequency of the 2nd harmonic. Increasing any of the cap's dimensions causes the susceptance of the cap to decrease. This

¹¹ Smith G.M.,(Thesis), Transferred Electron Oscillators at millimeter wave frequencies and their characterisation using quasi-optical techniques, pgs.119-122.

again lowers the fundamental frequency and hence the frequency of the 2nd harmonic. However, from Haydl's¹⁰ experiments on the effect of cap diameter, it was shown in addition, that the power output is increased with increasing diameter. Therefore, as a general rule of thumb it is advisable to use the cap dimensions to optimise power output from the device and to use the post dimensions to achieve the desired frequency of operation.

(3.3.5) The Third Section

The third section of the oscillator block houses the safety circuit, as depicted in figure(3.8).

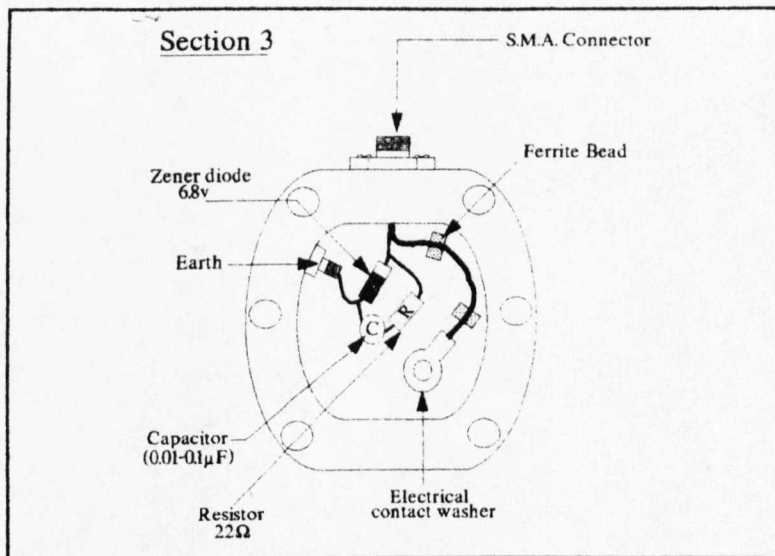


Figure (3.8)

The safety circuit prevents damage to the diode from various electrical hazards. A 6.8 volt Zener diode protects the Gunn diode from any accidental overbiasing or spurious voltage spike. The 22Ω resistor and 0.01-0.1μF capacitor prevent any bias oscillations occurring between the bias supply and the diode. Finally, the ferrite beads help to suppress any RF from the bias supply and hence, reduce noise. The current is drawn from via the S.M.A connector which is located on the outside of the block's section, through the safety circuit and is supplied to the insulated inner circuit of the

choke by means of the electrical contact washer.

(3.4) 2nd Harmonic Generation & Millimeter-wave Production

When in operation, the Gunn diode oscillates at what is known as its fundamental frequency (f_{FUND}). For GaAs, this fundamental frequency occurs at 40-45GHz. This is clearly too low in frequency for W-band operation which requires frequencies of 75-110GHz. A novel solution was found to obtain higher frequency operation by exploiting the higher frequency harmonic modes that also exist. These harmonic modes are due to nonlinearities in the diode, as documented by Eddison and Brookbanks¹². These nonlinearities in the diode makeup, cause power to be coupled into higher frequency harmonics of the fundamental frequency. The first harmonic mode, known as the 2nd harmonic, exists at twice the fundamental frequency ($2f_{\text{FUND}}$). Similarly the 3rd Harmonic exists at ($3f_{\text{FUND}}$) and so on. The lowest order harmonic contains the most power of all the harmonics and the power can be said to taper to zero at the final harmonic.

Due to the non-linearity of the diode, an entirely natural intrinsic frequency multiplier feature is open for exploitation in the form of these higher frequency harmonic modes. The 2nd harmonic is of particular importance, since it offers the highest power of all the modes and also exists at $2f_{\text{FUND}} \approx 80\text{-}90\text{GHz}$, for a fundamental of 40-45GHz¹³. Therefore, if one can form an arrangement to extract these higher order modes, one can achieve the desired higher frequencies of operation. This is the essence of 2nd Harmonic mode operation which will now be described. By arranging the cutoff frequency of the output waveguide of the oscillator block to be above that of the fundamental frequency of the diode, one can stop any propagation of the fundamental out of the block. Instead of

¹² Eddison I.G., Brookbanks D.M., Operating Modes of Millimeter-Wave Transferred Electron Oscillators, Electronics Letters, Vol.17, No.3, 5th Feb. 1981.

¹³ The position of the fundamental and hence that of the 2nd Harmonic can also be varied by the length of the active region.

propagating out into freespace the fundamental mode is contained within the cavity structure of the oscillator block between the disc and post, as described by Carlstrom¹⁴ and depicted in schematically figure(3.9). Erratic behaviour of the oscillator would result if the cutoff was below the fundamental. The coaxial cavity and the diode act as a resonator now for the fundamental frequency. Hence, by adjusting the length of the coaxial cavity one can alter the frequency of fundamental.

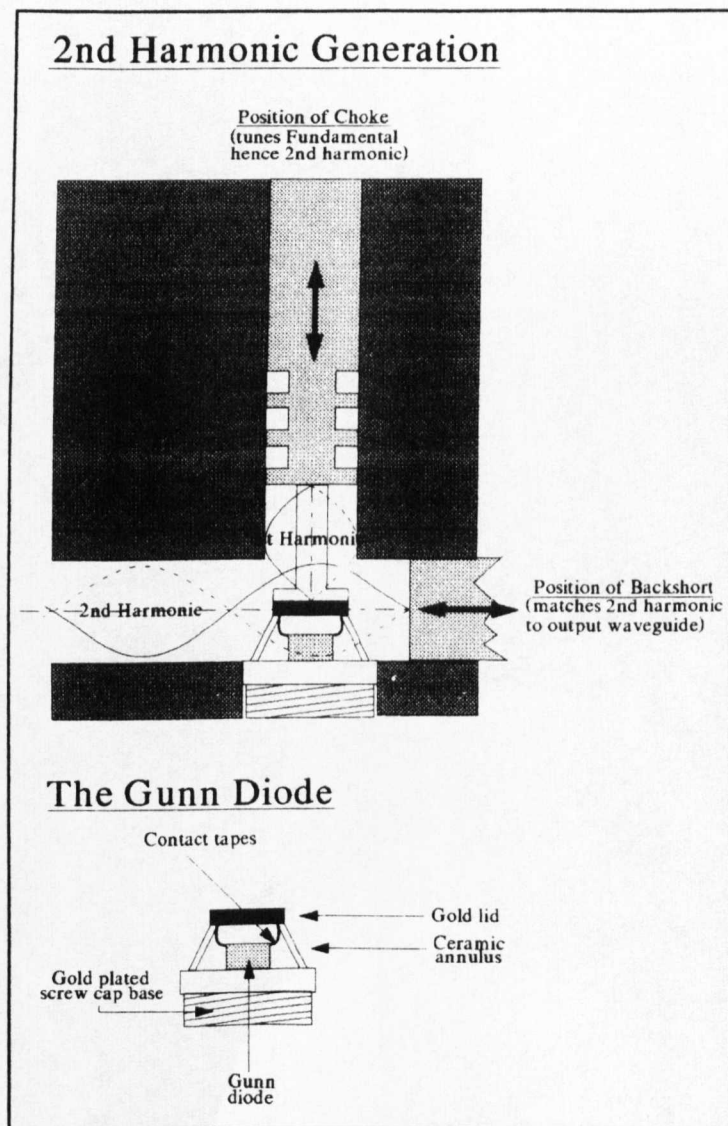


Figure (3.9)

¹⁴ Carlstrom J.E., Plambeck R.L., Thornton D.D., A Continuously Tunable 65-115GHz Gunn Oscillator, IEEE Transactions in Microwave Theory & Techniques, Vol.MTT-33, No.7, 1985.

The brass cap, of the cap and post structure, acts as a radial line transformer to match the low impedance of the diode to that of the waveguide. The backshort is used to match the 2nd harmonic to the output waveguide. Therefore, by tuning the frequency of the fundamental by adjustment of the length of the cavity, one also tunes the frequency of the 2nd Harmonic. This is because the 2nd harmonic frequency is dependent on the frequency of the fundamental, namely $f_{2nd\ Harm} = 2f_{FUND}$. Furthermore, by altering the position of the backshort one can match the frequency of the 2nd harmonic to the waveguide. Conversely, mismatching the 2nd harmonic to the waveguide results in a drop in power output. Hence, the backshort serves to vary the power output from the output waveguide. Figure(3.10) shows the modes of operation of Gunn oscillator block(F) which I constructed. The results were obtained from Fast Fourier Transforming the modulated output created by a Martin Puplett Interferometer from a Gunn oscillator block, where the ordinate scale is the log of the modulated output.

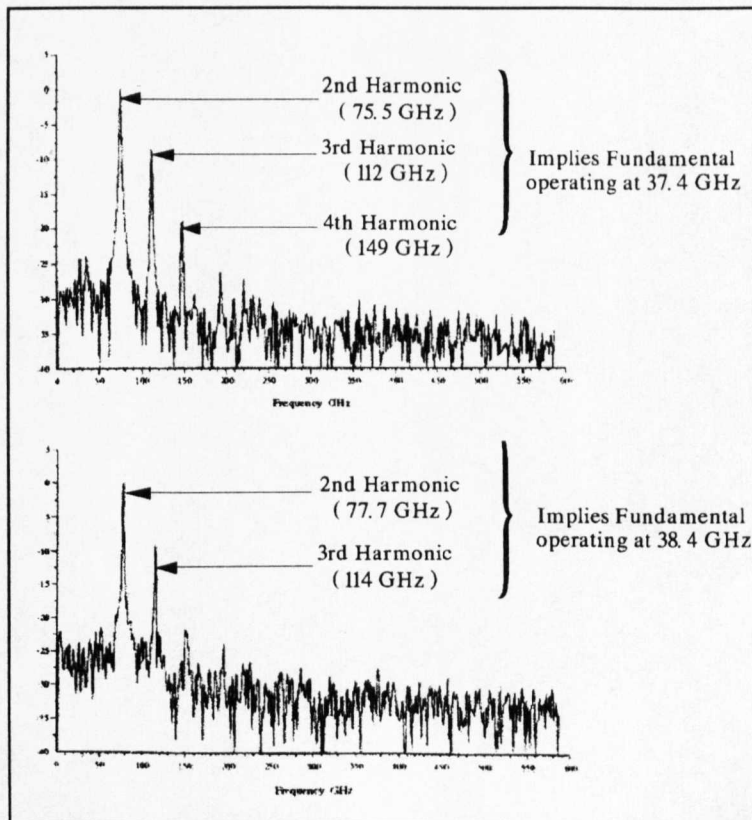


Figure (3.10)

The fundamental frequency is not in the FFT since it is contained within the cavity. This is due to the waveguide cutoff frequency being above that of the frequency of the fundamental. As can be seen, up to 90% of the output power is contained within the second harmonic. And up to the fourth harmonic mode is present in the FFT of the upper plot.

(3.5) Characterisation of the Gunn Oscillator

After the oscillator has been constructed it is necessary to determine how well it performs. This is termed as 'Characterising' the oscillator block. This involves determining what position of the frequency micrometer corresponds to what frequency is observed. Similarly for each separate frequency, one needs to know what position of the backshort micrometer provides the maximum power output and what value this maximum power output is. The characterisation of block(Y) is shown below in figure (3.11). In characterising a block one becomes familiarised with frequency jumps that occur. These are usually associated to slight machining imperfections in the cap and post structure. Probably machining the post in three sections introduces slight discontinuities in its dimensions and hence these jumps. Another effect which is also associated to machining imperfections is a type of 'hysteresis' which is present in the frequency tuning and is dependent on the direction of tuning. This results in different frequencies being obtained at the same frequency micrometer position. This non-reciprocal tuning problem can be avoided, by simply tuning the oscillator always in one specific direction.

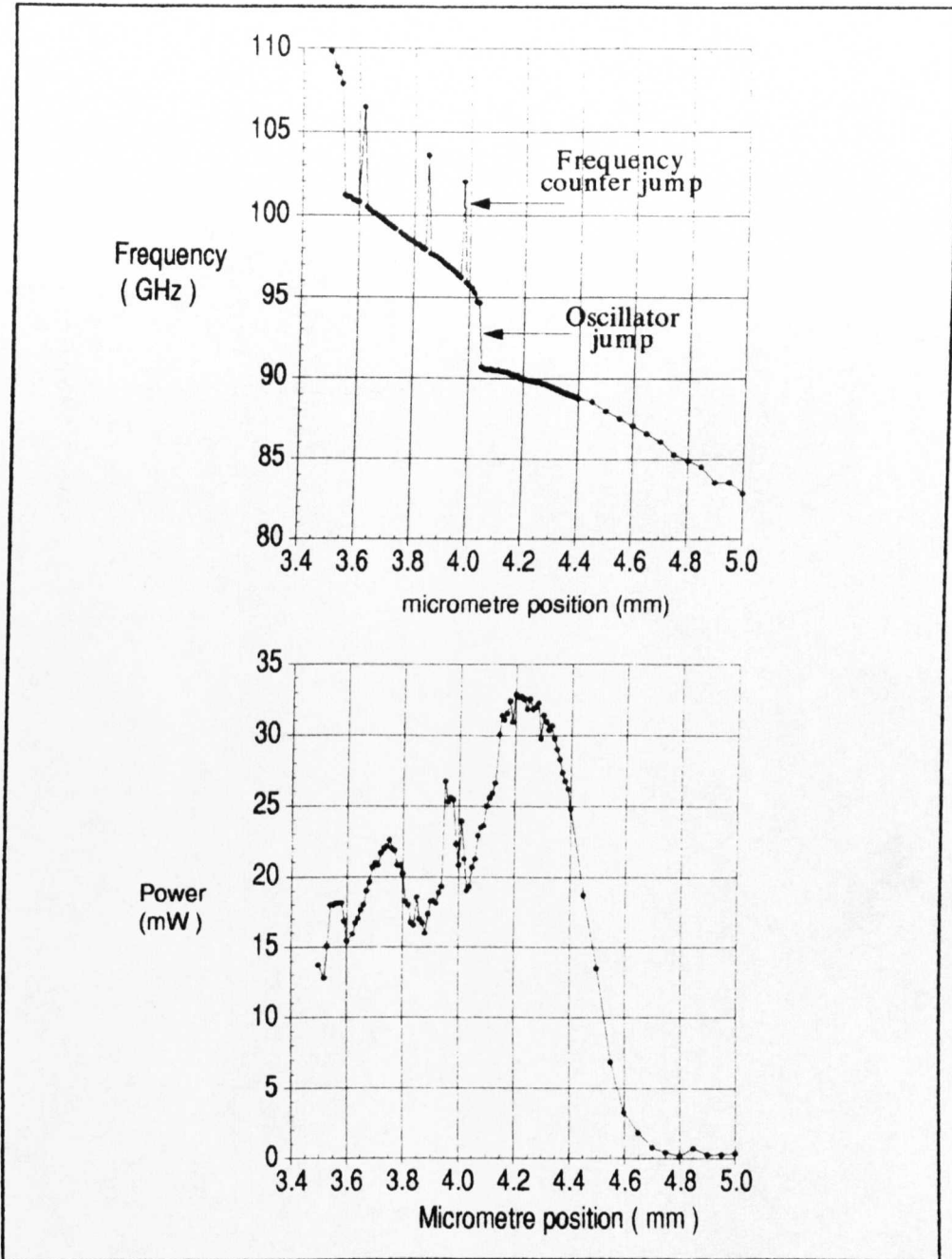


Figure (3.11)

This characterisation is performed manually and is a long and tedious process. This was one of the main reasons for the development of the 'Automatic Oscillator Tuning System' which is described in section(3.6.1). The frequency of the oscillator block can also be tuned over a few hundred megahertz by altering the bias of the supply. This is known as 'bias tuning' and is shown for oscillator block(Y) in figure(3.12).

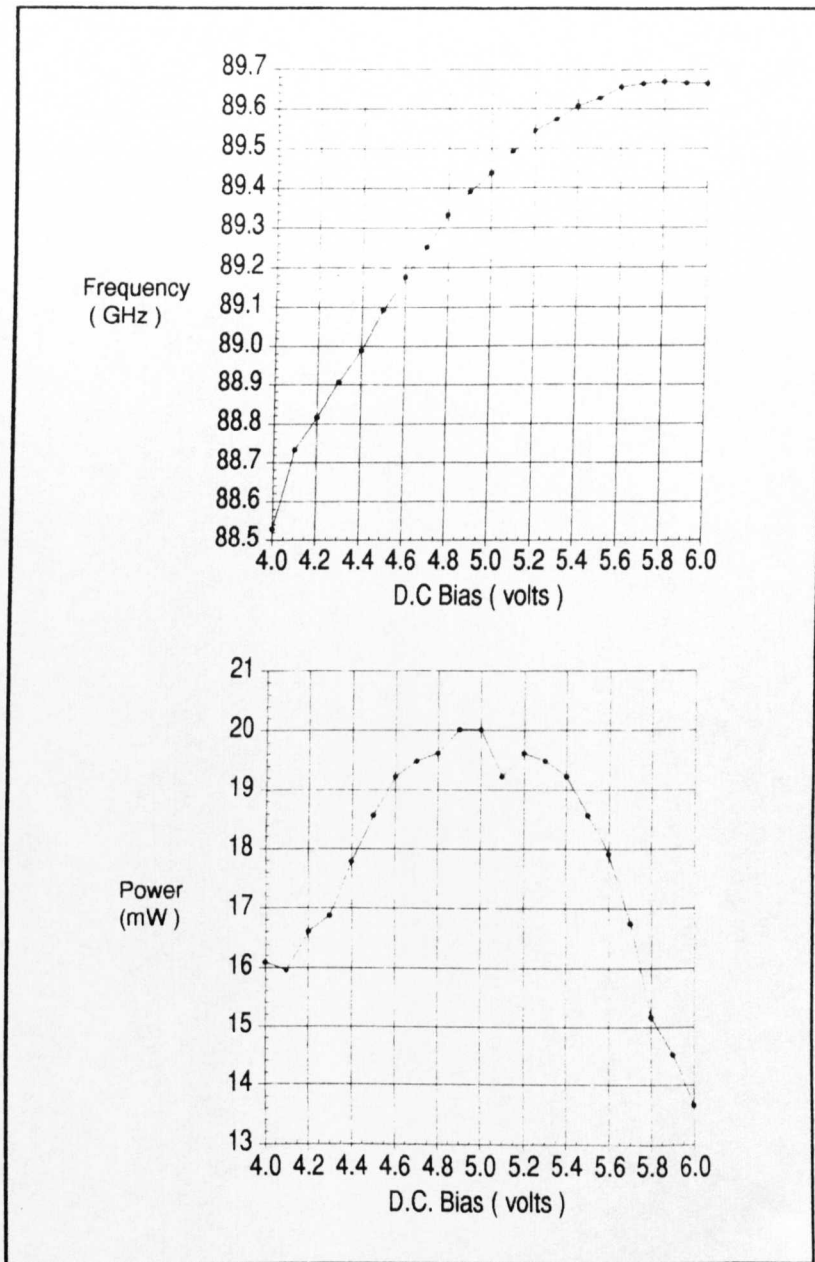


Figure (3.12)

(3.6) The Automatic Oscillator Tuning System (A.O.T.S.)

During the initial year of my study, I decided to construct a system that would help in the characterisation of an oscillator. As mentioned earlier in section(3.5), the manual characterisation of an oscillator is a particularly laborious, time consuming task. As will be described shortly, some means of automatically characterising an oscillator would prove very beneficial. This was the reason for the development of the 'Automatic oscillator tuning system' (AOTS).

With this system a program could be developed to not just characterise an oscillator but also to generally tune an oscillator in any manner the user required by the simple modification of the computer software. For example, such a system would allow one to be able to quickly sweep a range of frequencies over W-band. This was a prime feature necessary for the experiments performed using the 'Rotary Polariser Quasi-Optical System'. Without such a system, experiments like these would probably not be attempted due to the sheer amount of time necessary to perform them.

(3.6.1) AOTS system description

The 'Automatic oscillator tuning system' would be used to control the mechanical movement of the 'backshort' and 'frequency' tuners of a conventional Gunn oscillator. This was to be performed via an electronics unit which was interfaced to some mechanical fixtures affixed to the conventional Gunn oscillator block. Also the electronics unit was interfaced to a computer. Such a system with an appropriate computer routine could be used for 'characterising' Gunn oscillators, quickly accessing desired frequencies and the appropriate power level maximums. Previously, an automated version of bias tuning had been investigated by Robertson¹⁵ which proved successful. However, the bandwidth was limited to a couple of gigahertz of tuning. By mechanically tuning the frequency micrometer one could tune the oscillator throughout W-band.

Two machined mounting brackets were used, one for each tuner, to support a small motor, that would drive the tuner, either up or down via a wheeled cog mechanism. A small, linear, high precision, 10 turn potentiometer was also located on each mounting bracket, which was connected to the tuner via a small locking collar and could be used to determine the position of the micrometer by a reference voltage as its tuner moved. A seven way pin connector

¹⁵ Robertson D.A.,(Thesis) Millimeter-Wave, Quasi-Optical Signal Processing & Spread Spectrum Techniques, Chapt.4.

was also housed in the frequency tuner's mounting bracket, into which all the control wires of the motors and potentiometers were affixed. The fixtures had previously been designed by Harvey¹⁶ for a similar envisaged system which was never completed.

The computer was interfaced to the oscillator, via an electronics unit, which was designed and constructed in the laboratory and whose features will now be discussed.

The electronics unit consists of :

One 20 way pin connector,

To input 'digital signals from the computer in order to move the frequency and backshort tuners up and down. This made use of the 'Wildvision Card' of the Archimedes.

2 BNC connectors,

To output 'analogue' signals from the oscillator's frequency and backshort potentiometers, in the form of a reference voltage, in order to locate the micrometer position of the tuner. Each of the BNC connectors fed into a breakout box which in turn connected to the 'ADC channels' of the Archimedes 'Wildvision card' .

+15/-15 & Earth connectors,

To power the electronics unit.

The front panel of the unit, has manual override facilities, which follow.

One 7 way connector,

To interface unit to oscillator.

¹⁶ Harvey A.R., (Thesis) A Millimeter Wave, Quasi-Optical Complex Impedance Bridge, Chapt.4, pgs.98-100.

4 screw turn potentiometers,

To alter the 'up' and 'down' motor speeds of the backshort and frequency tuners.

2 Flat lever toggle switches(on-off-on),

To control the movement of the frequency and backshort tuners manually.

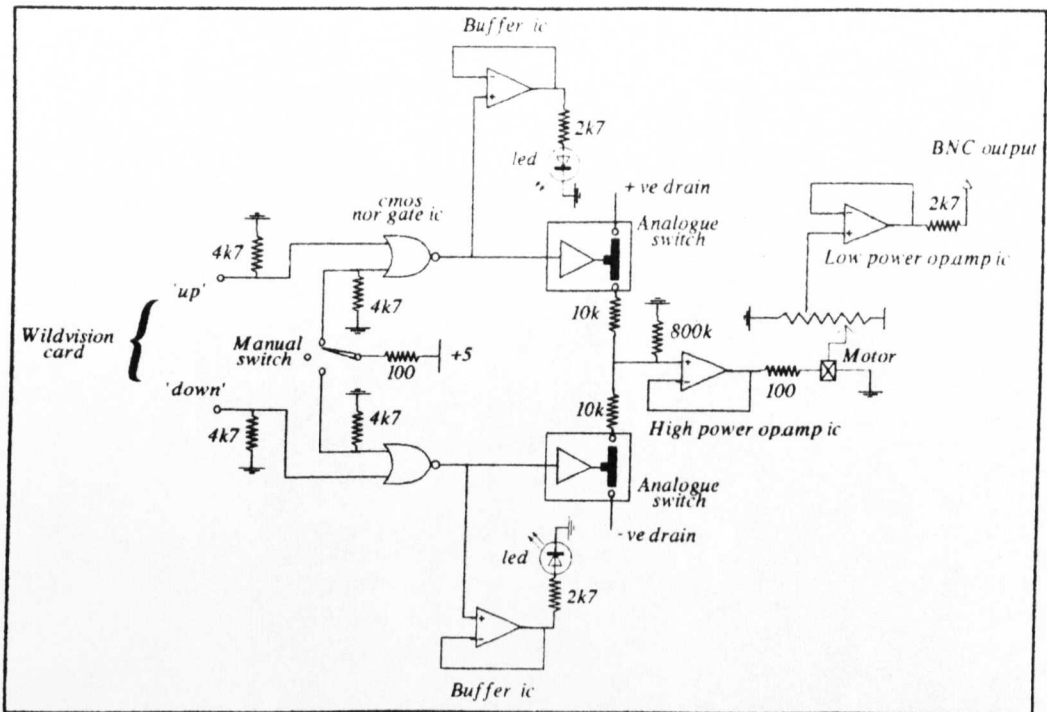
4 L.E.D's,

Two for each tuner. In order to display the direction of travel of the tuner.

(3.6.2) Circuitry necessary for AOTS operation

Initially, two circuits were developed, but it was decided to favour one, due to the facilities available in the lab. The chosen circuit was originally constructed on a 'protoboard'. After satisfactory testing, the chosen circuit was then transferred onto circuit board. Figure(3.13) depicts the diagrammatic version of circuit necessary to control the 'up' and 'down' movement of one of the tuners. Therefore, two of the circuits shown in figure(3.13) were necessary for complete control of the oscillator's frequency and backshort tuners.

As one can see from the circuit, the motors could be driven by sending (+5v) signals from the computer, via 2 of the 8-way digital input/outputs of the wildvision card. Similarly, the (+5v) signal could be sent by a manual switch. The 'NOR' gates would then respond appropriately by sending a (+5v) signal to the Analogue Switch and LED. The LED lights upon receipt of a signal and the Analogue Switch closes. Depending whether the initial signal from the wildvision card is to move the tuner 'up' or 'down' a (+ve) or (-ve) bias is applied respectively to the High Power Op-Amp. The High Power Op-Amp in turn drives the motor clockwise or anticlockwise. As the tuner is rotated by the motor, the 10-turn pot is also rotated in synchronisation. This provides a reference voltage at the BNC output which can be used to locate the position of the



Figure(3.13)

micrometer anywhere in its travel. The BNC is fed directly to a breakout box which is connected to the ADC card of the computer. In this way, the circuit provides a way of automatically tuning the micrometers of the oscillator whilst monitoring their positions.

When the circuit board was working, work began on constructing a more robust version of the circuit, on a 'Printed Circuit Board' (PCB). This involved learning a computer PCB designing package, known as "Easy P.C.", in order to create the circuit. Once the circuit had been designed it was projected onto 'acetate film'. In manufacturing the PCB, certain photolithographic processes had to be employed. This involved exposing, developing and etching the image correctly and tinning the final circuitry. This was all performed in the electronics workshop. The layout of the final PCB design is shown below in figure(3.14).

(3.6.3) Housing the Circuitry

After the PCB design was complete, the circuitry had to be housed. An appropriate box was purchased. The front and back panels of the box were cut and drilled for the appropriate switches and fixtures in the physics workshop and labels were affixed finally to the unit. Figure(3.15), shows the construction of the oscillator block + fixtures and figure(3.16) shows the electronics unit respectively.

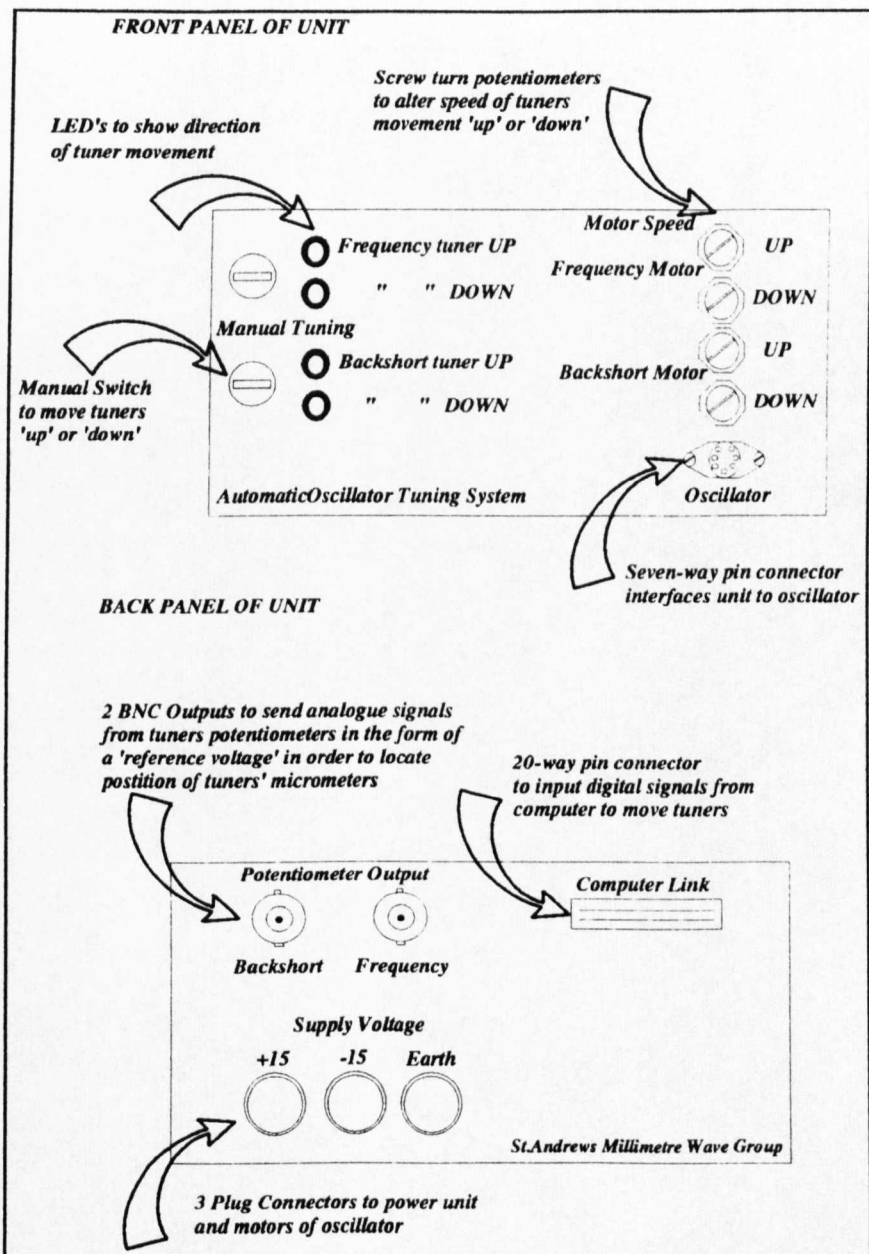


Figure (3.16)

(3.6.4) Program development

The next few sections, will explain the computer¹⁷ package that was developed to allow automated characterisation of a Gunn oscillator. As will be shown procedures were developed for use with the 'Wildvision card' of the Acorn computer. These procedures were used to operate the AOTS. Procedures were also developed for the GPIB which allowed one to read the EIP frequency counter and Boonton Power Meter. When the GPIB and wildvision card procedures were used in conjunction with each other, one could write a program to fully characterise a Gunn oscillator. This was achieved in the program 'CharOsc'.

(3.6.4.1) Overview of the Characterisation Program - CharOsc

All the procedures used in the program will be described in the following sections but the general operation of the program is as follows. Firstly, initialisation takes place. This is where parameters are set to their initial values and any computer controlled instrumentation is made ready for remote operation. Furthermore, the frequency tuner is moved to its start position and the backshort is adjusted to obtain a maximum power output. After initialisation, the characterisation of the oscillator begins. The frequency is determined by the EIP counter. The frequency value is passed to the Boonton power meter which calibrates its power output accordingly for the specific frequency. The power is returned in milliwatts and the frequency in gigahertz to the computer together with the voltage locations of both the frequency and backshort micrometer tuners. These values are stored in separate columns of the first row of an array. A repetitive process then begins by stepping the frequency tuner through small increments. After every increment, the backshort is scanned and positioned at the place of maximum power output. The frequency, power and voltage locations of both tuners is then

¹⁷ The computer package was developed for use with the 'Acorn Archimedes' computer. The language used was 'BBC Basic V'.

determined and placed in their specific columns of the next row of the array. This process continues until the voltage of the frequency tuner's potentiometer is less than or equal to some limiting value which is specified in the initialisation parameters. The separate columns of the array which correspond to the monitored variables are then saved as datafiles in the RAMdisc of the computer, ready for retrieval and display by the user.

What now follows is a description of the commands that were necessary to operate the GPIB and the 'Wildvision Card'. Using these commands, procedures could be built up to operate the various instruments in a variety of ways. A description of these main procedures is also included in the following sections.

(3.6.4.2) General Purpose Interface Bus Commands

The 'General Purpose Interface Bus' (GPIB) of the computer was connected to EIP frequency counter and to the Boonton Power Meter. This could be used to talk and listen to these instruments using various GPIB keywords. By using the GPIB to interface to the EIP and the Boonton, the frequency and output powers of the oscillator for various micrometer positions could be determined.

There were only three main GPIB commands which I needed to operate the EIP and Boonton. These were PROCadrandoutput, PROCadrandinput and FNserial_poll commands which allowed one to 'Talk', 'Listen' and enquire about the 'Status' of a specific device respectively. These commands will now be explained.

The two procedures are very similar. They both consist of three parameters that are specified by the user. In the case of the PROCadrandoutput command, the first parameter describes the type of terminator character that will signify the end of a command to the device and will be appended to the end of the command. The terminator character used was a carriage return <CR>, specified as a zero and was the same for both devices. The second parameter was the device address. For the EIP the device address was 19 and for

the Boonton the address was 3. The final parameter was the actual command to be sent to the device. This is device specific and list of GPIB commands can be found in the manual for each device¹⁸. In the case of the PROCadrandinput command, again the first parameter denotes the terminator which is to be expected from the device which is the same as that for the PROCadrandoutput command. The second parameter again denotes the device address. Finally, the third parameter specifies the maximum number of bytes of information to input from the device. This value can be anything up to 255 bytes which was chosen.

The command FNserial_poll is a function employed to access the status of a device in the form of a serial poll. All one has to specify is the device address with the function and the command is executed. A number is returned from the device which specifies its current status. This is a very useful command which can be used to see whether the device is ready to receive/send information, is searching for a measurement, is overloaded or is requesting attention. Again this is device specific and the codes returned have to be interpreted differently for each device.

Using these three commands, procedures could be built up to perform various operations from the instruments and will now be described.

PROCgo_eip_go

This procedure is employed to extract the correct frequency from the EIP frequency counter . It also calls three other eip related procedures PROCrun_poll_eip, PROCTake_value and PROCchange_band.

The PROCrun_poll_eip requests the EIP for its status. The EIP then responds with a number which will correspond to one of the

¹⁸ Boonton Electronics Corporation Instruction Manual for Model 4220 RF Power Meter, pgs. 4-13 to 4-23.
EIP Microwave Inc. 575 & 578 Source Locking Microwave Counters Manual, Sect.10, pgs.06-1 to 06-7.

various states it can be in. There are two states which are important. When the value returned is the number one, the EIP is responding with a 'Measurement Available' status. If this is the status, PROCtake_value is called which reads the frequency of the EIP. This is stored in the variable 'frequency' and the procedure is exited. Furthermore, a flag, known as lockflag\$, is set to 'L' which corresponds to a 'Locked' frequency. When the value returned is the number two then the EIP has a status which implies it is 'SEARCHING' for a frequency. The procedure then constantly polls the EIP for a further 10 secs to see if a measurement will become available, afterwhich lockflag\$, is set to 'U' which corresponds to 'Unlocked' and the procedure exited. The significance of lockflag\$ will be explained shortly.

PROCchange_band

When called from the main procedure the band of the EIP is changed. The bands of the EIP correspond to frequency ranges detectable. Over W-band, Band 43 is used for frequencies below 90GHz and Band 44 is used for frequencies above 90GHz. In the initialisation of the EIP the band is set to Band 44 and is contained in the variable BAND\$ which is set to 'B44'. When called from PROCgo_eip_go the procedure will check BAND\$. If it is equal to 'B44' then the band will be changed to Band 43 and BAND\$ will become 'B43'. Conversely, if the EIP is in Band 43 it will be changed to Band 44 together with BAND\$.

The whole of the main procedure PROCgo_eip_go now runs as follows and its operation is dependent on the value of lockflag\$, mentioned earlier. Firstly, the procedure evokes PROCrun_poll_eip. If a frequency is located then lockflag\$ is set to 'L', the frequency is taken and the main Procedure is exited. If after 10secs a frequency cannot be located by the serial poll then lockflag\$ is set to 'U'. This could mean that the frequency has shifted into the adjacent band and cannot be detected by the EIP. For this reason, the main

procedure calls PROCchange_band. Another serial poll is evoked in the new band. Again, if the frequency is found the main procedure is exited. If the frequency is still not found, this implies that the power flowing to the EIP is possibly too low to detect and that the original band could well have been the band at which the frequency occurred if the power was great enough. Therefore, the main procedure re-calls PROCchange_band and flips back into its original starting band. The serial poll is re-called and retried again. In the event of the frequency not being found the frequency is stored as a zero and the procedure is exited.

PROCread_boonton

This procedure is used to obtain a frequency calibrated power reading from the Boonton Power Meter. The Boonton is initially setup to operate with its W-band sensor. This is calibrated from 75-100GHz. The power measurements are frequency dependent and have to be calibrated manually or remotely via GPIB accordingly. This is accomplished by the following. Firstly, the frequency obtained from PROCgo_eip_go, in the variable 'frequency', is changed to a string value and appended to the letters "FR". This is stored in the string freq_string\$. An example of the string could be freq_string\$="FR94.32". The command PROCadrandoutput (0,3,freq_string\$) is sent to the Boonton which calibrates its power measurement to the frequency. A limit has to be imposed on the frequencies values sent to the Boonton since any frequencies outside 75-100GHz will result in an error response from the meter. This was overcome by imposing limits on the frequencies sent. Any frequency over 100GHz was set to be calibrated at 100GHz, with freq_string\$="FR100". And any frequency below 75GHz was set to be calibrated at 75GHz, with freq_string\$="FR75". After the power level was calibrated correctly to the frequency, a reading could easily be taken from the Boonton with a PROCadrandinput command. The reading returned from the Boonton was in milliwatts.

(3.6.4.3) Wildvision Commands

The electronics unit was interfaced to the computer via a 'Wildvision card'. This consists of an 8-way digital input/output and 8 ADC channels. As mentioned in section(3.6.2), two outputs were required for each tuner, in order to move it either up or down. Therefore, a total of four digital outputs were necessary for the control of both of the oscillator's tuners.

Of the eight ADC channels available on the wildvision card, one channel was required to read the analogue voltage of each of the 10-turn potentiometers that would be used to locate the position of the micrometers. Therefore, a total of two ADC channels were necessary.

Certain 'Wildvision' commands had to be used in conjunction with Basic, in order to access the 8-way digital input/output and to select the specific ADC channel. These commands will now be explained.

In order to use the 8-way digital input/output of the wildvision card, one first had to establish which of the 8 pins are to be used for input and which for output. This is achieved by the first telling the computer that one requires to send information. To send information one uses the SYS ViaWrite command. Similarly, to receive information one uses the SYS ViaRead% command. The next command specifies where one is going to send the information to. In this case, one wants to send the information to the Data Direction Register which is responsible for the assignment of the pins to either that of a digital input or digital output. The Dat_Dir_Reg% command is used to specify this. Finally, the last command specifies the information we are going to send. this is in the form of a eight bits which can be either (0) or (1). The first bit corresponds to the first pin, the second bit to the second pin and so on. If a (0) was allocated to the first bit, namely the first pin, it would assign that pin as a digital output. If (1) was allocated the pin would be assigned as a digital input. Since, we want to assign four pins as digital inputs, four of the eight bits should be set to (1). The following command

assigns pins 3-6 inclusive as digital outputs and pins (1,2,7 and 8) as digital inputs.

SYS ViaWrite%,IORegisterB%,%00111100

After the pins have been assigned to be dedicated digital inputs or outputs, one can then proceed to send or receive signals appropriately.

To send the (+5v) signals from the digital outputs, one has to specify firstly that one requires to send information via the SYS ViaWrite command. This time the information is to be sent to the input/output register of the wildvision card. This is specified by the IORegisterB% command. And finally one specifies which pin a (+5v) signal is to be applied to. To move the frequency tuner up, one would apply the (+5v) signal to pin 6. To move the frequency tuner down, pin 5 would be selected. The commands necessary to move both tuners or to stop the movement to the tuners is shown below.

SYS ViaWrite%, IORegisterB%, %00000100	<FREQUENCY Tuner 'UP'>
SYS ViaWrite%, IORegisterB%, %000001000	<FREQUENCY Tuner'DOWN'>
SYS ViaWrite%, IORegisterB%, %00010000	<BACKSHORT Tuner 'UP'>
SYS ViaWrite%, IORegisterB%, %00100000	<BACKSHORT Tuner'DOWN'>
SYS ViaWrite%, IORegisterB%, %00000000	< ALL Tuners 'STOP'>

The procedures known as PROCmoveft_up, PROCmoveft_down, PROCmovebs_up, PROCmovebs_down and PROCstop respectively contain these commands. Hence, calling the desired procedure will execute the movement of the desired tuner.

To read the ADC channels of the wildvision card a similar set of commands are required which will now be described. Firstly, one has to specify which of the ADC channels are going to receive the analogue signals. The SYS Channel% command is used here. ADC

channel one was used to receive voltages from the backshort pot and ADC channel two was used for the frequency pot, as shown below.

```
SYS Channel%,1 < Channel 1 to be read - backshort pot>
```

```
SYS Channel%,2 < Channel 2 to be read - frequency pot>
```

Finally, the `SYS ADC%,samples,channel,buffer%` command will take a number of four bit samples (at 167kHz) from a specified channel and store them concurrently in `buffer%`. The full range of the ADC is (-5 to +5 volts = 10volts). It is also 12 bit, therefore there exist ($2^{12} = 4096$) number of discrete steps. within the 10v range. Thus the quantisation error, in the specified range is ($=10/4096 = 2.5\text{mV}$). By averaging over 20 samples the quantisation error can be reduced in this manner. The functions `FNreadbs_pot` and `FNreadft_pot` employed the above mentioned commands. Hence, in calling the functions the backshort and frequency pots could be read respectively.

Besides the procedures already mentioned, others were created to move and read the tuners in particular ways. These are briefly described below.

PROCposition_ft

When characterising an oscillator manually, there are obviously critical limits which one should not tune the micrometer beyond. In the case of the frequency tuner, one does not want to wind the micrometer too far down else there is a risk of crushing the oscillator's diode. Similarly, one doesn't want to move the micrometer to far up else one would needlessly tune the oscillator below the cutoff of the waveguide. Similar limits exist for the backshort tuner. In the case of the AOTS, the above mentioned limits could be specified as voltages. These voltages are specific to

each oscillators' performance. In this procedure, the critical frequency tuner limits are stored in the variables `crit_ft_up=3.00` and `crit_ft_down=4.38`, for oscillator block (D4). Similarly, the critical limits for the backshort are given by `crit_bs_up=4.46` and `crit_bs_down=4.29` variables. Upon calling this procedure the frequency tuner will initially move to the `crit_ft_down` position which corresponds to the highest frequency the oscillator can obtain without damage to the diode occurring. The frequency tuner will then stop and move up to a start position which is slightly lower in frequency. The start position is held in the variable `ft_start_pos=4.28`. The reason for winding the frequency micrometer all the way down and then up slightly, is to avoid the frequency hysteresis that occurs with the oscillator, mentioned in section(3.5).

PROCscan_bs

This procedure scans the backshort through the entire voltage range specified by the variables `crit_bs_up` and `crit_bs_down`. Whilst traversing this range the Boonton power meter is monitored simultaneously, using procedures described in the next section. The reference voltage to which a power maximum occurs is stored in the variable (a). After the range has been scanned, the backshort micrometer is moved to the optimum power position.

PROCstep_ft

Once the frequency tuner is located at its start position and the backshort has been positioned for maximum power. The frequency tuner is stepped in small increments up to its final position specified by `crit_ft_up`. Each time the tuner is stepped one division, a frequency reading can then be taken from the EIP and the power maximum determined by the Boonton. It was found with the size of the step increment being very small (≈ 0.01 volts) the error created in reading the frequency tuner pot was significant. On occasions this would result in the frequency tuner not being stepped at all ! This

was probably due to noise effects on the line. This problem was overcome by firstly starting the frequency tuner moving, having a short time delay and then stopping the tuner. After a few test runs, it was found that a time delay of 2.3 secs ($\approx 200\text{MHz}$) would step the tuner by approximately 0.02volts and a delay of 1.2secs ($\approx 100\text{MHz}$) would step the tuner through 0.01volts. The delay is stored in the variable 'wait'. This method proved very successful and offers a variety of resolutions for stepping the frequency tuner. Although, the step would be approximate rather than precise, it would always result in a small movement of the tuner which is all one required to characterise an oscillator.

(3.6.5) Results obtained from Automatic Characterisation.

The Gunn oscillator block(D4) was characterised using the AOTS and the CharOsc program. The experimental setup is shown in figure(3.17).The frequencies and maximum power obtained were plotted separately against the voltage of the frequency micrometer which are shown in figure(3.18).

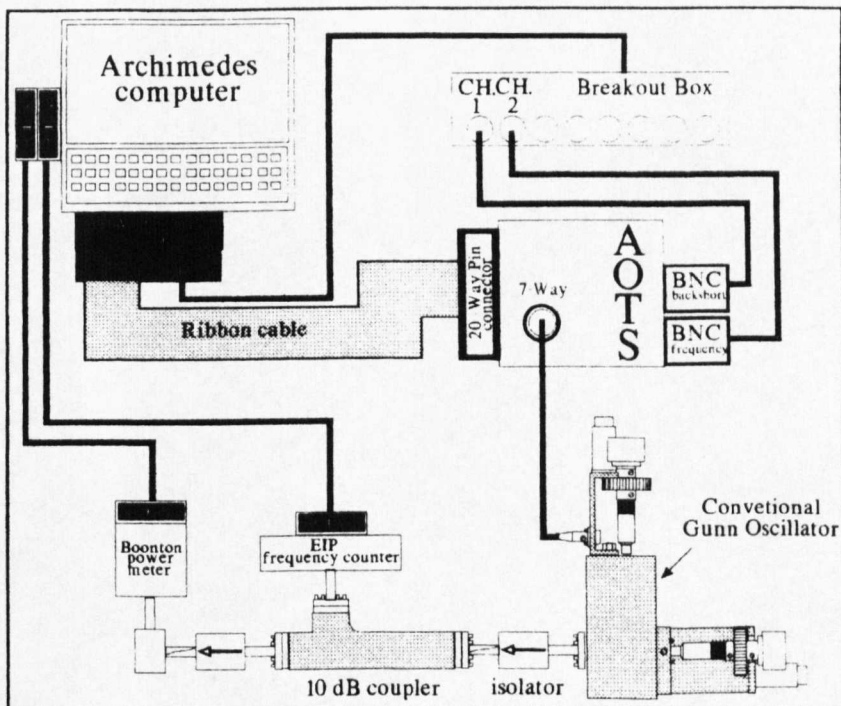


Figure (3.17)

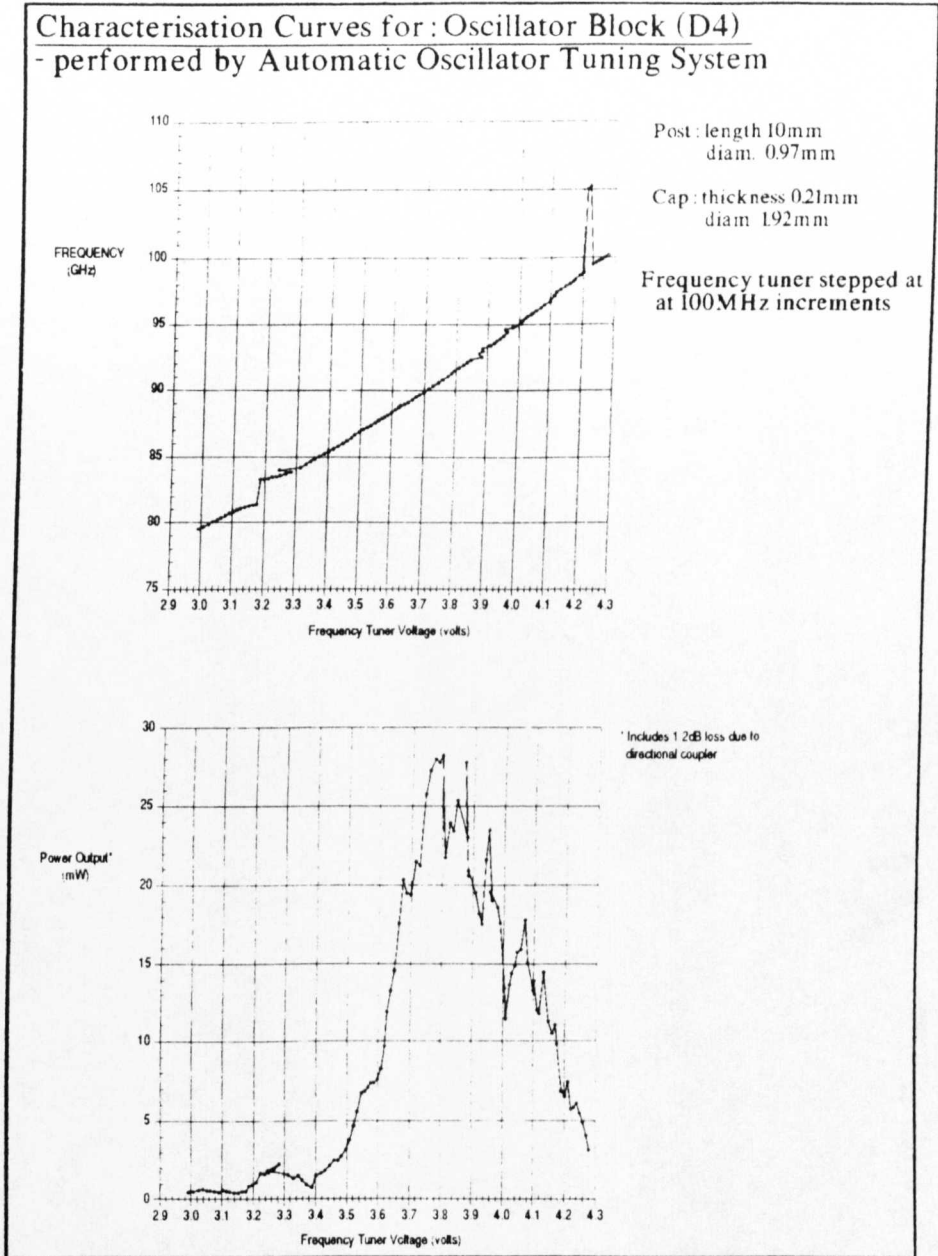


Figure (3.18)

These results were performed with frequency micrometer stepping increment of ($\approx 100\text{MHz}$). As can be seen from the uppermost figure, only one true frequency jump occurs with oscillator block(D4) at around 83GHz. This is the only frequency jump that occurs over the whole of W-band and spans $\approx 2\text{GHz}$. The other jump that can be seen is due to the EIP miscounting. The number of EIP frequency miscounts can be greatly reduced at this high resolution of stepping.

Chapter 4

Magnetic Behaviour

Introduction

Contained within the pages of this chapter, is the relevant magnetic theory necessary to describe the micro and macroscopic processes that occur within different types of magnetic material. Knowledge of the theory and terminology mentioned here will provide the necessary basis to allow one to proceed in understanding about the 'Faraday Effect', mentioned in the next chapter. The chapter starts with a discussion about how the proximity of the neighbouring atoms of a material can determine how it behaves as a whole magnetically. Special attention is paid to the exchange interaction that is responsible for magnetic materials being able to retain an internal magnetic field. The concept of Domain and Bloch wall formation is then discussed and shows how the domains can be influenced by an externally applied field and lead to a magnetically polarised material. The chapter is concluded by describing how the magnetisation of a magnetic material is temperature dependent such that it is reduced to zero as the temperature approaches the Curie point.

(4.1) What determines whether a material is Paramagnetic, Ferromagnetic or Antiferromagnetic ?

It is the proximity, the closeness, of the neighbouring magnetic atoms in a material that determine the magnetic nature of the material, in question. All ferromagnetic and antiferromagnetic materials can be thought of as special cases of the paramagnetic case. Whereby, in a paramagnetic material the atoms are far apart and in ferromagnetic and antiferromagnetic materials the atoms are

much more closely packed. As will be explained shortly, as the magnetic atoms of a material are brought closer together, they start to interact with each other. It is these 'close proximity' interactions that are responsible for and are the essence of ferromagnetism and antiferromagnetism. By first taking a look at the more simple paramagnetic system, we can hope to understand what happens in the more complex systems of ferromagnetism and antiferromagnetism.

(4.2) Paramagnetism, The Bohr Magneton & Orbital-Spin Coupling.

In a typical atom an electron of mass (m) and charge (q) describes an orbit of radius (r) and area (A) about the nucleus, as shown in figure (4.1). This gives rise to an 'orbital magnetic dipole moment' (μ_L). The orbital magnetic dipole moment can be calculated by likening it to that of a current (i) flowing in a closed loop of area (A), where (c) is the speed of light, such that :

$$\mu_L = \frac{i A}{c} = \frac{i \pi r^2}{c} \quad \dots(4.1)$$

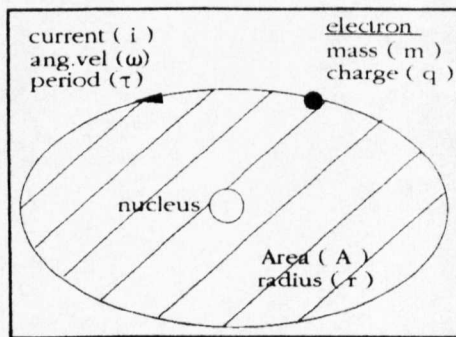


Figure 4.1

Now let the current be circulating with a period (τ) and an angular frequency (ω) therefore :

$$i = \frac{q}{\tau} = \frac{q\omega}{2\pi} \quad \text{since, } \tau = \frac{2\pi}{\omega} \quad \dots(4.2)$$

Subst. (4.2) in (4.1)

$$\mu_L = \frac{q\omega r^2}{2c} \quad \dots (4.3)$$

multiply (4.3) by $\frac{m}{m}$:

$$\mu_L = (m\omega r^2) \frac{q}{2mc} = P_L \left(\frac{q}{2mc} \right) \quad \dots (4.4)$$

where, the term $(m\omega r^2)$ corresponds to the 'orbital angular momentum' (P_L). From the Bohr model of the atom we know that angular momentum is quantized in units of $(h/2\pi)$, therefore :

$$\mu_L = k \left(\frac{qb}{4\pi mc} \right) = k \mu_B \quad \dots (4.5)$$

Where (k) is an integer and (μ_B) is a quantity known as the 'Bohr Magneton' and is the unit of 'magnetic moment'. Hence, the orbital magnetic dipole moment is an integral multiple of this quantity.

However, this is not the only magnetic dipole moment to exist. There is another contributor, which is larger than that of the orbital magnetic dipole moment and cannot be explained classically. The second contributor is due to a purely quantum mechanical effect. As well as the electron orbiting the nucleus it also spins about its own axis (See Figure 4.2).

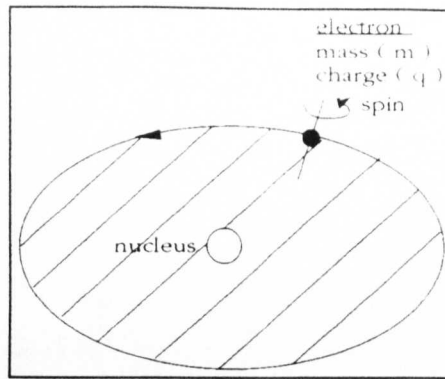


Figure 4.2

This spin gives rise to another magnetic dipole moment known as the 'spin magnetic dipole moment' (μ_s), which is given by :

$$\mu_s = P_s \left(\frac{q}{m c} \right) = k \left(\frac{q h}{2\pi m c} \right) = k (2\mu_B) \quad \dots (4.6)$$

where, (P_s) is the spin angular momentum.

As one can see, comparing equations (4.5) and (4.6), for a given angular momentum, the spin gives twice the magnetic dipole moment to that associated with the orbit.

Therefore, the 'total magnetic dipole moment' of the atom (μ_T) can be given by :

$$\mu_T = \mu_L + \mu_s = J g \mu_B \quad \dots (4.7)$$

where, (μ_T) is quantized and (J)¹ is the 'total angular momentum quantum number', which is a vector sum of the 'orbital angular momentum quantum number' (L) and the 'spin angular momentum quantum number' (S), such that :

$$J = (L + S) \quad \text{where, } L = 0, \pm 1, \pm 2\dots$$

$$S = \pm 1/2, \pm 1, \pm 3/2\dots \text{ for atom} \quad \dots (4.8)$$

¹ Also explained as 'Russell-Saunders Coupling'. pg 242, Ref [2]

(J) can have the values such that: $J = 0, \pm 1, 2, \pm 1, \pm 3/2, \dots$

Therefore, $(2J+1)$ discrete energy values exist for the total angular momentum.

The 'Lande spectroscopic splitting factor'^{2,3} (g) is used to describe a measure of the spin-orbit coupling that exists between the spin and orbital magnetic moments, where :

$$g = \frac{3}{2} + \frac{S(S + 1) - L(L + 1)}{2J(J + 1)} \quad \dots (4.9)$$

when $g=1$, only the orbital magnetic dipole moment contributes to (μ_T) and when $g=2$, only the spin magnetic dipole moment contributes to (μ_T).

In a paramagnetic solid the magnetic atoms are far apart, such that the orbits of the atoms' electrons do not overlap and there is no interaction or influence between the neighbouring atoms. The only influence on the electrons is a thermal one, which causes their magnetic dipoles to point in arbitrary directions as a consequence of the thermal agitation. Each dipole can be thought of as an individual, independent entity that is totally disconnected from the influences of its neighbours within the solid. Therefore, when an external field is applied, each of the dipoles will align independently in the same sense as the external field. However, when the external field is removed the dipoles will become disrupted and randomly oriented again due to thermal agitation. It is due to this independent alignment of the individual magnetic dipole moments on application of an external field that defines a paramagnetic material.

² pg 14, Ref [3]

³ pg 62, Ref [1]

(4.3) Ferromagnetism, Antiferromagnetism and the 'Exchange Interaction'.

Now consider what happens when we bring the atoms, of a paramagnetic material closer together. It can be seen from figure(4.3), that the orbits of the electrons now begin to invade the orbits of adjacent atoms' electrons.

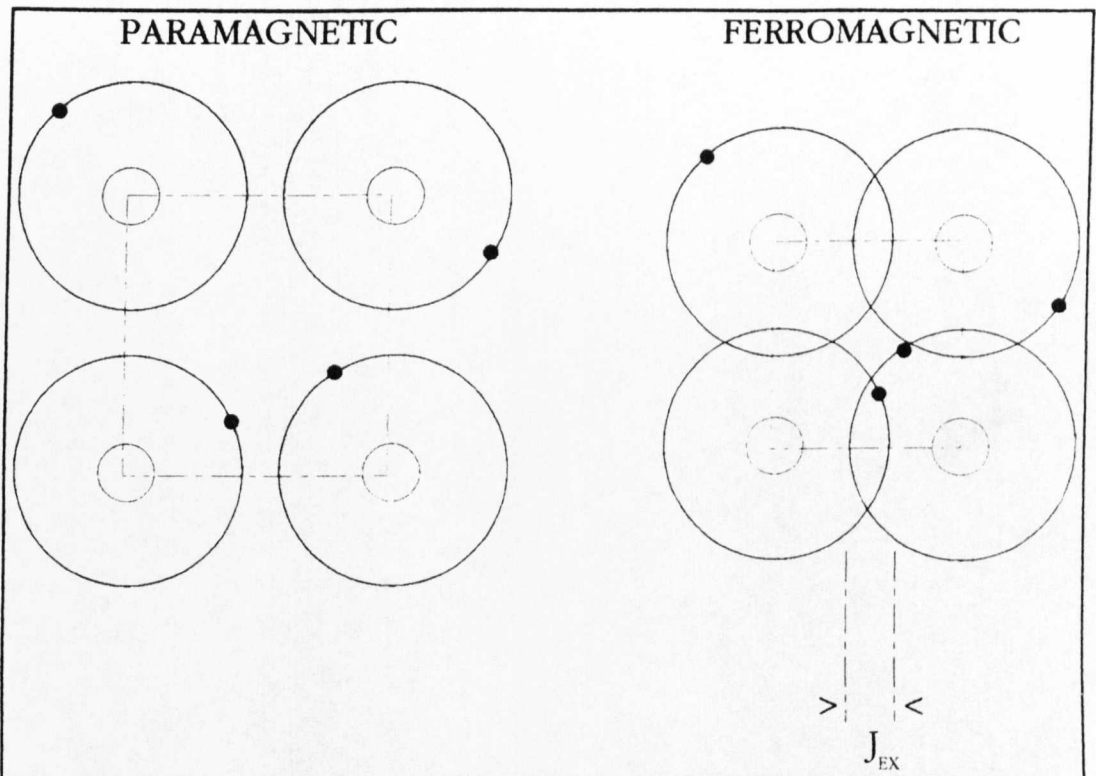


Figure 4.3

This creates an overlap of charge. As one can see in the paramagnetic case, the orbits of the electrons do not overlap and since the wavefunctions of the electrons decrease exponentially with distance, no interactions occur.

As the atoms are brought closer in proximity, the wavefunctions of the electrons start to overlap into the vicinities of the other electrons' wavefunctions. Statistically from, quantum mechanics, the electrons

spend part of their time around the nucleus of other adjacent atoms. This creates a strong electrostatic coulomb repulsion between the electrons. In order to keep the energy to a minimum the spins are aligned parallel⁴. Now, since the electrons spend time around each others nucleus and in each others orbits, it is possible for two electrons to exist in the same energy state and also have the same spin orientation. This is forbidden due to the 'Pauli Exclusion Principle'. Therefore, the neighbouring atoms exchange electrons between themselves. This is a purely quantum mechanical process of which there is no classical analogue. The energy required for this exchange of electrons is known as the 'Interaction Energy' or 'Energy of Exchange' (E_{ex}) and is expressed as :

$$E_{ex} = -2J_{ex}(S_i \odot S_j) \quad \dots (4.10)$$

Where, (S_i) & (S_j) are the electron spins of two adjacent atoms.

(J_{ex}) is known as the 'Exchange Integral' and is a very sensitive function of the separation between adjacent atoms. It can be thought of as a measure of the overlap of the wavefunctions of the two electrons. The exchange integral involves the wavefunctions of the two electrons and the Coulomb repulsion between them, which is responsible for their parallel alignment, given by⁵ :

$$J_{ex} = J_{ij} - 2 S_{ij} V_{ij} \quad \dots (4.11)$$

Where, (J_{ij}) is the 'True Exchange Integral'. (S_{ij}) is the 'Overlap' and (V_{ij}) is the 'Cross-Matrix' elements of the attractive potential, which is due to the electrons with antiparallel spin in non-orthogonal wavefunctions. By looking at how the exchange integral (J_{ex}) varies

⁴ A calculation demonstrating the preference of parallel alignment for minimisation of energy can be found on pgs 112-113, Ref [2]

⁵ pg 27, Ref [4]

with interatomic spacing⁶, one can categorize the various types of magnetic material as shown below :

Atoms far apart \Rightarrow no interaction $\Rightarrow J_{ex} \approx 0 \Rightarrow$ PARAMAGNETISM

Atoms close \Rightarrow spins align parallel $\Rightarrow J_{ex} > 0 \Rightarrow$ FERROMAGNETISM

Atoms very close \Rightarrow spins antiparallel $\Rightarrow J_{ex} < 0 \Rightarrow$ ANTIFERROMAGNETISM

As an aside, there are actually four different types of exchange mechanism that can exist. Very briefly the four different types of exchange mechanism are :

(4.4) Itinerant Exchange :

Which describes the exchange between itinerant electrons to one another within a metal.⁷

(4.5) Direct Exchange :

Describes the exchange between the spins of electrons whose atoms are separated enough to have 'free electron' characteristics.⁸

(4.6) Indirect Exchange :

Describes the exchange between electrons in the conduction band of a metal to those with localised spins within the unfilled inner shells.⁹

(4.7) Superexchange :

Describes the exchange between electrons of magnetic atoms, which are separated by non-magnetic ones.¹⁰

The type of exchange mechanism that is adopted depends on the

⁶ taken from pg 65, Ref [1]

⁷ Chapter 1, Ref [6]

⁸ Chapter 1, Ref [5]

⁹ Chapter 3, Ref [5]

¹⁰ Chapter 2, Ref [4]

atomic configuration of the system. For example, the structure of a metal would favour itinerant or indirect exchange. Whereas an insulator may tend to superexchange and a gas would adopt the mechanism of direct exchange. The types of exchange mechanism should not be thought of as disconnected from each other. The mechanisms all overlap with each other, some more than others as shown in figure(4.5)¹¹.

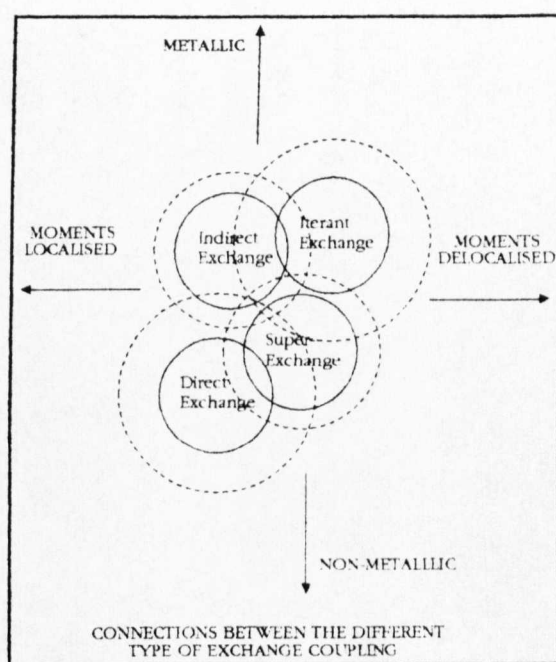


Figure 4.5

From the 'Electrostatic effect' of the Coulomb repulsion, which aligns the spins of the electrons all in the same sense. So too the magnetic dipole moments of the electrons align in the same sense, since they are parallel to the spin, therefore producing a net 'Magnetic effect', which results in Ferromagnetism. As we bring the atoms even closer the electrons spins are forced to align antiparallel and we get the phenomena of Antiferromagnetism. An

¹¹ Taken from Chapter 2, pg 3, Ref [6]

antiferromagnetic material can be envisaged at two separate sublattices which interact with one another. One sublattice consists of the moments that are aligned in one sense. The other sublattice is composed of the moments that are aligned in the opposite sense. The net moments of both sublattices are equal in magnitude. Thus the total moment of the bulk material is reduced to zero.

The materials investigated in chapter six, are known as 'ferrimagnetic', hence the name 'ferrite', which is a special case of antiferromagnetism. This type of magnetic behaviour exists when the two sublattices have different magnitudes. Hence, there is a net magnetisation in one particular orientation. The materials investigated were Barium ferrite ($\text{BaO} \cdot 6(\text{Fe}_2\text{O}_3)$) and Strontium Ferrite ($\text{SrO} \cdot 6(\text{Fe}_2\text{O}_3)$). As will be shown later, these materials are hexagonal in structure, have a high Anisotropy field along their c-axis and are magnetically hard in their sintered polycrystalline form with (Curie Temperature, $T_C = 500\text{-}800^\circ$).

As well as the exchange interaction there is another interaction due to the close proximity of the atoms. But before we can describe it we will first take a closer look at the atomic makeup of the ferromagnetic material, iron.

(4.8) Hund's Rules & the electron configuration within an atom.

Hund's Rules are a set of axioms that determine which of the available energy states shall be occupied within an atom. By following these rules, electrons can be distributed within the shells and the atom built up.

The rules state that, the electrons will occupy energy states within a shell such that :

(i) The max. total atomic spin (S) of a shell is equal to the sum of

the separate spins (m_s) of the electrons in the shell, namely :

$S = \sum m_s$ and doesn't violate Pauli's exclusion principle.

(ii) The max. total orbital momentum (L) of a shell is equal to the sum of the separate orbital momentum (m_l) of the electrons in the shell, namely :

$L = \sum m_l$ and is consistent with (S).

(iii) The total angular momentum (J) = $|L - S|$ when shell $< 1/2$ full.

for a shell = $|L + S|$ when shell $> 1/2$ full.

= S , since $L=0$ when shell = $1/2$ full.

The rules¹² imply that, the electrons will occupy the energy states within a given shell as far as possible, such that all the spins are parallel thus providing an atom with the 'maximum number of unpaired spins. For a 3d metal, such as iron, the orbital angular momentum is usually "quenched" by the crystal fields. In these materials the net magnetic moment therefore arises from an imbalance of spins. Hence, it is the magnetic moments of the unpaired spins that are responsible for the magnitude of the magnetization of a material. Conversely, if all the energy states of a shell are full, namely all the electron spins are paired ('up' to 'down'), the total orbital angular momentum ($L=0$) and the total spin angular momentum ($S=0$). For iron, with 26 electrons, the unpaired spins exist in the 3d shell.(See figure 4.6).¹³

¹² Rules taken from pgs. 239 - 240, Ref [2]

¹³ Customised from pg 49, Ref [1]

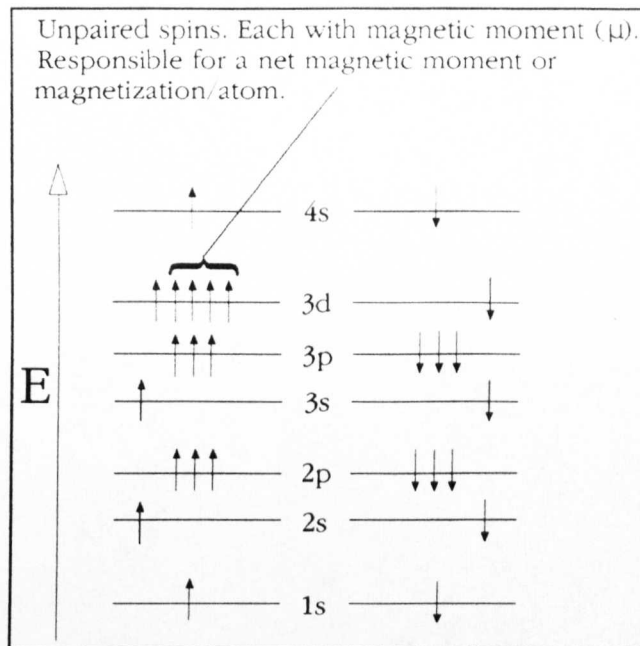


Figure 4.6

Where the letters (s,p,d, correspond to the state of the orbital angular momentum ($L = 0, 1, 2$) respectively.

This is the configuration of the free iron atom. Also nickel and cobalt have the unpaired spins in the 3d state and also exhibit ferromagnetism.

Having acquainted one's self about the distribution of electrons within a typical ferromagnetic material, we can now look at the second interaction due to close proximity. This is the redistributing of electrons between the 3d and the 4s state. The electrons cannot be viewed as localised particles anymore, like in the free model. Just like the electrons have a probability of being found in the orbits of neighbouring electrons, due to the exchange interaction, so too the electrons have a probability of occurring in the 3d or 4s state. Therefore, we get a smearing of charge between the 3d and 4s states. This smearing of charge forms bands of energy which overlap by various amounts depending on the separation of the atoms. For ferromagnetic solids of the iron group, the bands overlap as shown schematically in figure (4.7).¹⁴

¹⁴ Taken from pg 66, Ref [1]

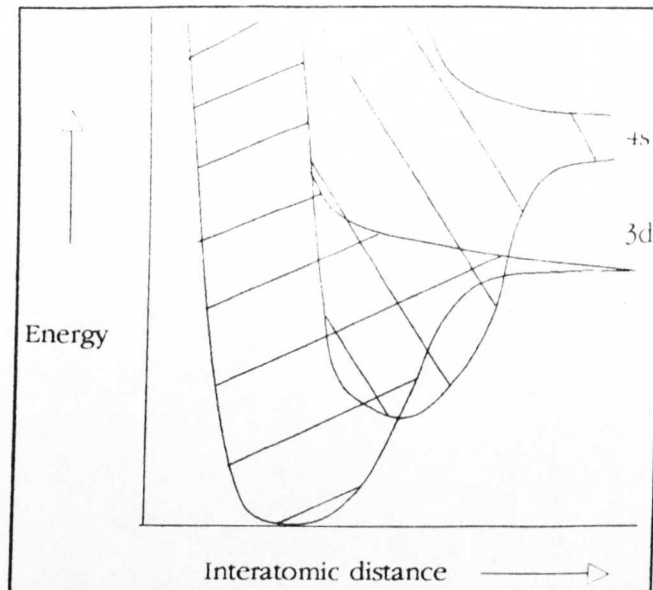


Figure 4.7

In comparison to the free atom of iron for the 3d and 4s states we see a non-integral distribution of spin (See figure 4.8).

FREE ATOM		IN SOLID	
↑	4s	↑	4s
↓		↓	
5↑	3d	4.8↑	3d
↓		↓	
NET SPIN 4		NET SPIN 2.2	

Figure 4.8

Therefore, in a ferromagnetic solid one can imagine, due to the close proximity of the atoms, two effects. One is the alignment of spin of the electrons and therefore the magnetic dipoles to minimise energy. Due to the Pauli exclusion principle this results in the swapping of the electrons between the atoms in order to avoid to electrons existing with the same set of quantum numbers. The other effect is the delocalizing of the electrons as they are allowed to redistribute between the 3d and 4s states.

These are the interactions that occur on the interatomic scale. We would now expect a ferromagnetic material to be spontaneously

magnetised, due to the alignment of the dipoles and a net magnetisation to exist, however, this is not the case. This is due to the formation of domains, another energy minimization process, which will now be discussed.

(4.9) Domain Formation.

Recapping, from the previous explanation on ferromagnetism one would expect that, without the need of any external field, as in the paramagnetic case, all the spins and therefore the magnetic dipole moments, in a ferromagnetic material would be aligned parallel and it would be spontaneously magnetised. However, it is found that a ferromagnetic material seems to be in an unmagnetised state and it is only after placing it between the poles of an external magnet that it then becomes magnetic and retains this magnetism after the external field is removed. Therefore, why is the ferromagnet not spontaneously magnetised? What causes this unmagnetised state? And by what mechanisms does the unmagnetised state employ to create the magnetised state? These questions were resolved by Weiss who suggested the idea of domain formation in order to minimise the magnetic energy.

Weiss suggested that a ferromagnetic material is composed of small regions called 'domains'. Each domain is a collection of magnetic dipole moments, approximately 10^{12} - 10^{15} dipoles/domain, which are all aligned parallel and can therefore be said to be magnetically polarised. However, the magnetically polarised domains, in relation to each other, are all randomly oriented such that their vector sum is zero, shown in figure(4.9). Hence, resulting in a seemingly unmagnetised state. The reason why the domains form and create this unmagnetised state is a direct consequence of the system adjusting the 'Magnetic Energy' of the solid to attain an absolute minimum.

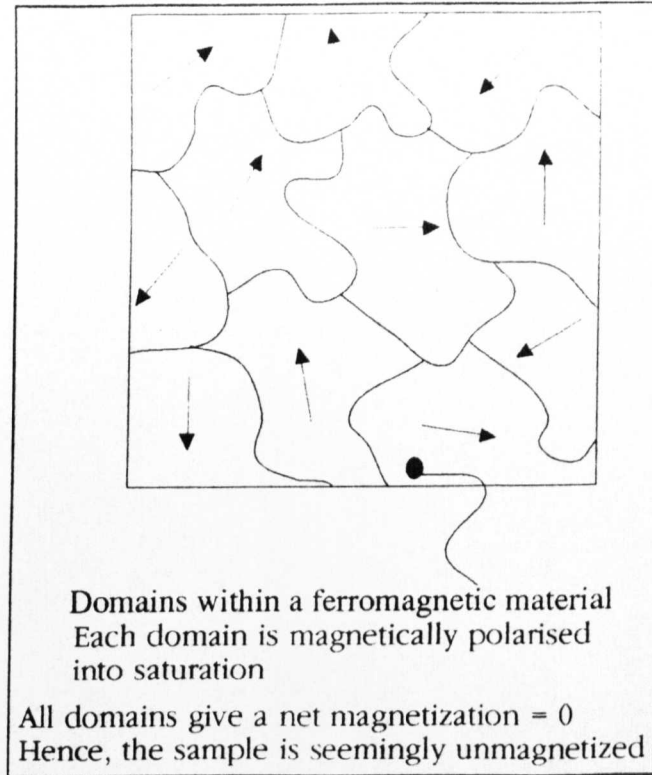


Figure 4.9

In a single crystal the domains are more regularly arranged, highlighted in figure(4.10).¹⁵

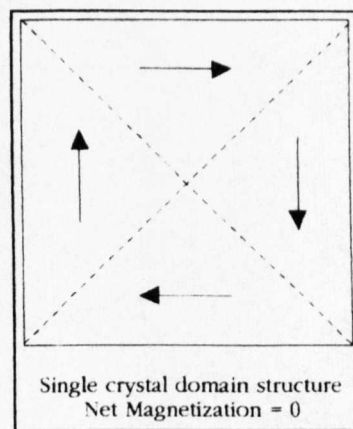


Figure 4.10

When this pseudo-unmagnetised state is placed in the external poles of a magnet. Then the domains try to orient themselves in the same direction as the external field.

¹⁵ Diagrams (4.10), (4.12) and (4.13) customised from pg 172, Ref [7]

Three mechanisms are involved in this reorientation process. These are 'Domain Boundary Displacement', 'Domain Rotation' and 'Coherent Domain Rotation'. The strength of the external field determines which mechanism is employed. (See figure 4.11)

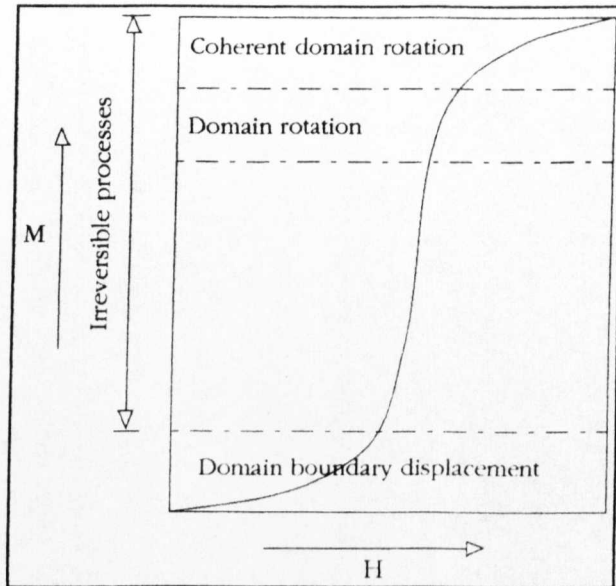


Figure 4.11

(4.10) Domain Boundary Displacement :

When the external field is weak, the mechanism of 'Domain Boundary Displacement' is employed. This is a reversible process and if the external field were removed the domains would revert back giving the original unmagnetised state. During 'Domain Boundary Displacement', a domain which is oriented in the more desirable sense to that of the external field will invade into the domain of a less desirable oriented neighbour. Therefore, the desirably oriented domain grows in magnitude (See figure.4.12).

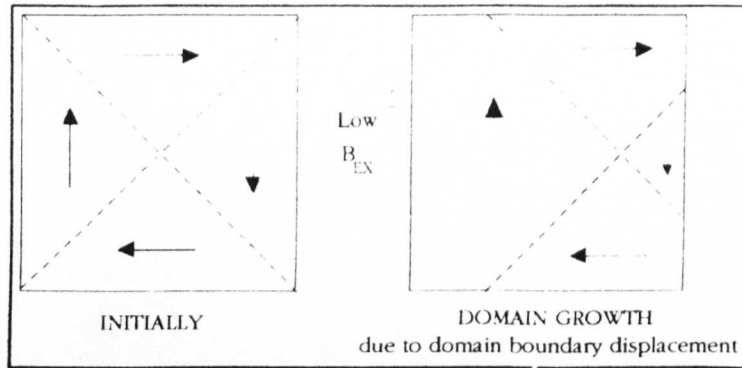


Figure 4.12

(4.11) Domain Rotation :

At moderate external fields, 'Domain Rotation' occurs. This is where a less desirable oriented domain overcomes the 'Anisotropy Energy', which will shortly be discussed, and rotates from its original direction into that of one of the crystallographic 'Easy Axes' which will also be explained shortly, (See figure.4.13).

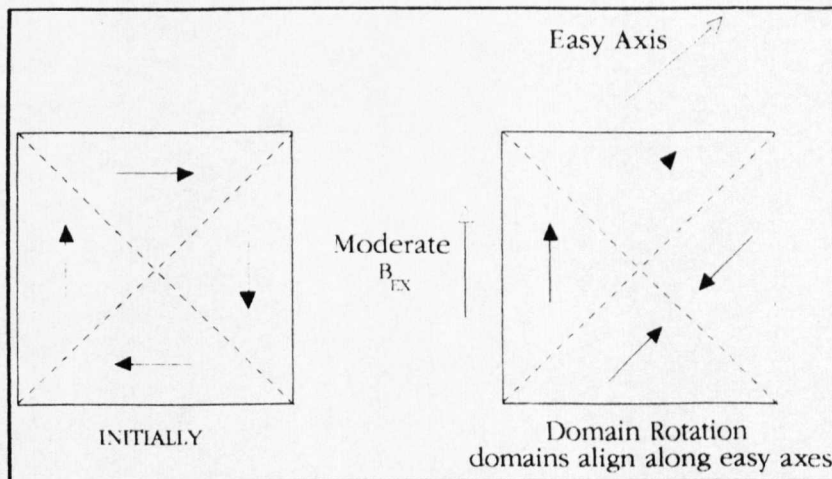


Figure 4.13

(4.12) Coherent Domain Rotation :

At high external fields, the mechanism of 'Coherent Domain Rotation' occurs. This is where all the domains rotate simultaneously such that the whole sample becomes magnetically polarised in the

same direction of the field (See figure.4.14).

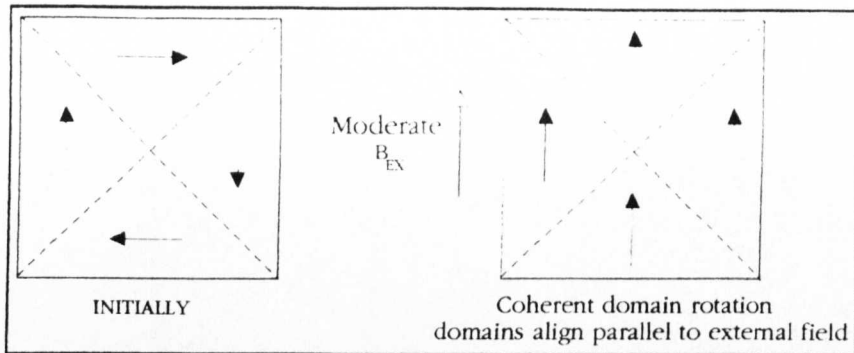


Figure 4.14

The domain structures formed in the pseudo-unmagnetised state of a ferromagnetic material are solely to keep the magnetic energy of the system to an absolute minimum. When placed between the poles of an external magnet the domains will reorient and adjust themselves to allow for this magnetic energy to be minimised. As a consequence of this we get a system which retains magnetism ferromagnetically.

The magnetic energy that is minimised exists in four different forms. That of Magnetostatic Energy (E_{MS}), Anisotropy Energy (E_{AN}), Magnetoelastic Energy (E_{ME}) and Exchange Energy (E_{EX}), which will now be discussed.

(4.13) Magnetostatic Energy (E_{MS}).

The best way to describe this form of magnetic energy is by looking at how it is associated with the simple system of a permanent magnet. The Magnetostatic energy can be thought of the energy required for the poles of a magnet to create the lines of flux that link them. The magnetostatic energy that is associated with the external lines of flux that connect the poles at the surface of a magnet is known as the 'Demagnetization Energy'. By looking at how the demagnetization energy changes with the intervention of multidomains we can see, schematically, how the magnetostatic energy of the system varies as a whole.

In a single domained sample, one can see, the external field is quite large. Hence, the magnetostatic energy required to create the field is also large. Now if the sample forms domains, such that adjacent domains are magnetically polarised antiparallel to one another. One can see that there is a significant reduction in the external field and hence, the magnetostatic energy required to produce it (See figure 4.15). Since, the system desires the magnetic energy to be minimised then this configuration is preferred.

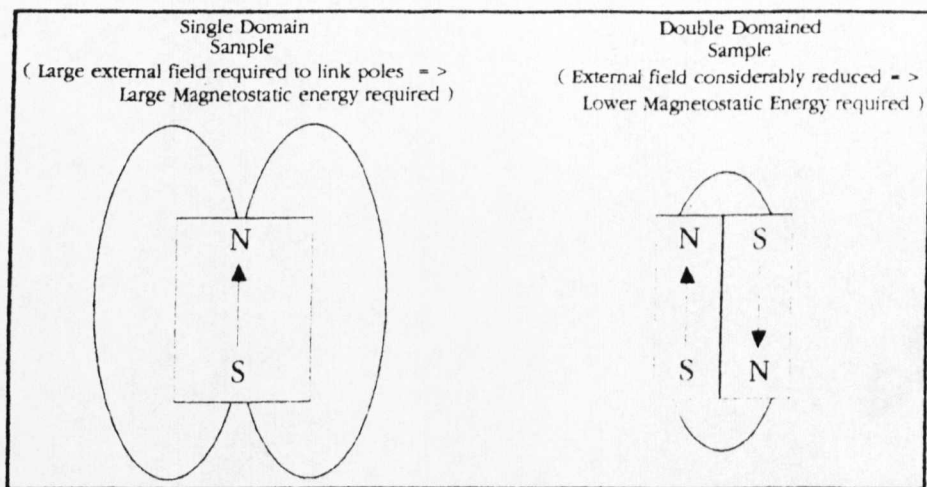


Figure 4.15

This process of subdividing continues, shown in (4.16) and hence, the magnetostatic energy is reduced. However, each time a domain is formed a boundary known as a 'domain wall' or 'Bloch wall', which will be described later, must also be formed in order to separate the domain from it's neighbouring domains. The formation of a Bloch wall also requires energy. Hence, the process of subdivision will finally be halted when the magnetostatic energy is equal to that of the total energy required in the creation of the Bloch walls in the solid.

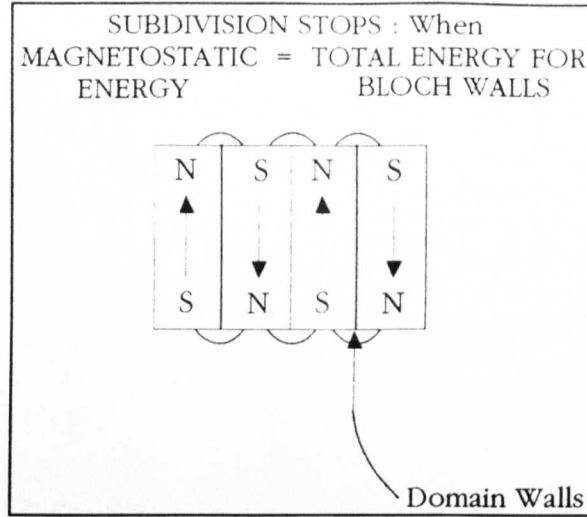


Figure 4.16

The Magnetostatic Energy can be calculated by considering the energy of a dipole of moment (\mathbf{m}) in an external magnetic field of magnetic induction (\mathbf{B}). The energy of the dipole is defined as the work done in the turning force to align the dipole parallel to the field. Hence,

$$E = -\mathbf{m} \cdot \mathbf{B}$$

Now $\mathbf{B} = \mu_0 \mathbf{H}$,

$$E = -\mu_0 \mathbf{m} \cdot \mathbf{H}$$

Now for a domain, which is a collection of magnetically polarised dipoles of Magnetization (\mathbf{M}) we get :

$$E = -\mu_0 \int \mathbf{H} \cdot d\mathbf{M}$$

Now the domain is subject to its own demagnetising field (\mathbf{H}_D), which is due to the poles at the surface of the domain, where :

$$\mathbf{H}_D = -N_D \mathbf{M}$$

Where (N_D) is the demagnetization factor¹⁶ and negative, since (\mathbf{H}_D) is antiparallel to (\mathbf{M}).

$$\therefore E = \mu_0 N_D \int \mathbf{M} \cdot d\mathbf{M}$$

Hence,

$$E_{MS} = \frac{\mu_0}{2} N_D M^2 \quad \dots (4.12)$$

Also as a point to note, the domains can be arranged such that the magnetostatic energy at the surface, the demagnetization energy, vanishes. These are known as 'domains of closure'. (See figure 4.17). They provide a closed circuit for the magnetic flux. And they are the first type of domains to evolve in the demagnetization process, since they provide a return path for the magnetic flux within the solid.

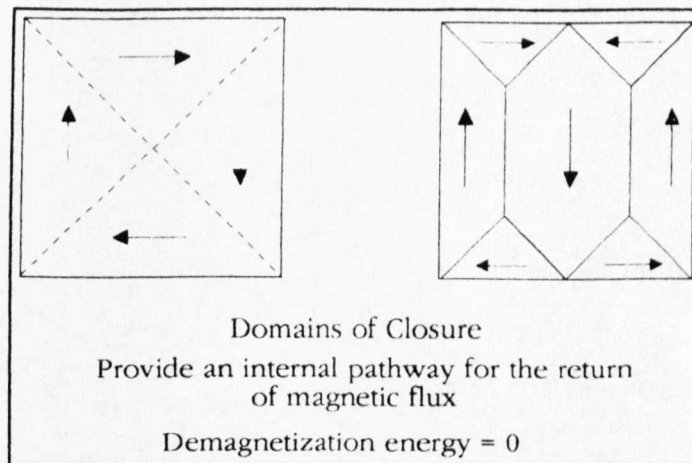


Figure 4.17

(4.14) Anisotropy Energy (E_{AN})

Due to the crystallographic structure of a material. There are certain preferential directions in which the domains will align. These preferred directions are known as 'Easy Axes' of magnetisation, (As mentioned in figure(4.13) & domain rotation). It is found that exposure to an external field along the easy axes require the smallest field to saturate. Also there are 'Hard Axes', which require

¹⁶ pg. 36-38, Ref [2], described in (5.6.2).

the largest field to saturate.

The Anisotropy energy is defined as the difference in energy required to align the magnetic dipole moments or to saturate the sample along the easy axes to that of the hard axes. For the Anisotropy energy to be minimised the domains would be aligned along the easy axes.

For the 'Cubic' crystallographic structure of iron there are three preferential axes. The easiest of which is the $\langle 111 \rangle$ axis along the cube diagonal

However, for the cubic structure of nickel the easy axis is along the $\langle 100 \rangle$ axis .(See Figure 4.18)¹⁷

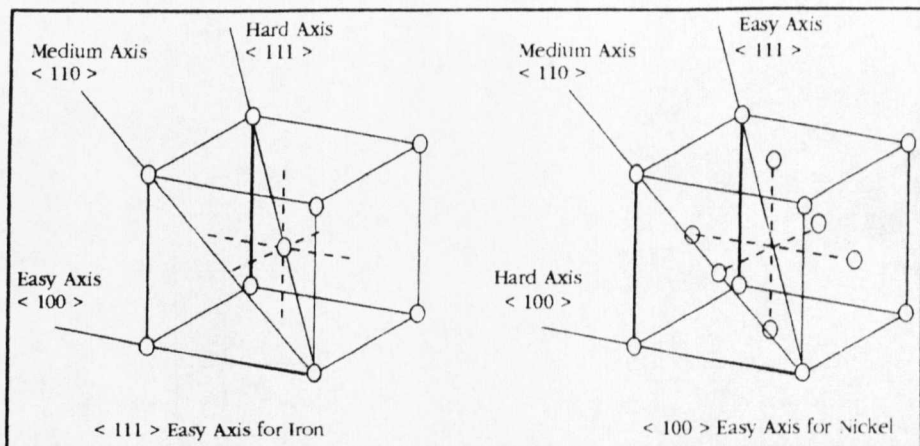


Figure 4.18

For a cubic structure the anisotropy energy is :

$$E_{AN} = K_1(\cos^2\theta_1 \cos^2\theta_2 + \cos^2\theta_2 \cos^2\theta_3 + \cos^2\theta_3 \cos^2\theta_1) \dots \quad (4.13)^{18}$$

where, θ_1 , θ_2 and θ_3 are angles the magnetisation makes relative to the three crystal axes $\langle 100 \rangle$, $\langle 110 \rangle$ and $\langle 111 \rangle$.

For cobalt or ferroxdure, which is hexagonal, there is only one preferred axis (and these structures are known as 'uniaxial') which

¹⁷ Taken from pgs 205 - 206, Ref [2]

¹⁸ Taken from pg 23, Ref [2]

lies along its hexagonal axis. (See figure 4.19)

For a hexagonal structure, the anisotropy energy is given by :

$$E_{AN} = K_1 \sin^2\theta + K_2 \sin^4\theta + \sin^4\theta \sin 6\varphi \quad \dots (4.14)$$

where, (θ) is the angle between the applied external field and the easy-axis. (K_1) & (K_2) are the anisotropy constants typical to a material at room temp.¹⁹

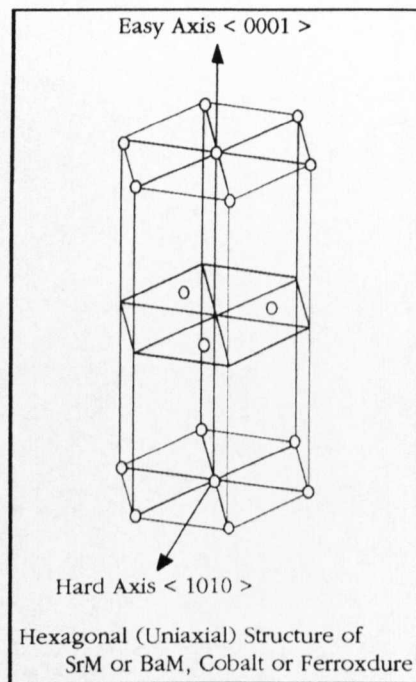


Figure 4.19

(4.15) The Magnetoelastic Energy (E_{ME}) or Magnetostriction.

As a ferromagnetic material is magnetised into saturation there is a dimensional change, which is due to the reorienting of the domains parallel to the external applied field. Shown schematically below in figure (4.20)²⁰.

¹⁹ Calculation of a typical Anisotropy field can be found in pgs 122 - 123, Ref [2]. The 1st term of equation(4.14) is the uniaxial symmetry term and the 3rd term describes the hexagonal anisotropy.

²⁰ Customised from pg 99, Ref [2]

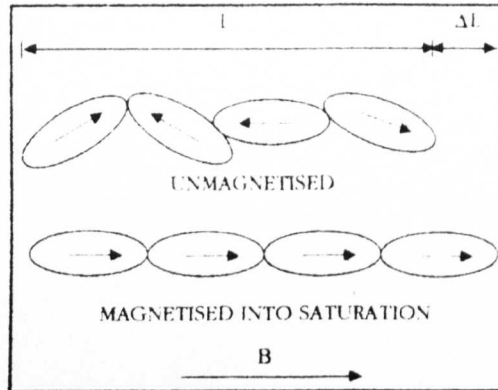


Figure 4.20

The fractional change (ΔL) in dimension (L) due to magnetisation is called the 'Magnetostriction'. The best way to visualize what is happening is to consider a cubic crystal structure, say that of iron. As we already know iron has 3 axes of magnetisation, which are along its cube edges. Therefore, for the anisotropy energy to be minimised the domains could line up in any one of these preferential directions. In fact (See figure 4.21) the ordinary domains align along one easy axis and the domains of closure align along another easy axis.

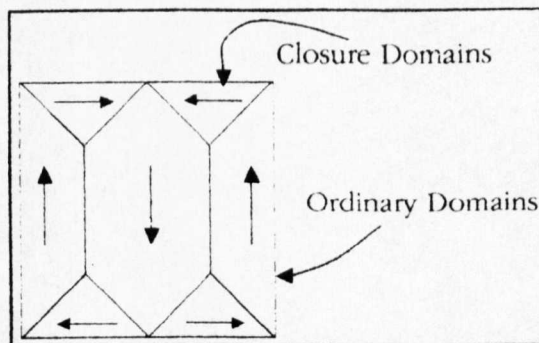


Figure 4.21

Now as the external applied field increases, magnetostriction occurs. As one can see schematically (See figure 4.22), since the ordinary domains are aligned along a different easy axis to the domains of closure they tend to become elongated, due to magnetostriction, along the axis they are aligned. The magnetostriction also elongates

the domains of closure, but along the axis which they are aligned. Therefore, the domains of closure and the ordinary domains force themselves into one another. This evokes a strain on the domains as they are restricted from expanding.

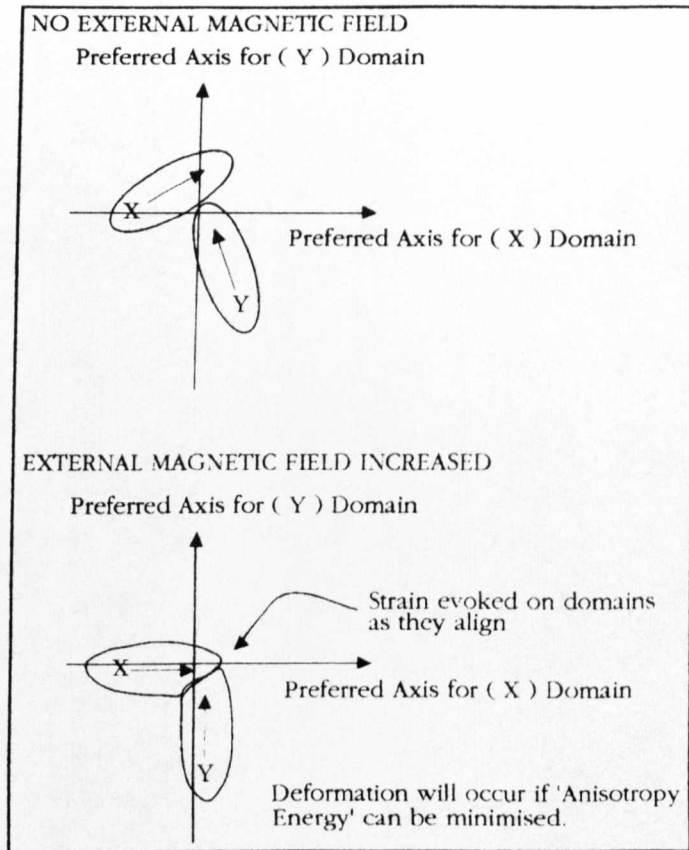


Figure 4.22

The work that has to be done to combat these elastic forces is the 'Magnetoelastic Energy', where :

$$E_{ME} = \lambda_s \sigma \sin^2 \theta \quad \dots (4.16)^{21}$$

where, (λ_s) is the saturation magnetostriction, which is the fractional change (ΔL) in length (L) of the sample. (Which is assumed to be isotropic in this case).²²

²¹ Taken from pg 119, Ref [8]

²² For the Anisotropic case see, 'Magnetostriction & Magnetomechanical Effects',

Where, (σ) is the stress and (θ) is the angle between the stress and the magnetisation.

Also the magnetostriction brings about a change in the 'anisotropy energy' of a domain. If a domain can minimise its anisotropy energy by deforming then this will occur. Therefore, the 'magnetoelastic energy' can be considered as an additional term in the 'anisotropy energy'. Therefore, the 'total anisotropy energy' ($E_{TOT. AN}$) is given, for a cubic crystallographic structure, by :

$$E_{TOT. AN} = (K_1 + \Delta K)(\cos^2\theta_1 \cos^2\theta_2 + \cos^2\theta_2 \cos^2\theta_3 + \cos^2\theta_3 \cos^2\theta_1) \dots (4.17)$$

where, (ΔK) is the change in anisotropy energy due to magnetostriction.

(4.16) Exchange Energy (E_{EX}) & Bloch Walls.

As described earlier, the 'exchange interaction' and the energy associated with this interaction is responsible for ferromagnetism. Where the exchange energy is given by (4.10)

As will now be explained it is the 'exchange energy' and the 'anisotropy energy' that are responsible for the creation of Bloch walls and their size.

Bloch suggested that due to the domain formation, it was possible for two domains to exist next to each other which were magnetically antiparallel in polarization on the condition that an intermediate region existed between the two, in which there was a gradual transform of the orientation of the magnetic dipoles from one polarisation state to the other. (See figure 4.23)

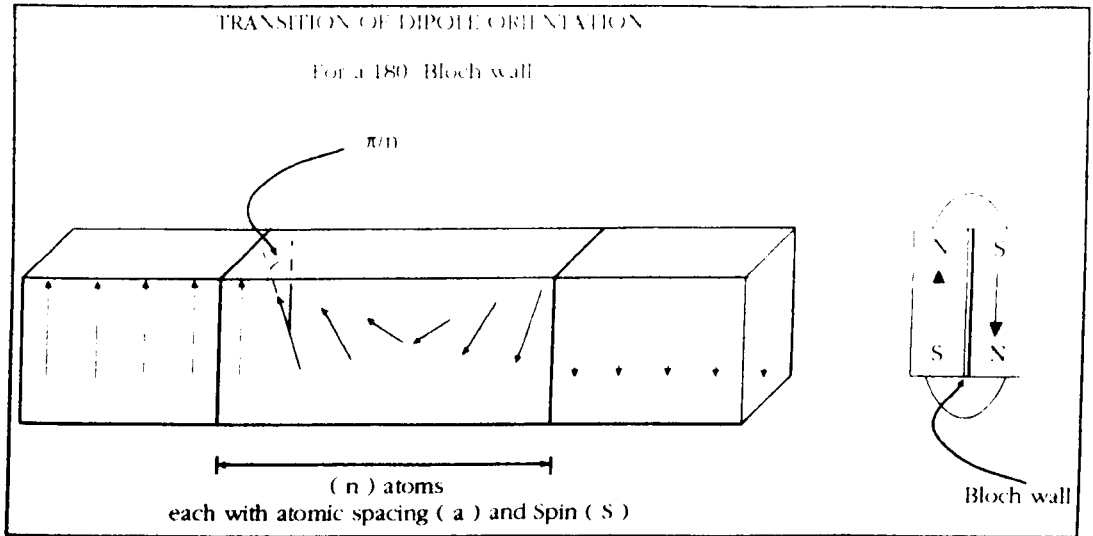


Figure 4.23

The reason the Bloch wall exists is to counter the dilemma one encounters when we look at the requirements for 'exchange energy' minimisation and 'anisotropy energy' minimisation at a domain boundary.

For 'exchange energy' minimisation, the spins, therefore the magnetic dipoles must be parallel to one another.

For 'anisotropy minimisation', the spins, therefore the magnetic moments, must be aligned along a certain 'easy axis'.

Therefore, within a Bloch wall for the exchange and anisotropy energies to be minimised a compromise of the above two statements must be met. This results in spins which are not parallel to an easy axis of the crystal and are not parallel to each other.

The energy required for domain wall formation is a direct sum of the 'exchange energy' and the 'anisotropy energy' :

$$E_{WALL} = E_{EX} + E_{AN} \quad \dots (4.18)$$

If the atomic spacing between the atoms is (a) and a wall consists of (n) atoms, where each atom has a spin (S) and the exchange integral is (J_{EX}). It can be shown that the contribution from the exchange term is :

$$E_{IA} = \frac{\pi^2 (J_{IA}) S^2}{na^2} \quad \dots (4.19)$$

It can be shown that the contribution from the anisotropy term is :

$$E_{AN} = Kna \quad \dots (4.20)$$

Therefore,

$$E_{WALL} = \frac{\pi^2 (J_{EX}) S^2}{na^2} + Kna \quad \dots (4.21)$$

Since the exchange interaction requires the dipoles to be parallel this term tends to increase the width of the wall. And since the anisotropy tends to align the dipoles along an easy axis, then this term tends to reduce the width. By minimising equation (4.21) with respect to (n) it can be shown that the width of a wall is ≈ 100 dipoles.

(4.17) Temperature Dependence Of A Magnetic Material & The Curie Point.

As the temperature of a ferromagnetic material is increased from absolute zero to a specific temperature, which is associated with the material, known as the 'Curie Temperature' (T_C) it can be shown that, the magnetization of the sample in question decreases from the saturation value (M_S) to zero at (T_C). At the Curie Temperature (T_C) and above, the thermal energy becomes great enough to overcome the exchange interaction within a ferromagnetic material and the system becomes paramagnetic. Before the intervention of interatomic interactions by quantum theory, Weiss explained the dissipation of the magnetization at the Curie temperature (T_C) thermodynamically. He postulated a fictitious field called the Weiss field (H_W), which is now explained by the exchange interaction, and is linked to the magnetization (M) such that :

$$\mathbf{H}_w = \lambda \mathbf{M} \quad \dots (4.22)$$

where, (λ) is known as the 'Weiss constant' and is specific to a material.

He deduced the magnitude of the Weiss Field, or the exchange interaction, to be equal to the thermal energy which is required to dissipate it at the Curie Temperature (T_C). Hence :

$$\mathbf{H}_w \approx \frac{k T_C}{g S \mu_B} \approx 10^7 \text{ Oersteds} = 125 \times 10^3 \text{ A/m} \quad \dots (4.23)$$

Which is much larger than the external field required to magnetise the ferromagnet into saturation.

It can be shown that the susceptibility (χ) of a ferromagnetic material is related to the Curie temperature (T_C) by the expression :

$$\chi = \frac{C}{T - T_C} \quad \dots (4.26)$$

where, (C) is the 'Curie Constant' and $T_C = C \lambda$ (for a ferromagnetic material). The behaviour of the susceptibility for the Paramagnetic and Ferromagnetic cases is shown graphically below (See Figure 4.24)²³

²³ Customised from pg 188, Ref [7]

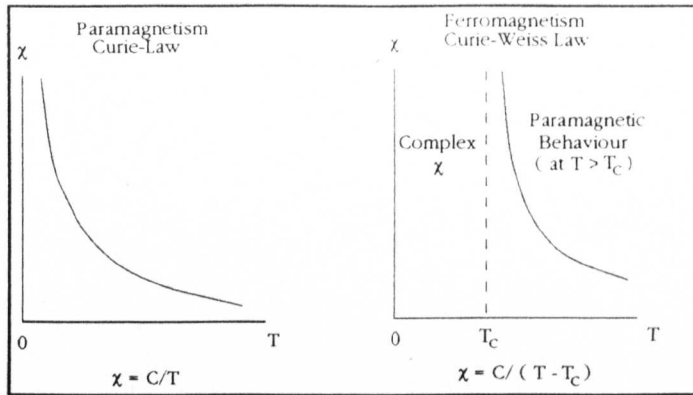


Figure 4.24

Therefore, as can be seen for the ferromagnetic case at temperatures $> T_c$ the curve represents that of the paramagnetic case and the ferromagnetic material behaves paramagnetically, due to the thermal energy overcoming that of the exchange energy.

Eight texts were mainly used in preparation for this chapter, which describes the fundamentals of magnetic behaviour. These are listed below.

Ref [1] Microwave Ferrites & Ferrimagnetics, B.Lax & K.Button, McGraw Hill.

Ref [2] Introduction to Magnetism & Magnetic Materials, D.Jiles, Chapman & Hall.

Ref [3] Magnetism & Metallurgy, Berkowitz & Kneller.

Ref [4] Magnetism Vol.I, Rado & Suhl.

Ref [5] Magnetism Vol.IIB, Rado & Suhl.

Ref [6] Magnetism Vol.IV, Rado & Suhl.

Ref [7] Solid State Physics, C. Kittel, New York, Wiley & Sons.

Ref [8] Reports On Progress In Physics Vol.XXIV (1961). Chapter on Magnetic Domains.

Chapter 5 Freespace Faraday Rotators & Quasi-Optical Isolators

Introduction

Faraday rotators are devices which exploit the non-reciprocal nature of the Faraday effect in their operation. The Faraday effect allows a Faraday Rotator to rotate a propagating linear polarised beam through a fixed angle. In addition, its non-reciprocal nature will rotate a forward travelling wave differently to that from a wave travelling in the reverse direction. A whole host of devices such as Faraday Rotators, Isolators and Circulators have incorporated this effect into their design. I intend to present in this chapter, an explanation of the criteria necessary to produce 'High Performance Freespace Quasi-Optical Faraday Rotators & Isolators'. The first sections will describe the Faraday Effect which defines the operation of the Faraday Rotator device. The proceeding sections will give an explanation of how one can create a Faraday Rotator and Quasi-Optical Freespace Isolator. A description of the materials used in Faraday Rotators/Isolators and how they maintain their 'High Internal Biassing Field' is then discussed. This is followed with a brief section on the processes involved in ferrite manufacture. The final sections will describe two experimental methods which I used to determine suitable magnetic materials for use in Faraday Rotators. The chapter is closed with an explanation of how one associates a figure of merit to an Isolator and the advantages that a Freespace Faraday Rotator/Isolator has over a conventional waveguide isolator.

(5.1) The Faraday Effect

The previous chapter on 'Magnetic Behaviour', details how ferrites and ferrimagnetic materials have the ability to retain their magnetism after being saturated by an externally applied magnetic field. As well as being magnetic, ferrites and ferrimagnets are also insulating. This provides a suitable medium to accommodate the interaction between the electromagnetic field of a propagating beam with the electrons of a ferrite. As will be shown, it is the magnetic dipole moment associated to the electrons' spin (μ_s) and its interaction with the magnetic field of the incident beam which are responsible for the non-reciprocal Faraday effect. Therefore, it is necessary to take a closer look at the spin magnetic dipole moment. It will be shown that the Faraday Effect can be described by firstly, examining how the spin-magnetic dipole moment is affected by a static magnetic field and then extending the examination by the introduction of an applied a.c. magnetic field of an incident beam into the scenario. Both these cases will now be considered separately.

(5.1.1) The Effect Of An Applied Static Magnetic Field On (μ_s).

Recapping from the previous chapter on 'Magnetic Behaviour', in addition to an electron orbiting an atom, it also rotates, or spins, about its own axis. This rotation of charge gives rise to the spin-magnetic dipole moment (μ_s) which is twice that of the orbital-magnetic dipole moment (μ_l), associated to the the electron's orbital motion, as described in section(2.2). The electron can be considered to spin with a constant spin-angular momentum (P_s). Furthermore, the direction of (μ_s) is antiparallel to the spin-angular momentum vector (P_s) and dependent on the direction of rotation of the spin. These intrinsic features of the electron are summarised in figure(5.1).

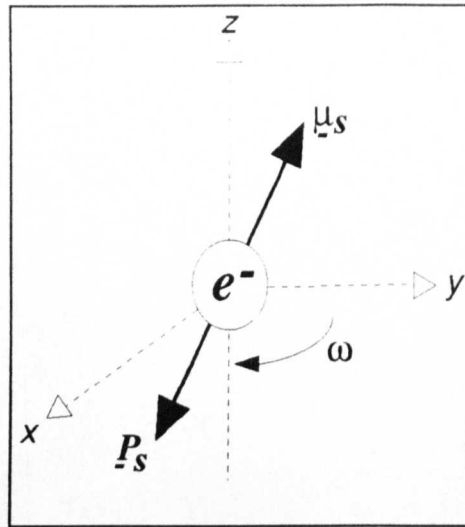


Figure (5.1)

As described by Hund's Rules, in section(2.8), there are a number of unpaired electron spins which each have an associated (μ_s). This gives rise to a net magnetic dipole moment which can be associated with each atom. For the unmagnetised case of the ferrite, domain formation occurs in order to minimise the magnetic energy of the sample, section(2.9), which effectively reduces the magnetisation of the sample to zero. In the magnetised case, all the domains align and the sample retains a magnetisation after the external field is removed. However, upon magnetically saturating the ferrite the electrons' behaviour is changed. This is due to the interaction between the static magnetic field and the spin contribution of the magnetic dipole moment.

As one can probably guess, the spin-magnetic dipole moment will be influenced by the static magnetic field in such a way that it lines up with it in order to decrease its magnetic potential energy. This will cause the electron to precess about an axis parallel to the static magnetic field, as shown in figure(5.2).

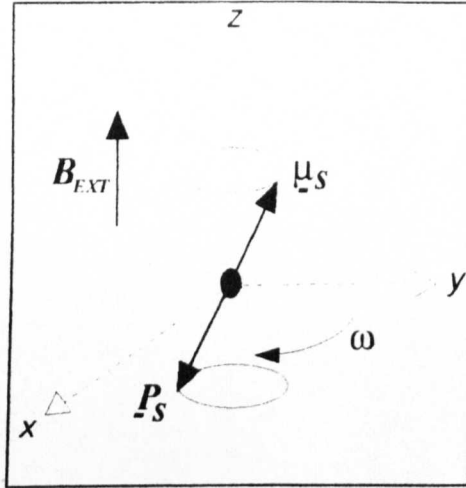


Figure (5.2)

An equation of motion can be derived to express this precession, by simply considering the torque (\underline{T}) that the external magnetic field (\underline{B}_{EXT}) on the spin-magnetic dipole moment ($\underline{\mu}_S$).

$$\underline{T} = \underline{\mu}_S \otimes \underline{B}_{EXT} \quad \dots (5.1)$$

The ratio of the spin-magnetic dipole moment ($\underline{\mu}_S$) to the spin-angular momentum (\underline{P}_S) is known as the 'gyromagnetic ratio' (γ) and is also expressed as :

$$\gamma = \frac{\underline{\mu}_S}{\underline{P}_S} \quad \dots (5.2)$$

Torque (\underline{T}) can also be expressed as the rate of change of angular momentum ($\frac{d\underline{P}}{dt}$). Thus, combining both of the above equations we arrive at the equation of motion. Where the (-ve) sign represents the antiparallel vector of (\underline{P}) in relation to ($\underline{\mu}_S$).

$$\underline{T} = \frac{d\underline{P}_S}{dt} = -\gamma \underline{P}_S \otimes \underline{B}_{EXT} = \gamma P_S B_{EXT} \sin\theta \quad \dots (5.3)$$

The angular velocity (ω_0) of the precessional motion can be expressed as :

$$\omega_0 = \gamma B_{EXT} \quad \dots (5.4)$$

Hence, the equation of motion can be re-expressed as :

$$\mathbf{T} = \frac{d\mathbf{P}_s}{dt} = \omega_0 \gamma P_s \sin\theta \quad \dots (5.5)$$

Where, (θ) is the precession angle that (μ_s) makes with (B_{EXT}) and (ω_0) is sometimes referred to as the 'Larmor frequency'.¹ This precession at the Larmor frequency is sometimes referred to as 'free precession'. The materials I investigated which will be described in Chapter(6) had Larmor frequencies ($\omega_0 \approx 50\text{GHz}$).

As explained in section(2.3), due to the proximity of the electrons in a ferrite, the exchange interaction causes a bulk effect precession of all the electrons in the solid. This linkage of all the individual precessions, gives rise to the solid having its own internal magnetic field (B_{INT}), such that :

$$\mathbf{B}_{INT} = \mu_0 \mathbf{H} + \mathbf{M} \quad \dots (5.6)$$

One can also rewrite the gyromagnetic ratio for a bulk solid. Since, the bulk analogue for magnetic dipole moment is 'Magnetisation' (\mathbf{M}) we get :

$$\gamma \propto \frac{\mathbf{M}}{\mathbf{P}_s} \quad \dots (5.7)$$

This can be shown to give an equivalent equation of motion for a bulk solid ferrite with its own internal magnetic field as :

$$\frac{d\mathbf{M}}{dt} = \gamma \mathbf{M} \otimes \mathbf{H} \quad \dots (5.8)$$

¹ Foundations for Microwave Engineering, Scholnik, Sect.6.6, pgs.(287-312),
 Microwave Propagation in Ferrites,

Where, the external magnetising magnetic field strength is denoted as (H) .

(5.2) The Effect Of A Propagating Beam Through A Magnetised Ferrite.

From the description above, one can now visualize the magnetised ferrite as a collection of magnetic dipoles that are all precessing in the same sense at the Larmor frequency. This is depicted in figure(5.3).

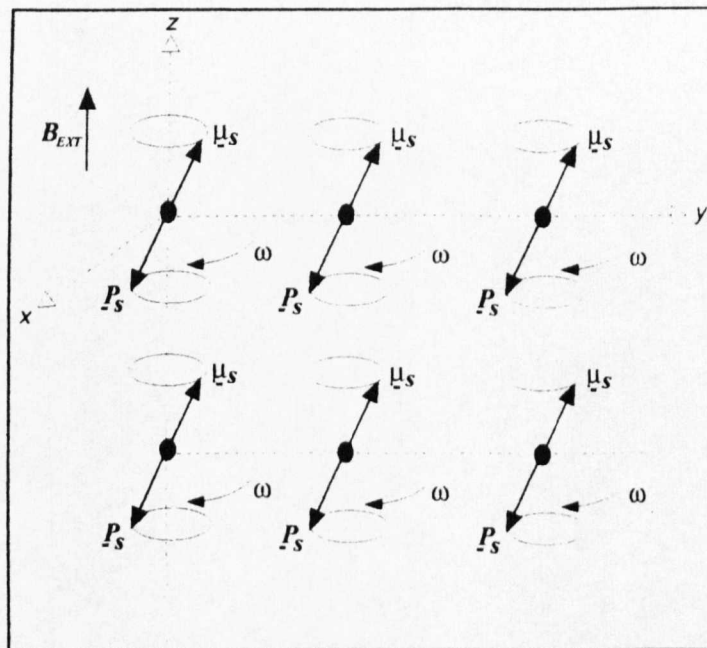


Figure (5.3)

The mathematical discussion of this interaction is described by Baden Fuller². From figure(5.3) the electrons are precessing in a clockwise manner. This is also referred to as a (+ve) or right handed sense. The best way to describe the effect of a linear polarised beam on the spin-magnetic dipole moment is to firstly decompose the linear polarised beam into its two constituent circular components. From the law of superposition, a linear polarised beam can be described as two equal in magnitude, counter rotating circular

² Microwaves 2nd Edition - An Introduction To Microwave Theory & Techniques, A.J. Baden Fuller, Chapter 7, Ferrite Media.

polarised states. One could intuitively expect, two different types of interactions to occur between each of these circular states and the precessing electrons. The type of interaction being dependent on the sense of rotation of the circular state with respect to the precessing electrons. This is in fact what happens ! As will be described, if the electrons are precessing in the same sense as the circular state then the circular state will have one particular permeability through the medium. However, if the electrons are precessing contrary to the circular state, the circular state will have a different permeability through the medium. Hence, an 'Effective permeability' can be associated to each circular state, as shown below :

$$\mu_{\pm} = \mu_0 \left(1 + \frac{\omega_m}{(\omega_0 \mp \omega)} \right) \quad \dots (5.9)$$

Where, (ω_0) is the Larmor frequency. Furthermore, $(\omega_m = \gamma\mu_0M)$ where, (γ) is the gyromagnetic ratio, (μ_0) the permeability of freespace and (M) is the magnetisation of the ferrite.

Similarly, a 'Propagation constant' (β_{\pm}) can be assigned to each circular state. The propagation constant is connected to the effective permeabilities (μ_{\pm}) , as shown below :

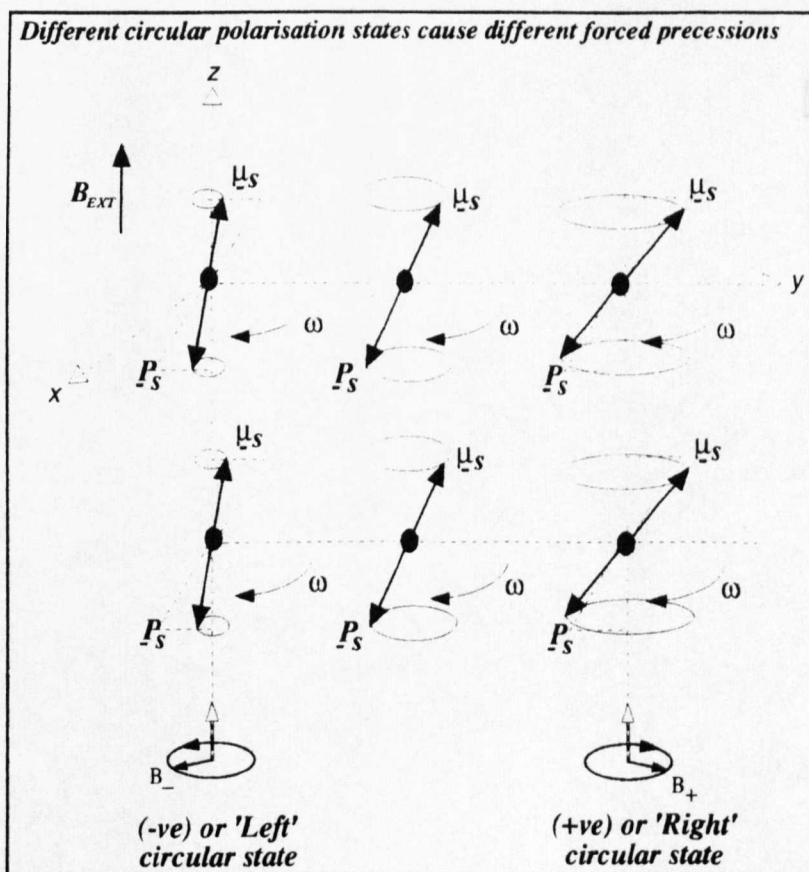
$$\beta_{\pm} = \omega\sqrt{\epsilon\mu_{\pm}} \quad \dots (5.10)$$

Where, (ϵ) is the permittivity of freespace and $(\omega = 2\pi f)$ where, (f) is the frequency of the incident radiation.

By convention, the electrons are taken to precess in the (+ve) or right handed sense, as shown in figure(5.3). Furthermore, since a circular polarised state still remains circular after propagation through the ferrite, it is known as the 'Fundamental mode' of

propagation of the ferrite.

As shown in figure(5.4), when the (-ve) or left circular state propagates through the medium, it will exert a torque on the electrons' spin-magnetic dipole moment ($\underline{\mu}_s$). The torque is such that it forces the electrons to reluctantly precess around a smaller circumference as compared to that during free precession. This type of precession is known as 'forced precession'. Due to the contrary rotation of the circular state, the electrons serve to retard the circular state and increase its path-length through the sample. For the (+ve) or right handed circular state, the electrons again undergo a forced precession. However, this time they are forced to describe a larger circumference to that described in free precession. Since the electrons and the (+ve) circular state are precessing in the same sense, a certain amount of interaction goes on together with an



Figure(5.4)

energy exchange. The amount of interaction that occurs between the electrons and the (+ve) circular state depends on the frequency of the radiation which will be described shortly. In general, the electrons serve to accelerate the circular state through the medium via a shorter path-length compared to that of the (-ve) circular state. When both the circular states combine together on exit of the ferrite, they will be out of phase with each other due to the different path-lengths that they each traversed. This will result in a linear beam that has been rotated through a given angle (θ), depicted in figure(5.5). The amount of rotation that is incurred upon the linear polarised beam is dependent on the propagation constants (β_{\pm}) of the two circular states and the thickness (L) of the ferrite :

$$\theta = \frac{L}{2}(\beta_{-} - \beta_{+}) \quad \dots (5.11)$$

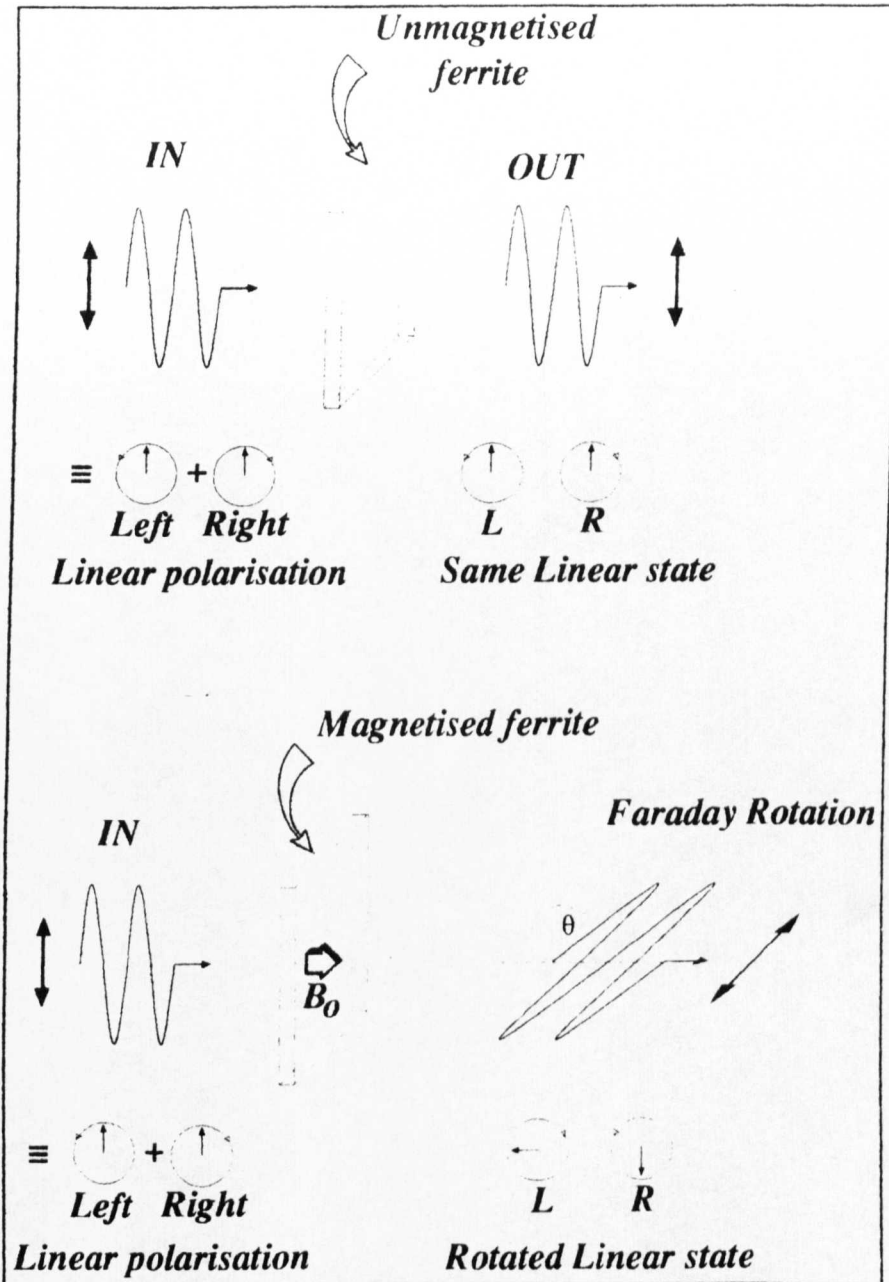


Figure (5.5)

(5.3) Frequency Dependent Interaction Of The (+ve) Circular State.

As mentioned earlier, the amount of interaction between the (+ve) or right circular state is dependent on the frequency (ω) of the incident radiation. As can be seen, equation(5.9) becomes infinite when $\omega \Rightarrow \omega_0$. The section will explain this region of interest together with what interactions occur between the (+ve) circular state and

the precessing electrons as (ω) is increased from below (ω_0) , through it and beyond. In order to understand the interactions it is necessary to take a closer look at the spin states that are possible for an electron and their interconnection with the magnetic dipole moment.

(5.3.1) Electron Spin States & Electron Spin Resonance

The existence of electron spin was first proved during the Stern-Gerlach experiment, in which a beam of silver atoms was split into two components by an inhomogeneous magnetic field. This is known as the 'Zeeman effect' and is shown in figure(5.6)

As described in section(5.1.1), the spin-magnetic dipole moment ($\underline{\mu}_S$) of the electron is antiparallel to its 'spin angular momentum' vector (\underline{P}_S) and directly proportional to it. However, the electron can exist in two spin configurations or states. There is the low energy spin state which I shall denote as $||\alpha\rangle$, sometimes referred to as the 'down' state. And a high energy spin state exists which I shall denote as $||\beta\rangle$, sometimes referred to as the 'up' state.

The Zeeman effect can be observed, when one places an electron in a uniform, static magnetic field (\underline{B}), of magnitude (B_0), say in the (z) direction. This causes a separation of the two spin states $||\alpha\rangle$ and $||\beta\rangle$, by an amount of energy (ΔE). This can be seen in figure(5.6). This is essentially what is happening when ferrites own internal magnetic field(B_{INT}) is acting on the electrons.

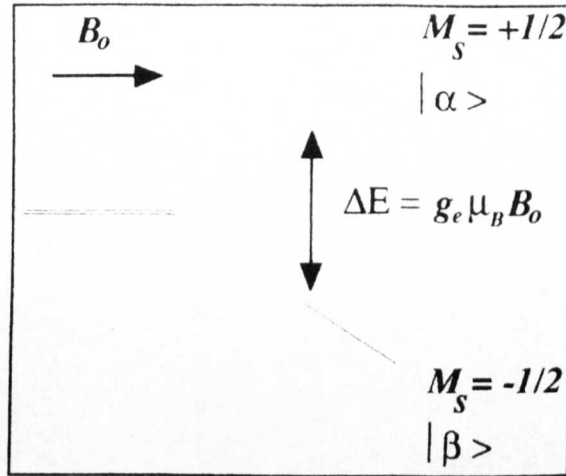


Figure (5.6)

The quantum of radiation (ΔE), which separates the two spin states can be described as :

$$\Delta E = h\nu = g \mu_B B_o \quad \dots (5.12)$$

Where, ($\mu_B = e\hbar/2m_e$) is the Bohr magneton and (g) is the 'G' factor of the electron which is equal to 2.0023.

This is known as the 'Bohr Frequency Condition' and is the amount of energy required to cause an electron's spin state to flip to the other spin state.

Now consider the a.c. magnetic field (B_1) of the (+ve) circular state, where ($B_1 \ll B_o$), which is rotating about the z-axis with some frequency (ω) and is in the same sense as the (ω_o) of the precessing electrons.

When $\omega < \omega_o$

The precessing spin-magnetic moment ($\underline{\mu}_s$) of the electron is not seriously affected by the field (B_1). This is due to the electron's oscillating xy component of ($\underline{\mu}_s$) passing in and out of phase with (B_1). This will result in very little coupling between the ($\underline{\mu}_s$) and (B_1). Hence, the resultant interaction will be very small.

However, when $\omega = \omega_0$

Due to thermal equilibrium, the electron will be initially in the lower spin state $|\beta\rangle$. One can by quantum mechanics work out the probability of the electron transitioning to the upper spin state $|\alpha\rangle$ ³. The most probable time for a spin transition to occur is when the 'Bohr Frequency condition', described by equation (5.12) is satisfied. This will occur when the energy brought into the system by the rotating magnetic field (B_1) is equal to or greater than the energy difference between the two spins states $|\alpha\rangle$ and $|\beta\rangle$. At the time when the frequency of rotation of (B_1) in the xy plane matches the 'Larmor Frequency' (ω_0) the Bohr frequency condition is satisfied and the system is said to be at 'Resonance'^{4,5}.

What this actually implies is that the magnetic field (B_1) now remains in phase with the electron's spin-magnetic moment ($\underline{\mu}_s$). Thus, from the electron's perspective, it sees a constant (\underline{B}) field. Since, the magnetic field of the circular state and the magnetic dipole moment are precessing at the same frequency, energy from the circular state is transferred to the electron. As described above, the energy transferred by the circular state allows the electron's spin to make a transition from the lower spin state $|\alpha\rangle$ to the higher spin state $|\beta\rangle$. After one quanta has been exchanged the electron will revert back to the lower spin state again. This process manifests itself by causing the electron's magnetic moment ($\underline{\mu}_s$) to eventually spiral down, over the surface of a sphere, until its projection on (-z) has the same value as it did at (+z). This is shown in figure(5.7). The electron will then resonate between these two extrema as long as the external, rotating (\underline{B}) field remains at the frequency (ω_0).

³ Principles Of Electron Spin Resonance, N.M. Atherton.

⁴ The Theory Of Ferromagnetic Resonance Absorption, C. Kittel, Physical Review, Vol.73, No.2, January 15th 1948.

⁵ Ferromagnetic Resonance, International Series Of Monographs In Solid State Physics, Pergamon Press, Vol.4, Editors S.V. Vonsovskii, 1966.

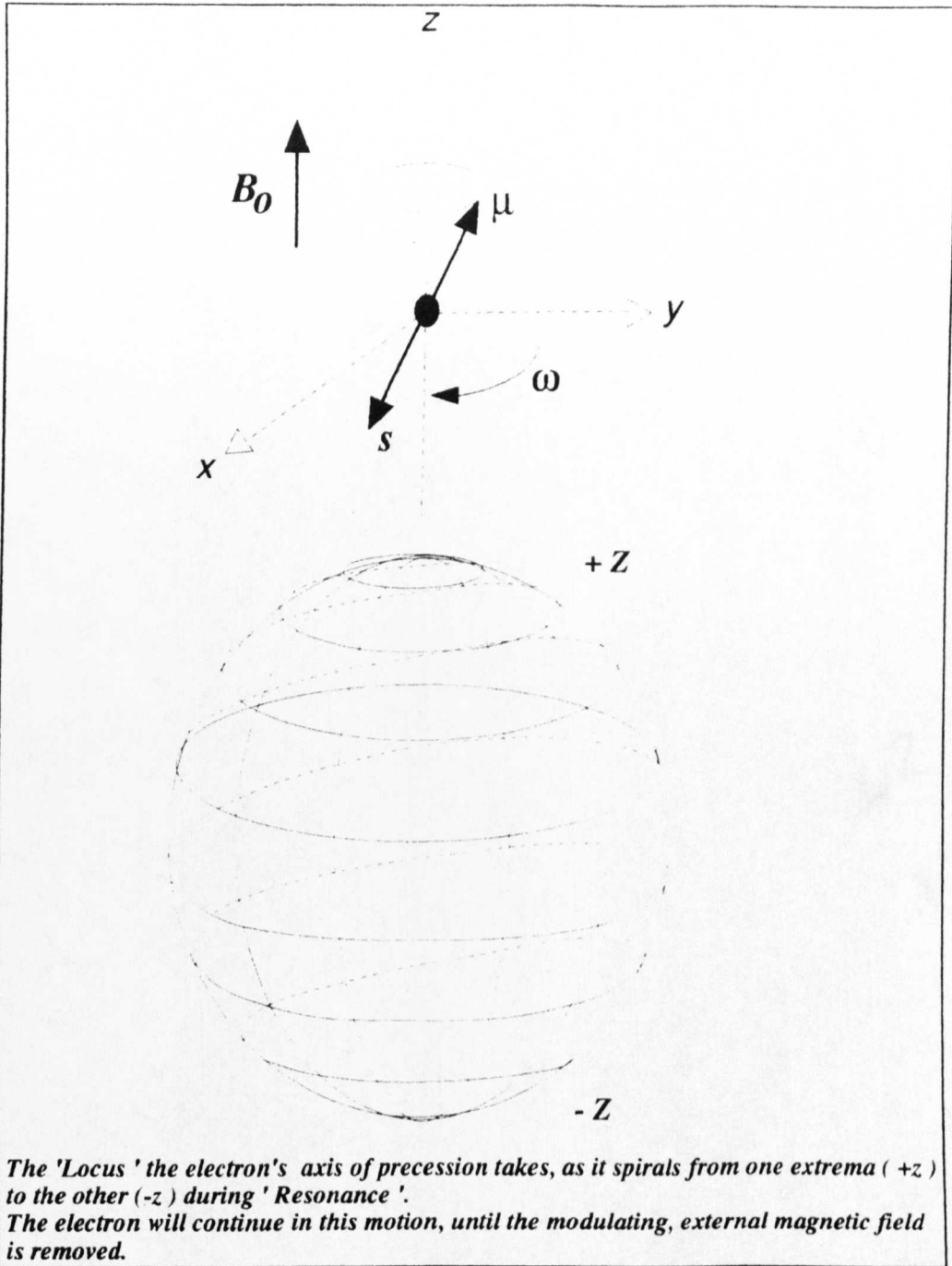


Figure (5.7)

At Resonance the energy possessed by the (+ve) circular state will be transferred to the electrons to be dissipated as heat. Hogan⁶ illustrates very well, the high attenuation of the (+ve) circular state due to resonance.

⁶ The Ferromagnetic Faraday Effect At Microwave Frequencies & Its Applications, C.L. Hogan, Reviews Of Modern Physics, Vol. 25, No.1, January 1953.

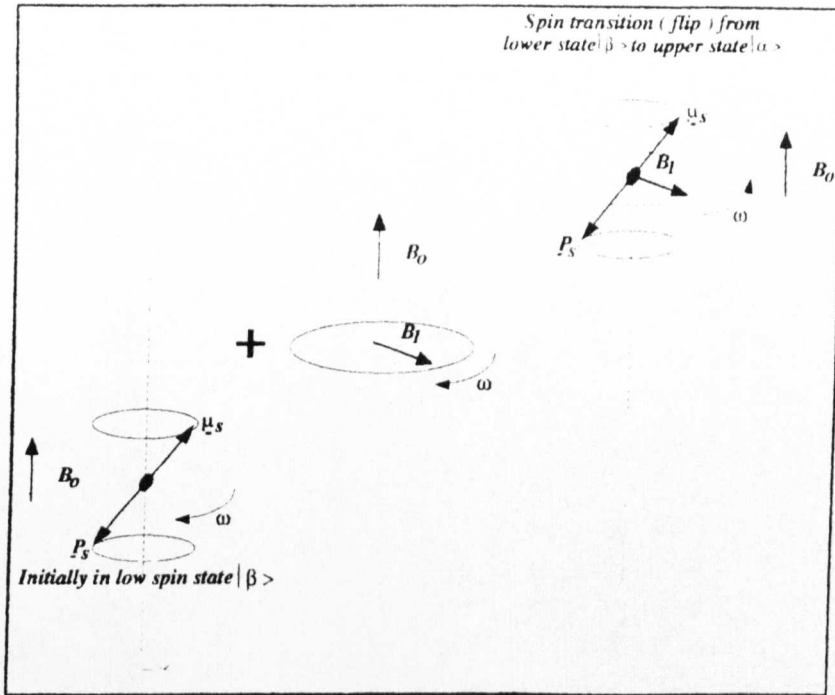


Figure (5.8)

When $\omega > \omega_0$

As (ω) is increased above (ω_0) , the rotating (B) field of the circular state loses synchronisation with the precessing electrons. Less energy is exchanged with the field and the electrons and the rotation exhibits a $(1/f)$ dependence as described by Lax and Button⁷. The dramatic change of rotation and the point of resonance can be seen in the rotation versus frequency plot of figure(5.9). As a short aside to accompany figure(5.9), the region in which the rotation varies with frequency is said to be the 'frequency dependent region'. Also there exists a region that occurs at $(\approx 4 \times \omega_0)$ in which the rotation remains constant with frequency. This is termed as the 'frequency independent region'. Both regions are depicted in figure(5.9). It is assumed that the graph represents the rotation of a typical BaM or SrM Hexaferrite which has a resonant frequency $(\omega_0 \approx 50\text{GHz})$. This implies that the frequency independent region exists at and above 200GHz.

⁷ Microwave Ferrites & Ferrimagnetics, B.Lax, K.Button, McGraw Hill Book Company, New York, 1962.

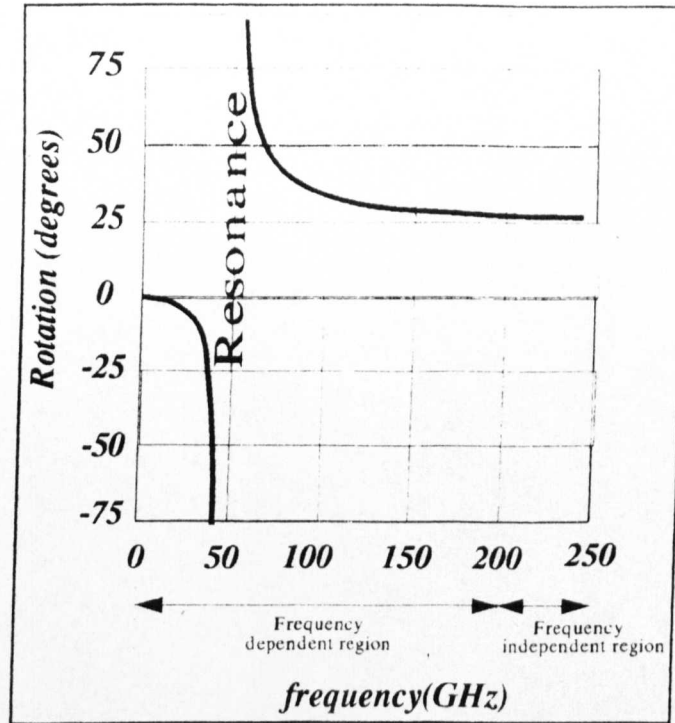


Figure (5.9)

(5.4) The Freespace Faraday Rotator.

The 'Freespace Faraday Rotators' which we produce here at St. Andrews basically consist of the following elements. The principle element consists of a square sheet (100mm^2) of ferrite material. The materials we have used up to now have consisted of 'Polycrystalline, uniaxial, anisotropic Barium or Strontium Hexaferrite' with a 'Magneto-plumbite' structure. However, this study also examined the same powdered material that has been embedded in a plastic matrix. (See Chapter(6), concerning the work on 'Plastoferrites'). Tests are firstly performed on the sample, to determine what the required thickness must be in order to give a 45° rotation on a single pass. All the tests are performed on a sample with its c-axis which contains the 'easy axis', described in section(2.14), to be perpendicular to the plane of the ferrite. After which the material is machined to the appropriate dimensions. The reason the c-axis is oriented in such a manner is in order to allow easy magnetisation of the sample. The sample is then placed in a 2 Telsa field with its

plane perpendicular to the lines of flux. This magnetically saturates the ferrite sample and when it is removed it exhibits the Faraday effect. The only other thing necessary, it to match the ferrite to freespace. This will allow a Gaussian beam to couple in and out of the ferrite easily. Thus minimising reflections from its surface. A suitable material is chosen which has a refractive index which is equal to the square-root of the refractive index of the ferrite. The thickness of the matching layer should be a quarter of a wavelength of the operational frequency of the device. However, in practice three quarter wavelength matching is employed. This is because at millimetric wavelengths, quarter wavelength matching is extremely thin and sometimes hard to machine accurately to this tolerance. Finally, one matching layer is affixed to either side of the ferrite with a thinned adhesive mixture. The 'Freespace Faraday Rotator Device' can be seen in figure(5.10)

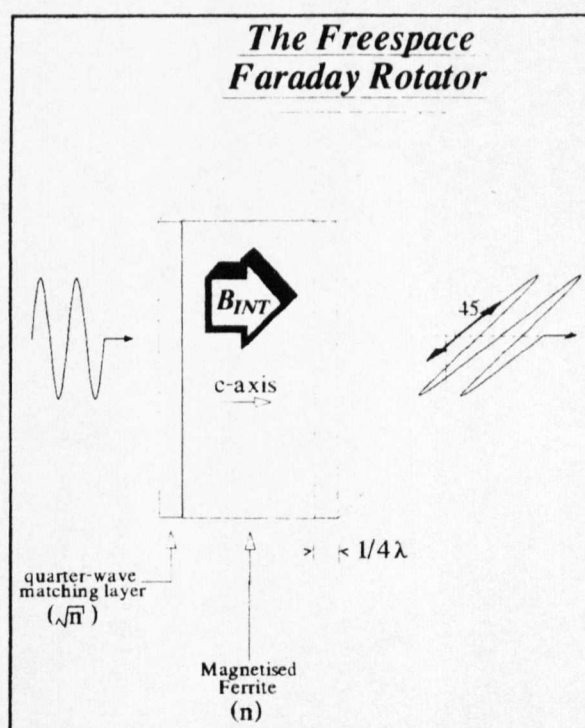
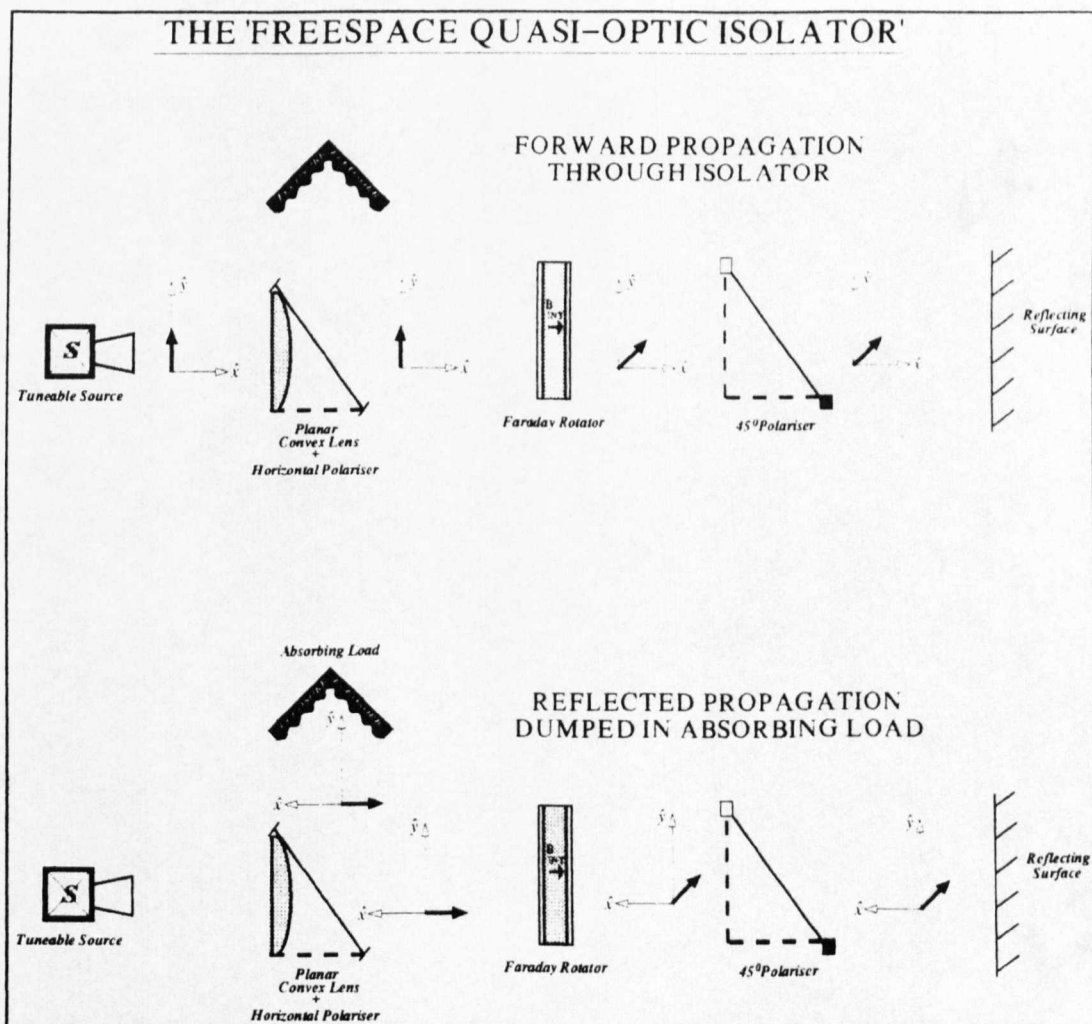


Figure (5.10)

(5.5) A Freespace Quasi-Optical Isolator

An Isolator is a device which employs a Faraday Rotator in its

makeup. The isolator is designed to divert any reflection which propagates back to the Faraday Rotator to a load. A quasi-optical isolator can be easily constructed by placing a horizontal polariser before the Faraday Rotator and by placing a 45° polariser after it, as shown in figure(5.11). Thus a vertically linear polarised beam will initially pass through the polariser and the Faraday Rotator. The Faraday Rotator will rotate the incident beam through 45° , thus passing through the 45° polariser. If one arranges for a reflecting surface to be located after the 45° polariser, the beam will propagate back through the 45° polariser, be rotated again through another 45° . This time, however, the (E) field is parallel to the horizontal polariser and is instead reflected to an Eccosorb load.



Figure(5.11)

The first freespace isolator that required no external field was developed by Wylde⁸ in 1985, using Ferroxdure 330. He attained 17dB's isolation at an operating frequency of 115GHz. Also a contribution was made by Dionn, Weiss, Allen and Fitzgerald in 1988⁹. Furthermore, the idea of a heat dissipative quasi-optical reflection circulator was suggested for high power applications at millimetric frequencies¹⁰. Here at St. Andrews a lot of work has been achieved developing High Performance Freespace isolators centred at 94GHz. This work was initiated by Webb¹¹ who produced a small aperture isolator of ≈ 30 dB's isolation. The work that involves Plastroferrite Isolators, covered in this thesis has been submitted in various papers^{12,13,14}.

(5.6) Suitable Materials¹⁵

The following section describes the material aspect of the Faraday Rotator/Isolator design. The main prerequisite of a material suitable for use in a Faraday Rotator/Isolator is that it possess a high internal biasing field (B_{INT}). This is in order to rotate the incident beam

⁸ R.Wylde, (Thesis) Chapter 4, Queens Mary College, England, 1985.

⁹ A Quasi-Optical Ferrite Rotator For Millimeter Waves, G.F.Dionne, J.A.Weiss, G.A.Allen, W.D.Fitzgerald, MTT Conference Symposium Digest, pgs. 127-130, 1988.

¹⁰ A Quasi-Optical Reflection Circulator, B.Lax, J.A.Weiss, N.W.Harris, G.F.Dionne, IEEE Transactions On Microwave Theory & Techniques, Vol.41, No.12, December 1993.

¹¹ A Millimeter-Wave Four Port Quasi-Optical Circulator, M.R.Webb, International Journal Of Infrared & Millimeter Waves, Vol.12, pgs.45-63, January 1991.

¹² Design, Analysis & Application Of High Performance, Permanently Magnetised, Quasi-Optical Faraday Rotators, G.M. Smith, C.P.Unsworth, M.R.Webb, J.C.G.Lesurf, IEEE MTT-S International Microwave Symposium (San Diego) Digest, 1994.

¹³ Microwave, Millimeter Wave & Submillimeter Wave Freespace Faraday Rotators, G.M.Smith, C.P.Unsworth, S.Kang, E.Puplett, D.Franklin, J.C.G.Lesurf, IEEE MTT-S International Microwave Symposium (Orlando) Digest, 1995.

¹⁴ Design & Applications Of High Frequency Quasi-Optical Faraday Rotators, G.M.Smith, C.P.Unsworth, S.Kang, D.Franklin, J.C.G.Lesurf, Berlin Conference 1996.

¹⁵ Magnetic Materials For Millimeter Wave Applications, G.P.Rodrigue, IEEE transactions On Microwave Theory & Techniques, Vol.MTT-11, pgs.351-356, September 1963.

through 45° in the shortest possible path-length possible. Thus minimising the attenuation incurred upon the beam. A variety of methods have been attempted in the past to obtain high biasing fields within a ferrite sample^{16,17,18,19,20}. Still as yet, however, the use of the 'Uniaxial, Hexagonal Barium or Strontium Magneto-Plumbite' compound ($\text{BaO} \cdot 6(\text{Fe}_2\text{O}_3) \equiv \text{BaO} \cdot \text{Fe}_{12}\text{O}_{19}$ or $\text{SrO} \cdot \text{Fe}_{12}\text{O}_{19}$) has not yet been superseded. The compounds are usually written in a shorthand notation BaM and SrM respectively, where (M) denotes the magneto-plumbite structure. As these materials have been the main source of this study some time will be spent explaining how their structure enables them to retain such a high internal biasing field.

The Barium Version was first developed by 'Philips Laboratories' who patented it as Ferroxdure 330^{21,22}. Although these were originally developed for use in permanent magnets and magnetically soft cores at frequencies at UHF, they also have found a major use in microwave applications. It is the hexagonal crystal structure of BaM and SrM that is responsible for its high internal biasing field. The internal magnetic field (\underline{B}_{INT}) consists of several contributing factors, as described in equation(5.13).

$$\underline{B}_{INT} = \mu_0(\underline{M} - \underline{H}_D + \underline{H}_A) \quad \dots (5.13)$$

Where, (μ_0) is the permeability of freespace, (\underline{M}) the magnetisation

¹⁶ Effects Of Some Additional For The Magnetic Properties Of Ba & Sr Oxide Magnets, H.Kojima, Sci.Rep.Res.Inst.Tohoku University, pgs. 175-182, 1958.

¹⁷ New Magnetic Anisotropy, W.H.Meiklejohn, C.P.Bean, Physical Review, Vol.105, No.3, February 1, 1957.

¹⁸ Hexagonal Ferrite Isolators, D.R.Taft, Journal Of Applied Physics, Vol.35, No.3, March 1964.

¹⁹ The Effect Of Grain Size On Saturation Magnetisation Of Barium Ferrite Powders, K.Torkar, O.Fredriksen, Powder Metallurgy, No.4, 1959.

²⁰ Anisotropy Fields Of Ba-Ferrite & Other Particulate Media, D.E.Speliotis, IEEE Transactions On Magnetics, Vol.24, No.6, November 1988.

²¹ Ferroxdure - A Clan Of New Permanent Magnet Materials, J.J.Went, Philips Tech.Rev., 13[7], pgs.194-208, 1952.

²² Ferroxdure II & III - Anisotropic Permanent Magnet Materials, A.L. Stuijts, G.W.Rathenau, G.H.Weber, Philips Tech.Rev., 16 [5-6], pg.141, 1954.

of the ferrite, (\underline{H}_D) the Demagnetisation Field and (\underline{H}_A) the Anisotropy Field. As will be shown it is the large (\underline{H}_A) field that is the source of the high internal biasing field (\underline{B}_{INT}).

(5.6.1) The Magnetisation Of The Sample (M)

The Magnetisation of the sample (\underline{M}) is defined as the total magnetic dipole moment per unit volume. Thus, for (η) dipoles ($\underline{\mu}_s$) the magnetisation can be expressed as :

$$\underline{M} = \eta \underline{\mu}_s \quad \dots (5.14)$$

The magnetisation acts in the direction which we have defined the magnetic dipole to point, i.e. from 'South to North'.

(5.6.2) The Demagnetisation Field (\underline{H}_D)

The Demagnetisation field is another contributor to (\underline{B}_{INT}) and as its name suggest its serves to demagnetise the sample. This can be explained by considering the magnetic flux lines created by a simple bar magnet. As is explained in section(2.13) the 'magnetostatic energy' is the energy provider for the magnetic poles of the magnet to link each other with magnetic flux lines. However, this flux linkage occurs within the sample, linking the 'North to the South' pole which is in opposition to the Magnetisation Field (\underline{M}). This internal linkage of flux can be described as a field (\underline{H}_D). Known as the 'Demagnetisation Field' it can be expressed as :

$$\underline{H}_D = N_D \underline{M} \quad \dots (5.15)$$

Since the Magnetisation (\underline{M}) effectively creates this field, the size of the 'Demagnetisation Field' is dependent on (\underline{M}). In addition, (\underline{H}_D) is also dependent on the geometric shape of the bulk solid. This as known as the 'Shape Factor' (N_D). As mentioned earlier, the Freespace Faraday Rotators/Isolators consist of a square sheet of

ferrite which has its c-axis perpendicular to its planar face. Magnetising the sample in the direction of the c-axis results in a shape factor ($N_D \approx 1$).

(5.6.3) The Anisotropy Field (H_A)

Since the electrons lie in a crystal lattice they cannot freely change their orientation in space. Instead there is an effective coupling between the individual spins of the magnetic ions with the crystalline electric fields associated to their neighbouring ions²³. Depending on the configuration of the neighbouring ions the spins will be aligned in a particular orientation. Due to the hexagonal symmetry of the crystalline structure there will be preferred directions of the orientations of the spins. As described in Chapter(4), these preferred orientations are known as 'Easy-axes'. Therefore, in the unmagnetised state the system will have spins aligned in certain orientations due to its own crystal structure. Since the crystalline structure effectively orients the magnetic spins, one can express this as a magnetic field associated to the crystalline structure of the material. This is known as the 'Anisotropy Field' and is expressed to the first order as:²⁴

$$\mathbf{H}_A = \frac{2K_1}{\mu_0 M} \quad \dots (5.16)$$

The hexagonal crystalline structure can be seen in figure(2.19) in Chapter(4). In BaM and SrM there is only one easy-axis which is aligned along the hexagonal axis, commonly referred to as the c-axis. When the c-axis and the easy-axis are aligned in this manner the material is said to be 'Uniaxial'²⁵.

²³ In fact the crystalline electric field actually couples directly to the orbital angular momentum. This in turn is directly coupled with the spin angular momentum.

Therefore, Indirect coupling exists between the crystalline electric field and the spin angular momentum.

²⁴ The full expression can be found in Chapter(4) equation(2.14).

²⁵ In the case, where the 'Hard-Axis' is aligned along the c-axis the material is referred

In reference to the last three sections and the main equation(5.13) one can see that for a Freespace Faraday Rotator/Isolator, such as the ones produced at St.Andrews, the Demagnetisation field (H_D) negates the Magnetisation (M). Therefore, the 'Internal biasing field' (B_{INT}) of the ferrite becomes²⁶ :

$$B_{INT} = \mu_0 H_A = \frac{2K_1}{M} \quad \dots (5.17)$$

Hence, the 'Internal biasing Field' is due solely to the Anisotropy Field.

BaM and SrM have extremely large 'Anisotropy Fields'

For BaM, $H_A = 17,000$ Oe. and $M = 5000G$ ²⁷.

For SrM at 94GHz, $H_A = 18,870$ Oe. and $M = 4700G$ ²⁸.

(5.7) Manufacturing Processes

Although it is really beyond the scope of this study, it is also worth pointing out that the manufacture of the material can be very crucial. In this section, I will highlight briefly some of the main areas of interest to my study and give reference for further reading.

A typical manufacturing process for Polycrystalline ceramic ferrite is shown in figure(5.12).

to as 'Planar'.

²⁶ Handbook Of Microwave Ferrite Materials, W.H.von Aulock (Editor), Academic Press.

²⁷ The Effect Of An Applied Magnetic Field On The Complex Permeability Of A Hexagonal Ferrite, G.G.Bush, IEEE Transactions On Magnetics, Vol.25, No.5, September 1989.

²⁸ Characterisation Of Strontium Hexaferrite For Millimeter Wave Applications, M.Labeyrie, T.M.Robinson, IEEE Transactions On Magnetics, Vol.Mag-22, No.5, September 1986.

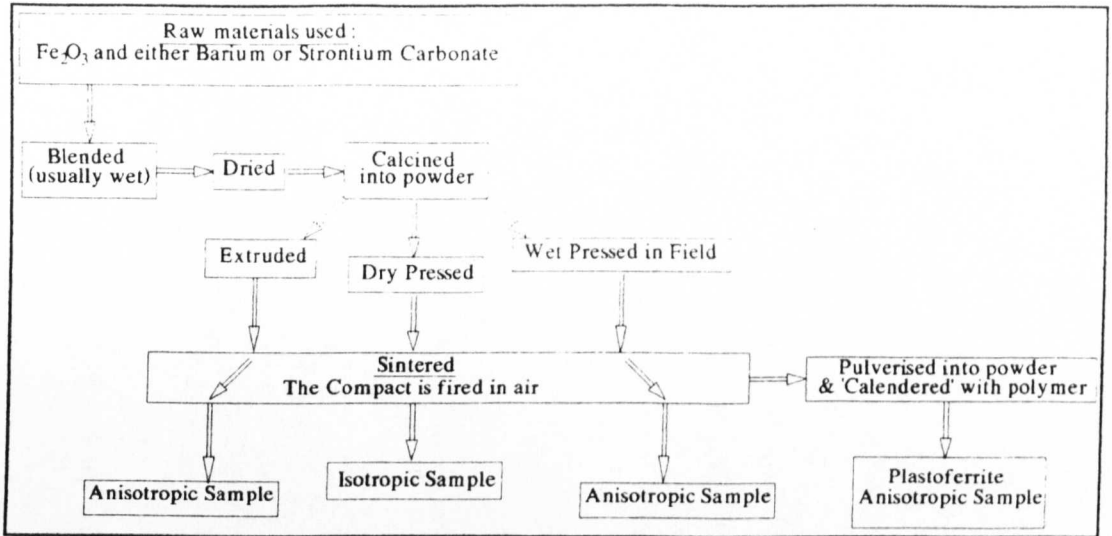


Figure (5.12)

There are various methods of macroscopic alignment which are employed.

'Die Pressing', where the material is injected into a compression space which is in the shape of a die. Magnetic coils around the die are then activated which tend to orient the particles with the field. The material is then compacted then demagnetised and removed.

During 'Extrusion', the ferrite material in the form of a paste is injected through a region that has a uniform magnetic field. In the case of BaM the platelike shape of the particles also assists in the orientation process. However, a degree of anisotropy is imposed on the material.

Factors such as permeability, Loss, alignment and porosity can all be affected by the manufacture process^{29,30}.

In a 'Calendering' process, a mixture of polymer and ferrite are passed closely between two rotating rollers. The rollers are rotating at different speed and hence shear the mixture. As well as dispersing the powder it also acts to orient the plate-like particles.

²⁹ Soft Ferrites - Properties & Applications, E.C.Snelling.

³⁰ Understanding Ferrites, A.Goldman, Ceramic Bulletin, Vol.63, No.4, 1984.

(5.7.1) Manufacturing Terminology

To add to the confusion, the manufacturers use a similar terminology to that used in the description of a ferrite's crystalline structure. The words 'Anisotropic', 'Isotropic' and 'Semi-Anisotropic' are all used in the manufacturers specification of the material. However, the words refer to the macroscopic alignment of the platelike particles within the material. Thus, a material specified to be Anisotropic after manufacture would suggest that there exists a common axis in which all the axes of the platelike particles align parallel to. This usually implies that the material has been exposed to some kind of field or has been calendered in order to orient the particulate. Similarly, when the manufacturers specify an 'Isotropic' sample, there is no preferential orientation of the axes of the platelike particulate. The above manufacturing terminology should not be confused with terminology used to describe the microscopic crystalline makeup of the ferrite. The hexagonal nature of the ferrite will lead it to be optically Anisotropic. This is an intrinsic optical feature of the material and is responsible for the 'high internal biasing field' and also the Linear Birefringence of the material. All the manufactures specification really tells us is whether the material will require a high external magnetic field to saturate the sample or not. In Chapter(6) which describes the plastoferrite work I undertook, I decided to use the manufacturers' specification of the materials investigated. This was in order to distinguish a particular batch of plastoferrite material from another.

For the Polycrystalline ceramic ferrites

A pore-free, dense structure is preferable. The grain size should be uniform and not a duplex structure. Inhomogenities, inclusions, stresses, cracks should be avoided. Sometimes, coprecipitation of $\text{BaFe}_{12}\text{O}_{19}$ before sintering is performed. This has been proved to create almost defect free single domain powders, discussed by

Haneda, Miyakawa and Kojima³¹.

At Low microwave frequencies close to resonance ($\approx 50\text{GHz}$)

An increase in porosity leads to a larger range of frequencies at which the resonance exists.

At High microwave frequencies

Small grain size is desirable and some porosity may be preferred to a dense structure³².

PlastoFerrites

Plastoferrites are composite materials. They are made up of the pulverised powdered form of BaM and SrM. The powder is then embedded in a plastic matrix which is a low loss polymer at the frequency of operation. In this plasticised form the ferrite is extremely robust.

(5.8) Limiting Features Of BaM and SrM

Ironically, the hexagonal nature of the BaM and SrM ferrites is also responsible for limiting their performance. The crystalline anisotropy of the material causes it to exhibit 'Linear Birefringence'³³. Namely, the material has two orthogonal axes within its plane which have different refractive indices. This serves to impose an ellipticity on the incident beam and to reduce performance of the device. However, as will be described in Chapter(9), there are ways in which one can overcome this problem to a certain extent.

(5.9) Experimental Methods Used To Determine Ferrite Material Parameters

There are a variety of methods one can characterise ferrites, as

³¹ Preparation Of High Coercivity BaFe₁₂O₁₉, K.Haneda, Miyakawa, H.Kojima, Research Inst. For Scientific Measurements, Tohoku University, Sedai, Japan, 1974.

³² Magnetic Properties Of BaFe₁₂O₁₉ Small Particles, K.Haneda, A.H.Morrish, IEEE Transactions On Magnetism, Vol.25, No.3, May 1989.

³³ As opposed to the 'Circular Birefringence' of the ferrite, where discrimination between circular states occurs with each being refracted differently.

described by Rachford and Forester³⁴ and also Afsar³⁵. The next two sections will describe the two methods which I employed to determine the material parameters for various ferrite samples. These methods are the Reflectance/Transmission Method and the Faraday Angle Resonance Method.

(5.9.1) The Reflectance/Transmission Method

One conventional way of determining the material parameters of a ferrite is by observing variation in the propagation of both circular states. The discussion of this method will be brief since it is covered in detail in Chapter(6). A detector can be positioned to examine this variation in either reflection or transmission of the circular state. Since the circular states traverse different path-lengths within the ferrite, it will result in different attenuation of each circular state. The variation of this attenuation with frequency can be measured for both circular states in unmagnetised and magnetised versions of the sample. From the measured data one can predict the variation in refractive index for each circular state with frequency. From the refractive indices of both circular states it is then possible to determine the required thickness of ferrite necessary for 45° rotation and how the thickness varies with frequency. As will be shown in Chapter(6), these types of measurement prove very laborious and time consuming. It is also necessary to take results for both the unmagnetised and magnetised versions of the sample for both circular states. In addition, at least three samples are needed of varying thicknesses to determine the final parameters of the ferrite.

(5.9.2) The Faraday Angle Resonance Method

The exploitation of a phenomena known as Faraday Angle

³⁴ Characterisation Of Magnetic/Dielectric Materials At Millimeter-Wave Frequencies, F.J.Rachford, D.W.Forester, IEEE Transactions On Magnetics, Vol.Mag-19, No.5,Sept.1983.

³⁵ The Measurement Of The Properties Of Materials, M.N.Afsar, Proceedings Of The IEEE, Vol.74, No.1, January 1986.

Resonance was recently proved as a new method to determine material parameters for ferrite materials. The method of assessing magnetic samples was suggested and demonstrated experimentally by Raum³⁶ at 290GHz. Raum obtained results for Trans Tech TT1-105 and Philips Ferroxdure 330 which agreed very well to the manufacturers specification. This method of assessment has advantages over the 'Reflectance/Transmission' measurements, described earlier. These advantages are as follows :

- Complete determination of material parameters from one experimental run
- Parameters calculated from very simple formulas
- Determination of Faraday Rotation/single pass, Dielectric constant (ϵ_r), Saturation Magnetisation (M_s) and also an estimate of the loss factor ($\tan\delta$).

Faraday Angle Resonance exploits the internal multipath reflections that occur within an unmatched ferrite. If a linear polarised wave passes through a ferrite it will be rotated by the Faraday Effect through an angle (θ). When it reaches the air/ferrite interface at the other side of the ferrite, part of it will be transmitted and part reflected back into the sample. These multiple reflections within the ferrite sample will also produce further transmissions at the same air/ferrite interface. However, these transmissions will have accumulated different amounts of Faraday rotation depending on their path-lengths traversed. Therefore, the resultant beam that travels toward a detector will be a superposition of these multiple transmissions which could be very different to the rotation incurred on a single pass through the ferrite. Raum calculated in his paper, that because of the multipath effect the resultant Faraday angle will differ with frequency for an unmatched magnetised ferrite. Furthermore, he discovered that the Faraday Angle will oscillate with frequency between two extreme angles in a resonant type manner. These extreme angles are referred to as the maximum and

³⁶ Quasi-Optical Measurement Of Ferrite Material Parameters At Terahertz Frequencies By A New Method: Faraday Angle Resonance, Michael Raum, International Journal Of Infrared & Millimeter Waves, Vol.15, No.7, 1994.

minimum Faraday angles, namely ($\Delta\varphi_{MAX}$) and ($\Delta\varphi_{MIN}$) respectively. Raum demonstrated that by very simple measurement of these extreme angles one can determine the amount of Faraday rotation that occurs in a single pass ($\Delta\varphi$) through the ferrite. This is expressed in equation (5.18) below :

$$\Delta\varphi = \tan^{-1} \sqrt{\tan(\Delta\varphi_{MAX}) \tan(\Delta\varphi_{MIN})} \quad \dots (5.18)$$

The optimum thickness (L_{OPT}) required for 45° rotation can also be deduced as :

$$L_{OPT} = L \cdot \frac{\pi}{4\Delta\varphi} \quad \dots (5.19)$$

where, (L) is the thickness of the ferrite sample.

Furthermore, the product ($M_s\sqrt{\epsilon_r}$) can be calculated. Where (M_s) is the 'Saturation Magnetisation' of the ferrite, measured in (A/m) and (ϵ_r) is the dielectric constant.

$$M_s\sqrt{\epsilon_r} = \left(\frac{2cm_e}{\mu_0q_e} \right) \frac{\Delta\varphi}{L} \quad \dots (5.20)$$

where (c) is the speed of light, (m_e) the mass of an electron, (μ_0) is the permeability of freespace and (q_e) the electronic charge.

A course estimate to the dielectric constant (ϵ_r) can be made which is shown below :

$$\epsilon_r = \left(\frac{c}{4L |f_{MAX} - f_{MIN}|} \right)^2 \quad \dots (5.21)$$

Where (f_{MAX}) and (f_{MIN}) are the frequencies at which the maximum and minimum Faraday angles occur.

The experiments that Raum performed were at 290GHz with ferrites that had a resonant frequency of (≈ 50 GHz). This means that the results, shown in the schematic profile of figure(5.13), occurred in the frequency independent region of the ferrite and are reflected in

the fact that $(\Delta\varphi_{MAX})$ and $(\Delta\varphi_{MIN})$ remain constant. This means that the rotation/single pass $(\Delta\varphi)$ will also remain constant and hence (L_{OPT}) will remain constant which is to be expected for this region.

The 'Fully Automated Millimetric Rotary Polariser Quasi-Optical System' that I developed, described in Chapter(9), can also be used to assess ferrites using this method. However, the profile of the results is expected to be different. This is because the experiments will be performed in the frequency dependent region of the ferrite. The profile one intuitively expects is also shown schematically in figure(5.13). Since the rotation is now varying with frequency one expects this to be evident in a variation of $(\Delta\varphi_{MAX})$ and $(\Delta\varphi_{MIN})$.

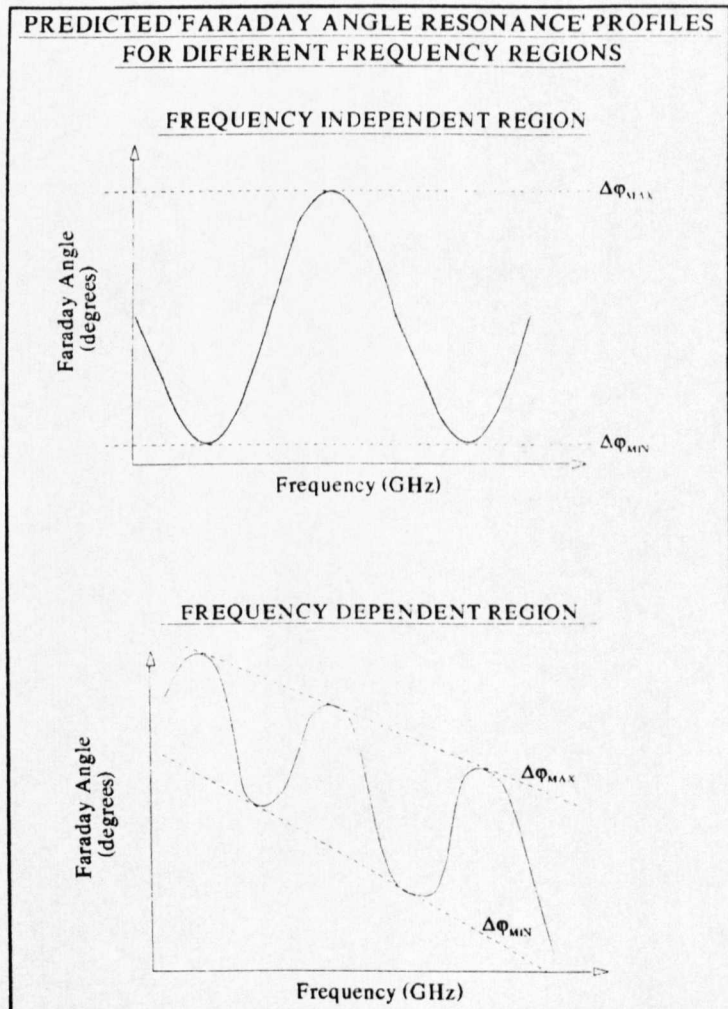


Figure (5.13)

The variation in (Δq_{MAX}) and (Δq_{MIN}) will also result in different optimal thicknesses being required for different frequencies. It is expected to show with the final fully automated system that this trend does in fact result in the millimetric frequency dependent region of the ferrite. It is hoped this will give a further insight into the study of Faraday angle Resonance and also to compliment the original work performed by Raum.

(5.10) Characterisation Of A 'Freespace Faraday Rotator & Isolator'.

The final section of the chapter, will discuss the performance criteria required in order to produce a High Performance Faraday Rotator or Isolator.

There are two key factors which describe how an isolator performs. These factors are its 'Isolation' and 'Insertion Loss'. The isolation is a measure of how efficiently the Faraday Rotator or Isolator is rotating the (E) field through 45° . Therefore, a high performance isolator would have a very high isolation figure, expressed in dB's. The insertion loss is a measure of the material loss of the isolator in a single pass, assuming the ferrite is perfectly matched. Again this is expressed in dB's. Manufacturers usually supply graphical records of the isolation and insertion loss for the range of operating frequencies of the device. The method by which one can experimentally determine these figures is described in Chapter(2).

As well as isolation and insertion loss, the operating bandwidth of the device is sometimes specified. This is accompanied by the value of the lowest isolation occurring in the region. Sometimes if particularly high isolations have occurred they are specified as 'Spot Frequency Isolations'.

In addition, the linearity of the polarised beam must be preserved. When characterising isolators conventionally, the ellipticity is never measured directly. However, an ellipticity evoked upon the beam will tend to reduce isolation and increase the insertion loss figure. In the final Chapter, the ellipticity issue will be addressed and an

experimental arrangement will be described in which this factor can be measured.

Therefore, in order to produce a 'High Performance Freespace Faraday Rotator/Isolator' the desirable features are :

- High Isolation
- Low Insertion loss
- Large operating Bandwidth
- Linearity Of The Polarised Beam (No ellipticity incurred)

The Advantages of the Freespace version of the Faraday Rotator/Isolator over a conventional waveguide isolator can be summarised in the table below:

<u>Freespace Faraday Rotator</u>	<u>Conventional Waveguide Isolator</u>
No External Field required	Biassing Permanent Magnet Needed
Large Aperture	Limited to a Waveguide aperture
High Isolation >20dB	Moderate Isolation 15-20dB
Low Insertion < 1dB	Moderate Insertion 1.5dB
Bandwidth 20GHz	Bandwidth 20GHz
Freestanding Fits into existing Quasi-Optics	Needs to be Interfaced with Waveguide
Plastoferrite Versions Extremely Robust	Fairly Robust
Easy To Manufacture	Hard To Manufacture
Low Cost (≈ £100)	Very Expensive (≈ £3000 +)

Chapter 6

Plastoferrite Investigation

Introduction.

The purpose of this chapter is to determine the suitability of three commercially available plastoferrites for use as the integral part of a 'Free-space, Quasi-optical Faraday Rotator'. The essential features of a high performance Faraday rotator involve a combination of large rotation/mm and negligible loss/mm of sample. By investigating the reflectance variation of -ve and +ve circular polarised light in magnetised and unmagnetised versions of a sample, I will demonstrate how the above mentioned features can be assessed and hence determine the most suitable plastoferrite for use in this application. The chapter consists of several subsections which introduce the reader to the experimental apparatus involved, a methodology (describing how the measurements were taken and interpreted), experimental results obtained for each of the three types of plastoferrite and curvefitting techniques to model the data obtained. The final sections document the performance of three Freespace Faraday Rotators that were constructed from the plastoferrite materials. The chapter is concluded by a summary of how the plastoferrite Rotators perform in comparison with conventional rotators and whether the plastoferrites are a viable option for use in Faraday Rotators.

(6.1) Experimental Reflectance Setup.

This subsection describes the experimental setup that was used to investigate the three types of plastoferrite. As will be discussed in more detail, in the experimental methodology section (6.2), the objective of the experiment was to create left and right circular

polarised wave states and to allow them to propagate through unmagnetised and magnetised versions of each of the three types of plastoferrite. This would allow one to then observe how the refractive index of each circular state behaved with frequency. It is necessary to create the circular states and to observe how their refractive indices behave with frequency because, as we know, it is these circular states which propagate through a magnetised sample at different rates (which can be observed as a differing refractive index for each circular state).¹ And it is this difference in the refractive index, that is responsible for the 'Faraday rotation' in the sample. The refractive index cannot be measured directly through experiment, but instead can be determined indirectly from measurement of how the reflectance of the sample varies with frequency, the relationship of which will be explained in section (6.2).

Therefore, the objective of the experimental setup was to :

- Create right and left circular polarised states.
- to record the variation in reflectance of each circular state for a given sample.

The experimental apparatus I used to satisfy the above two criteria, which I will now refer to as the 'Reflectance Setup', consisted of a modified version of the 'Martin-Puplett Interferometer' (MPI)². The MPI is a commonly used circuit configuration in optics and has a whole host of uses. In its basic operation (See Figure 6.1) it consists of two polarising structures: one horizontal polariser and the other a 45⁰ polariser (the beamsplitter), separated by a planar convex lens. In the reflection and transmission arms of the beamsplitter are located a fixed roof mirror and a moveable roof mirror respectively.³

¹ As described in sections (5.2 & 5.3)

² A polarising version of the Michaelson Interferometer

³ Millimeter-Wave Optics, Devices & Systems, J.C.G.Lesurf, Adam Hilgar Publishers, Chapter 9 for a more thorough discussion on the MPI.

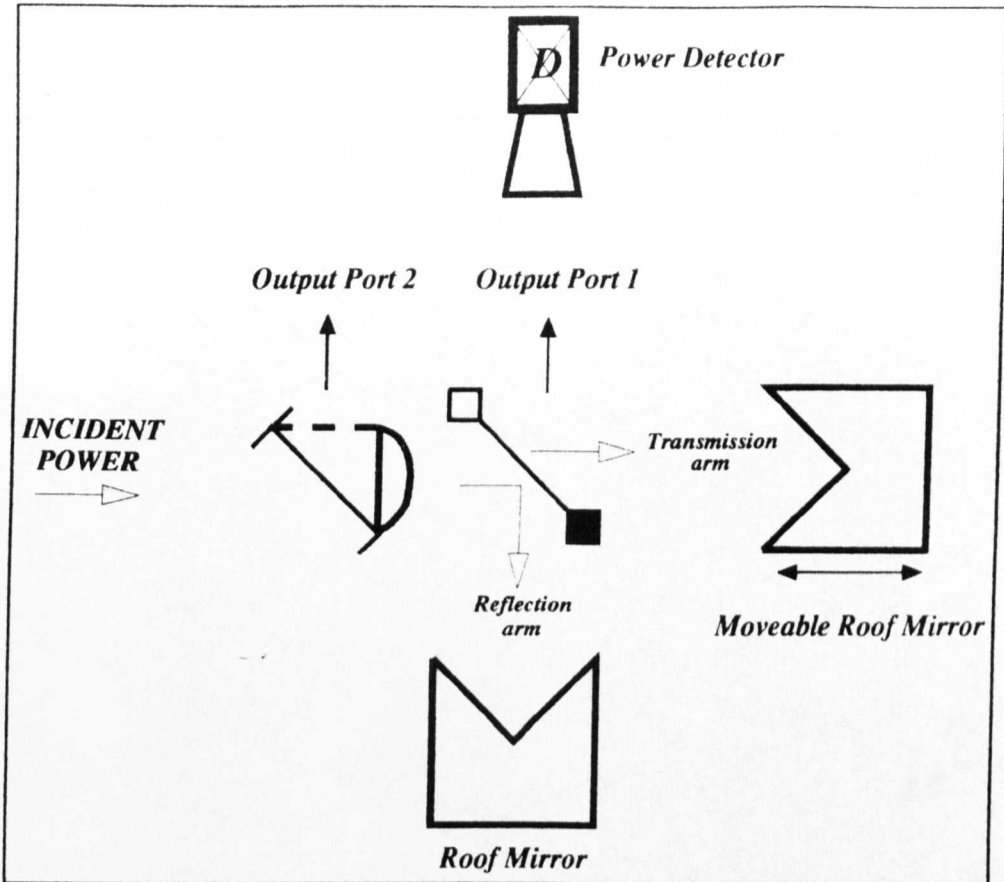


Figure 6.1

Incident power can then be modulated by adjustment of the moveable roof mirror, which is then sensed by a detector located at output port 1.

The experimental objectives can be satisfied by modifying the above mentioned MPI setup, in the following manner. The right and left circular states can be created by the adjustment of the moveable mirror. This will be explained in detail in the 'Experimental Methodology', section (6.2). The reflectance of the sample can be determined by interchanging a polished reflecting surface with a ferrite sample at output port 1 and relocating the detector to output port 2, in the basic MPI configuration, also to be described further in section (6.2). The new Reflectance Setup is shown in Figure (6.2)

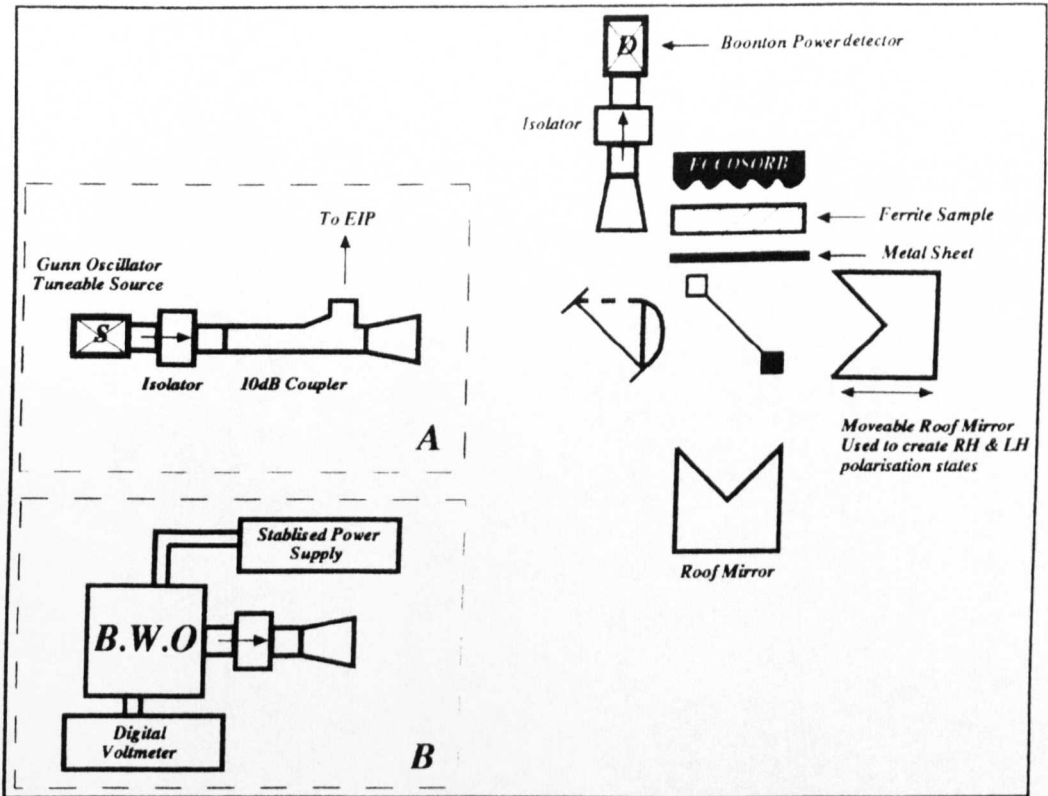


Figure 6.2

The experiments were performed over the frequency range 70 - 160 GHz, which starts at the W-band, millimeter, region and moves into the low end of the submillimeter region, at approximately 100GHz. Since measurements were being performed in two different regions of the electromagnetic spectrum. It was necessary to use appropriately designed equipment, specific to the two regions in question. This is to ensure correct production and efficient propagation of the radiation to freespace. Each region required a suitable source, feedhorn and correctly sized waveguide structures. Measurements from 70-100 GHz were performed using standard W-band equipment (namely, Gunn oscillator, waveguide 27 isolator, 10dB coupler and a corrugated feedhorn - Setup A). The frequency of the source was determined by an EIP frequency counter. Measurements from 100-160 GHz were performed with Setup B (namely, Backward Wave oscillator (BWO), stabilised power supply, waveguide 29 isolator and corrugated feed). The frequency of operation of the BWO was determined by means of taking the

digital voltmeter readout and referring to a lookup chart (Figure 6.3).

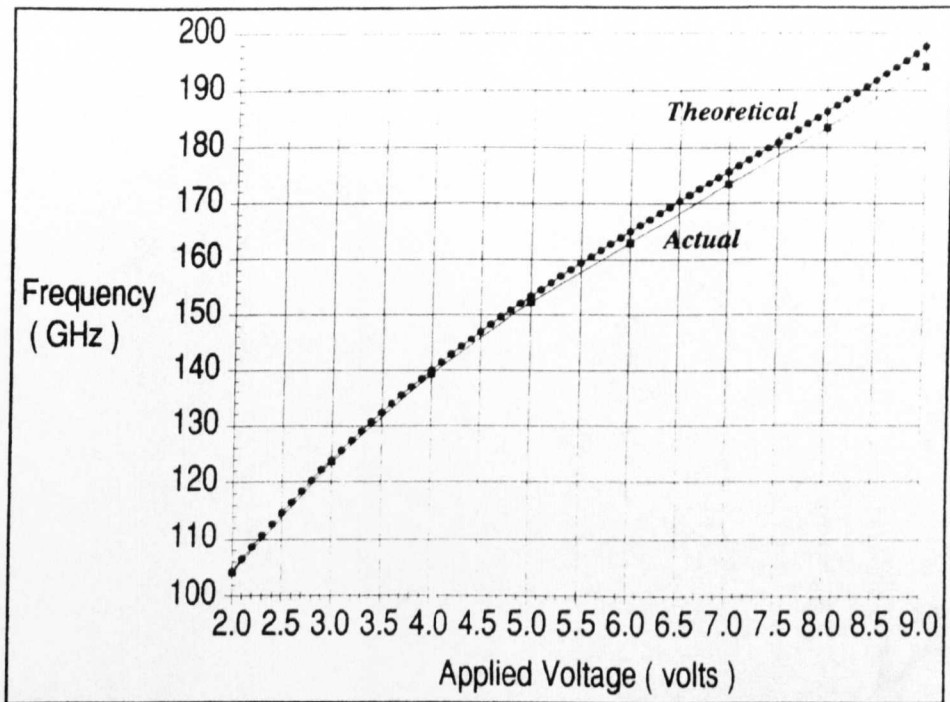


Figure 6.3

The source and detector feedhorns of Setup B were of a much greater radius than the standard W-band horns normally employed. Although, the half-cube, quasi-optical structures used here at St. Andrews were designed for W-band⁴, they would still operate efficiently above this region and also our region of interest. However, different lenses would have to be incorporated into the 'Reflectance system' and new Z_{IN} 's (> 2.5 times that at W-band) would have to be calculated to allow correct propagation of the submillimeter radiation through the system. It was found in order to give optimum performance (i.e. to have good beam to lens coverage and good throw) that 2 lenses were required for the 100 - 160 GHz range. The lenses to be used were determined as follows.

⁴ Designed by Andy Harvey. See Harvey A.R., Thesis, A Millimeter Wave Quasi-Optical Complex Impedance Bridge, Chapter 4.

The feedhorn had a radius $a = 1.2 \times 10^{-2} \text{ m}$

\Rightarrow effective beamwaist radius of $\omega_0 = 0.6435a = 7.7 \text{ mm}$

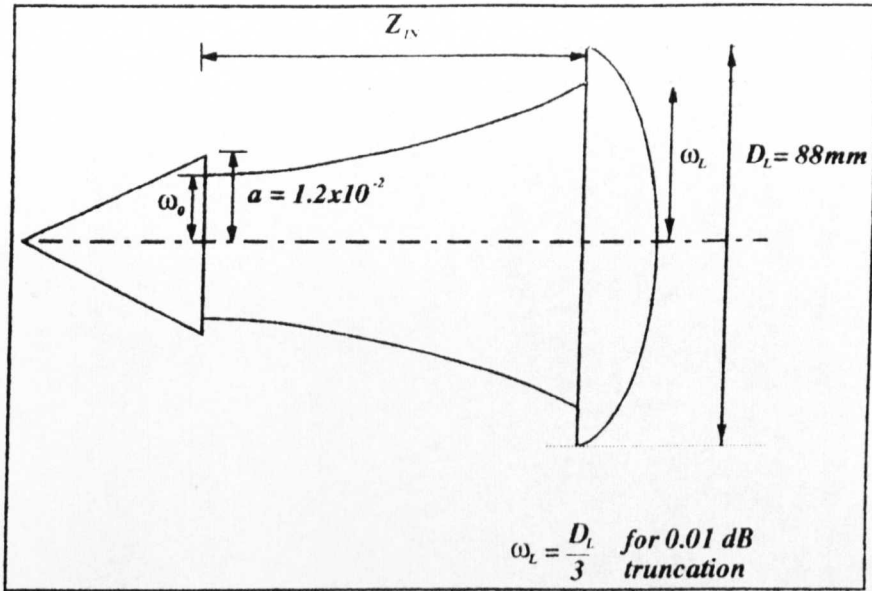


Figure 6.4

The reflectance system was designed to incorporate planar convex lenses of diameter ($D_L = 88 \text{ mm}$). In order to keep truncations to a minimum ($< 0.01 \text{ dB}$) and to have good beam to lens coverage the beamwaist radius (ω_L) at the lens should be no greater than $(\frac{D_L}{3})$. (See fig 6.4). The beamwaist radius (ω_L) at the lens was calculated using :

$$\omega_L = \omega_0 \sqrt{1 + \left(\frac{Z_{LN}}{Z_R} \right)^2} \quad \dots (6.1)$$

And the corresponding Z_R 's and ω_L 's determined for each lens (See figure 6.5)

	17.9mm lens		9.7mm lens	
frequency	100GHz	130GHz	130GHz	160GHz
λ (mm)	3.0	2.3	2.3	1.9
Thickness (mm)*	17.9	17.9	9.7	9.7
Z_{IN} (mm)	209.3	199.0	277.6	272.3
Z_R (mm)	62.1	80.7	80.7	99.3
ω_{LENS} **	27.1	20.5	27.5	22.4
Max throw (1/2 cubes)	4.1	3.8	4.6	4.7

* Includes 3mm lip.
** < 29.3mm for 0.01dB truncation

Figure 6.5

(6.2) Experimental Methodology

The following section is a detailed explanation of how the experiment was performed. As mentioned in the earlier section (6.1) there were two main objectives of the experiment. The first objective was to create right and left circular polarised wave states from a input which is a linear polarised wave The second objective was to record the variation of the reflectance of each of the circular states with frequency. The way in which these objectives were achieved will now be discussed.

A circular state can be defined when two orthogonal components are out of phase by ($\pm \frac{\pi}{2}$ rads). The creation of either a right or left circular state from a linear polarised wave was achieved using the 'Reflectance Setup' by adjustment of the moveable mirror. The creation of the above mentioned circular states initially started at the 45° polariser (or beamsplitter) where the incident linear polarised state is split into two orthogonal components. One component is reflected intially by the beamsplitter and propagates to the roof mirror, where its \underline{E} vector is rotated by 90° before it re-enters the beamsplitter where it is now transmitted and recoupled back with the other orthogonal component. The other orthogonal component is intially transmitted toward the moveable roof mirror, its \underline{E} vector

also being rotated through 90° . However, the distance it travels could be varied by the moveable mirror, hence resulting in a change of phase, with respect to the other orthogonal component. By varying the roof mirror, so that the component travels $(\pm \frac{\lambda}{2})$ further/shorter than the other orthogonal component one can create either a left or right circular state when both components recouple back at the beamsplitter before moving toward the sample.

After creating the desired circular state, the next objective was to record the reflectance of the sample, which was performed in the following way. Firstly, one needed to calibrate the detector to a standard known reflectance. This was achieved by allowing the newly created circular state to propagate firstly to a highly reflecting, flush metal plate where it is totally reflected back to the beamsplitter, where the reverse of the above mentioned process occurs except the resultant linear polarised \underline{E} vector has been rotated through 90° to the incident \underline{E} vector and is therefore reflected by the horizontal polariser and registered by the detector. The detector can now be zeroed and this zero point will represent 100% reflection of the system for this particular frequency. A ferrite sample can now be inserted in place of the metal sheet and the reflection noted in dB's.

For the magnetised ferrite, instead of locating both circular states by the moveable mirror. Only one circular state needed to be located and the other could be created by simply turning the ferrite around. In turning the ferrite around the electrons that rotate in one particular sense, in the magnetised case, from the point of view of the radiation will appear to rotate in the opposite sense. Conversely, the electrons will see a circular state rotating in the opposite sense. (See Figure 6.6).

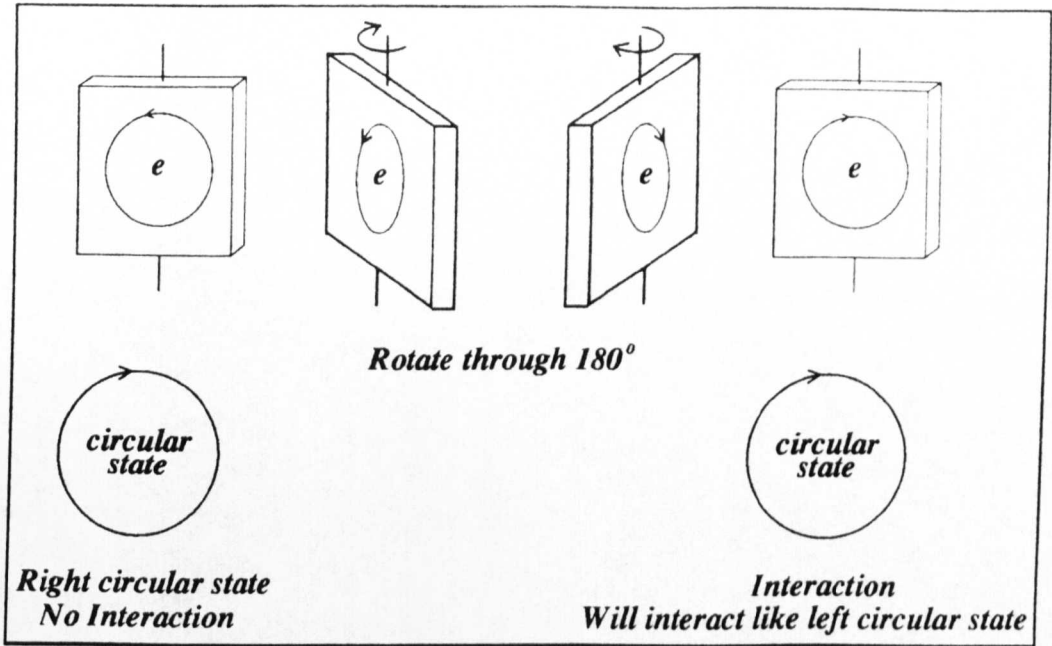


Figure 6.6

The above procedure, was the experimental method employed. This method was repeated over the desired frequency range, hence, obtaining a plot of reflectance versus frequency for each circular state. This was performed for magnetised and unmagnetised versions of each type of plastoferrite under investigation.

(6.3) Predicted nature of the 'Reflectance vs. Frequency' curves.

What now follows is a discussion about the behaviour one would expect to see in the reflectance vs. frequency curves for an unmagnetised and magnetised version of a ferrite sample. The reflectance curves, as will be demonstrated shortly, over a frequency range will behave sinusoidally. The sinusoidal nature can be attributed to the ferrite sample behaving as a 'Fabry-Perot' structure, as will now be explained.

A Fabry-Perot structure can be thought of as two semi-reflecting surfaces which are placed parallel to one another (See Figure 6.7).

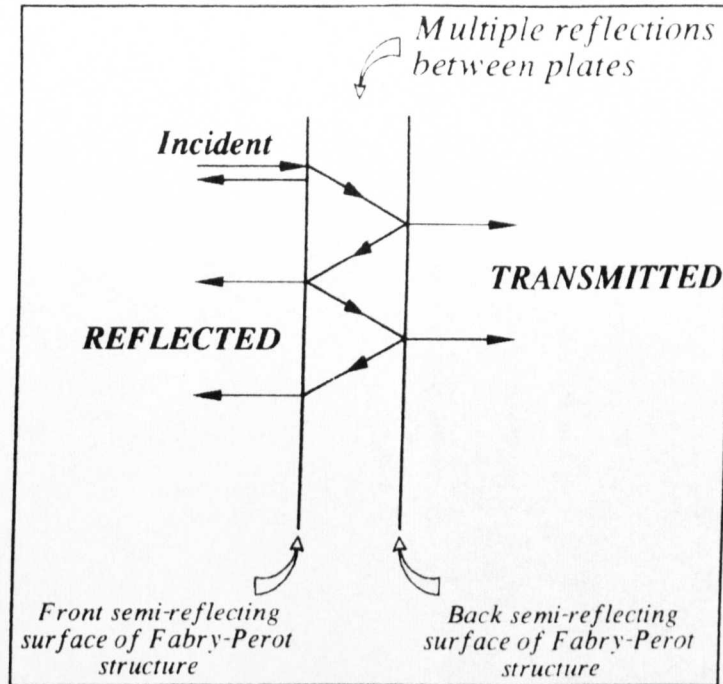


Figure 6.7

An incident beam will initially be partially reflected from the front surface before being transmitted into the region between the plates. Upon being transmitted into this region it undergoes a series of multiple reflections, each time being partially transmitted when it encounters a surface. This results in some of the incident signal being partially transmitted from the back face of the structure and the rest of the signal being reflected from the front face of the structure. The amount of signal that is reflected will depend whether the reflected rays interfere constructively or destructively. This is determined by the distance traversed within the region between the plates, namely the path length, and also the wavelength of the radiation. The ferrite sample can be considered analogous to the Fabry-Perot, since its front and back surfaces partially reflect and transmit, which is the basis of a Fabry-Perot structure. Therefore, one can expect this sinusoidal nature, which is intrinsic to a Fabry-Perot structure, to feature in the reflectance vs. frequency results. There is, however, one modification to be made and that is that the region between the semi-reflecting surfaces is a ferrite medium, which will absorb radiation. This introduces a loss factor/mm, which

is intrinsic to the medium, which is the other important feature of a Faraday rotator and will be explained in section (6.13).

The next question that needs to be addressed is whether one should expect a difference in the reflectance graphs for the magnetised and unmagnetised versions of a sample. And if so, how will the graphs differ in nature. The answer to this is in the affirmative, since the ferrite medium behaves differently in its unmagnetised state compared to its magnetised state. Therefore, one should also expect this difference to be evident in the reflectance vs. frequency results. How the graphs will differ can also be predicted by using a Fabry-Perot analogy, now explained.

In the unmagnetised case, as we know, both circular states propagate through the medium at the same rate. Explaining this from a Fabry-Perot perspective both the circular states will follow the same path within the medium, (i.e. traversing the same distance and, therefore, having the same path length). This will result in, (See Figure 6.8), the occurrence of constructive and destructive interference at the same wavelengths for both circular states. This implies that, the peaks and troughs of their reflectance curves will occur at the same places and hence, they can be said to be 'inphase' with each other.

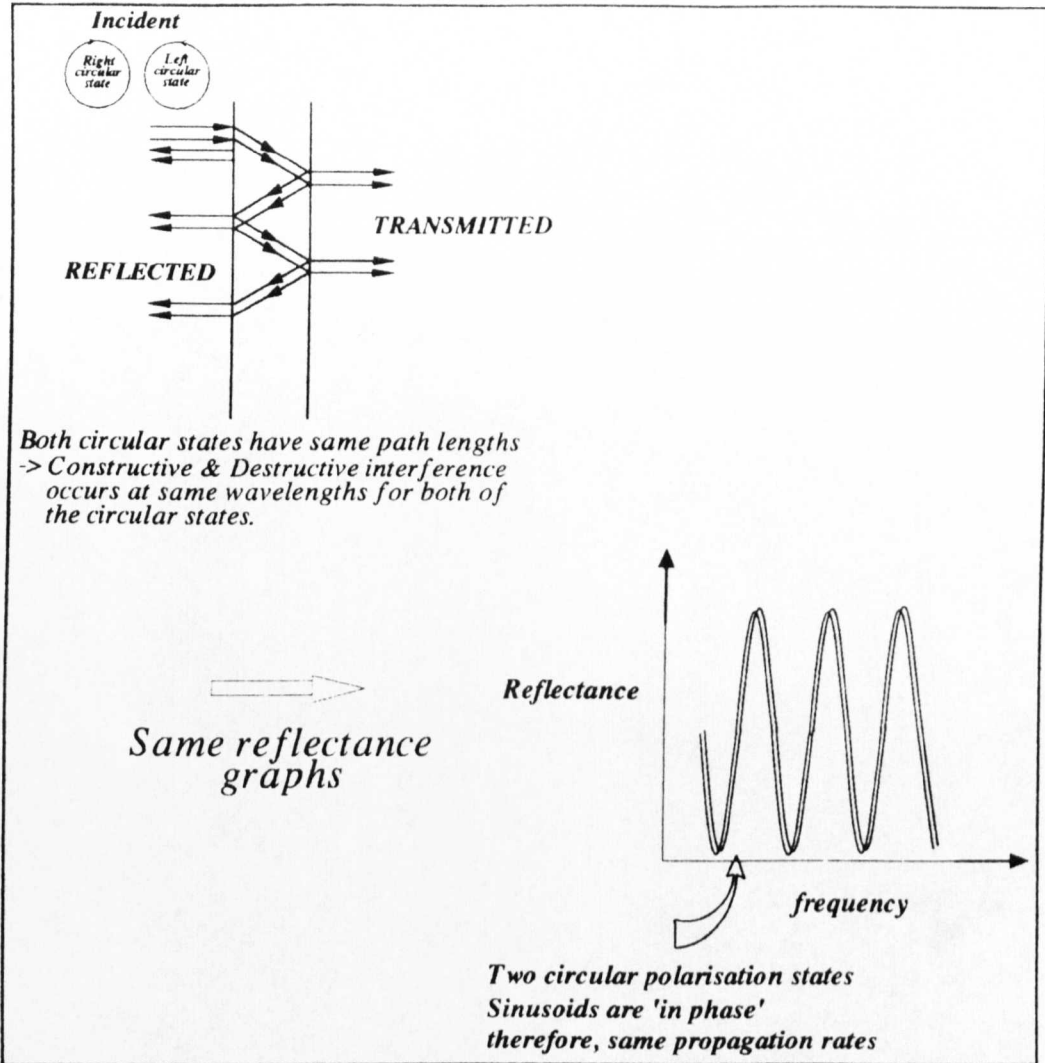


Figure 6.8

For the magnetised case, since the electrons precess in a certain circular sense they can be said to discriminate between the circular polarised states by causing them to propagate at different rates⁵. From the Fabry-Perot analogy since the circular states propagate at different rates they therefore traverse different paths within the medium and consequently have different path lengths. This results in the occurrence of destructive and constructive interference at different wavelengths for the circular states, which implies that the reflectance vs. frequency curves will be out of phase with each other, as shown in figure(6.9).

⁵ The medium can also be said to be circularly birifringent.

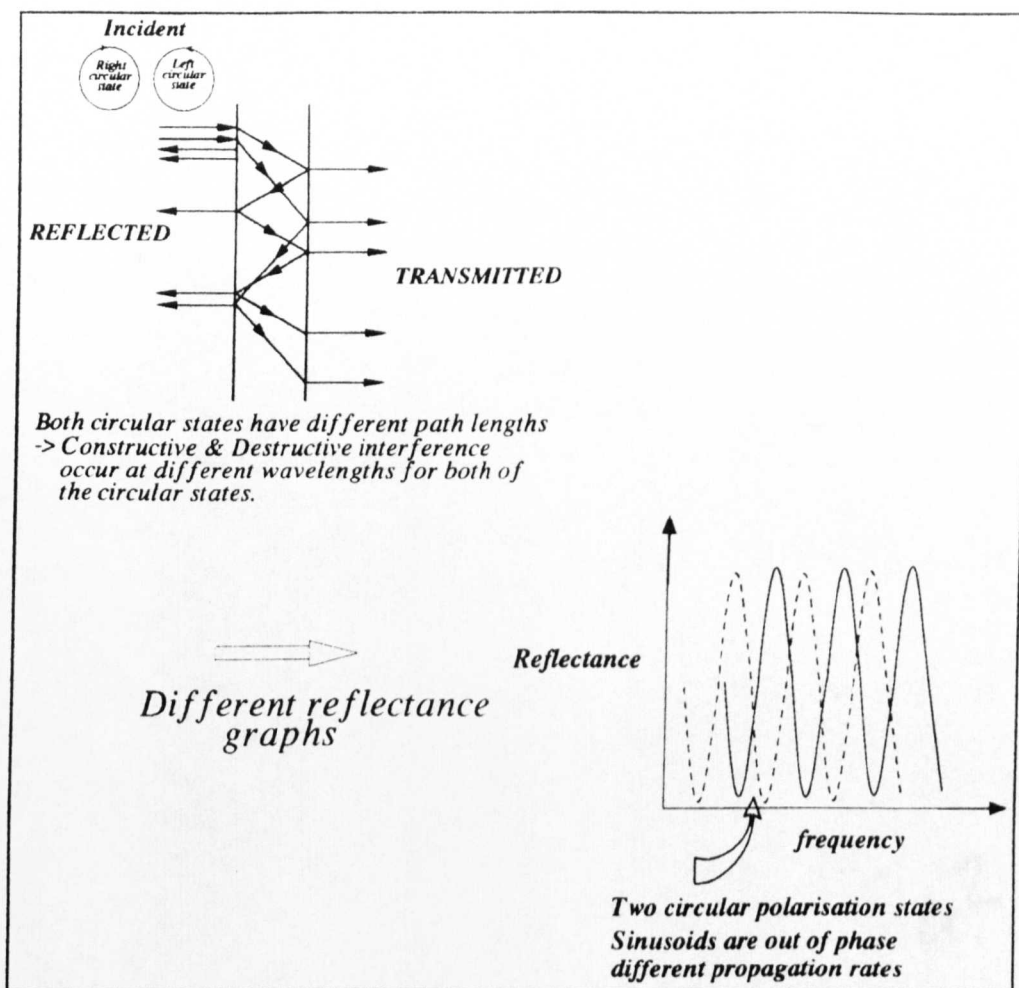


Figure (6.9)

Summarising the last section, one can expect the reflectance vs. frequency curves to be sinusoidal in nature, due to the Fabry-Perot nature of a ferrite. Also in the unmagnetised case, since both circular states propagate through the medium at the same rate, the sinusoids for each circular state will be in phase in their reflectance curves. Whereas, in the magnetised case, since both circular states propagate at different rates through the medium the sinusoids for each circular state will be out of phase of their reflectance curves.

(6.4) Determination of refractive index from reflectance measurements.

After understanding how to predict the nature of the reflectance vs. frequency graphs the next step is to determine the refractive index

from the reflectance measurements. This will involve finding a relationship between the refractive index and some parameter which is associated with the reflectance measurements. This section will describe how this link was made. As will be demonstrated shortly, it is the minimas in the reflectance curves that are the link to determining the refractive index. This can be explained by, again, likening the ferrite to a Fabry-Perot structure. Let us start by considering the ferrite to be of a thickness (L) and to have an unknown refractive index (n). (Figure 6.10).

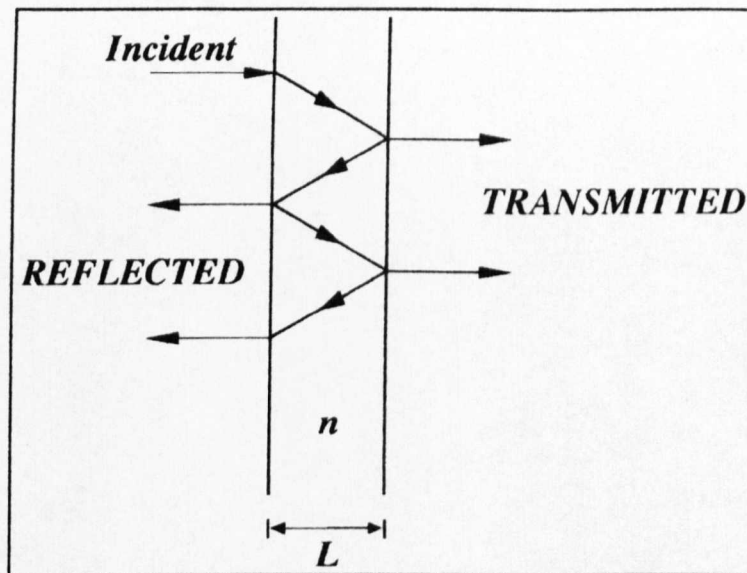


Figure 6.10

By Likening the ferrite to a Fabry-Perot structure, one can describe the distance traversed between adjacent pairs of reflected rays or adjacent pairs of transmitted rays as the path length (ΔP), described as:

$$\Delta P = 2nL \quad \dots(6.2)$$

Now destructive interference between emerging reflecting rays or emerging transmitted rays will occur when the path length (ΔP) is an integer (m) number of wavelengths, given by :

$$\Delta P = m\lambda \quad \dots(6.3)$$

Similarly, constructive interference between emerging reflecting rays or emerging transmitted rays will occur when $\Delta P = (m + \frac{1}{2})\lambda$. However, I will only consider the destructive case. This is one of experimental choice, since in the destructive case very little signal will be reflected back. This will greatly reduce any error due to standing waves, therefore a measurement will be at its most accurate here. Whereas, in the constructive case, large standing waves can be generated, which will in turn produce large errors in the measurements. This is evident in all the data I have obtained, where the destructive data is located at the smooth minimas of the reflectance curves and the constructive data is located at the maximas of the reflectance curves, which are not smooth, but erratic due to standing wave error. (Figure 6.24 is a very good example of this).

Therefore, considering only the destructive case and using (6.2) and (6.3) \Rightarrow

$$nL = \frac{m\lambda}{2} \quad \dots (6.4)$$

where, (m) is the order number which is an integer. A particular (m) corresponds to a particular minima in the reflectance vs. frequency curve. Therefore, by examination of equation (6.4) one can determine the refractive index (n) of the ferrite for a specific frequency once the order (m) is known. Now the problem shifts to one of determining the order (m).

The way the order was determined is as follows. If one considers two dips that occur on the same reflectance vs. frequency curve at frequencies (f_0) and (f_e) for an unmagnetised sample. The reason I state it has to be an unmagnetised sample, is because of an assumption I will make very soon. If the minima at (f_0) has order (m_0) and if (f_e) is located (e) minimas away from (f_0), then (f_e) will have order ($m_0 + e$). (Figure. 6.11).

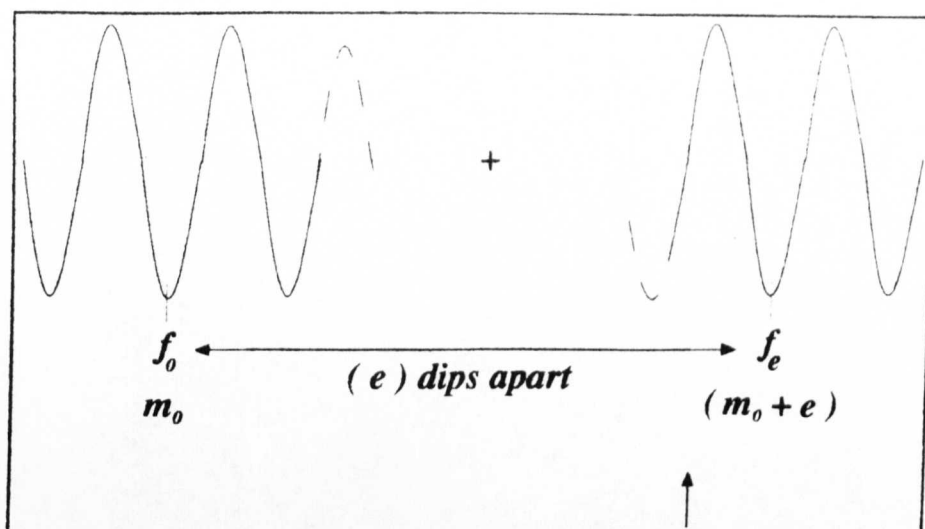


Figure 6.11

Now the assumption I am going to make is that the refractive index remains constant over the frequency range between the two mentioned minimas. This assumption can only be applied to the reflectance graphs for the unmagnetised sample, since the refractive index is constant in the unmagnetised case⁶. Therefore, using equation (6.4) we can derive expressions for (nL) at positions (f_0) & (f_e) , such that :

$$nL = m_0 \frac{\lambda_0}{2} \quad \dots (6.5)$$

$$nL = (m_0 + e) \frac{\lambda_e}{2} \quad \dots (6.6)$$

Since we have assumed (n) to be constant in the unmagnetised case, we can say $(6.5) = (6.6) \Rightarrow$

$$\frac{\lambda_0}{\lambda_e} = 1 + \frac{e}{m} \quad \dots (6.7)$$

⁶ In the magnetisation of a magnetic material the refractive index cannot be considered constant. This is because the permeability of the magnetised material is a tensor quantity. This varying relationship of (μ) can be seen in the 'Hysteresis' curve which characterises the variation of (B) with (H) for a magnetised material.

A derivation of the tensor permeability can be found in, *Microwaves* (2nd Ed.), A.J.Baden Fuller, Pergamon Press, 1979, pgs.169-171.

The Hysteresis behaviour can be seen in, *Introduction To Magnetism & Magnetic Materials*, D.Jiles, Chapman & Hall Publishers, 1991, pgs.70-71.

where, $c = f\lambda \Rightarrow$

$$\frac{f_c}{f_0} = 1 + \frac{c}{m} \quad \dots (6.8)$$

$$\therefore m_0 = e \left(\frac{f_c}{f_0} - 1 \right)^{-1} \quad \dots (6.9)$$

Usually, one sets $e=1$, since if there was a refractive index change between the two minima, the error in (m) would be reduced to a minimum. Hence, one can determine what the order is. However, upon calculation the order does not always turn out to be an integer value. This can be due to inaccurate determination of where the minima actually lies, which will give an error in the frequency of (f_0) or (f_c) . Or infact, (n) could be varying slightly. This presents an error in the predicted order of (m_0) by (± 1) . Therefore, the true value for order (m_{TRUE}) could lie in the range :

$$m_{TRUE} \text{ lies in the range} = (m_0 - 1), m_0, (m_0 + 1)$$

$$\text{corres. } n_{TRUE} \text{ range} = n_{m_0-1}, n_{m_0}, n_{m_0+1}$$

The way one can completely determine the correct order is to repeat the same experiment for differing thicknesses of sample for the same material. In thin samples the values of the refractive index for adjacent orders, $(m_0 - 1)$ and $(m_0 + 1)$, is much greater or much smaller than the central value (m_0) . In the thick samples, however, the refractive index of the adjacent orders, $(m_0 - 1)$ and $(m_0 + 1)$, is very similar to the central value (m_0) . Hence, one can with two or three samples tally which is the common refractive index and hence determine the order.

One can firstly determine the order of the unmagnetised samples by the above method. After magnetising the same samples one can determine the order of the circular states of the now magnetised sample by using the fact that the minima of the circular states of a particular order (m) will fall adjacent to minima of the same order

(m) of the unmagnetised state. (Figure.6.12).

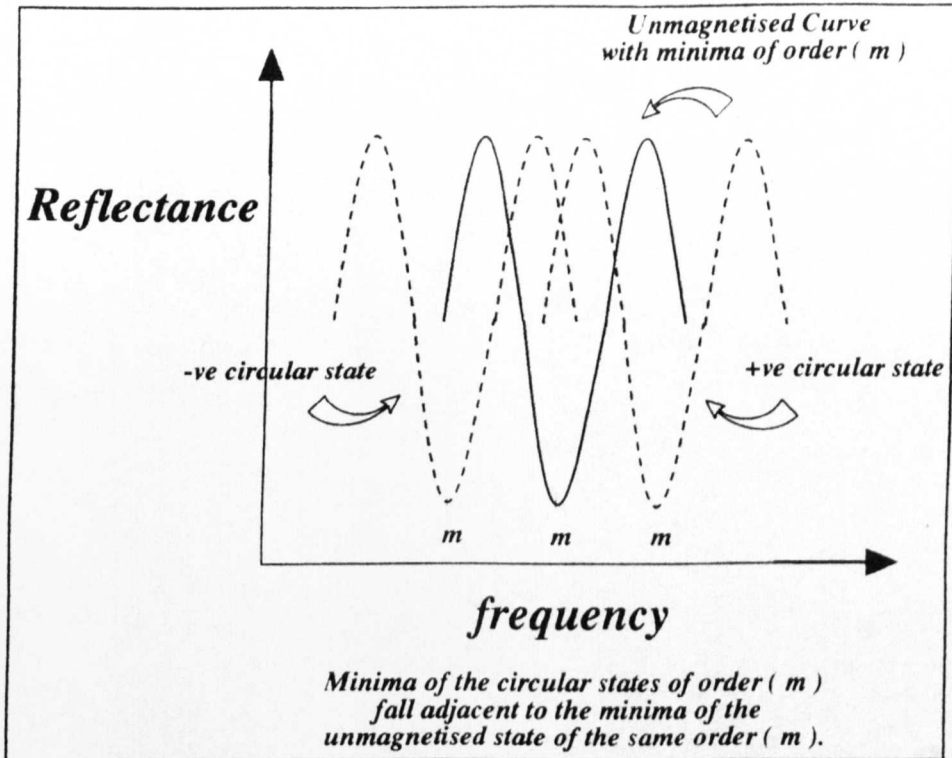


Figure 6.12

Therefore, in this section I have presented how one could determine the refractive indices from the reflectance data. Sections (6.5, 6.6, 6.7) present the 'Reflectance vs. Frequency' curves, that represent the data obtained for the three types of plastoferrite, namely Anisotropic, Semi-Anisotropic and Isotropic, in their unmagnetised and magnetised states. As mentioned earlier a variety of samples, that varied in thickness, was required for each type of plastoferrite to determine the correct orders and therefore the correct refractive indices of the minima of the reflectance vs. frequency curves.

(6.4.1) Materials Used In Study

As mentioned above, three different types of material were studied. All the materials were commercially available and of the Strontium Hexaferrite $\text{SrO} \cdot 6(\text{Fe}_2\text{O}_3)$ type embedded in a plastic matrix.

⁷ Nonreciprocal Magneto-Optics For Millimeter Waves, G.F. Dionne, J.A. Weiss, G.A.Allen, IEEE Transactions On Magnetics, Vol.24, No.6, November 1988.

The Anisotropic material was purchased from 'Magnetic Developments'. The material was supplied in 6mm thick sheets. 100mm squares were cut and machined to appropriate sample sizes. The Semi-Anisotropic and Isotropic materials were purchased from 'Anchor Magnets'. These materials were supplied in a rolled form. Also remnant magnetic flux lines, from the manufacturer process, could be seen to lie in the plane of the material and parallel to its rolled length. The thickness of the material was $\approx 1\text{mm}$. Thus, several sheets had to be cut and affixed by a thinned glue to form the samples described.

(6.5) Anisotropic SrM Plastoferrite Reflectance vs. Frequency curves.

Five samples, of varying thickness, were used to achieve a broad range of refractive indices for the 70 - 160 GHz region. The samples involved were :

SAMPLE 12 (3.73mm), SAMPLe 4 (3.02mm), SAMPLe 3 (3.33mm), SAMPLe 2 (5.99mm) and SAMPLe 1 (5.93mm) the results of which now follow :

Results for Sample 12

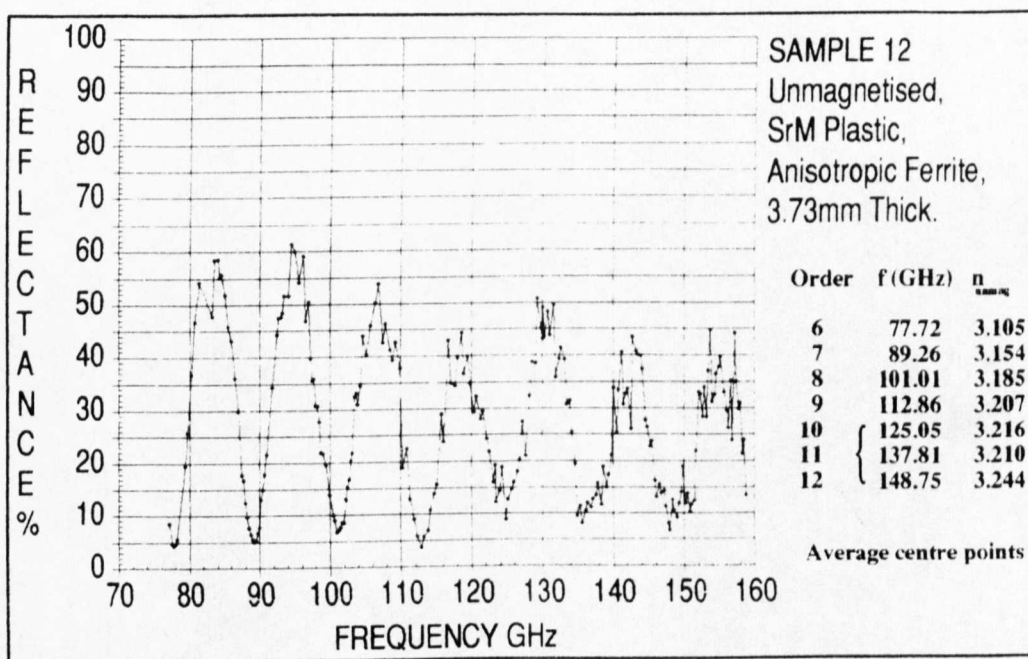


Figure 6.13

Results for Sample 4

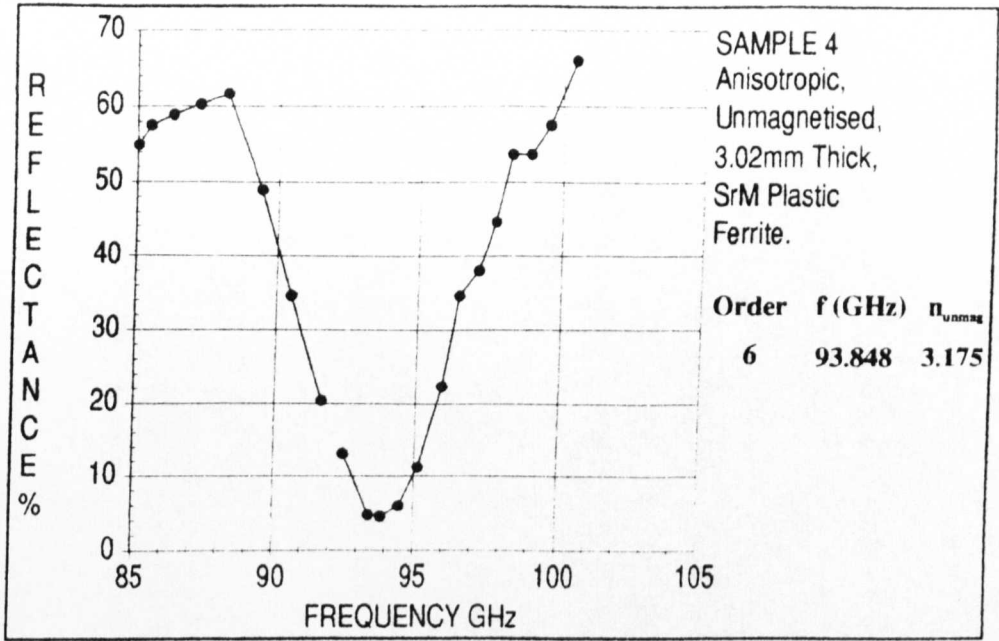


Figure 6.14

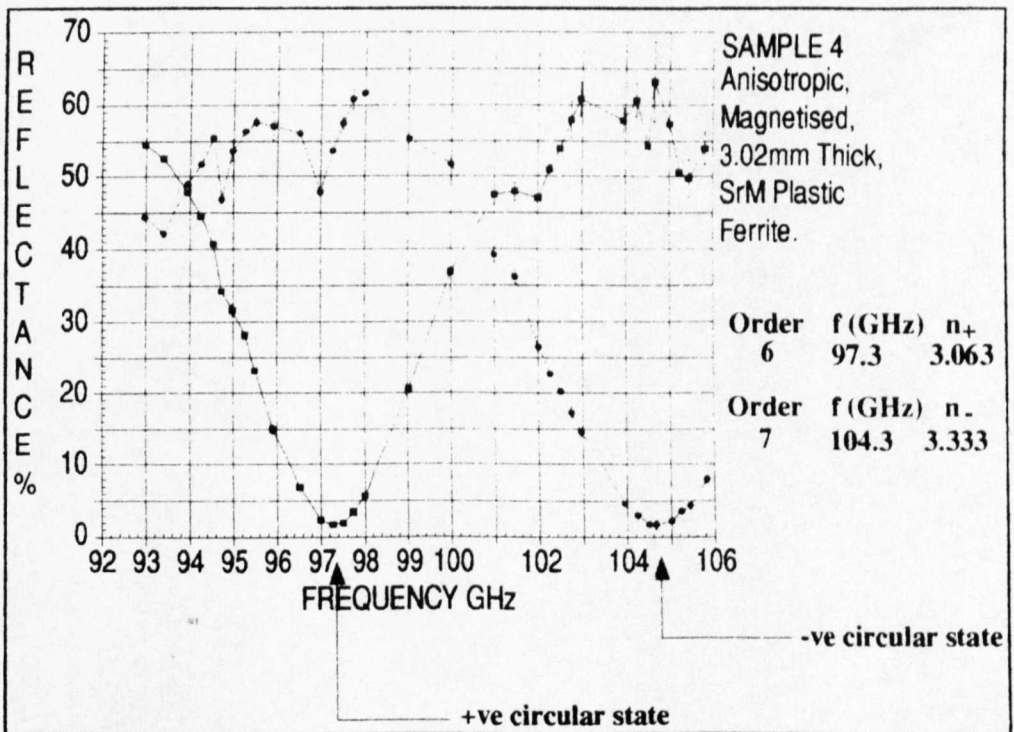


Figure 6.15

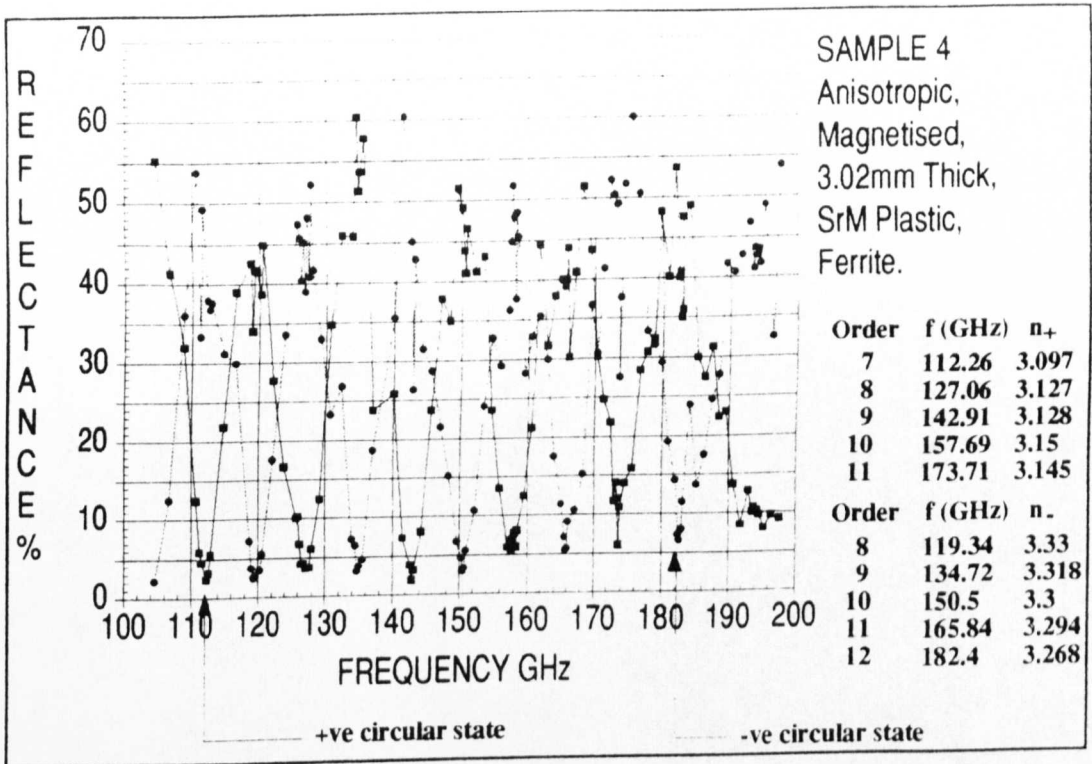


Figure 6.16

Results for sample 3

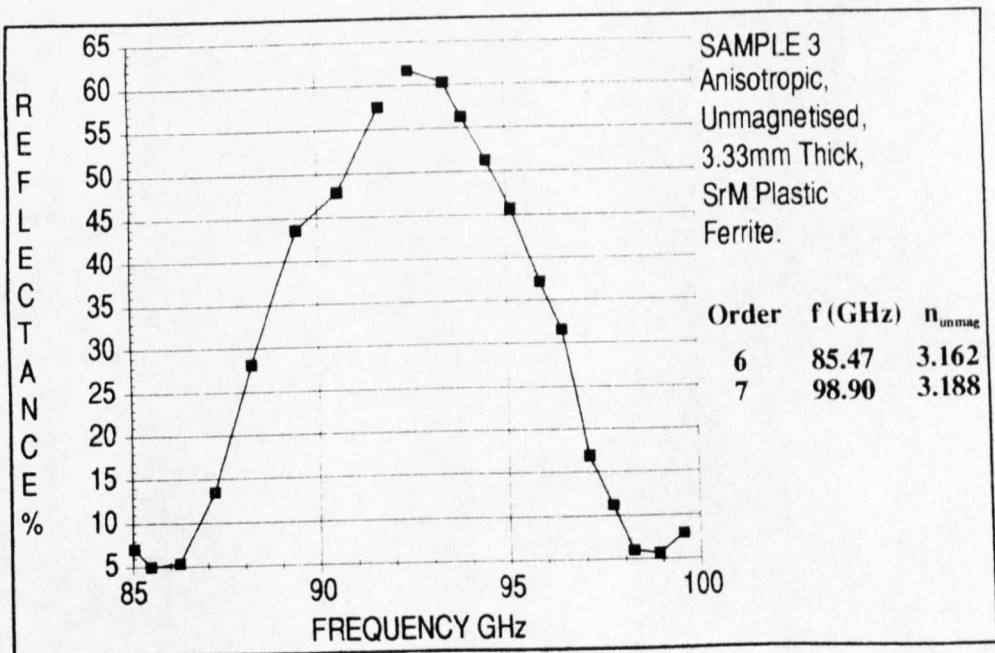


Figure 6.17

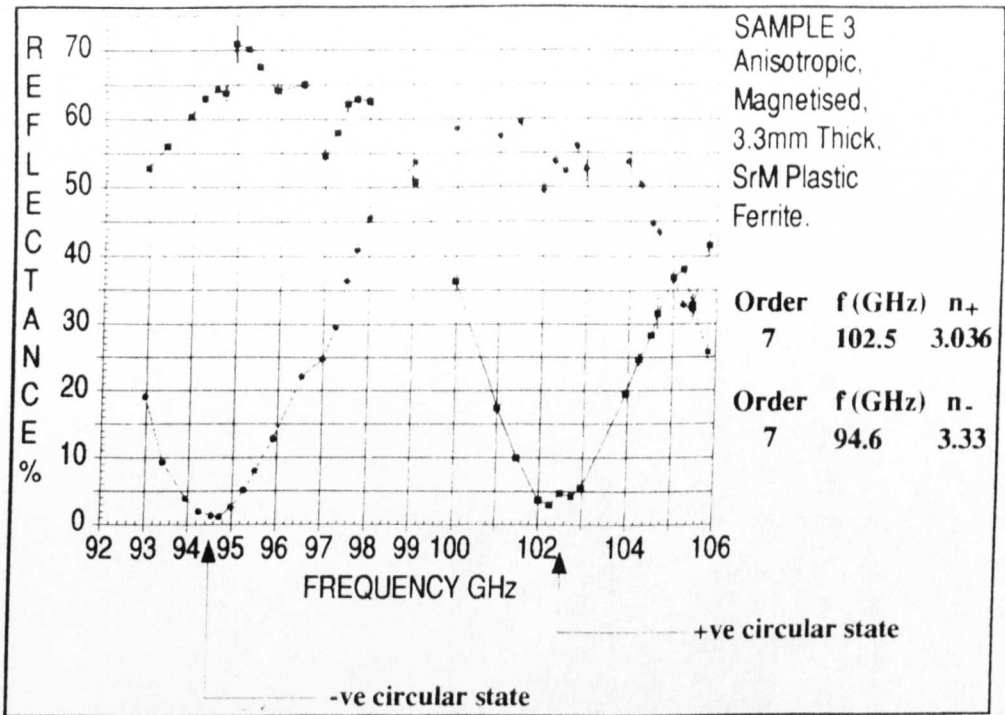


Figure 6.18

Results for Sample 2

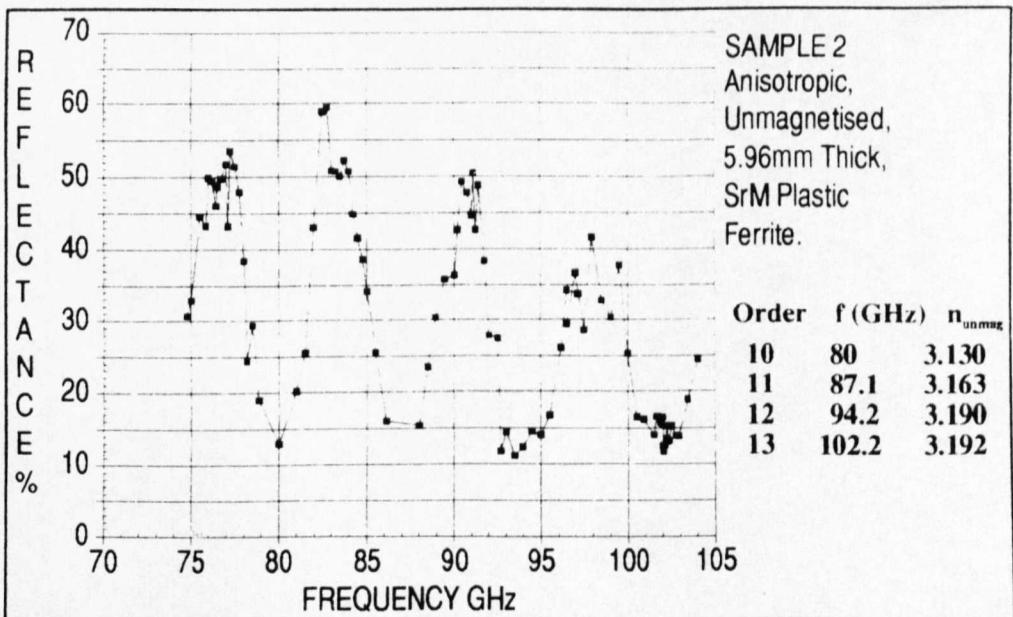


Figure 6.19

Results for Sample 1

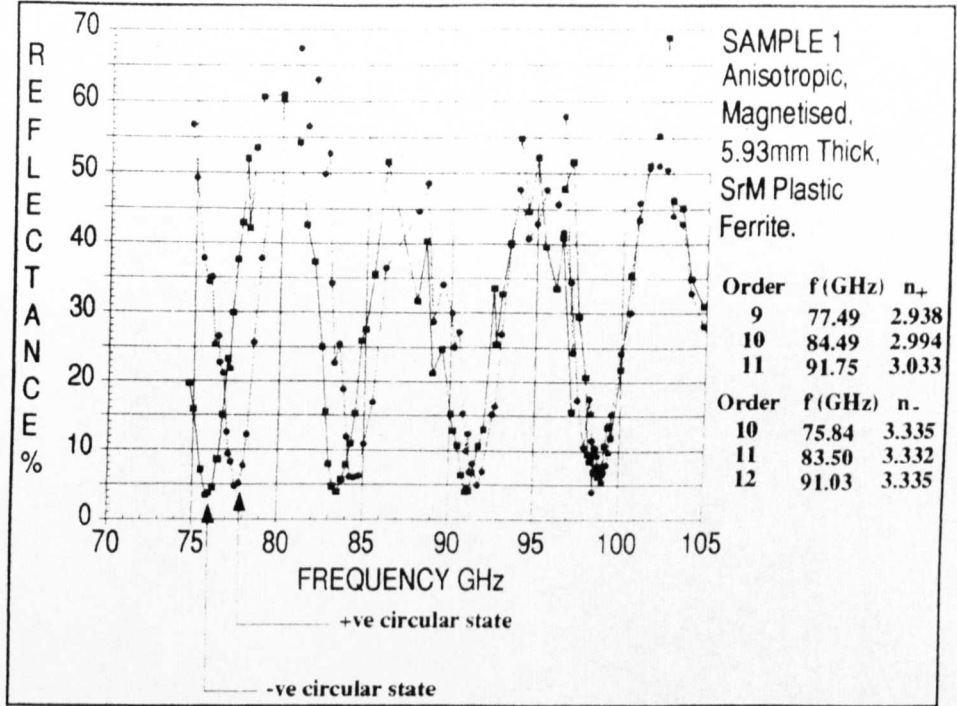


Figure 6.20

(6.6) Isotropic SrM Plastoferrite Reflectance vs. Frequency curves.

Four samples were involved in the Isotropic measurements. These samples were : SAMPLE 6 (1.48mm), SAMPLE 7 (1.48 mm), SAMPLE 9 (4.77mm) and SAMPLE 10 (5.834 mm).

Results for Sample 6

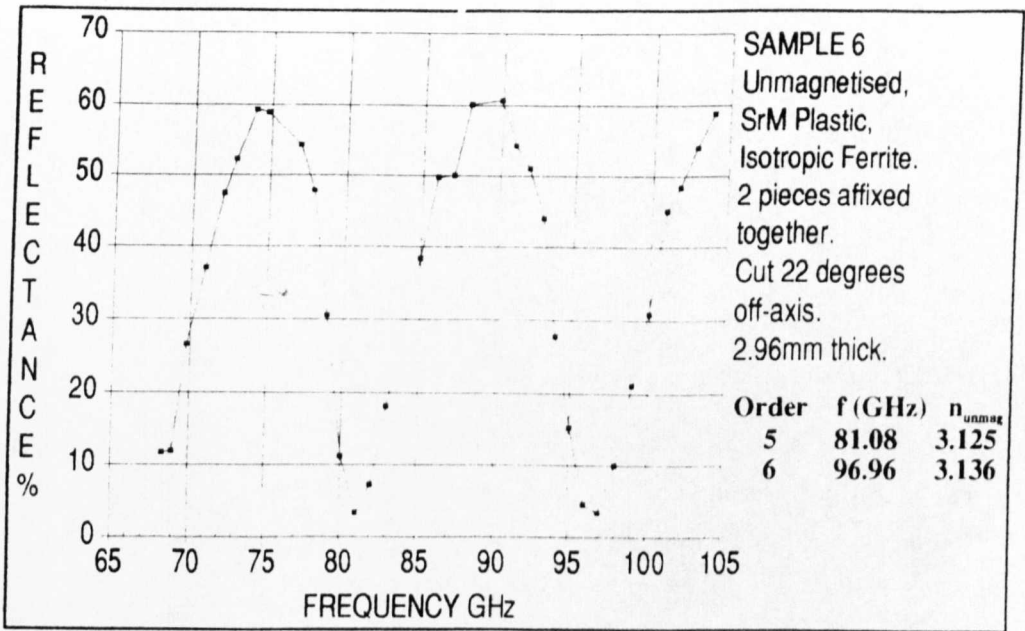


Figure 6.21

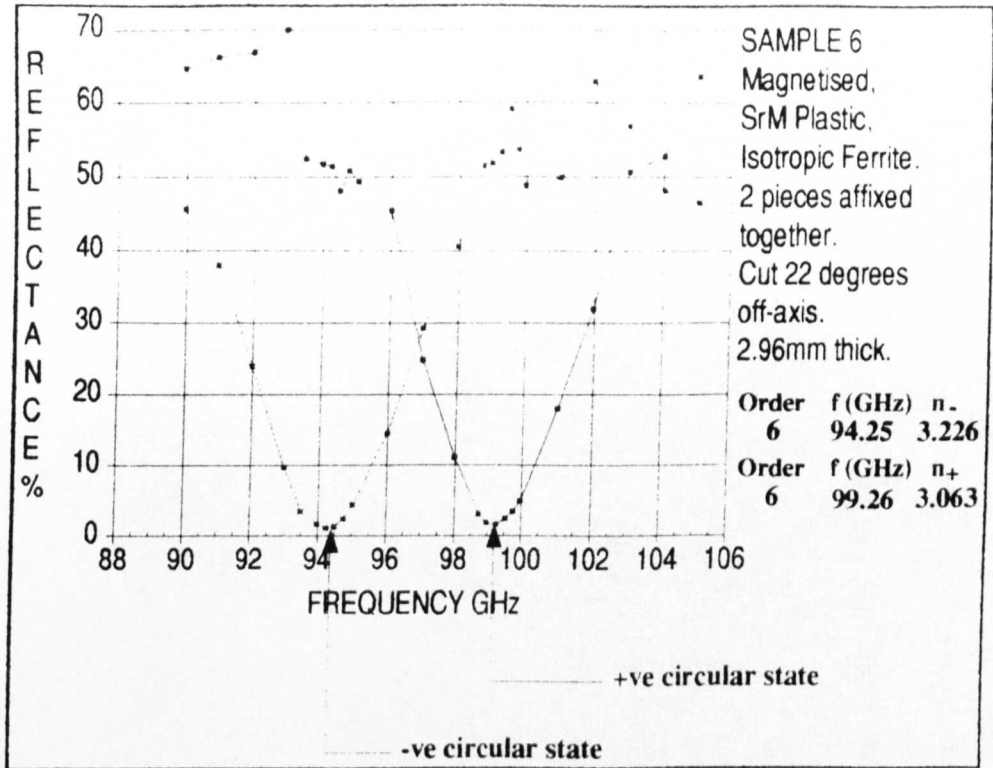


Figure 6.22

Results for Sample 7

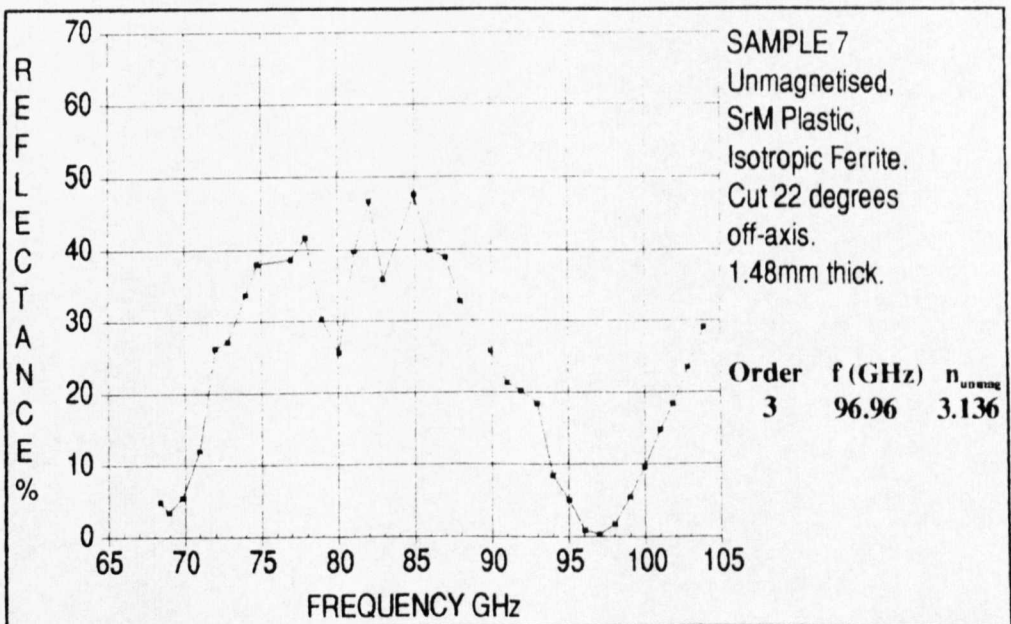


Figure 6.23

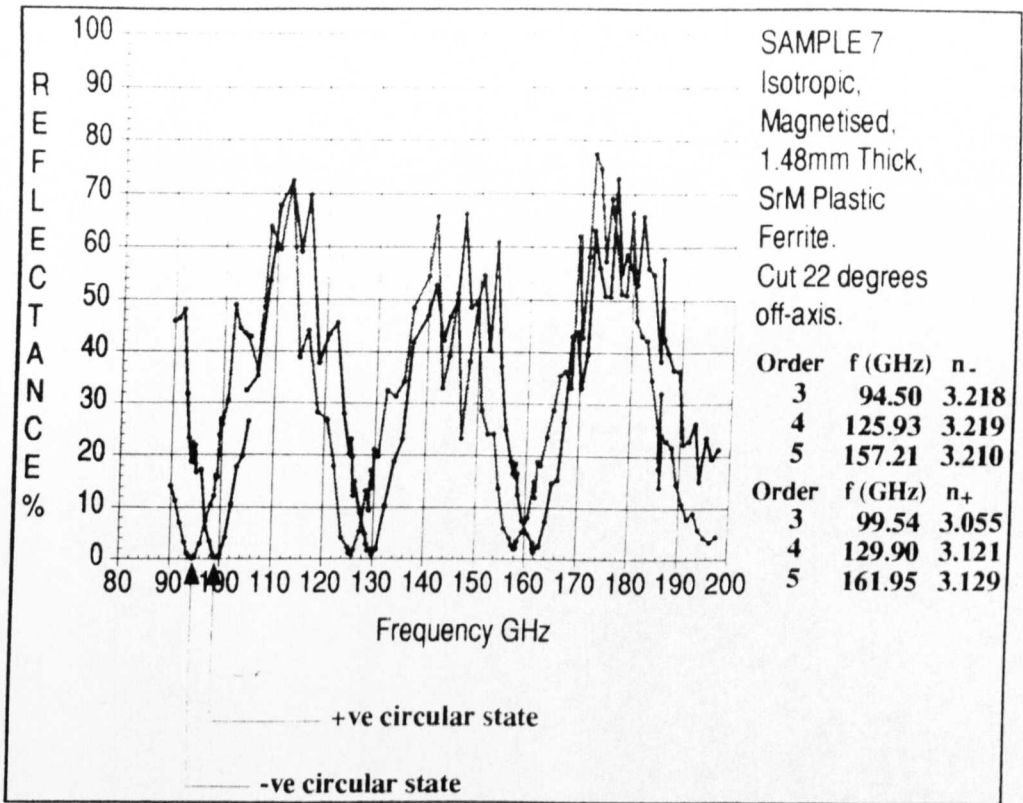


Figure 6.24

Results for Sample 9

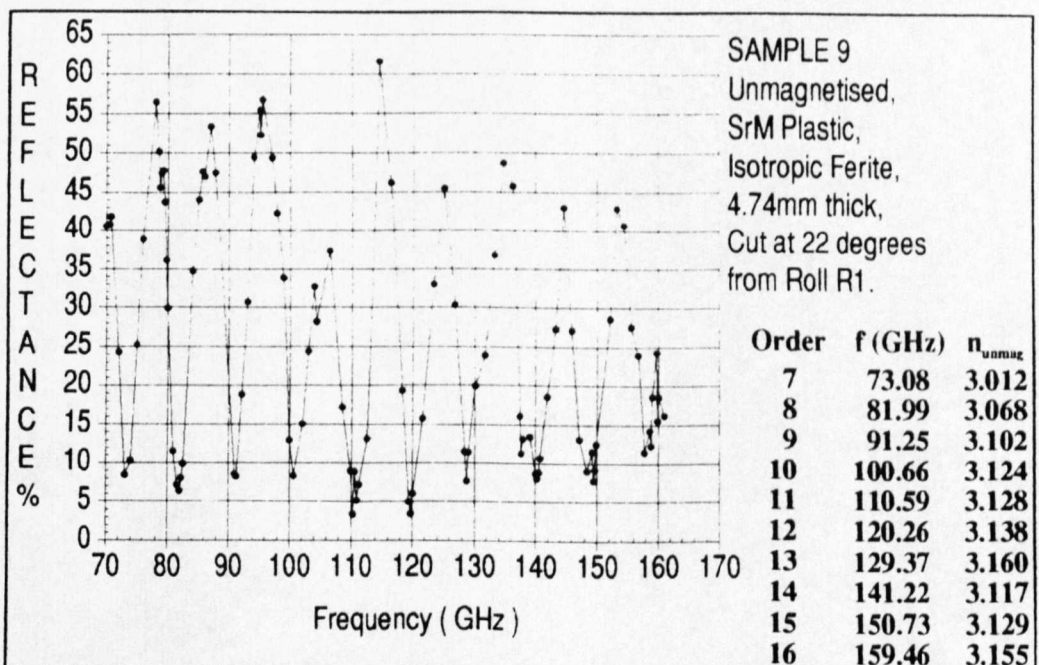


Figure 6.25

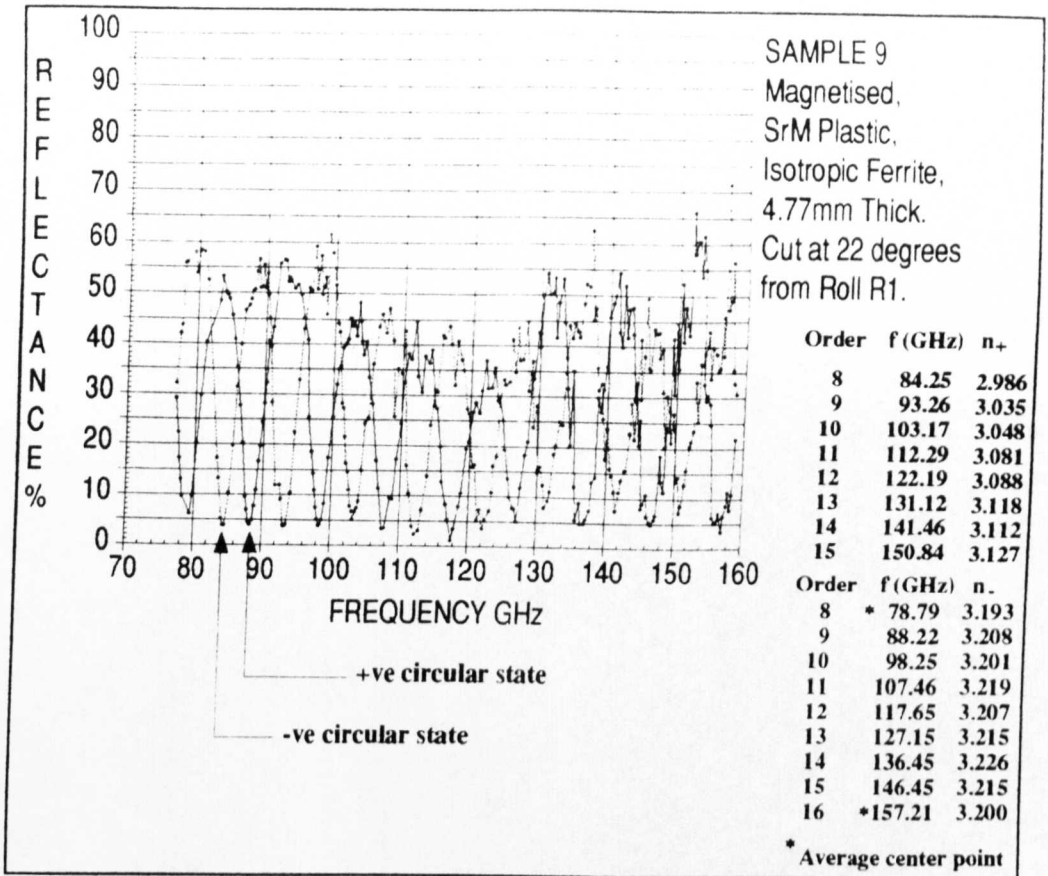


Figure 6.26

Results for Sample 10

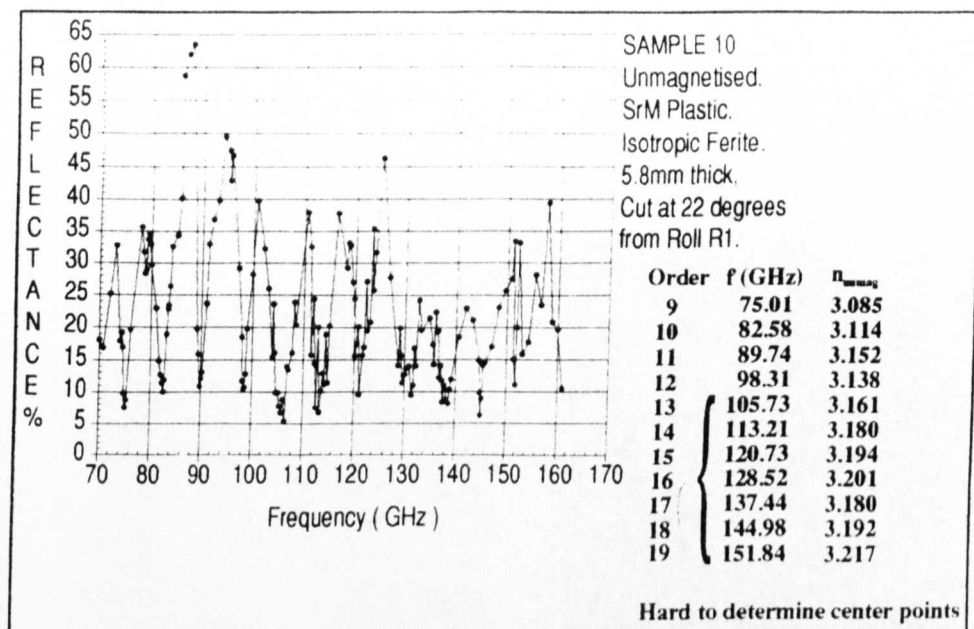


Figure 6.27

(6.7) Semi-Anisotropic SrM Plastoferrite Reflectance vs. Frequency curves.

Two samples were involved in the semi-anisotropic measurements. These were : SAMPLE 8 (1.535mm) and SAMPLE 11 (3.05mm). Results for Sample 8

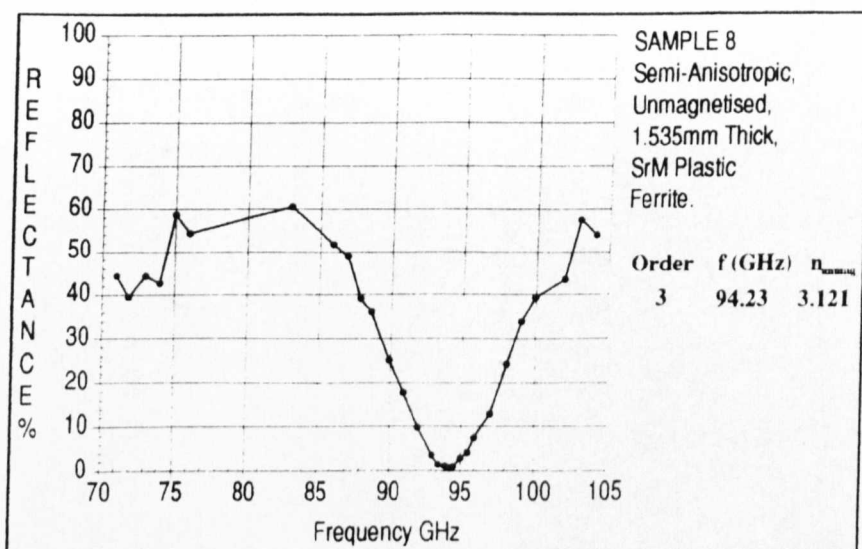


Figure 6.28

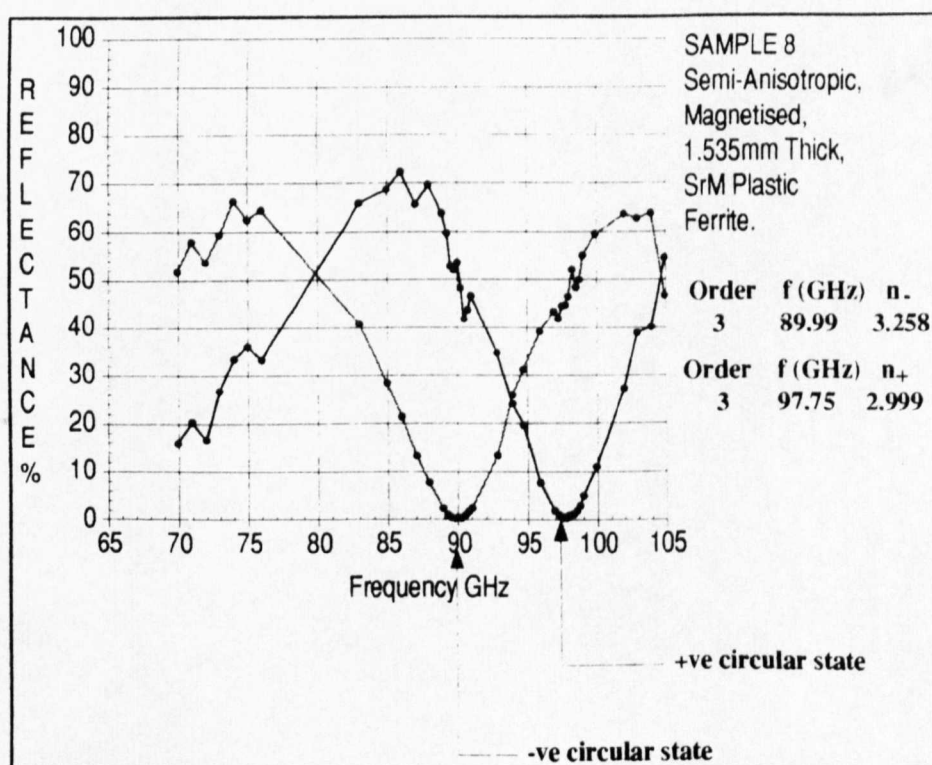


Figure 6.29

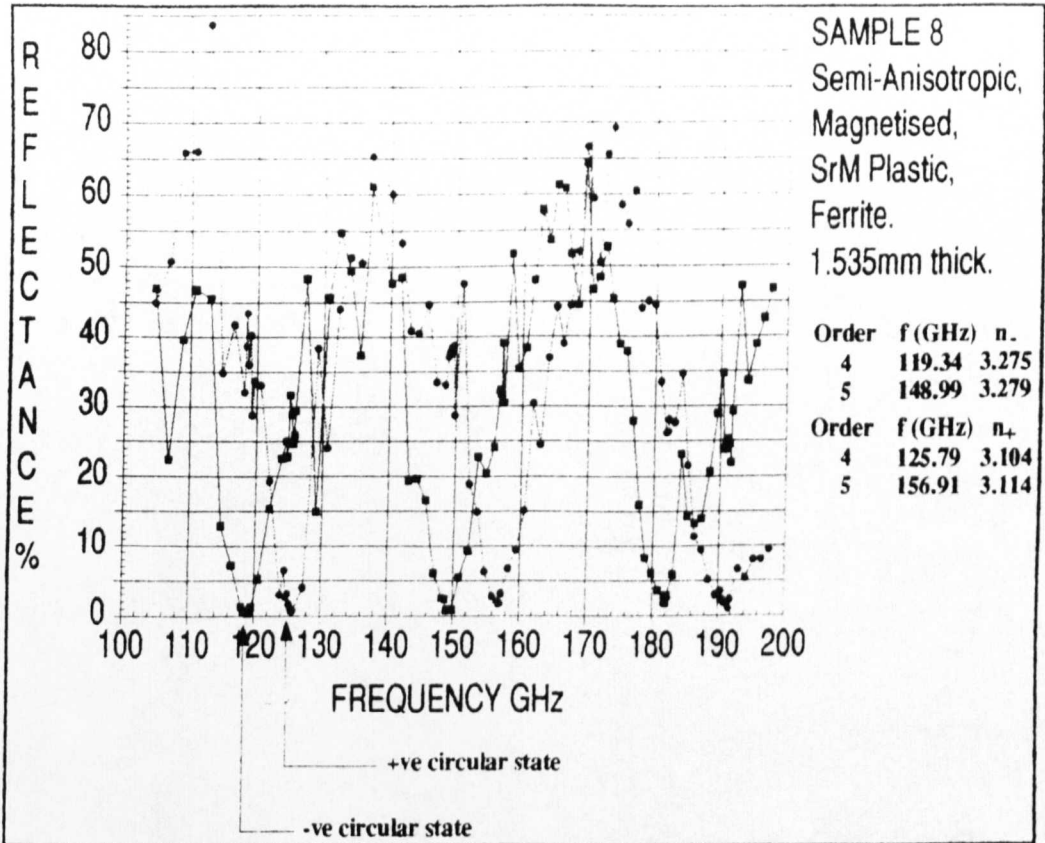


Figure 6.30

Results for Sample 11

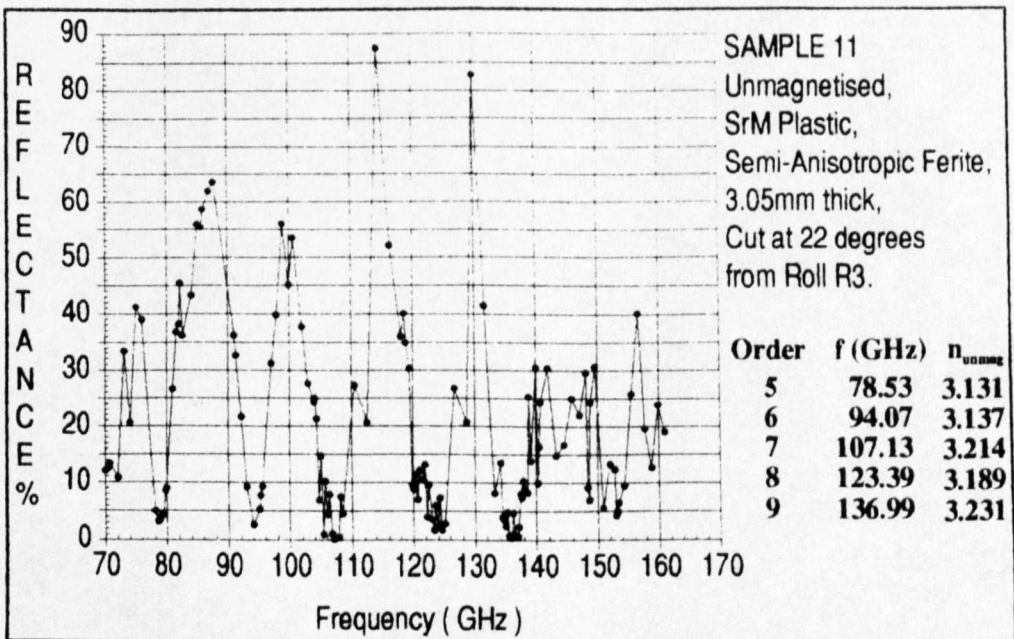


Figure 6.31

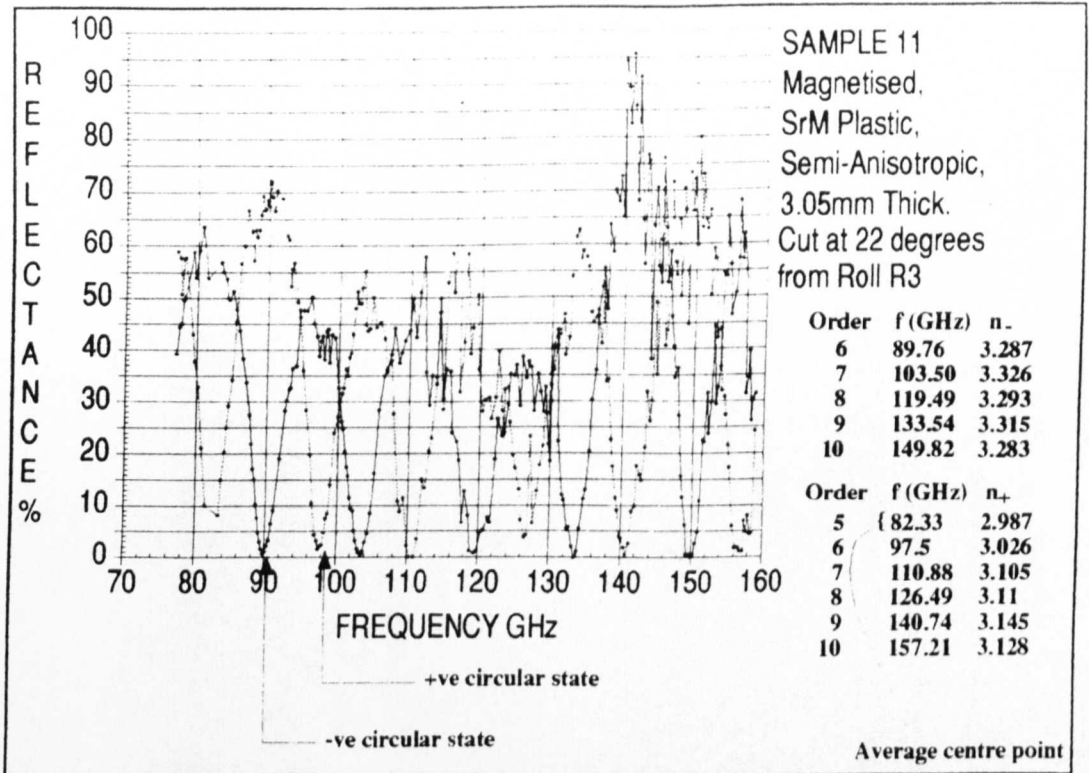


Figure 6.32

(6.8) Predicted nature of the refractive index.

After determining the refractive indices for each of the circular polarised states of the unmagnetised and magnetised versions of the sample. It was necessary to predict the nature of these refractive indices. This section describes how suitable expressions derived from theory can be obtained to predict the nature of the refractive index, for the various circular states and for unmagnetised and magnetised versions of a sample. Once determined one can then computerfit these expressions to the refractive index data and hence, determine the behaviour of the ferrite at any frequency.

The first part of this section, will determine theoretically the nature of the refractive indices for the circular states of a magnetised sample.

One can start by using the relations for the propagation constants (β_{\pm}) and the effective permeabilities (μ_{\pm}) for the right and left circular states, shown in equations (6.10) and (6.11), respectively.

$$\beta_{\pm} = \frac{2\pi}{\lambda} n_{\pm} \quad \dots(6.10)$$

$$n_{\pm} = \mu_0 \left(1 + \frac{\omega_m}{\omega_0 \mp \omega} \right) \quad \dots(6.11)$$

Where (ω_0) is the Larmor, or resonant angular frequency and $(\omega_m = \gamma\mu_0 M_s)$, where (γ) is the Gyromagnetic ratio, (μ_0) the permeability of freespace and (M_s) is the magnetisation of the sample. An expression for the behaviour of the the refractive indices (n_{\pm}) for each circular state can then be determined in the following manner : Arranging (6.10) for (n_{\pm}) , where $c = \lambda f$ and $\omega = 2\pi f$

$$n_{\pm} = \frac{\beta_{\pm} c}{2\pi f} = \frac{\beta_{\pm} c}{\omega} \quad \dots(6.12)$$

Also (β_{\pm}) can be represented as :

$$\beta_{\pm} = \omega \sqrt{\epsilon \mu_{\pm}} \quad \dots(6.13)$$

Substituting for (μ_{\pm}) from (6.11) in (6.13) and then for (β_{\pm}) from (6.13) in (6.12) results in :

$$n_{\pm} = c \sqrt{\epsilon \mu_0 \left(1 + \frac{\omega_m}{\omega_0 \mp \omega} \right)}$$

Now $c = \frac{1}{\sqrt{\epsilon_0 \mu_0}}$ and $\epsilon = \epsilon_r \epsilon_0$,

$$\therefore n_{\pm} = \sqrt{\epsilon_r} \sqrt{1 + \left(\frac{\omega_m}{\omega_0 \mp \omega} \right)} \quad \dots(6.14)$$

A discussion of the nature of the refractive index curves, expressed in equation(6.14) will follow shortly. The behaviour of these curves is shown schematically, in Figure (6.33), below.

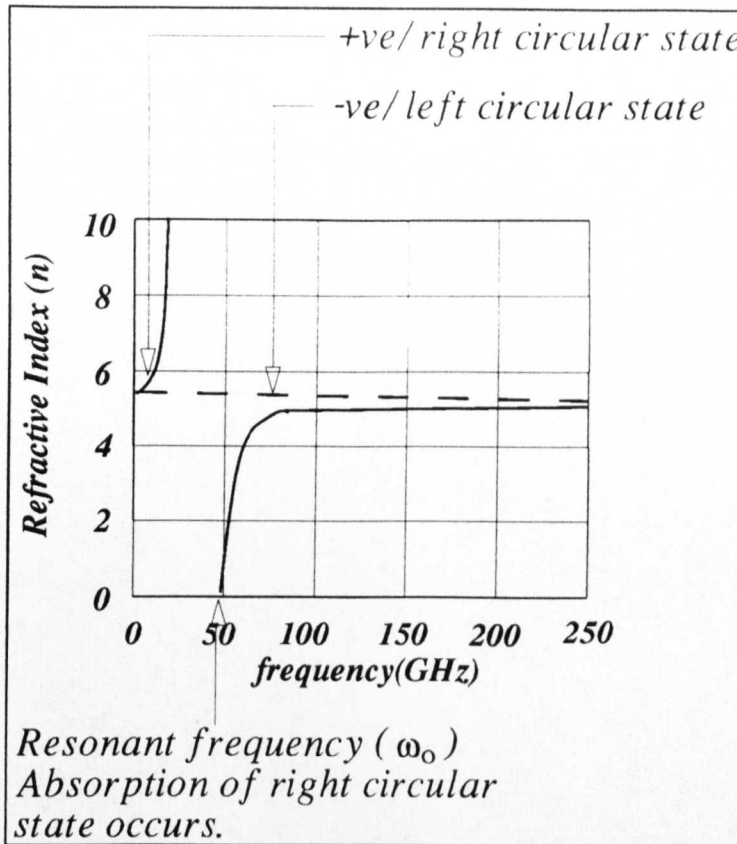


Figure 6.33

The solid line represents the behaviour of the +ve/right circular state, whilst the broken line represents the -ve/left circular state. In the frequency region below (ω_0), in Figure (6.33), one can see that the refractive index for the +ve circular state is greater than that of the -ve circular state. This results in a rotation of the linear polarised wave in a -ve/left-handed sense, shown in Figure(6.34). At (ω_0), the resonant frequency, the +ve circular state that is rotating in the same sense as the electrons, will also be rotating at the same rate (ω_0) as the electrons. This results in the absorption of the +ve circular state, described in section(5.3.1). Beyond, (ω_0) the refractive index for the -ve circular state is greater than that of the +ve circular state which results in a rotation of the linear polarised wave in a +ve/right-handed sense. The rotation will decrease with increasing frequency beyond (ω_0), due to the changing refractive indices of the -ve and +ve circular states. At very high frequencies (above 160GHz) the refractive indices for the -ve and +ve circular states will become

constant and these curves will become parallel. This will result in the rotation of the linear polarised wave also remaining constant. In this region the rotation can be said to frequency independent.

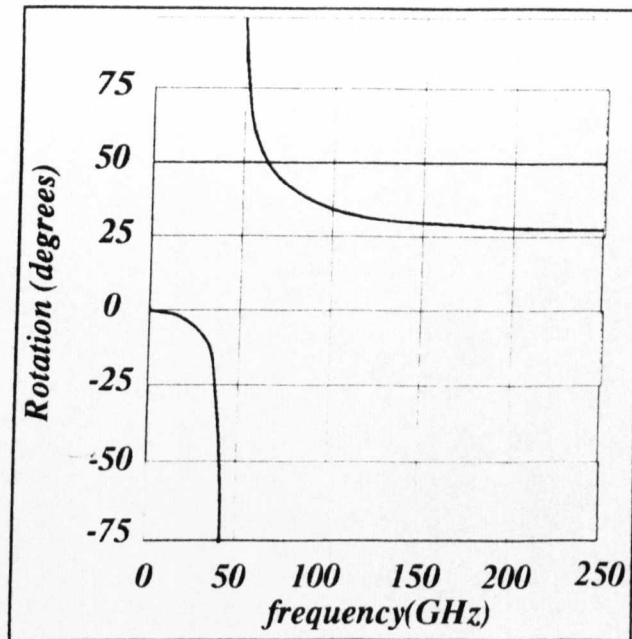


Figure 6.34

The final part of this section will now describe how the refractive indices for the unmagnetised circular states were determined theoretically.

For the unmagnetised state the refractive index (n_{unmag}) can be expressed simply as :

$$n_{unmag} = \sqrt{\epsilon_r \mu_r} \quad \dots (6.15)$$

The theoretical curves, given by equations (6.14) and (6.15), were fitted with the aid of a curve fitting package.⁸ In the computerfit, the variables (a) and (b) were assigned to $(\sqrt{\epsilon_r})$ and (ω_m) respectively in equation (6.14). (ω_0) was set to 50 GHz, since this is the resonant frequency for Strontium hexaferrite.

Where, $\mu_r = 1$ for the unmagnetised state. Therefore, it is quite obvious from equation (6.15) that one would expect a constant

⁸ The curve fitting was achieved via 'Easyplot'.

value over the whole frequency range for the unmagnetised circular states.

(6.9) Computerfitted curves to the refractive index results

After determining theoretically what the nature of the refractive index curves should be one could then computerfit the curves to the refractive index data. This next section is a presentation of the computerfits, described in the previous section (6.8), to the refractive index data for each type of plastoferrite under investigation.

Each graph contains four curves. The top curve represents the computerfit to the -ve/left circular state in the magnetised case. And is a fit to the refractive index data with the circular data markers. The second curve is actually a constant predicted value for $\sqrt{\epsilon_R}$. The third curve represents the computerfit to the circular states of the unmagnetised case. And is a fit to the refractive index data with the triangular data markers. The bottom curve represents the computerfit to the +ve/right circular state for the magnetised case and is a fit to the refractive index data with the square data markers.

The refractive index vs. frequency computerfits to data for the Anisotropic plastoferrite are shown below :

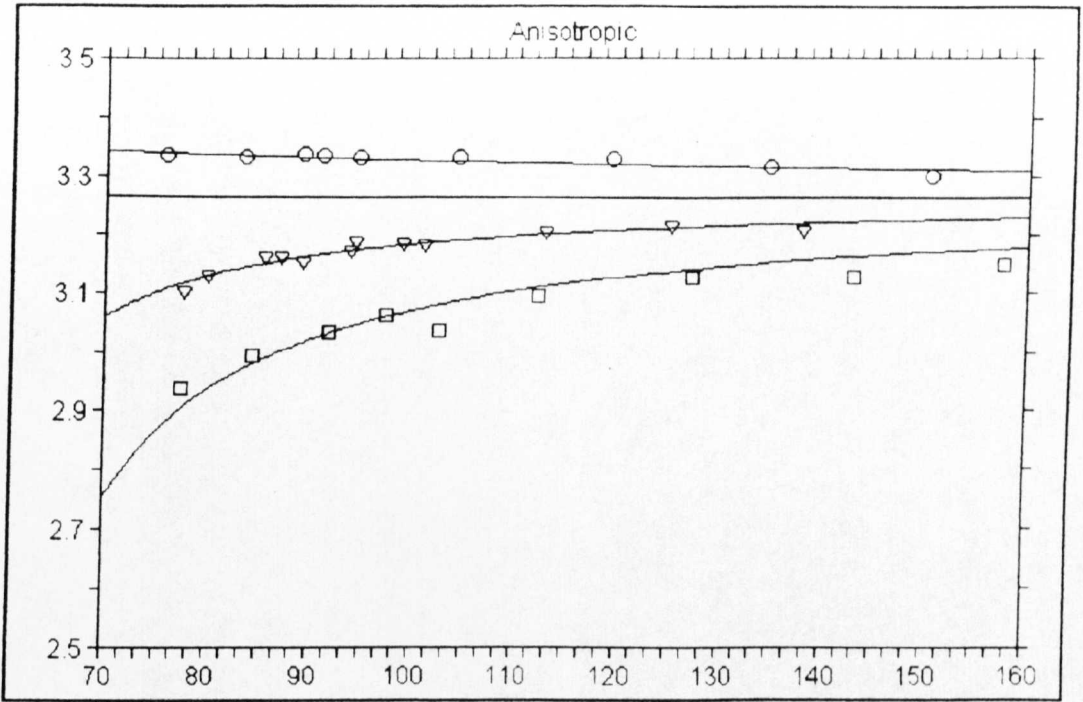


Figure 6.35

From the computerfits, $(\sqrt{\epsilon_R})$ and (ω_m) were determined to be :
 $\sqrt{\epsilon_R} = 3.26$, $\omega_m = 5.79$

The computerfits to the refractive index vs. frequency data for the Isotropic plastoferrite are shown next:

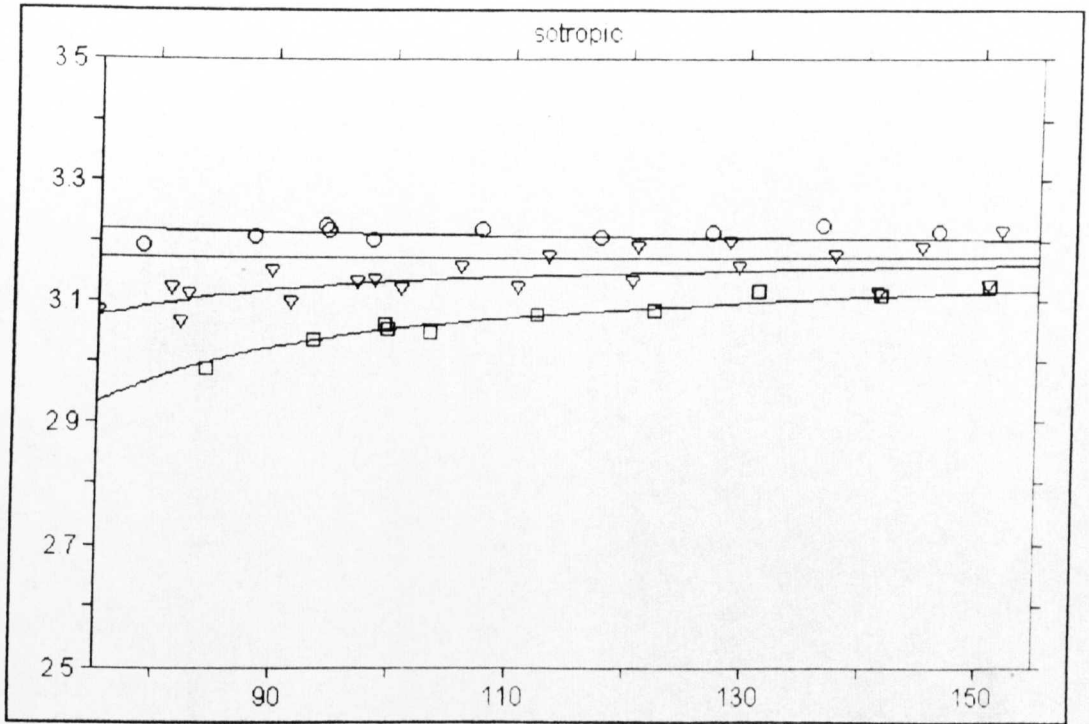


Figure 6.36

From the computerfits, $(\sqrt{\epsilon_R})$ and (ω_m) were determined to be :

$$\sqrt{\epsilon_R} = 3.17, \omega_m = 3.71$$

The computerfits to the refractive index vs. frequency data for the Semi-Anisotropic plastoferrite are shown :

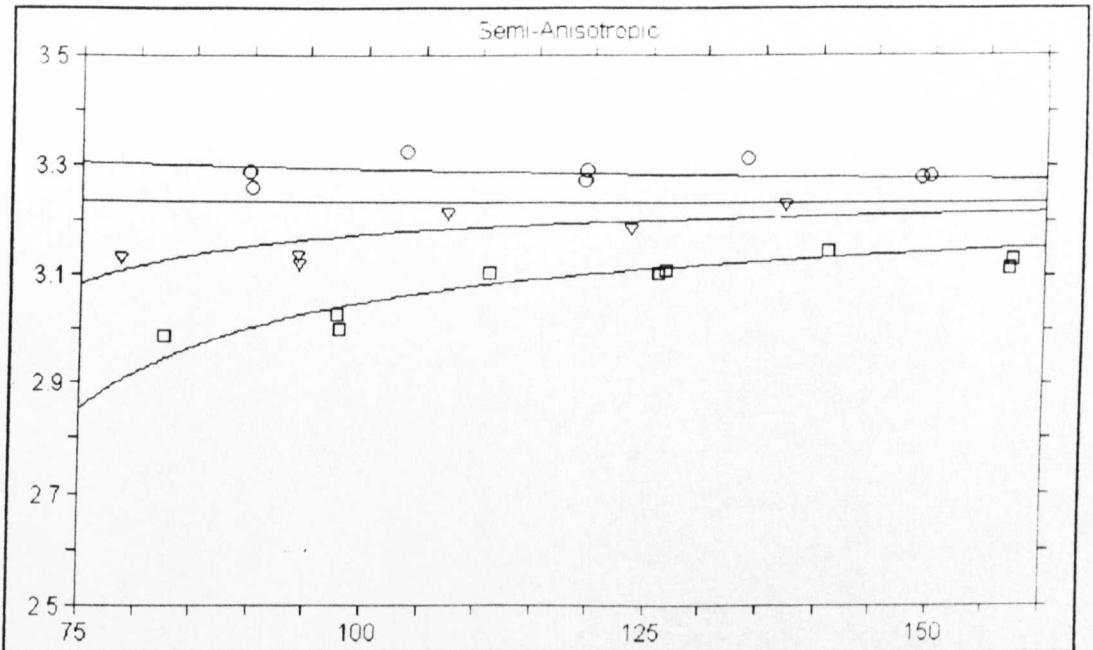


Figure 6.37

From the computerfits, $(\sqrt{\epsilon_R})$ and (ω_m) were determined to be :

$$\sqrt{\epsilon_R} = 3.23, \omega_m = 5.56$$

(6.10) Interpretation of the refractive index results.

This section will give an explanation of the refractive index results presented in section (6.9). The results for the magnetised versions of all the three types of plastoferrite behaved as predicted from section (6.8) except in the unmagnetised case. The unmagnetised curve showed a non-linear trend which did not correspond to a computer fit using equation(6.15). Therefore, an average of the computerfitted curves of the magnetised circular states was fitted instead. This non-linear trend is evident in all the three types of plastoferrite that were investigated. Examining equation(6.15) shows this could be an electric effect in which the relative permittivity (ϵ_r) is not constant. Another possibility is a magnetic effect that could cause the relative permeability $\mu_r \neq 1$ in the unmagnetised case. Also a combination of

both these effects could be causing the non-linearity. Examining the manufacturing process of the three types of ferrite suggests that the $\mu_r \neq 1$ could be significant in the production of the non-linearity. This implies that there is a preference to one circular state with respect to the other in the unmagnetised case, which could be due to an alignment in a specific direction induced by the manufacturing process. This is understandable in all the cases and is probably a consequence of the manufacture. The Anisotropic material was manufactured by 'Die pressing' and the Semi-Anisotropic and Isotropic materials were manufactured by 'Calendering'⁹. In both manufacture processes the particles are all oriented in some preferential direction which could lead the unmagnetised versions of the material to discriminate differently between the two circular states.

(6.11) Calculated 'Ideal Thickness' or 45 degree rotation vs. frequency.

This section describes how the ideal thickness, for 45⁰ degree rotation can be calculated for each of three types of plastoferrite. One can start by taking the computer generated equations, which were fitted to the refractive index for each type of plastoferrite. These equations can then be used to generate (β_{\pm}) values, from equation (6.10), over the desired frequency range. From these generated (β_{\pm}) values one can predict the optimal thickness (L) required for $\theta = 45^0 = \frac{\pi}{4}$ rotation from the equation (6.17).

$$\theta = \frac{L}{2} (\beta_- - \beta_+) \quad \dots(6.16)$$

$$\Rightarrow L = \frac{\pi}{2(\beta_- - \beta_+)} \quad \dots(6.17)$$

⁹ Described in section(5.7).

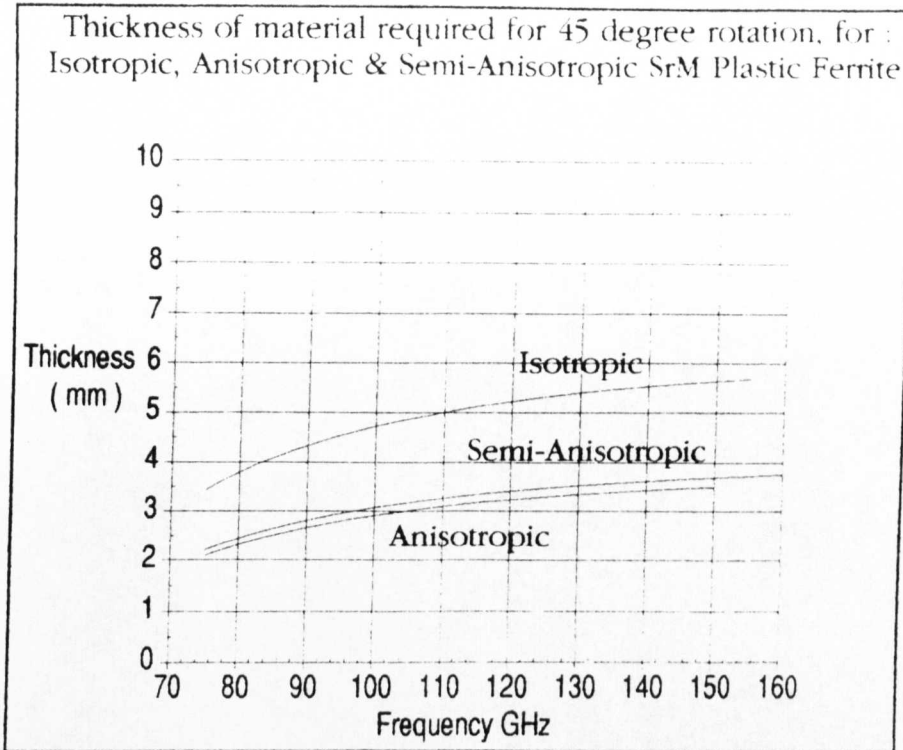


Figure 6.38

The predicted optimal thicknesses for 45° rotation are shown in Figure (6.38). Using the information from figure(6.38), I proceeded to construct three Faraday Rotators IA1, IA2 and I9. The following section, will describe their construction, how they were characterised and a discussion of how well they performed. The section will be concluded by determining whether the plastoferrites discussed are a viable option for use in quasi-optical Faraday Rotators.

(6.12) Plastoferrite, Quasi-Optical, Freespace Faraday Rotators

(6.12.1) Construction Of Faraday Rotators

As described above, three Faraday Rotators were constructed, a description of which now follows.

(6.12.1.1) Faraday Rotators (IA1) & (IA2)

Both Faraday Rotators were cut from the SrM, Anisotropic ferrite. This material was supplied in 6mm thick sheets for 'Magnet Developments'. 100mm×100mm squares were cut to form the

Faraday Rotator. The sides of the squares were parallel to the sides of the sheets from which they were cut. Faraday Rotator (IA1) was then machined to a thickness of 3mm and Faraday Rotator (IA2) was machined to a thickness of 2.75mm. On either side of the ferrites one ($\frac{1}{4}\lambda$) PVC matching layer was affixed. As a point to note, all of the isolators constructed used the adhesive 'Araldite'. Also a thinner was used, in the form of Toluene. The PVC layers for (IA1) were of thickness 0.45mm and (IA2) had layers of thickness 0.5mm. The main reason for the construction of the Faraday Rotators, was for use in a high frequency millimetric Electron Spin Resonance application¹⁰. Therefore, the thickness of the ($\frac{1}{4}\lambda$) matching was designed for operation at 150GHz & 166GHz.

(6.12.1.2) Faraday Rotator (I9)

The material used for (I9) was SrM Semi-Anisotropic Plastoferrite. This was supplied in a rolled form from 'Anchor Magnets'. The Faraday Rotator required two pieces of the material. Each of the two pieces was cut at 22.5° to the flux lines of the remnant magnetic field, as described in section(9.7.2). Similarly, (I9) was constructed for operation at 150GHz and therefore had 0.5mm UPVC matching.

(6.13) Experimental Setup Used To Determine Isolation & Insertion Loss

The quasi-optical experimental setup used to determine the performance of the isolators can be seen below in figure(6.39).

¹⁰ A Millimeter Wave Quasi-Optical Electron Spin Resonance Spectrometer, G.M.Smith, J.C.G. Lesurf, R.H.Mitchell, P.C.Reidi, Int.Conf.Inf.MM Waves, Berlin, 1996.

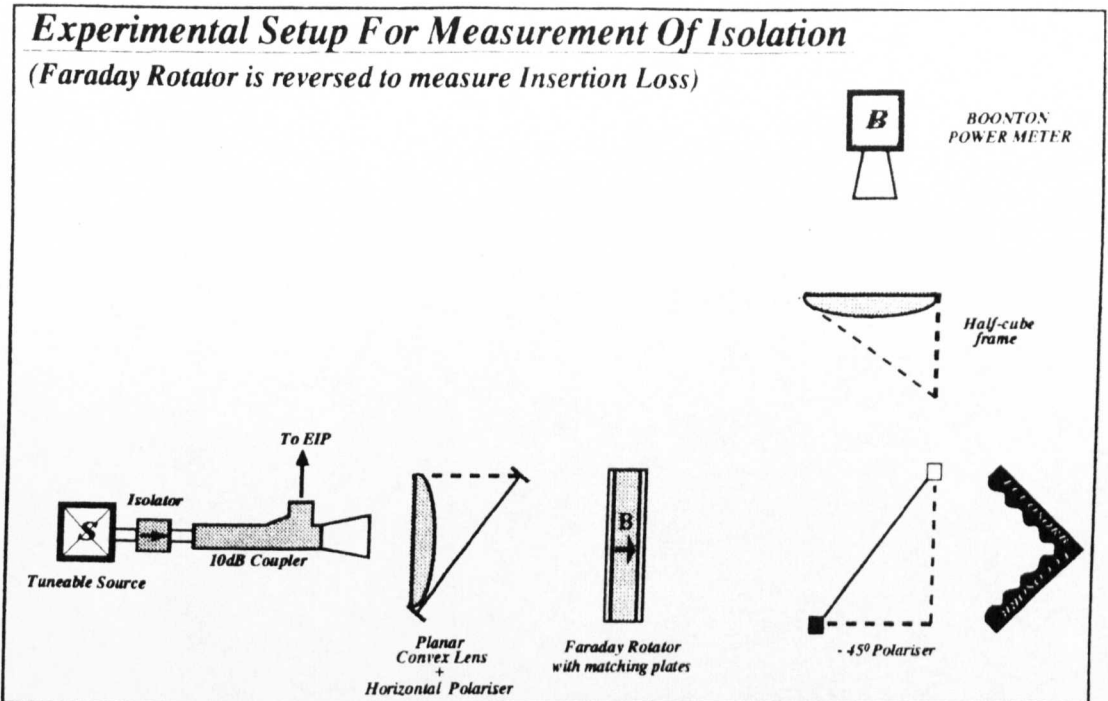


Figure (6.39)

The way in which the isolation and insertion loss was determined is as follows. Without the Faraday Rotator in the setup, due to the 45° polariser, i.e. beamsplitter, half of the incident power would get transmitted to the Eccosorb load and the other half reflected to the Boonton power meter. Initially, the Boonton is zeroed to this 3dB power level. Therefore, this represents 100% power. If a perfect Faraday Rotator were now placed in the setup, such that it rotates the vertical beam through 45° in a clockwise direction. Then from the orientation of the wires of the -45° polariser, all of the beam will pass through the polariser and get absorbed by the Eccosorb load. Hence, from the detectors's perspective it sees 0% power. Hence, a very large -ve dB value will be recorded. In the realistic case, were the beam is not rotated through exactly 45° or some ellipticity has been imposed on it. Then some small fraction of power will be reflected to the detector. The relative value measured is known as the 'Isolation'. The larger the -ve figure the more efficient the Faraday Rotator.

The 'Insertion Loss' can be measured simply by turning the ferrite around. In the ideal case, all of the power would be channelled to

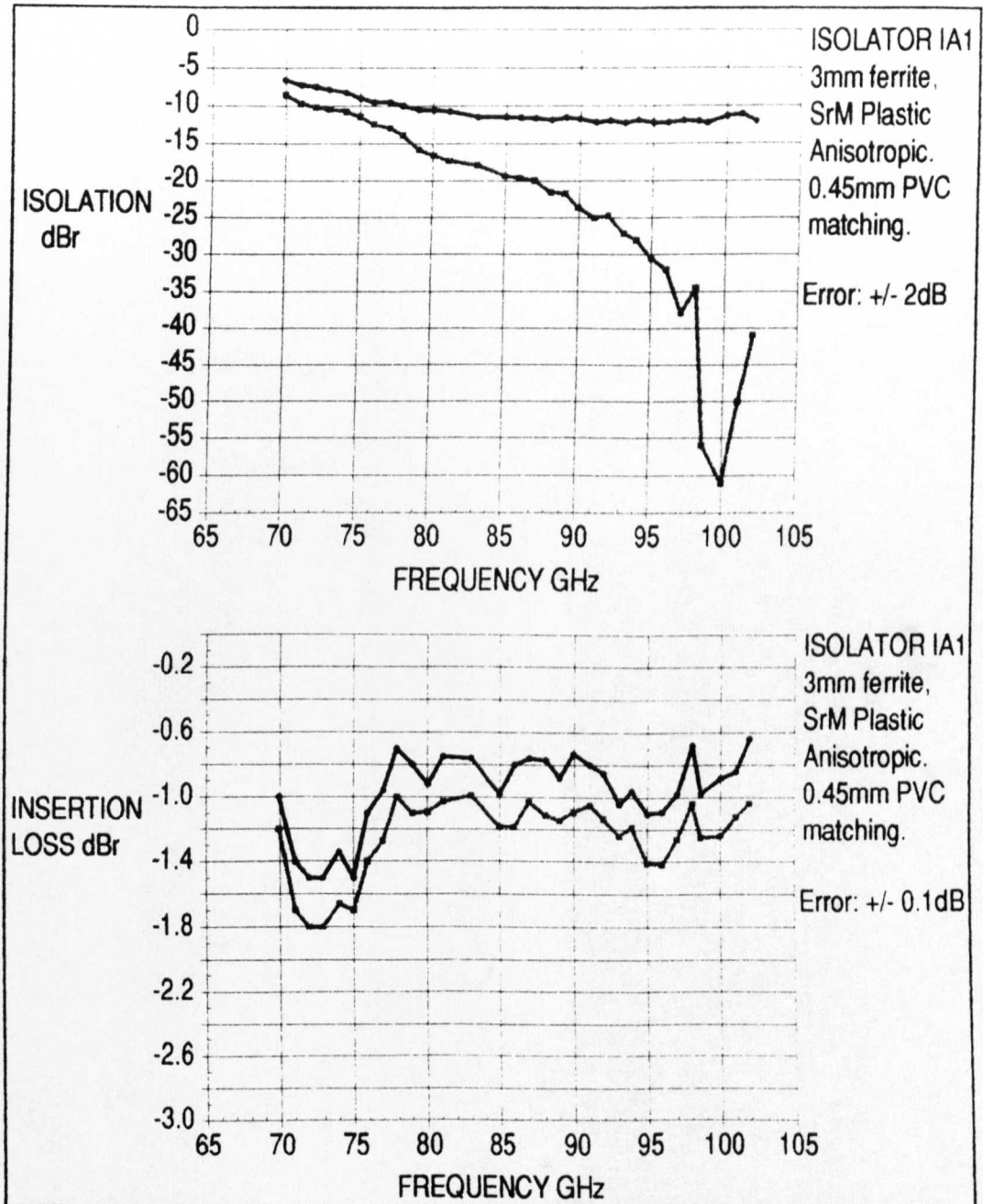
the Boonton power meter. The meter would therefore see twice as much power as it did without the device in the setup. Hence, 3dB's would be registered if the device were lossless. In the realistic case, this value will be less. The power detected is the amount of power that was successfully rotated and transmitted through to the detector. Thus, the insertion loss is recorded as 3dB less the detected value.

The Isolation and Insertion Loss of the Faraday Rotator (I9) was determined using the above method. The only difference in the methodology for (IA1) and (IA2) was that they were manually angled at ($\approx 22.5^\circ$) from the vertical. The reason for this is due to the spatial measurements described in section(9.7.2) which pointed to the materials being birefringent. Since, (I9) had already been cut specifically to allow for this, described in section(6.12.1.2), there was no need to angle it.

(6.14) Isolation & Insertion Loss Results For (IA1), (IA2) & (I9)

The results of the isolation and insertion loss experiments using the experimental setup of figure(6.39) are shown below.

(6.14.1) Results for (IA1)



Figure(6.40)

(6.14.2) Results For (IA2)

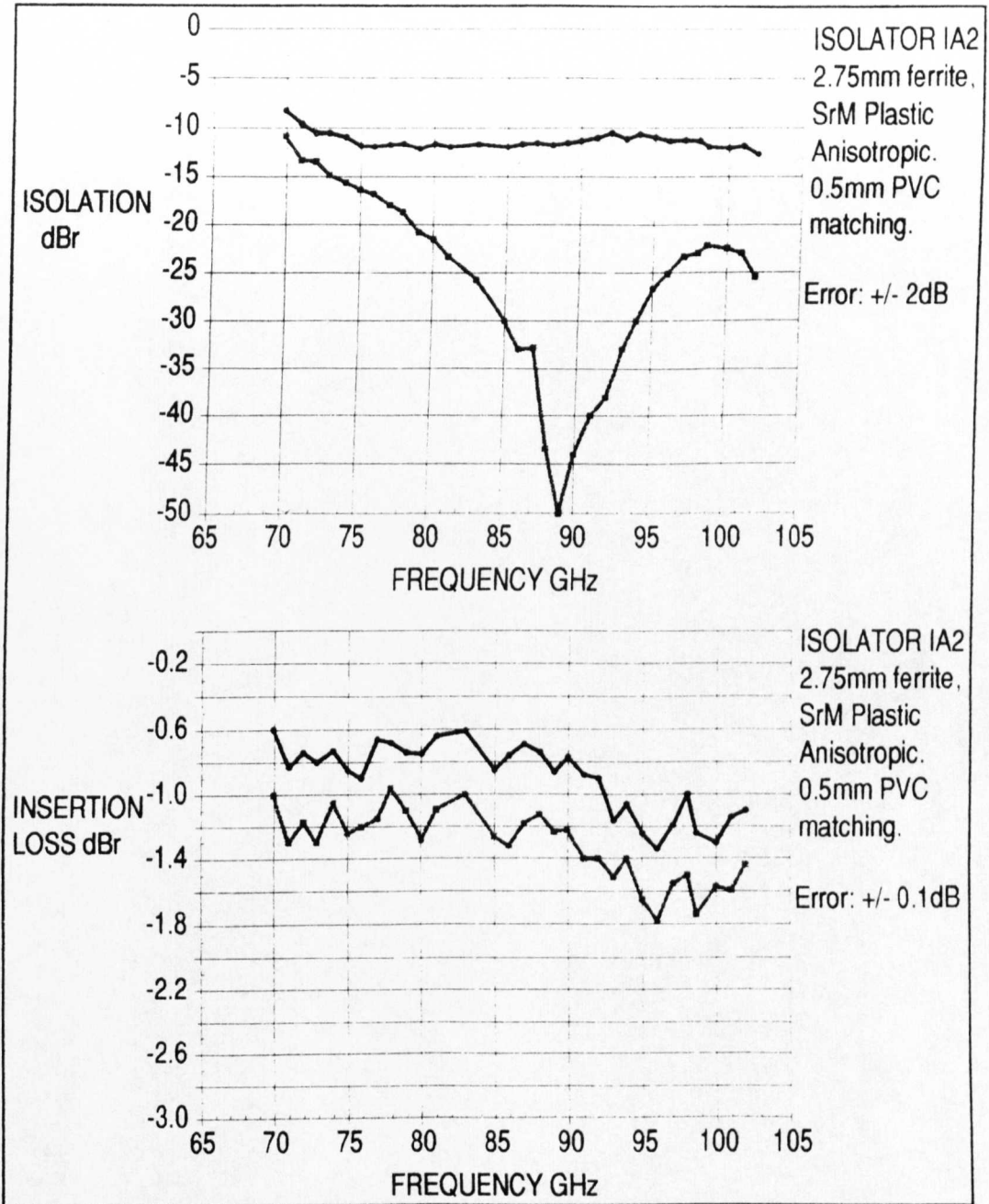


Figure (6.41)

(6.14.3) Results For (I9)

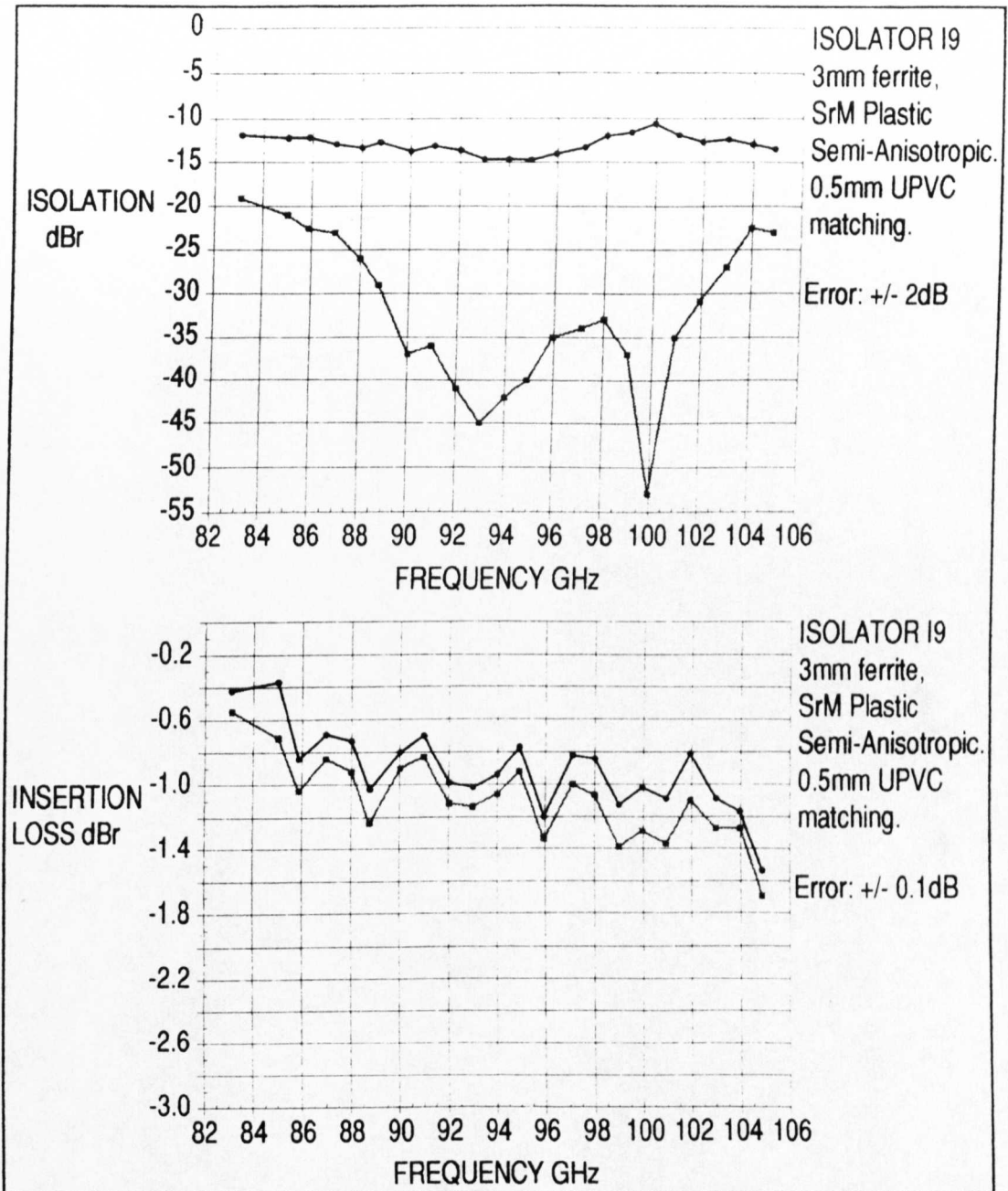


Figure (6.42)

(6.15) Results Analysis

(6.15.1) Results Analysis Of (IA1)

As can be seen from the isolation plot for (IA1), there is a definite spot frequency for the forward operation of the device which occurs at 100GHz giving an isolation of -61dB's. Figure(6.38) predicts the

frequency of operation for an Anisotropic Rotator of a 3mm thickness to be 104GHz. This gives an error of 4.0% in the prediction. However, this location could well be affected by the manual angling of the Rotator that was involved. The bandwidth at which > -20 dB's isolation occurs is 17GHz. This ofcourse would be larger, if measurements of the isolation had been performed at higher frequencies. The reverse isolation of (IA1) is considerably less than its forward counterpart. This is due to the birefringence of the material, as discussed in sections(5.8) and (9.7.2). The reverse isolation remained roughly constant at ≈ -12 dB's from 82.5 -102GHz. The insertion loss for the forward direction was > -1.0 dB's and < -1.8 dB's across the region. The reverse insertion loss was slightly better, > -0.62 dB's and < -1.5 dB's across the region.

(6.15.2) Results Analysis Of (IA2)

Very similar results were obtained for (IA2). Again there was a definite frequency of operation at 89GHz of -50 dB's isolation. Figure(6.38) predicts the frequency of operation for an Anisotropic Rotator of a 2.75mm thickness to be 93GHz. This gives a slightly larger error of 4.4% in the prediction and again this could have been influenced by the manual angling of the device. Over the region concerned, the > -20 dB bandwidth of operation of the device in its forward direction is 24GHz. The angling of the device gives it a poor reverse isolation which is similar to (IA1). However, the > -12 dB isolation persists over a larger 75- 102GHz region.

The insertion loss for the forward direction was no better than (IA1), even though the device was thinner. The figures were > -1.0 dB's and < -1.8 dB's across the region. The reverse insertion loss was slightly better than (IA1) giving figures of > -0.60 dB's and < -1.3 dB's across the region.

(6.15.3) Results Analysis Of (I9)

The forward isolation curve for (I9) has a operation frequency of

100GHz giving an isolation of -56dB's which is less than the (IA1) and greater than (IA2). Figure(6.38) predicts the frequency of operation for a Semi-Anisotropic Rotator of a 3.0mm thickness to be 97GHz. This gives an error of 3.1%. However, it should be noted that the Rotator was constructed from two pieces of ferrite which could serve to alter its frequency of operation. The >-20dB's bandwidth over the region of interest was 22GHz which is greater than the bandwidth of (IA1) and competitive with that of (IA2). The Insertion Loss was almost identical in both the forward and reverse directions. It was competitive with that of (IA1) and (IA2) in the forward directions and better than both in the reverse directions, even though it was thicker than (IA2). The figures ranged from values of > -0.6dB's to < -1.5dB's.

(6.16) Conclusions & Final Remarks

Figure(6.43) tabulates the frequencies at which the Faraday Rotators operate best at from the experimental results of figures (6.40 - 6.42). Also included are the frequencies predicted from the optimum performance figure(6.38).

Faraday Rotator	Pred.Op.Freq.	Actual.Op.Freq.	Error	Comment
IA1 (3.00mm)	104 GHz	100 GHz	4.0%	Angled Manually
IA2 (2.75mm)	93 GHz	89 GHz	4.4%	Angled Manually
I 9 (3.00mm)	97 GHz	100 GHz	3.1%	Two pieces Affixed

Figure (6.43)

As can be seen from the tabulated results, the predictions of the optimal thickness as shown in figure(6.38), have only a 4.2% average margin of error for the Anisotropic plastoferrite and a 3.1% margin of error for the Isotropic plastoferrite. The prediction of the optimal thickness for 45° rotation therefore gives a good agreement with experiment. As was mentioned in section(6.15.1), the

systematic error introduced in the manual angling of the (IA1) and (IA2) could influence the location of their frequencies of operation. Concerning (I9), the affixing of two ferrites could also introduce performance changes. In addition, problems were encountered when determining the thickness accurately for samples of the Semi-Anisotropic and isotropic type. This was because 2-3 layers of the rolled ferrite had to be used in order to produce a significantly thick sample. The glue used to bond the ferrite layers was 'Araldite'. Also a thinner was used, in the form of Toluene. Also there was no way of accurately predicting the thickness of the glue layers or the amount of ferrite that the Toluene thinner could dissolve in the bonding process.

Two attempts were made at constructing Rotators from the 'Isotropic' plastoferrite material. The results however were extremely poor. This is probably due to the fact that quite a thick sample was required to attain 45° rotation. Approximately five layers of ferrite were needed for operation at 94GHz. It was extremely hard to ensure that the different layers remained aligned in the gluing process. Also there was a higher risk of air becoming trapped between the layers. The high number of layers together with the matching layers could result in a high probability of multiple reflections occurring within the sample. This in turn would incur additional rotation on the beam and severely reduce the isolation and increase the insertion loss of the device. Thus, the difficulty in construction of an Isotropic Rotator proved the device to be unsuitable for use at millimeter wavelengths.

In conclusion, all of the plastoferrites offer a very high performance which is very competitive with their polycrystalline versions. All the materials were found to exhibit birefringence and therefore were angled at 22.5° to maximise isolation in one direction. They all have a $> -20\text{dB}$ isolation over bandwidths of 20GHz and also offer very good insertion loss up to -0.6dB 's. The tradeoff occurs in the reverse direction where isolation is reduced in comparison.

Both types of the plastoferrite studied offer a very high performance in different areas and choice really depends upon the users requirements, described below.

The Anisotropic plastoferrites offer an exceptional spot frequency performance (up to -60dB's) and would be very suited to spot frequency applications. In addition, their isolation does persist over a very large bandwidth (up to 24GHz+) and their insertion loss is better than a conventional waveguide isolator.

The Semi-Anisotropic plastoferrites still offer a very high isolation (up to -56dB's) as well as giving good isolation over a bandwidth of (22GHz+). They also offers a very good insertion loss in both the forward and reverse directions (up to -0.6dB's). These figures would probably be improved if the device could be made from a single layer of ferrite as opposed to 2-3 layers.

In general, it is worth sacrificing a small drop in spot frequency isolation of the Semi-Anisotropic material for the benefit gained in the low insertion loss in both forward and reverse directions.

Chapter 7 Instrument Development Of A Rotary Polariser

Introduction

The following chapter will describe how I developed a Rotary Polariser Instrument. The Rotary Polariser consisted of a circular polariser which could be rotated accurately by a stepper motor and monitored and controlled by a computer.

The chapter will consist of a discussion which will identify what the user wanted ideally from the instrument. I shall call these user requirements. Also what design features had to be incorporated to allow efficient propagation of a gaussian beam when it reflects and transmits at the polariser face. These I will class as design requirements. In addition, it was necessary to identify what type of motor and motor-drive should be used in order that correct movement be performed by the instrument and to identify any requirements of the motor and motor-drive that have to be fulfilled for successful operation (these are to be known as motor and motor-drive requirements). By determining a suitable compromise of the three types of requirements mentioned, the chapter will document a system solution that will produce efficient and successful operation for the application in question. The interconnection of the three above mentioned requirements is shown in (Figure 7.1).

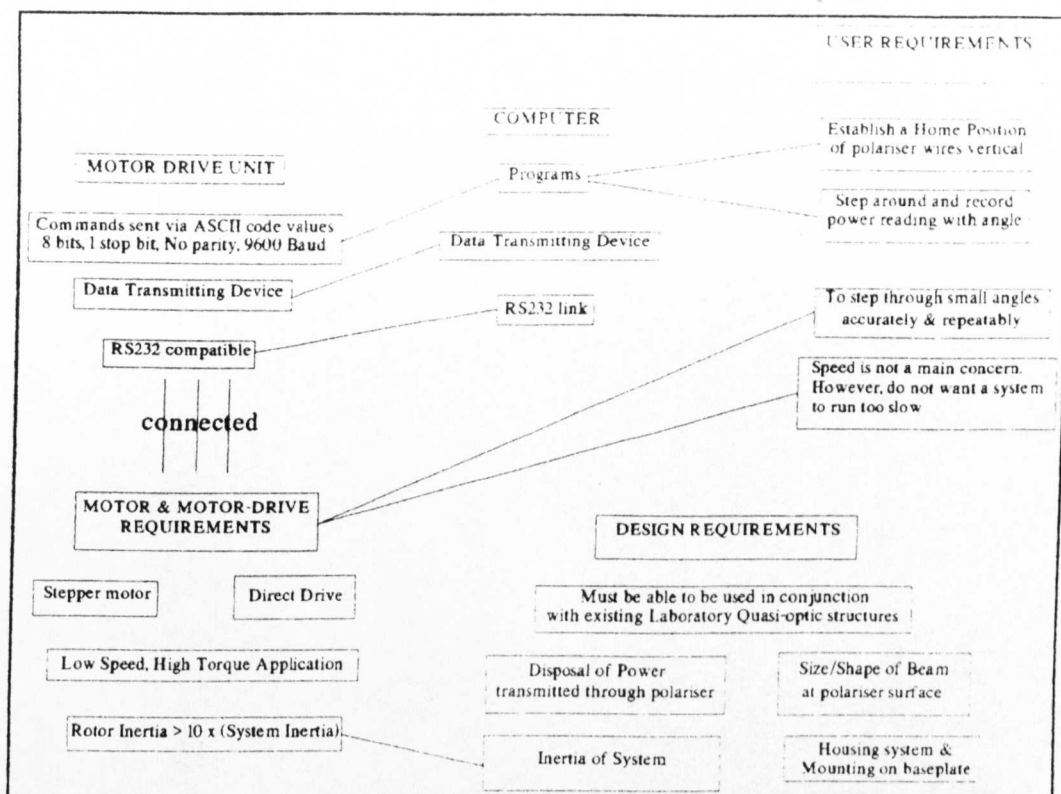


Figure 7.1

(7.1) Design requirements.

In the Rotary Polariser design several factors had to be considered. These factors determined the overall size and shape of the instrument, which will now be discussed.

(7.1.1) The Size Of The Circular Polariser.

The size of the circular polariser is very important. It is determined by the size and shape of the gaussian beam at the polariser face and is a consideration that cannot be overlooked. There are three factors that come into play when determining the size of the polariser.

The first and most important requirement is that the circular polariser is large enough to contain the beam which is projected on to its surface. If the polariser is not large enough this will result in clipping and truncation of the beam. If the polariser is too large, however, it will create unwanted excess inertia which could degrade the performance of the motor. The inertia of the system will be

described in more detail later.

The second requirement is an extension of the first. Not only does one have to encompass a beam that is projected onto the face of the polariser, but it is also necessary to take into account the inclination of the polariser face in relation to the beam. Since the polariser face is angled at 45° to the oncoming beam (See Figure 7.2), the beam will be elliptical in shape, at the plane of the polariser. The size of the major axis that the ellipse of the beam forms is the largest dimension of the beam. This dimension must be contained within the polariser to avoid any truncation of the beam and will serve to increase the size of the polariser in comparison to if the beam was circular (i.e. if the polariser was not inclined to the beam).

The final design requirement, is that the polariser will have to be used in conjunction with the existing laboratory quasi-optical structures. The quasi-optical structures which we use here at St. Andrews have an optical height of 60mm. The optical height of the rotary polariser is, as will be shown, larger than that of the quasi-optical structures. This will mean that the beam will not be concentric with the polariser and will fall in the lower half of it. This will also tend to enlarge the polariser in order to encompass the beam.

Taking all the design requirements into consideration. We want to design a polariser that will firstly encompass the largest beam that we expect to see at its face. The polariser will be located at the beam waist. Therefore, the largest beamwaist will occur at the polariser face when the beam at the lens is almost plane parallel. (Namely, when the beam has minimum diffraction effects occurring along its path). The largest beamwaist allowable at the lens, to avoid truncation is ($\frac{D_l}{3} = 29.3\text{mm}$), see figure (6.4). Therefore, we can assume the beamwaist to be the same as that at the lens, although in reality it is slightly less. Now let us take into consideration, the fact, that the polariser is inclined at 45° to the oncoming beam. Since one can assume the beam to be plane parallel, the elliptical

shape produced on the polariser surface will have a major axis of 126mm. The minor or vertical axis of the beam will remain preserved at (2x29.3mm). This is represented in (Figure 7.2) shown below.

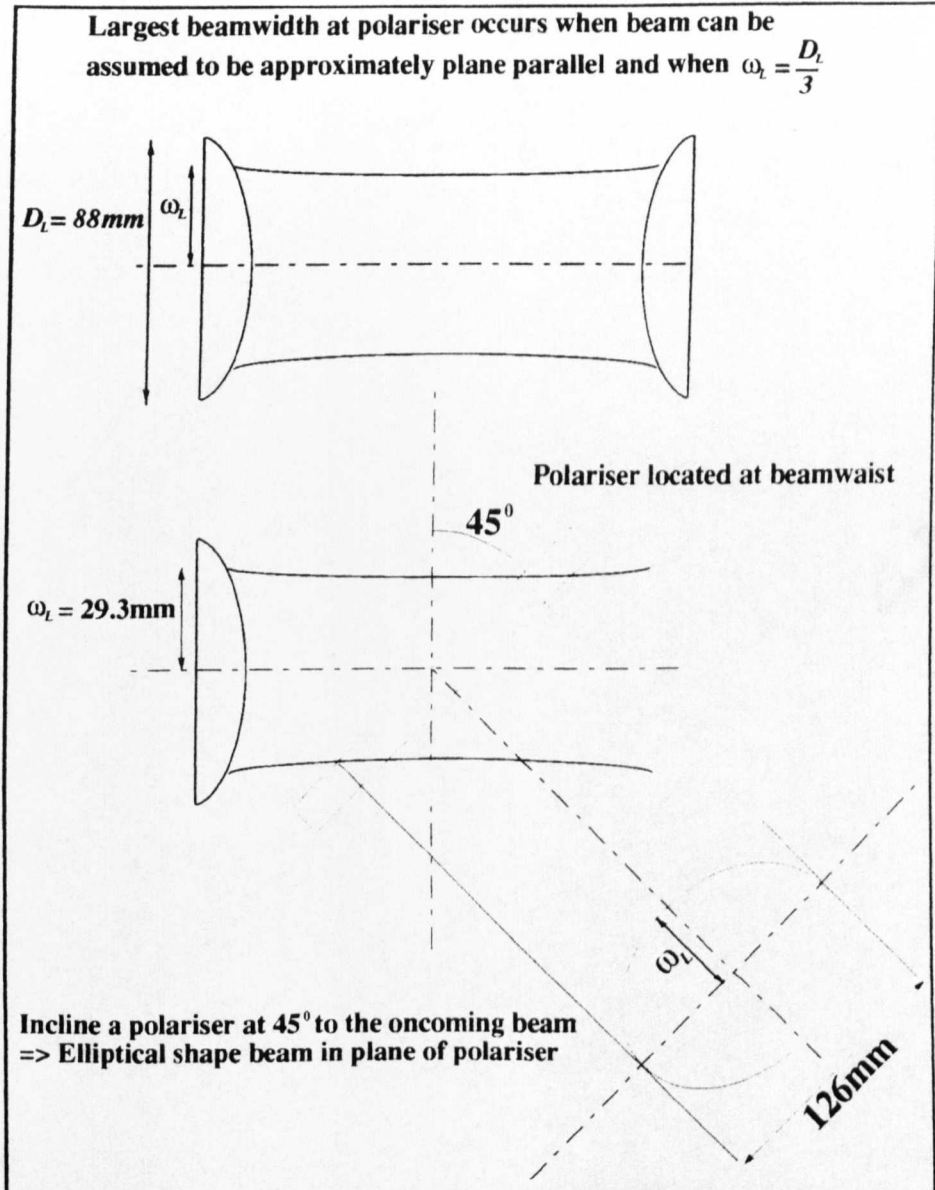


Figure 7.2

Since the optic axes, for the polariser and beam, are not concentric; the beam will fall in the lower half of the polariser. Therefore, the width of the polariser at the optic-axis of the beam (i.e. 60mm from the baseplate) will have to be at least 126mm. A polariser of radius

82mm would encompass this maximum beam size and also give an 11.6mm margin of clearance, either side of the beam's major axis. The polariser was wound on a circular frame of outer radius 92mm, inner radius 82mm and was 6.35mm thick (See Figure 7.3).

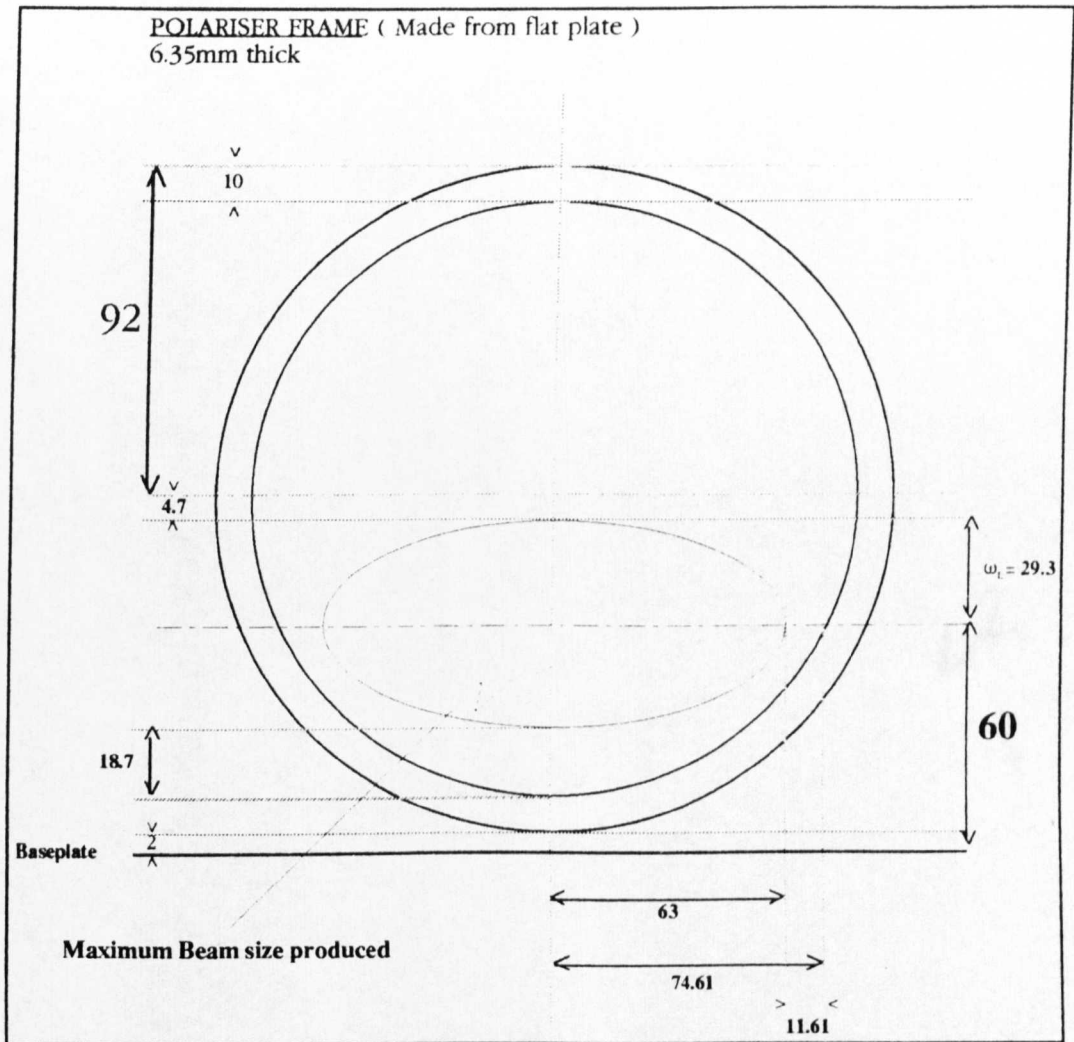


Figure 7.3

The frame was made from specially manufactured plate. This was ideal for winding a polariser structure onto due to its high surface finish. The polariser was wound with 25 micron tungsten wire at a pitch of 50 microns.

(7.1.2) The Length Of The Cavity & Disposal Of Transmitted Power.

Another problem that can arise and could be alleviated by design now follows. It is concerned with the power that is transmitted through the circular polariser wires. Now the polariser would have to be mounted on some type of framed structure which then can be connected to and driven by the motor. I shall refer to this as the 'cavity structure'. Whatever the design of the cavity structure, the rear face of it could reflect the transmitted power back through the polariser into the system. This reflected power could then set up standing waves in the system and serve to reduce the accuracy of any measurements made. I decided the cavity structure would consist of three aluminium rods which were connected to the polariser frame equally distant from one another. The three rods were then connected to a wheel like frame, which formed the back of the cavity. The wheel like frame was connected to a cylindrical hub .The hub was passed through the front of a housing unit which supported the whole instrument. The motor was connected to the back of the housing unit and its shaft was affixed rigidly within the hub. The housing unit could then be located on the baseplate (See Figure 7.4).

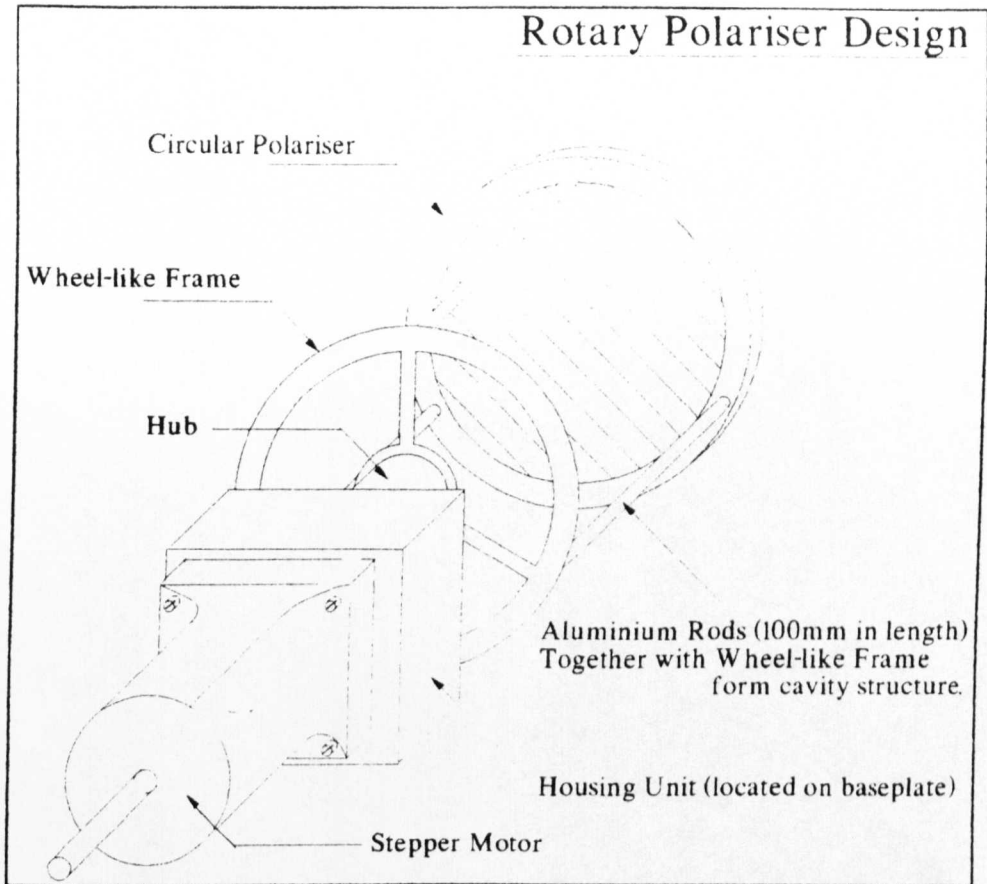


Figure 7.4

The reason I chose to have a cavity structure that consisted of three aluminium rods and a wheel like frame was for two reasons. The first reason is that it greatly reduces the inertia of the system which will be described later. The second reason is that any transmitted power that reflects from the back of the cavity can actually be reflected out of the sides of the instrument if the cavity length is large enough. As one can see from (Figure7.5).

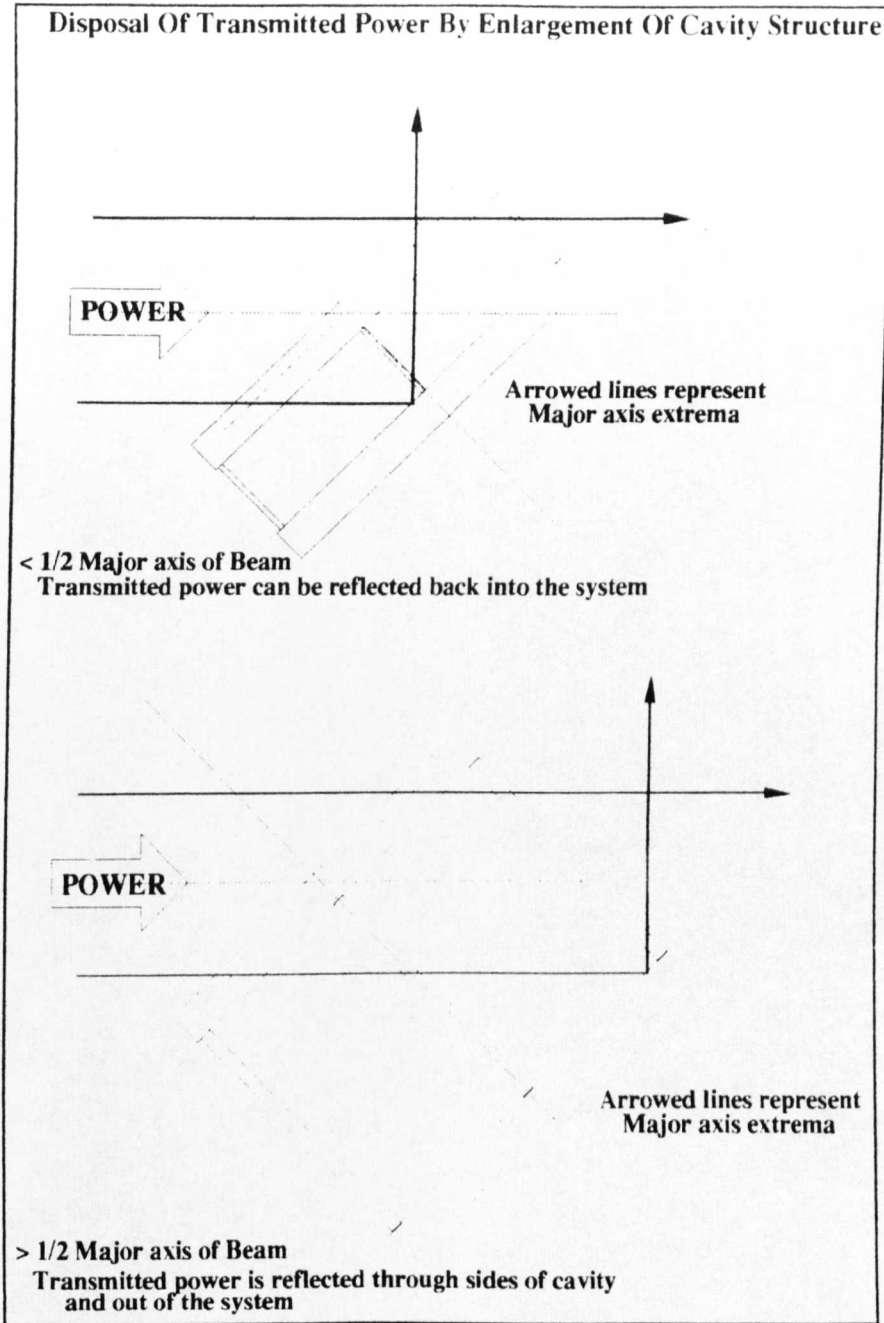


Figure 7.5

As long as the cavity length is greater than half of the radius of the beam then any transmitted power will be reflected out of the sides of the cavity. This corresponds to half of the major axis of our beam, since the instrument is inclined at 45° to the incoming power. Therefore, the minimum cavity length for our application could be 63mm. I chose a cavity length of 100mm. 20dB Eccosorb was also affixed to the back of the cavity for an extra safeguard.

(7.2) The Inertia Of The System

Before I describe the motor and motor-drive requirements, I will firstly discuss the inertia of the system. The inertia of the system is very important factor and is constrained by the size of the motor used.

The general rule of thumb is :

- rotor inertia \leq The system load inertia < 10 times the rotor inertia.

The motor needs a load of at least its own inertia to accelerate properly. Loads of less than the rotor inertia can cause resonance to develop within the motor and can also cause the motor to stall. This fact also deters one from just indiscriminately buying a large motor since these resonance are more pronounced when the rotor inertia forms the majority of the load. If the load inertia is greater than ten times the rotor inertia cogging and extended ringing can be experienced at the end of a move.¹ Resonance, ringing and the inertia of the system can be reduced by the type of motor one uses, which will be described later. The inertia of the motor I chose, served to limit the maximum weight of the system I could use and also curtailed my design of the system to that of (Figure 7.4). The Rotor Inertia² of the motor I chose was 10.24 oz.in². Therefore, the system load inertia for our application would have to fall between the limits :

- 10.24 oz.in² \leq System Load Inertia < 102.4 oz.in²

Bearing this in mind the inertia of the system was determined as follows :

¹ As explained in Engineering reference section pg. A12 of the 'Compumotor & Digiplan - Step Motor & Servo Motor Systems & Control Catalogue (1995)'.

² The unit (oz.in²) is the unit commonly referred to, when specifying motor inertia. Therefore, I will adopt this convention when referring to inertia.

Hub dimensions (Cylinder)³

cylinder of radius(r) = 25mm, length(l) = 120mm \Rightarrow Mass(M) = 636 g.

$$I_{\text{HUB}} = \frac{Mr^2}{2} = 0.199 \text{ gm}^2$$

Polariser Frame (Cylindrical Ring)

Outer radius(r_{out}) = 92mm, Inner radius(r_{in}) = 82mm, Thickness = 6.25mm
 \Rightarrow Mass(M) = 92 g.

$$I_{\text{POL}} = \frac{M}{2}(r_{\text{out}}^2 + r_{\text{in}}^2) = 0.6995 \text{ gm}^2.$$

3 Rods (cylinders) each of :

radius(r) = 2.5mm, length(l) = 100mm \Rightarrow Mass(M) = 5.3 g.

Use parallel axis theorem, since axis of rods is height(h) = 89.5mm above axis of rotation.

$$I_{\text{RODS}} = 3 \times \left\{ \frac{Mr^2}{2} + Mh^2 \right\} = 0.127 \text{ gm}^2.$$

Wheel-Like Frame (Can be considered to consist of a cylindrical ring,
a disc and 3 rectangular slabs)

Cylindrical ring

Outer radius(r_{out}) = 92mm, Inner radius(r_{in}) = 87mm, Thickness = 5mm
 \Rightarrow Mass(M) = 0.038 g.

$$I_{\text{RING}} = \frac{M}{2}(r_{\text{out}}^2 + r_{\text{in}}^2) = 3.05 \times 10^{-4} \text{ gm}^2.$$

Disc

Radius(r) = 25mm, Thickness(t) = 5mm \Rightarrow Mass(M) = 26.49 g.

$$I_{\text{DISC}} = \frac{Mr^2}{2} = 4.14 \times 10^{-5} \text{ gm}^2 .$$

3 Rectangular slabs (each of)

Length(a) = 67mm, width(b) = 5mm, Thickness = 5mm \Rightarrow Mass(M) = 4.5 g.

Use parallel axis theorem, since axis of slabs is height(h) = 33.5mm above axis of rotation.

$$I_{\text{SLABS}} = 3 \times \left\{ \frac{M}{2}(a^2 + b^2) + Mh^2 \right\} = 0.0203 \text{ gm}^2 .$$

$$\therefore I_{\text{WHEEL}} = I_{\text{RING}} + I_{\text{DISC}} + I_{\text{SLABS}} = 0.0206 \text{ gm}^2 .$$

³ All components of the Rotary Polariser were made from Aluminium ($\rho = 2698 \text{ kgm}^{-3}$).

$$\begin{aligned}\therefore \Rightarrow I_{\text{SYSTEM}} &= I_{\text{HUB}} + I_{\text{POI}} + I_{\text{RODS}} + I_{\text{WHEEL}} = 1.046 \text{ gm}^2 \\ &= (1.046)(1 \times 10^{-3})(5.46745 \times 10^{-9}) = 57.20 \text{ oz in}^2 \\ &\Rightarrow \frac{57.20}{10.24} = \underline{5.59 \text{ times Rotor Inertia.}}\end{aligned}$$

This value of the system inertia falls within the inertial limits calculated earlier.

(7.3) The Motor & Motor-Drive Requirements.

Basically, to move a load one requires a motor which is connected directly or indirectly, via a geared or belt mechanism, to the system. The motor is in turn driven by a motor-drive unit. This usually consists of a piece of electronics which takes information from a computer and translates it to a set of pulses. The pulses describe the values of the currents to be supplied to the motor and how they will vary etc. These pulses are then passed on to a power amplifier. The power amplifier acts on the pulses by supplying the desired currents to the motor. Hence, the motor is driven accordingly.

The type of motor and motor-drive one chooses depends on the application one is using it for. It is very important to choose the correct motor and motor-drive. This is because some motors and motor-drives that have one set of features and work well for a particular application, might not necessarily work well with another application that requires another set of features. The first step to determining the motor and motor-drive features is to identify what tasks the user requires the system to perform. The tasks I wanted the system to perform were :

- To be able to step through small angles accurately and repeatably throughout 360°
- Speed was not a main concern for this application, however I did not want the system to run too slowly.

After identifying the user requirements one can relate them to features available in typical motors and motor-drives. From the user

requirements, the set of features I built up were as follows :

- Repetitive movement
- High Positional Accuracy & Repeatability
- High Resolution
- Low Speed / High Torque
- Low-cost

From these features, I decided upon a motor that was :

- Brushless
- 2 phase and 5 amps/phase (switch reducible)
- 8 lead, Bifilar wound and Series connected
- Directly Driven

and a motor-drive that had the following features in one complete unit :

- MOSFET Circulating Chopper provides Ministepping with 400-4000 steps/rev (user-selectable)
- Indexer
- Power Amp and Switch Mode Power supply
- RS232C computer link

I will now explain what these terms mean and the significance of these to the application in question.

(7.3.1) The Motor Mechanism

There are in general two types of motor design. These are a brush and brushless design. Very briefly, Michael Faraday's D.C motor was the first brush type motor. This consisted of a coil connected to a commutator that fed current to the coil. The 'Brush' refers to the commutator. Depending upon the orientation of the coil, the commutator could reverse the flow of current through the coil. The coil was placed between two oppositely poled magnets (which are known as the stators). The interaction between the fields produced by the current carrying coils and the stators would cause rotation of

the coils.

The Brushless motor is basically the inverse of the brush motor. Where the coils are replaced by a permanent magnet and the stators are wound iron cores. The main advantage of a brushless motor is the lack of the commutator (brush). The commutator is always a source of wear and potential trouble. By choosing a brushless system this problem can be alleviated.⁴ Coils are wound on oppositely aligned stators and are connected together in pairs. The number of phases of a motor refers to the number of these pairs of windings. By energising various pairs of windings, phases, in a particular fashion a variety of step resolutions can be obtained. The motor I chose had two phases and can be represented schematically by figure(7.6).

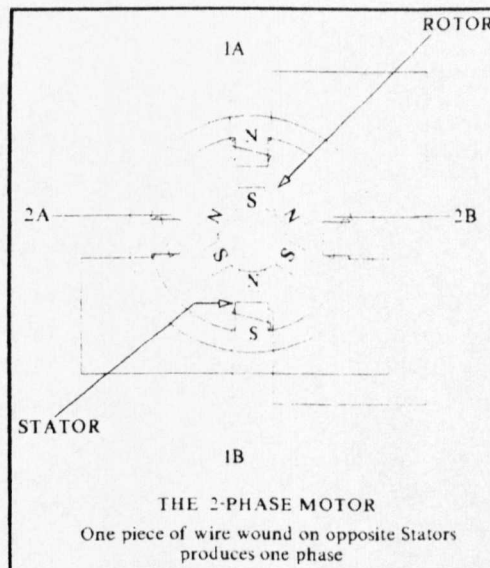


Figure 7.6

For a two phase motor, the simplest step resolution, the full-step, is achieved by keeping both the phases energised and then reversing the current in each phase alternately. Hence, reversing the polarity

⁴ The major disadvantage of a brushless motor, is rare earth magnets are required to achieve high torque and low inertia. Also more sophisticated electronics are necessary to control the current through the stator windings hence this increases the price.

of the stators and moving the rotor through a full-step (See Figure 7.7).

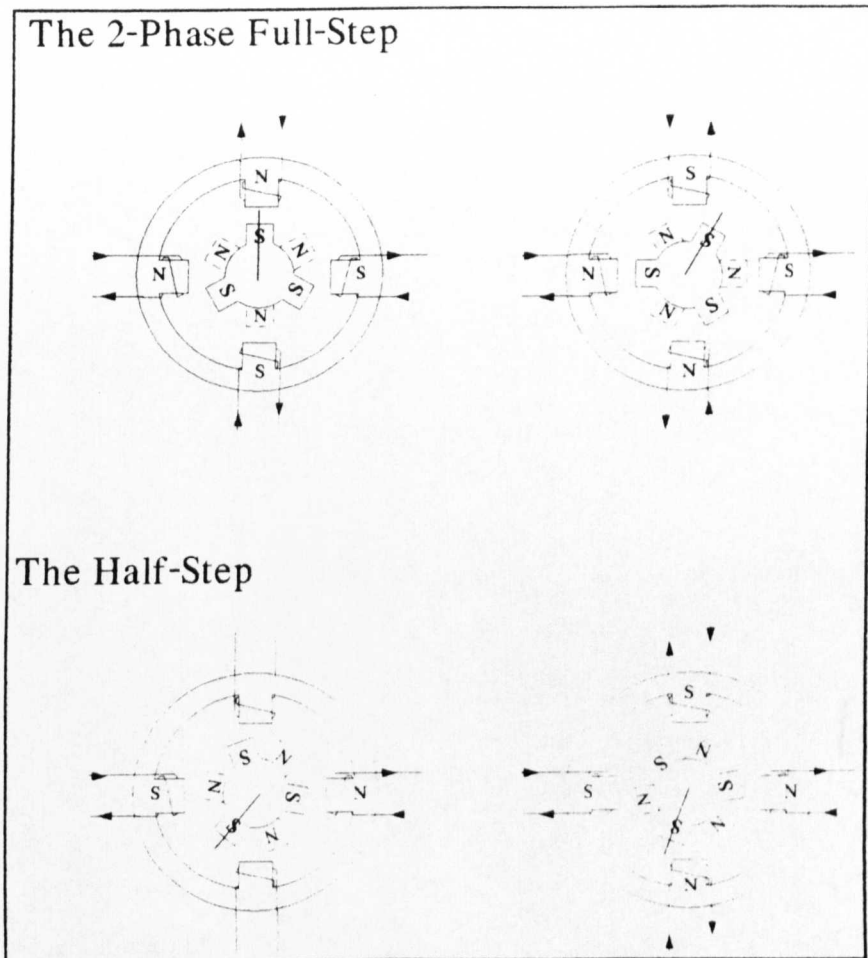


Figure 7.7

The half-step mode increases the step resolution by a factor of two (Figure 7.7). This can be achieved by alternately energising both phases and then only one.⁵ A higher mode of step resolution can be attained by proportioning the currents in the two phases, shown in figure (7.8).

⁵ This will produce a greater torque when both phases are energised in comparison to only one phase being energised. This can be alleviated by using a higher current level when only one phase is energised. This does not over dissipate the motor either because the manufacturers current rating assumes that two phases are energised.

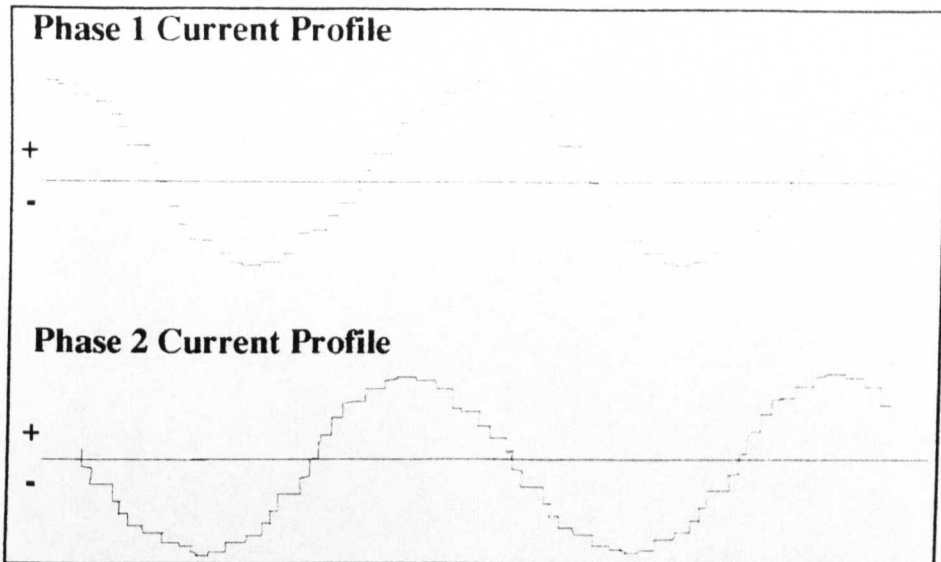


Figure 7.8

This will induce magnetic fields in the stators that are proportional in size to the currents in their windings. Hence, the rotor will shift a proportional distance. This effect is exploited by the micro and ministeping systems which reduces step size and also improves low speed smoothness.⁶

Going back to the list of motor features. The number of amps/phase refers simply to the maximum current that can be supplied to the motor phases. This current is switch reducible for the system I have. The recommended peak current for the motor is 3.448 Amps. I have set the peak current of the drive unit to 3.6 Amps.

Another point to note about the winding of the phases is whether they are Bifilar wound or not. Bifilar winding of a phase, is a technique employed to reverse the current in the phase. Hence, changing the polarity of the stator on which the phase is wound. The polarity of a stator can be changed by reversing the current flow in its phase. By the technique of Bifilar winding, namely by having two sets of windings on each stator which are wound in

⁶ Low speed smoothness is improved since the current profile that flows into the windings changes gradually in a sinusoidal manner. This results in a smooth step movement by the rotor. Whereas, in the full and half-step modes the current is either on or off which results in an abrupt movement.

opposite directions,⁷ one can instead of reversing the current in the phase transfer the current to the other winding. This helps to keep the drive simple. The main advantage of bifilar wound motor depends on how one connects the two sets of windings. If the windings are connected in parallel then only half the total resistance is produced and the motor inductance is halved. This can be an advantage when one requires a very fast step motion. Since the motor inductance is reduced, it is easier for the currents to reach there desired level quicker. Hence, giving significantly high torques at high speeds. When the windings are connected in series it is a lot harder to establish the desired currents at faster speeds due to high motor inductance. However, at lower speeds this serves to increase the torque available. Therefore, the bifilar pairs can be connected in series or in parallel depending on the requirements of the application. For my application I required low speed and high torque which led me to connect the bifilar windings in series. If all the coils in the bifilar-wound motor are brought out separately, there will be a total of eight leads. This is the most common configuration and is also the configuration of the motor chosen as shown in figure(7.9).

⁷ Actually the coils are wound in the same direction but different ends of the coils are connected.

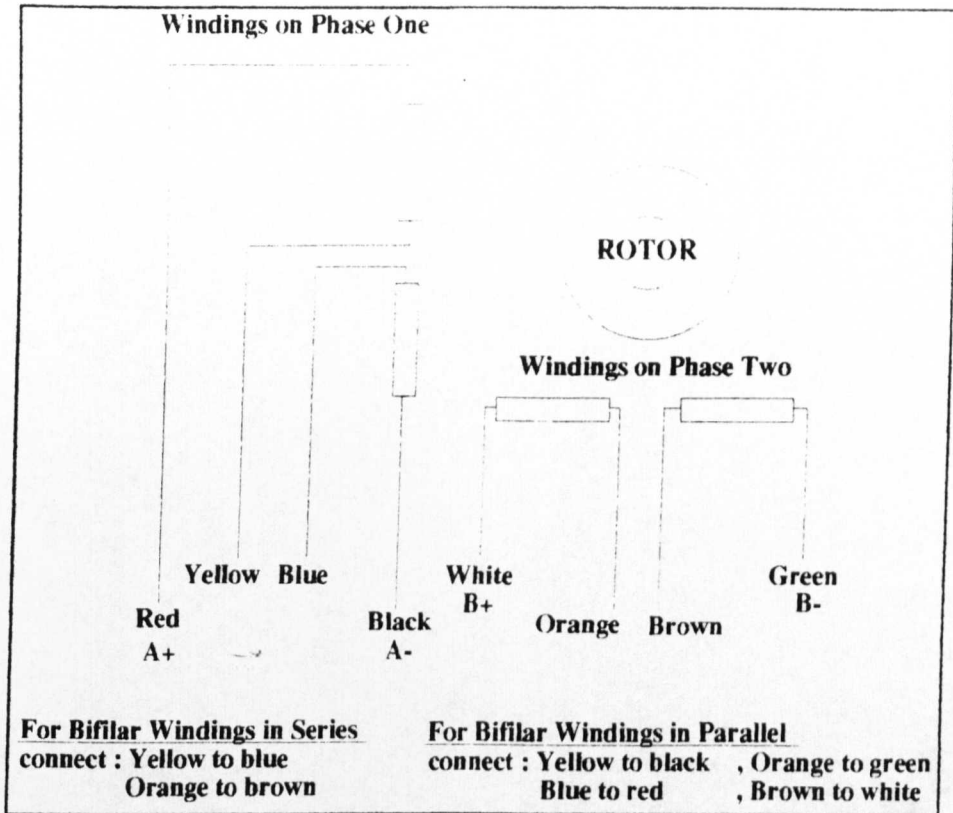


Figure 7.9

The torques available for the series and parallel bifilar winding configurations are shown in the torque/speed plot for a motor. The torque/speed plots which will be discussed in section(4.1), consist of two curves. The curves represent the torques available, at various speeds, when the bifilar windings are connected in series or in parallel.

The Direct Drive feature was the final criterion for the motor. This means the motor shaft is directly coupled to the load without the use of belts or gears. Although a geared or belt system can be used to move large inertial loads it also provides the worry of backlash and position loss. By directly driving the load, backlash can be eliminated and accuracy and repeatability are greatly improved. The only problem with a directly driven system is the criterion for the system inertia, as mentioned earlier, must be satisfied. Recapping, the criterion was :

$$\text{rotor inertia} \ll \text{system inertia} < 10 \text{ times the rotor inertia}$$

The above identity was satisfied, in the previous system inertia calculations. (See Section 7.2). Therefore, by directly driving the system one could make full use of the advantages offered.⁸

(7.3.2) The Motor-Drive Unit

The next section explains the features of the motor-drive unit I chose. The drive unit was a PDX15 single-axis ministep drive. The unit was compatible with the S83-135, size 34 motor chosen and both products were purchased from the company "Compumotor & Digiplan".

The unit provided the ministepping feature via a piece of electronics known as a 'MOSFET Recirculating Chopper Drive'. By means of the above mentioned, the regulation of the current can be maintained at the correct value by switching or "chopping" the supply to the motor. This electronic configuration improves efficiency in power consumption and also reduces drive heating. By this method, a resolution of 400-4000 steps/rev can be attained. This is user selectable and can be set from switches on the front panel of the unit. I set the resolution of the unit to 4000 steps/rev.

The PDX15 unit is a complete packaged system that provides everything necessary to power and ministep a compatible motor. The unit has five separate internal features. The internal features can be seen below (Figure 7.10) and are now explained.

⁸ For systems with large inertial loads a geared or belt driven system might have to be employed, maybe with a rotary encoder to provide feedback to determine position loss and correction.

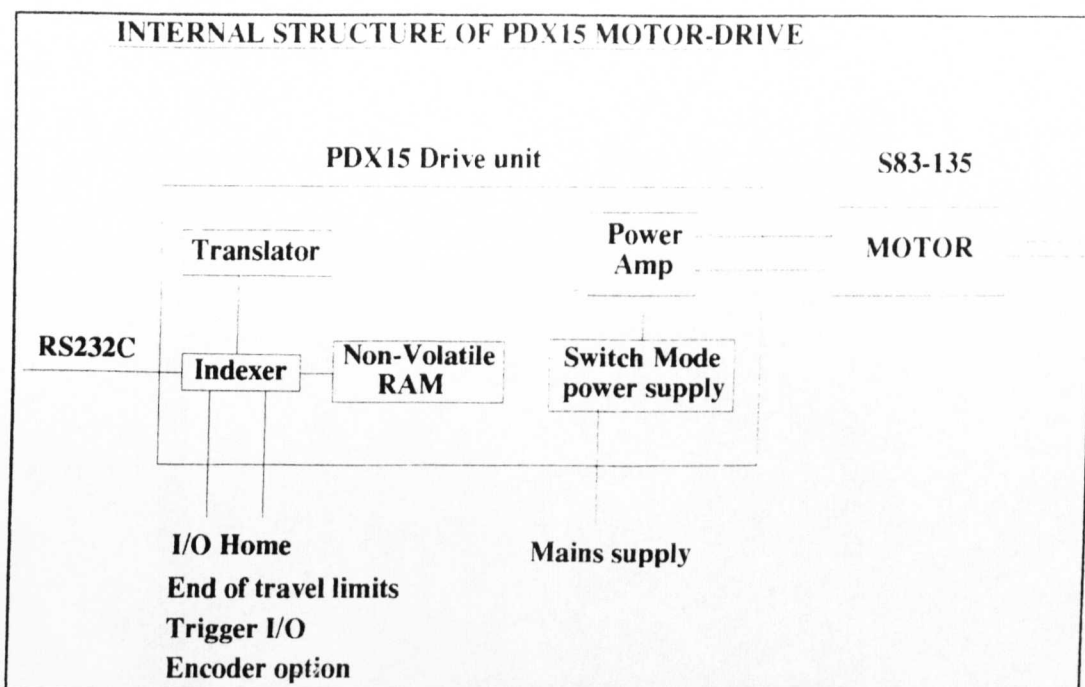


Figure 7.10

(7.3.3) The Indexer and Non-Volatile Memory

Commands are sent from a RS232C compatible device to the indexer within the unit. The indexer has a complete range of 'Motion Control' commands. Our RS232C compatible device was an Acorn Archimedes 410 computer. The user can send a series of these commands, separated by carriage returns, as a set of character strings to the serial port.⁹ These commands usually refer to speed, acceleration rate, distance to move etc. The indexer basically takes these commands and passes them to the translator. The Indexer also produces an echo of commands back to the sender and will output a status report back to the serial port if requested from the user. The indexer has the added feature that it can store up to seven complete motion control sequences in its non-volatile memory. These sequences can be pre-programmed by the user and then selected when necessary to perform a whole combination of moves. In addition, the indexer has dedicated inputs for home-position and end-of-travel limits switches. It also has provision for three

⁹ The range of commands available, known as 'X-Code', are documented in the PDX15 User Guide. A sample of the X-code commands can be found in section (7.5.3).

programmable user inputs and two programmable outputs. These can be used to monitor other functions on another device or to trigger a stored sequence when a particular external event occurs. The indexer can also be linked to part of a daisy chain network if necessary.

(7.3.4) The Translator

The indexer passes the commands from the RS232C port to the translator. It translates the commands into a sequence of useable currents, for the two phases and delay times between current changes in the phases. The Power Amplifier supplies the desired currents, determined by the translator, to the phases in the motor. Hence, a sequence of commands is turned into motion.

(7.3.5) The Switch Mode Power Supply.

In the PDX15 unit a switch mode power supply is available. This is used to perform a power factor correction to minimise losses from the A.C. supply. The whole unit is powered from a direct on-line mains supply.

(7.3.6) Summary Of Motor & Motor-Drive

The whole PDX15 package and motor was low-cost in comparison to buying the components separately (namely, the power amp, drive unit and motor). In addition, a considerable amount of time in wiring and installation was saved.

The microstepper is the most sophisticated system and with this comes expense. I did not require the resolution of the microstepper or the wave-trimming capability it offers. The ministepper provided an excellent lower resolution alternative at low-cost. The ministepper also provided smoothness and resolution which is superior to a full or half-step system.

(7.4) Determination Of Torque Required To Move Load

The next section will describe how the torque that was required to move the load was determined. I will show that by determining a "Move-profile" of the system how the torque can be calculated. I will then show that the torque necessary to rotate the polariser falls within the desired limits of the torque/speed plot for the motor I chose. I will first start, however, with a short explanation of the torque speed plot.

(7.4.1) The Torque/Speed Plot

Each motor has a specific torque/speed curve associated with it. As mentioned near the end of section (7.3.1), the torque/speed plots consist of two curves. One curve represents the torques available, at various speeds, when the bifilar windings are connected in series. The other curve represents the torque/speed relationship when the bifilar windings are connected in parallel. The torque/speed plot associated with the PDX15 drive and S83-135 motor is shown in figure(7.11).

When the bifilar windings of each phase are connected in parallel, half of the total resistance is produced. For the same power dissipation in the motor, the current may be increased by 40%. Therefore, a typical 5 amp motor will accept 7 amps for the parallel connection. This will give a significant increase in available torque. Also when the motor is run at high speeds (namely, when the currents in the phases have to change rapidly) it is easier to achieve the desired currents in the phases quicker. This is because by reducing the resistance we also reduce the inductance in the motor which would oppose a rapid current change. This results in high torques being available at high speeds.

When the bifilar windings of the phases are connected in series, double the total resistance is produced and also the inductance is increased. This reduces the current rating by a factor of 1.4 (giving a current of 3.5 amps for our 5 amp motor). Hence, a high torque is

available at low-speeds. And this also allows a motor to produce full torque from a low current drive.¹⁰

As a general rule parallel connection is preferred since it produces a flatter torque/speed profile, gives greater shaft power and reduces any chance of overheating the motor.

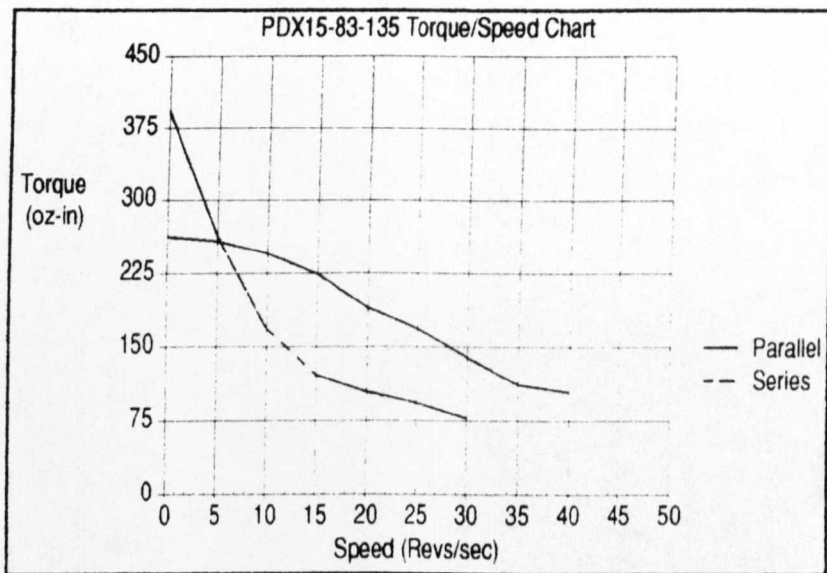


Figure 7.11

As one can easily see from the plot for a low-speed application, such as ours, a torque of no more than 262oz.in. can be achieved for a parallel connection and a torque of no more than ≈ 400 oz.in. can be achieved for a series connection. The way one can determine the torque needed to rotate the system will now be explained.

(7.4.2) The Move Profile

Before one can determine the torque requirements of an application, one firstly needs to determine the "Move-Profile" of the application. The move-profile helps one determine the velocities

¹⁰ However, care should be taken to avoid overheating of the motor since its current rating is lower than that actually supplied. Series connections carry the greater likelihood of resonance due to high torque which is caused from high acceleration of the load being produced in a low speed region.

and accelerations necessary when one only knows the distance(d), of the move, and the time(t), to move the given distance. Once the velocities and accelerations are known one can then proceed to calculate the torque for the application.

The move profile is a trapezoidal profile and consists of three parts. The first part is the acceleration(a) part which is performed over a distance($d/4$) in a time($t/3$). After this initial acceleration the system will have achieved its desired velocity, for which it is to run at. The second part, the velocity run, is performed over a distance($d/2$) in a time($t/3$). Finally the system must decelerate($-a$) to complete its move. This is performed over a distance($d/4$) in time($t/3$). See Figure(7.12).

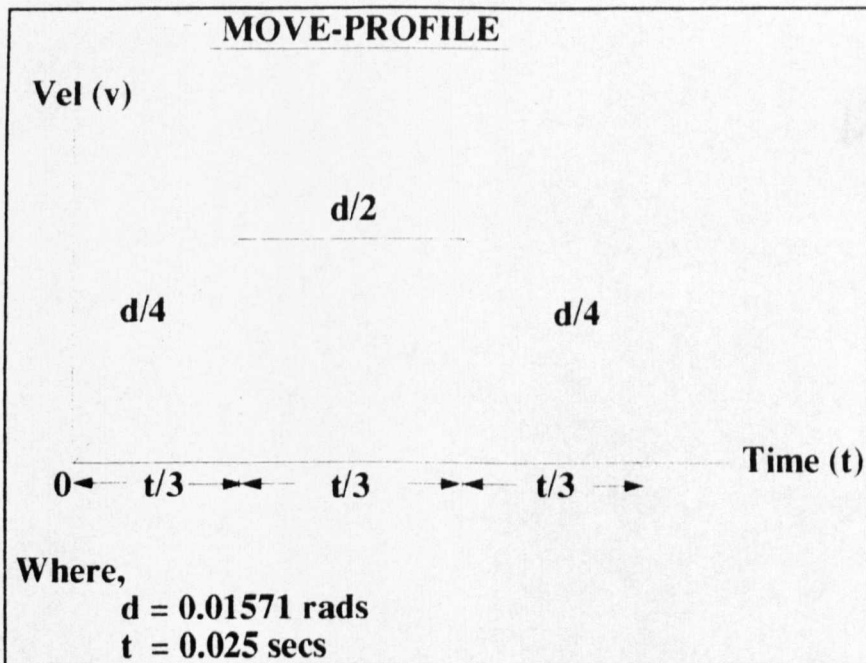


Figure 7.12

The resolution of the stepper was set to 4000 steps/rev. I defined one move to be 10 steps = 0.9 degree = 0.1571 rads. I decided the time for one revolution would take 10 seconds. Therefore, the time complete a move would take $\left(\frac{10\text{secs}}{2\pi} \times 0.1571\right) = 0.025$ secs.

$\Rightarrow d = 0.1571$ rads and $t = 0.025$ secs.

From the move profile the acceleration(a) and velocity(v) are given

as :

$$a = \frac{4.5 d}{t^2} = \frac{4.5(0.01571)}{(0.025)^2} = 113.112 \text{ rads/sec}^2 \quad \dots(7.4.1)$$

$$v = \frac{1.5 d}{t} = \frac{1.5(0.01571)}{0.025} = 0.9426 \text{ rads/sec} = 0.15 \text{ rev/sec} \quad \dots(7.4.2)$$

The maximum torque(τ) encountered during a move is during the initial acceleration. This is when we rapidly increase the velocity to its desired value. Therefore, by knowing the acceleration which has just been calculated one can determine the maximum torque(τ).

For a directly driven load the torque can be calculated by the following equation :

$$\tau = \frac{1}{g} (I_{SYSTEM} + I_{MOTOR}) \frac{\Delta v}{t} \quad \dots(7.4.3)$$

where, I_{SYSTEM} = Inertia of system = 57.20 oz.in.

I_{MOTOR} = Inertia of motor = 10.24 oz.in.

g = Accel. due to gravity = 386 in/sec²

$$\frac{\Delta v}{t} = \frac{\text{Diff. between initial \& final velocity}}{\text{time taken for change}} = a = 113.112 \text{ rads/sec}^2$$

Therefore, substituting in equation (7.4.3) we get : $\tau = 19.76$ oz.in.

For good operation we allow a 50% torque margin.¹¹ This allows for friction etc.

$$\text{Therefore, } \Rightarrow \tau = 29.64 \text{ oz.in.} \quad \dots(7.4.4)$$

By referring to the torque/speed plot for the motor and motor-drive (Figure 7.12) one can see that the motor can easily cope with this torque for the speed determined in either of the parallel or series configuration.

¹¹ The equations for the move profile and the torque can all be found in the System Calculations reference section pgs. A58 & A63 of the 'Compumotor & Digiplan - Step Motor & Servo Motor Systems & Control Catalogue (1995)'.

(7.5) Interfacing & Control of the Drive Unit

This section will describe how I interfaced the computer to the PDX15 Drive unit. This will be followed by a description of how one set up the initial parameters on the computer in order to allow communication flow between the computer and the drive. Then a short explanation of the main commands that were used to send and retrieve information from the computer will be given. To conclude this section and the chapter, a description of the three of the main operating programs, I developed to perform set stepping routines and data retrieval, will be given.

(7.5.1) Interfacing Drive to Computer

Both the Acorn Archimedes 410 and the PDX15 Drive unit have an RS232C Serial Port. However, the serial port for the Acorn computer is 9-pin and that of the PDX15 is a 25-pin. A three-wire (R_x, T_x and Signal Gnd) configuration is used. Both the computer and Drive unit are 'Data Terminal Equipment' (DTE)¹². And the PDX15 Drive does not support handshaking. The connections between the interfaces are shown in (Figure 7.13).

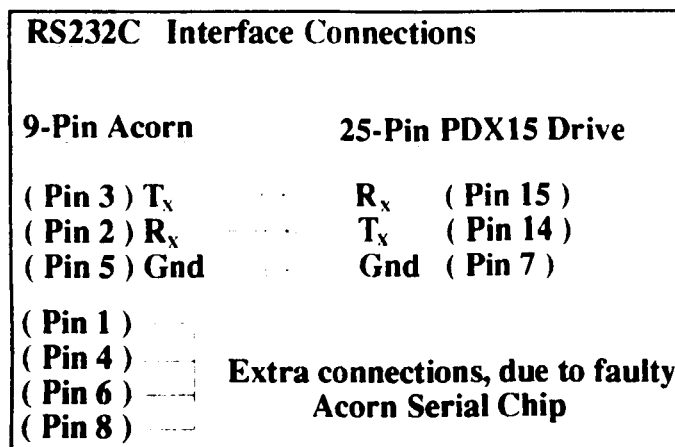


Figure 7.13

Extra connections within the 9-pin port, of the Acorn computer, had to be made. This is due to a flaw in the serial-chip of the Acorn 410

¹² A piece of equipment with a serial port can be a DTE, as mentioned, or it can be a 'Data Communication Equipment'(DCE).

and 510 models. Without these extra connections no communication can be established. The extra connections can also be seen in (Figure 7.13) and are concerned with the pins 1,4,6 and 8.

(7.5.2) Establishing Communication Flow

After interfacing everything correctly, communication flow between the Acorn computer and the Drive had to be established. This was achieved by setting Baud-rates, Data Format etc.

The PDX15 Drive interprets signals correctly that are transmitted at 9600 Baud, 8 data bits, 1 stop bit and no parity. It also sends signals back to the computer at these values. The Transmit and receive baud rates were set by the "SerialOp" commands in Acorn Basic. The SerialOp commands will now be discussed in the section that follows.

(7.5.3) Transmitting Commands & Receiving a Response

Commands could be sent to the PDX15 Drive in the 'X-code' format as mentioned earlier. One could send a series of these commands that specified acceleration, velocity, number of steps to move etc. In a command string, termed as "data\$". A typical command string would be written as :

```
data$ = CHR$(13) + "8D10" + CHR$(13) + "8G" + CHR$(13) + "8PR" + CHR$(13)
```

The breakdown of the command string is as follows. The CHR\$(13) is ASCII code for a carriage return. All command strings must start and end with a CHR\$(13). The sequence of numbers and letters in each pair of quotes is the X-code format which specifies a particular command to the drive. Note how each starts with the number '8'. This refers to the factory default device number which is '8' for the PDX15 Drive unit. All X-code commands must start with the device number. The first X-code command, "8D10", tells device number '8' to get ready to move a distance of 10 steps. This move will only be

executed when the device receives the X-code command "8G". This tells device '8' to "GO". The final X-code command of the data string is "8PR". This asks device '8' for a Position report. The indexer of the drive unit upon receiving this command will respond by transmitting its position, in steps, relative to some absolute position which can be set. As a final point to note all the X-code commands must be in 'uppercase'.

The command string is then sent to two procedures in my program. The first procedure is called PROCSEND_String(data\$). This takes the command string(data\$) and breaks it up into its character string components. Then it sends the ASCII code equivalent, which is a number, of each of character string components to the second procedure. The second procedure called, surprisingly, PROCSEND(byte%) takes each of the ASCII codes in turn and sends it to the output buffer of the serial port. This is achieved by use of the SerialOp commands in the following loop :

```
REPEAT
  SYS "OS_SerialOp",3,byte% TO ;flags%
UNTIL ( flags% AND %0010 ) = %0000
```

The loop takes a single ASCII code value which is stored in byte% in the SerialOp command and places it in the output buffer of the serial port which is represented by the number '3' in the SerialOp command. The ;flags% is the register value returned by the SerialOp command. This represents whether byte% is in the output buffer or has left it. The value returned in flags% is a 1 = %0001, in binary, if the ASCII code value is still in the output buffer. If the ASCII code value has left the output buffer then a 0 = %0000 is returned. Therefore, by constantly sending the ASCII code value to the output buffer, in the form of a repeat loop then logically 'AND'ing flag% with the number 2 = %0010 until 0 = %0000, which refers to the ASCII code value as being sent, is achieved we can make sure the

ASCII code value has actually been sent before continuing to send any other ASCII code values. This check is necessary in order to assure the commands are being sent correctly.

When receiving, a status report say, the analogous SerialOp command to retrieve ASCII code values from the input buffer of the serial port is used. This is in the procedure PROCGet_Byte which is:

```
SYS "OS_SerialOp",4 TO ,message%
```

The number '4' tells the SerialOp command to go to the input buffer of the serial port. And to store the ASCII code value, which is there, in the variable message%. Then this ASCII code value is run through the procedure PROCvalues_returned which basically performs the reverse of PROCsend_String and translates the ASCII back to a readable format for the user. There is one additional check that is made here. And this is to check that all the information from the PDX15 has been retrieved. This is achieved by the following statement which is all contained in the PROCvalues_returned procedure.

```
REPEAT  
PROCGet_Byte  
SYS "OS_Byte",152,1 TO Z,ZZ,ZZZ;Cflag%  
UNTIL (Cflag% AND %0110) = %0110
```

Basically we get an ASCII code value from the input buffer with PROCGet_Byte. Then by the "OS_Byte",152 command we can look and see if any new information has arrived in the input buffer, represented by the number '1' in this case. This is different to the SerialOp commands which actually take/put bytes from/to a buffer. Instead, the "OS_Byte",152 command looks at what is in the buffer without actually altering it. Again a value is stored in the register Cflag% which expresses whether the buffer is full or empty. Again

by 'AND'ing we can tell the program to jump out of the loop when there is no information left in the input buffer. Hence, one can retrieve all the desired information from the status report.

(7.5.4) Programs Developed

The following section gives a short description of the programs developed to satisfy the user requirements. There were three primary functions I wanted the Rotary Polariser to perform. These were :

- Step and Record
- Check the alignment of the polariser Grid
- Locate the polariser wires Vertical

The 'Step and Record' program basically steps around 180° in 200 steps. Where 1 step = 10 ministeps = 0.9° . The acceleration rate and velocity are initially set to the values calculated in the 'Move-Profile' in section(7.4.2). After each step the program waits one second to allow any resonance in the polariser to settle. This time delay also allows for the power reading on the meter to settle. Initially, at millimeter wavelengths, the power reading was determined by a Boonton power meter. The power values of the meter could be read by the computer via a GPIB interface.¹³ The power readings together with their corresponding angle, at which they were taken, is recorded in a file "StepRec" in the RAM disc. Later the data in the file can be retrieved and displayed as desired, via a C-program.¹⁴

The Grid Alignment program is an extension of the step and record program. The motor steps around 360° in 400 steps. If the polariser is aligned correctly then the power at an angle(θ) should be the same as the power at an angle($\theta + 180^{\circ}$) and the ratio of these powers should be unity. The program calculates this ratio and stores

¹³ In the final system the power was read from a TK Freespace power meter which will be described in detail in Chapter 9.

¹⁴ The retrieval and display of the data via a C program will be described in section(5.4)

them together with the corresponding angle in a file "Gridalign" in the RAM disc. Therefore, a deviation from unity in the plot of the above mentioned ratio versus angle, will detect any skew in the plane of rotation or identify any damaged wires that exist etc.

Finally the program designed to locate the wires vertical will now be described. It relies on the fact, that if one inputs radiation that is polarised in the vertical sense, then maximum power will be detected also when the polariser wires are located vertical. The program steps the polariser around recording the power readings and corresponding angles in a file "PosVert" in RAM disc. After this is completed, the polariser moves back to the position where maximum power was detected. Hence, locating the wires in the vertical sense. In addition there is a feature in the 'X-code' commands that allows one to define an absolute position. Basically the position counter is zeroed in the drive unit when the call is made. The call is made when the wires are in the vertical sense. Therefore in an experimental run, one can reference position relative to this absolute position of wires horizontal. Hence one can determine the angle of rotation relative to this zero position.

Chapter (8)

A Prototype Rotary Polariser Quasi-Optical System

Introduction

After the construction and interfacing of the rotary polariser was complete the next task was to test out the new instrument in a quasi-optical circuit. The purpose of this chapter, is to describe the first trials of the prototype 'Rotary Polariser Quasi-Optical System'. The first part of the chapter details the results of initial tests and corrections performed with the rotary polariser optical system. These tests and corrections were necessary in order to initialise the experimental setup for accurate measurement retrieval. The rest of the chapter is devoted to showing theoretically and verifying experimentally what one should expect from the working system. It will be shown that the system can uniquely identify linear, circular and elliptical polarised beams. Furthermore, it will be shown that Faraday rotation as well as ellipticity of the beam can be measured. The closing sections include results on isolator performance and ferrite characterisation. In addition, an example of the 'Faraday Angle Resonance' phenomenon is given.

(8.1) Preliminary Tests & Measurements

As mentioned in the previous chapter, a few initial tests and corrections have to be performed with the rotary polariser before it can be used accurately in experiment. There were two initial tests and one measurement correction that had to be performed before accurate results could be obtained. The description of the tests and measurement correction now follow.

(8.1.1) Grid Alignment Experiment

As mentioned in section(7.5.4) the grid alignment program was developed to detect any skew in the polariser grid as it rotated through 360° . Obviously the power detected when the wires are at angles (θ) and $(\theta+180^{\circ})$ should be the same. Therefore, any deviation in this ratio will give a measure of the skew in the plane of rotation of the polariser or locate any damaged wires. The results of the grid alignment test are shown below in Figure(8.1).

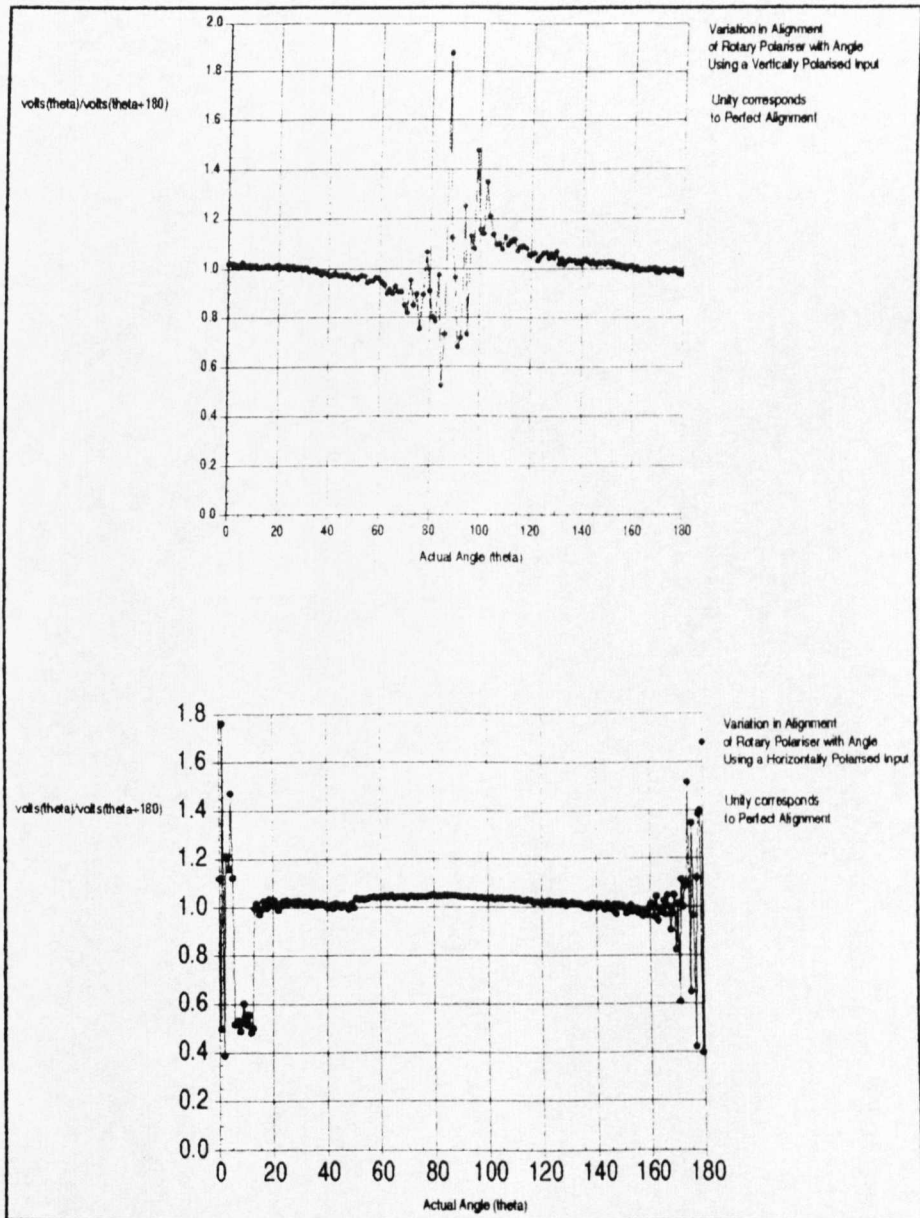


Figure (8.1)

Two measurements were necessary in order to assess the alignment of the polariser grid. This was because I was using a linearly polarised source. Therefore, when the wires are located orthogonal to the (E) vector of the linearly polarised input, the radiation would propagate through the wires and nothing would be detected. The irregularities that occur in fact are associated to the background noise the detector sees when no radiation is present. Therefore, performing two measurements which are orthogonal to one another, will allow one to assess the regions dominated by noise in the orthogonal polarisation. As one can see the polariser is virtually free from any skew that could exist due to misalignment.

(8.1.2) Offset Determination Of Polariser Wires From Vertical

Also mentioned in section(7.5.4) the offset determination of the polariser wires from vertical can be calculated and corrected initially. This is achieved by inputting a linear polarised beam in the vertical sense. Obviously a maximum reflection of power from the polariser wires will occur when the wires are in the same sense as the linear polarised beam. It is this power maximum that locates the wires when they too are in the vertical. The results of a typical offset test are shown below in Figure(8.2).

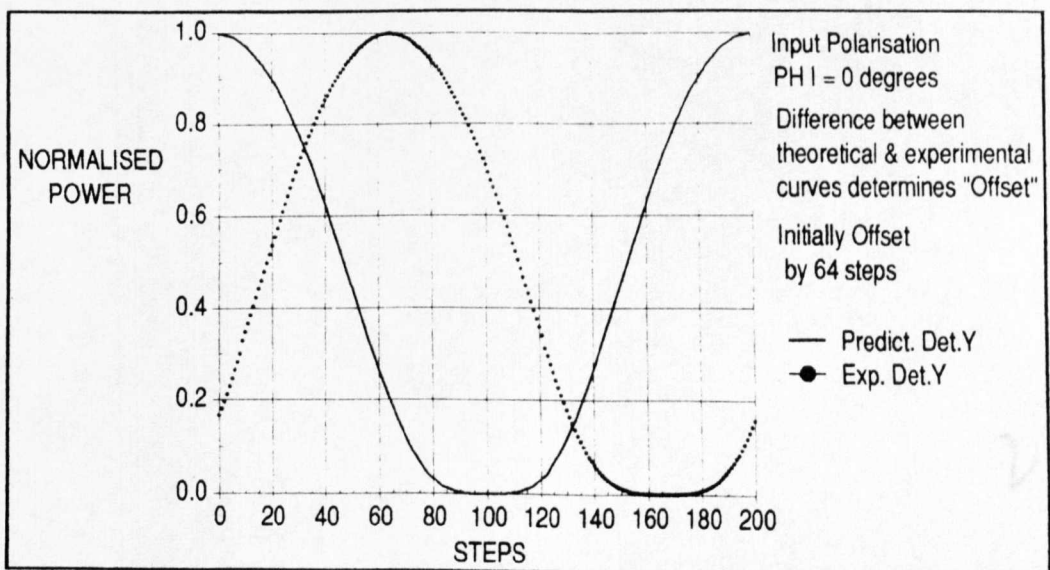


Figure 8.2

As one can see from the experimental results. The theoretical profile for wires vertical has been shifted 64 steps to the right. This corresponds to an offset angle of $(0.9 \times 64 = 57.6^\circ)$.

(8.1.3) Relationship Between Seen Angle (χ) & Actual Angle (θ)

Another correction to be made concerns the orientation of the rotary polariser to the input beam. Since the rotary polariser is inclined at $(\epsilon=45^\circ)$ to the input beam, a parallax error exists. This is because the angle of the polariser wires, as seen by the input radiation is different to that of the actual angle rotated by the stepper. Furthermore, the radiation reflected to the detectors will also be inclined at this "Seen Angle". A relationship between the "Seen Angle (χ)" and the "Actual Angle (θ)" can be determined as follows. In the most general case, let the rotary polariser be inclined at an arbitrary angle (ϵ) to the input beam, see Figure(8.3).

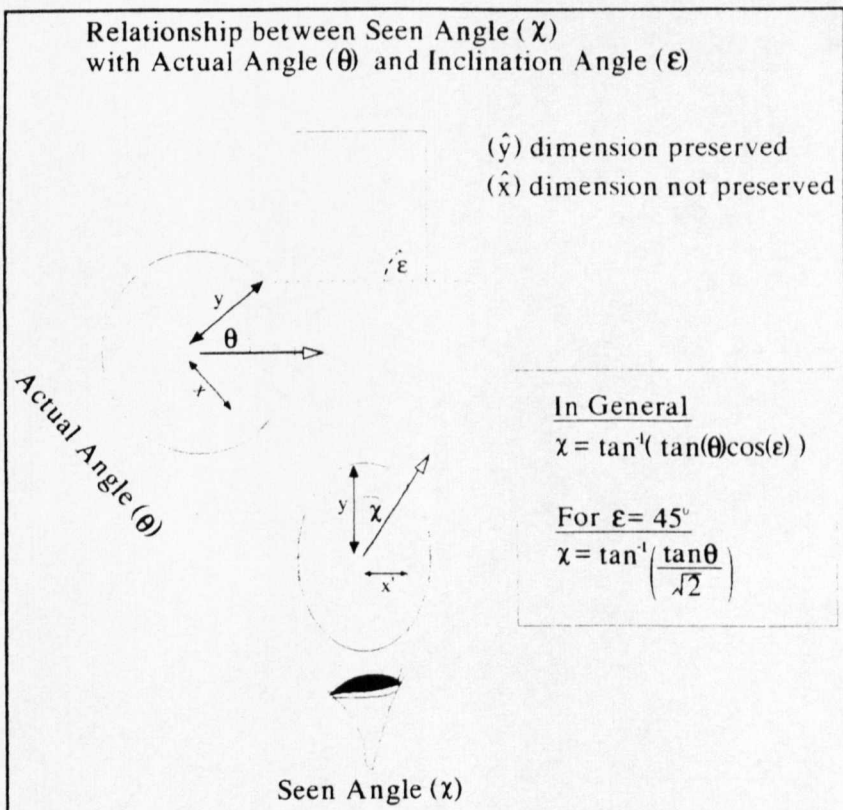


Figure 8.3

Now one can define the tangent of Actual Angle (θ) of the wires to vertical as :

$$\tan(\theta) = \left(\frac{x}{y}\right) \quad \dots(8.1)$$

A Seen Angle (χ) is viewed from the perspective of the input beam. The (y) dimension is preserved and the (x) dimension is not preserved. If the new (x) dimension is known as (x'), then we can define the tangent of the Seen Angle (χ) as :

$$\tan(\chi) = \left(\frac{x'}{y}\right) \quad \dots(8.2)$$

The (x) and (x') dimension are related by the inclination angle (ϵ) of the rotary polariser, such that :

$$\cos(\epsilon) = \left(\frac{x'}{x}\right) \quad \dots(8.3)$$

Substituting $\tan(\theta)$ and $\cos(\epsilon)$ into equation(8.2), the general relationship of how the Seen Angle (χ) varies with Actual Angle (θ) and Inclination Angle (ϵ) can be shown to be :

$$\chi = \tan^{-1} \{ \tan(\theta) \cos(\epsilon) \} \quad \dots(8.4)$$

Since the rotary polariser is inclined at ($\epsilon = 45^0$) to the input beam, the seen angle (χ) can be expressed as :

$$\chi = \tan^{-1} \left\{ \frac{\tan(\theta)}{\sqrt{2}} \right\} \quad \dots(8.5)^1$$

¹ Using this formula one can deduce that the 45^0 polarisers, used here at St.Andrews, have to actually be wound at 54.7^0 to act as a quasi-optical beam splitter.

A plot of equation(8.5) gives the following relationship which is seen to be negative for ($\theta > 90^\circ$) in the first graph of Figure(8.4).

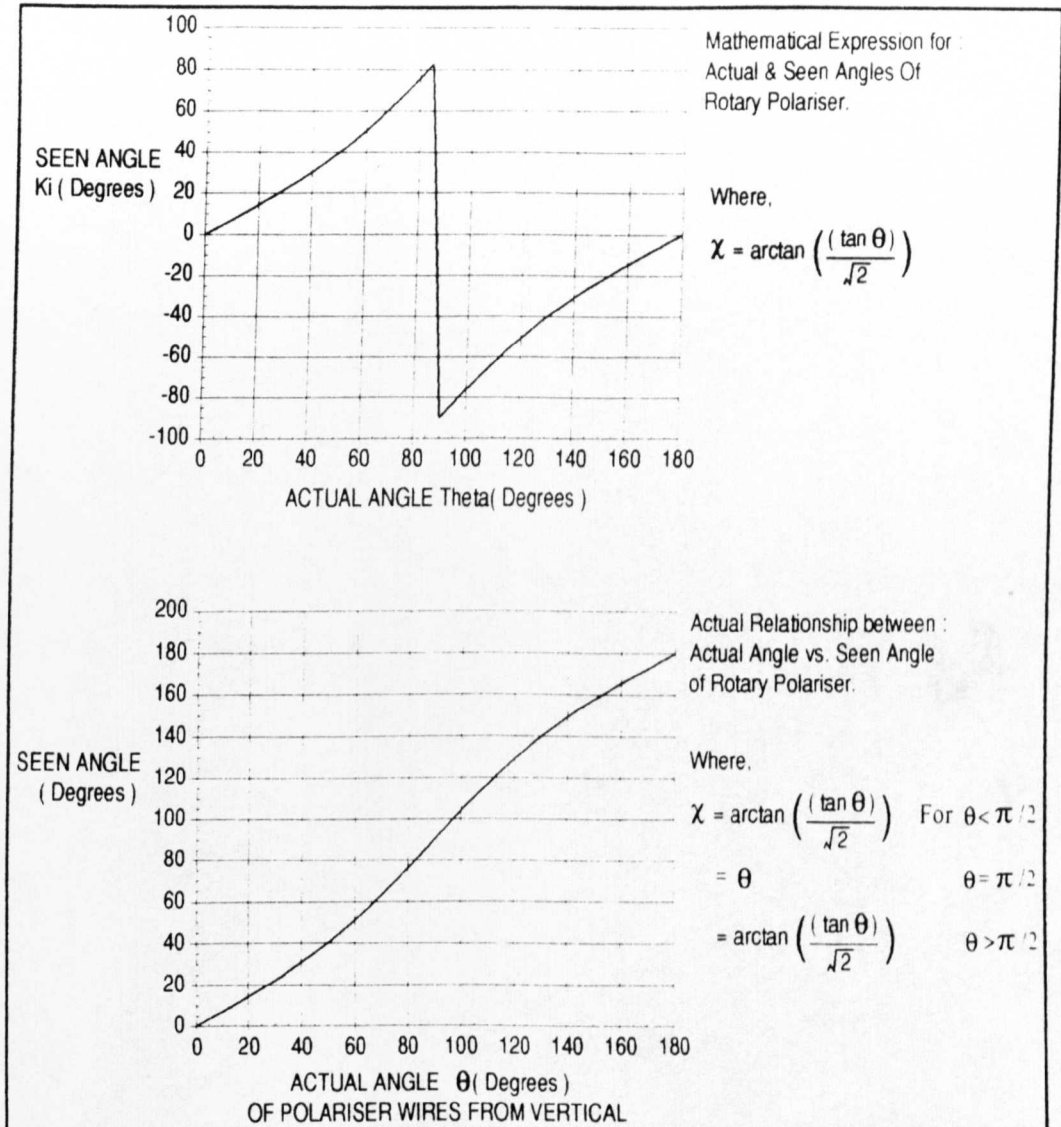


Figure 8.4

However, this is just the consequence of the mathematical solution to the problem. Obviously, an additional (180°) should be added to (θ) values greater than 90° to achieve the correct value for (χ) as seen in the second graph of Figure(8.4), such that :

$$\begin{aligned}
 \chi &= \tan^{-1} \left\{ \frac{\tan(\theta)}{\sqrt{2}} \right\} && \text{for } \theta < \pi/2 \\
 &= \theta && \text{for } \theta = \pi/2 \\
 &= \tan^{-1} \left\{ \frac{\tan(\theta)}{\sqrt{2}} \right\} + \pi && \text{for } \theta \geq \pi/2
 \end{aligned}$$

....(8.6)

(8.2) Polarisation Classification

The tests which I am about to describe are designed to investigate what linear, elliptical and circular polarised light is detected to be, after its propagation through the rotary polariser optical system. This is as the rotary polariser steps through half a revolution. By simulating the different types of polarisation states and then observing what the detectors of the system see, one can define a pattern of recognition for each type of polarisation state. The patterns of recognition can then be used to safely predict how a known input polarisation state has been altered upon its propagation through an unknown medium. The unknown medium being a ferromagnetic one in this instance. However, this analysis could be applied to any type of medium. It will be shown in the following sections that linear, elliptical and circular light can indeed be identified uniquely. Furthermore, a measure of the ellipticity of the beam can be determined by the system. In addition, if a ferrite sample is placed in the system the amount of rotation incurred by the ferrite can be determined.

(8.2.1) Case one : Linear polarisation

The simplest case to investigate and understand is that of linear polarised light propagating through "Rotary Polariser Setup (A)" shown in Figure(8.5). Once one has a firm understanding of what linear polarised light appears to be, from the point of view of the detectors, after it has passed through the experimental setup, one can then proceed to build upon this information, as in the next case, and deduce how the general elliptical form of light appears to the

detectors.

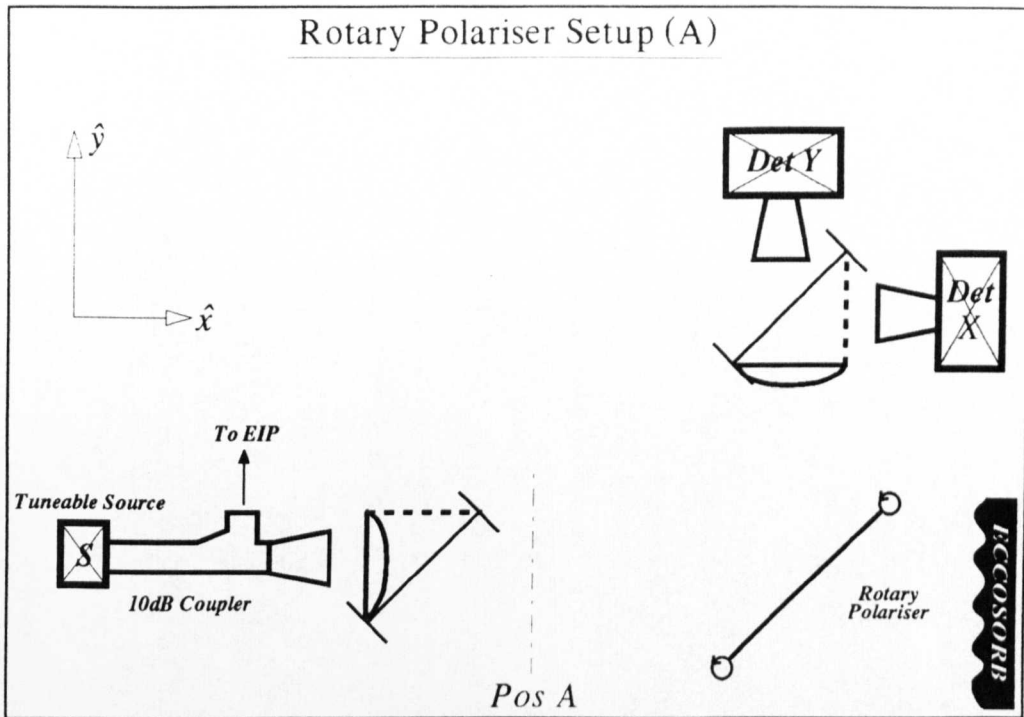


Figure 8.5

To determine theoretically what the detectors see as the rotary polariser steps around one can imagine the following scenario. Consider an (\underline{E}) vector, linearly polarised in the vertical (\underline{y}) direction with an amplitude (E_0), propagating through setup (A) in Figure(8.5). At position(A) in the experimental setup we can imagine an ideal magnetised ferrite that is isotropic, lossless and is perfectly matched to freespace. Its isotropic nature implies that there is no linear birefringence associated to the material, namely no ellipticity imposed on the input beam. Being lossless, there is no change in amplitude to the input beam. And finally, being perfectly matched to freespace there are no multiple reflections occurring within the sample. This results in a perfect linear beam being output from the ferrite. The only difference to the initial input state is that the output state has been rotated through an angle (φ). Now this output state propagates to the rotary polariser wires which are inclined at the Seen Angle (χ) to the vertical, as mentioned in section(8.1.3). The part reflected towards the detectors is the

component of the (\underline{E}) vector which is parallel to the rotary polariser wires. Similarly, the part which is transmitted out of the system is that component perpendicular to the rotary polariser wires. Therefore, the reflected part that travels towards the detectors is inclined at an angle (χ) to the vertical which was the angle of the rotary polariser wires. An (\underline{x}) detector would detect the horizontal component of this vector and similarly the (\underline{y}) detector would detect the vertical component of the vector. Vectorially, the propagation of the (\underline{E}) vector can be shown in Figure(8.6).

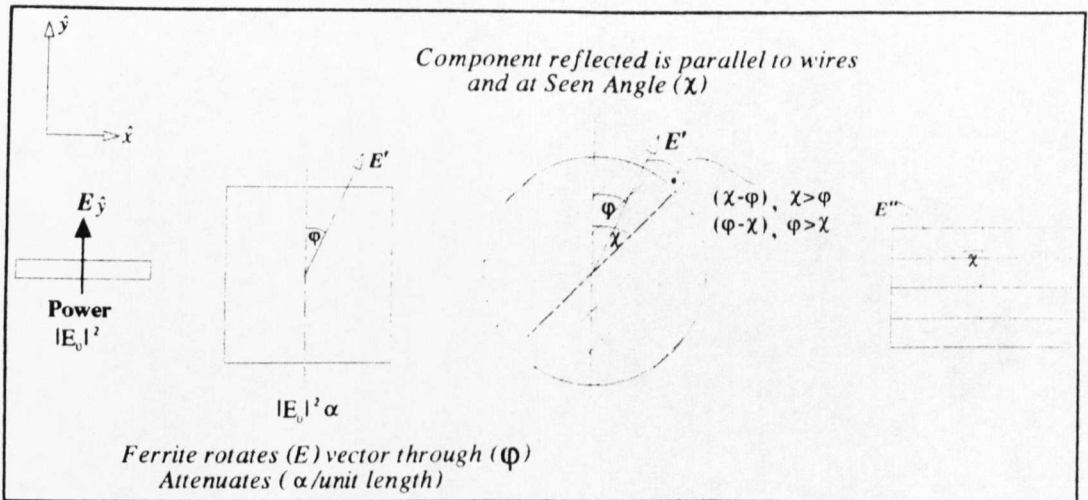


Figure 8.6

Mathematically this linear problem can be solved simply by a resolution of vectors. Let us consider the (\underline{E}) vector after it has passed through the ferrite and rotated by (ϕ). Including an attenuation constant (α) which describes the amount of attenuated power/unit length into the calculation. This would reduce the amplitude of the (\underline{E}) vector by ($\sqrt{\alpha}$). By resolving (\underline{E}') onto the wires the component reflected would be :

$$\underline{a} \cdot \underline{b} = |\underline{a}| |\underline{b}| \cos(\delta) = \sqrt{\alpha} |E_0| \cos(\chi - \phi) \quad \text{for } \chi > \phi \quad \dots(8.7)$$

$$= \sqrt{\alpha} |E_0| \cos(\phi - \chi) \quad \text{for } \phi > \chi \quad \dots(8.8)$$

Now $\cos(\chi - \phi) = \cos(\phi - \chi) \therefore \Rightarrow (8.7) = (8.8)$

$$\begin{aligned} \therefore \quad \text{Reflected Part} & \quad E'' = \sqrt{\alpha} |E_0| \cos(\chi - \phi) \\ \text{Transmitted (Lost) Part} & \quad E_{\text{LOST}} = \sqrt{\alpha} |E_0| \sin(\chi - \phi) \end{aligned}$$

(X) Detector sees :

$$E_{\text{DX}} = E'' \sin\chi = \sqrt{\alpha} |E_0| \cos(\chi - \phi) \sin\chi \quad \dots(8.9)$$

(Y) Detector sees :

$$E_{\text{DY}} = E'' \cos\chi = \sqrt{\alpha} |E_0| \cos(\chi - \phi) \cos\chi \quad \dots(8.10)$$

$$\text{Since, Amplitude} = (\underline{E.E})^{1/2} \quad \text{and} \quad \text{Power} = (\text{Amplitude})^{1/2} \quad \dots(8.11)$$

Power Detected : where $|E_0|^2 = \text{Input Power} = P_{\text{IN}}$

$$P_{\text{DX}} = \alpha \{ |E_0| \cos(\chi - \phi) \sin\chi \}^2 \quad \dots(8.12)$$

$$P_{\text{DY}} = \alpha \{ |E_0| \cos(\chi - \phi) \cos\chi \}^2 \quad \dots(8.13)$$

(8.2.1.1) Computer Model For Linear Polarisation

The computer models can be seen in (Figures 8.7 & 8.8). Each graph has three curves associated to it. Two of the curves represent what the (x) and (y) detectors would see separately. And a third curve is a summation of the powers of both detectors.

The (PHI) values mentioned in the graphs represent the angle of rotation induced by an ideal ferrite on a linear vertically polarised input beam. A PHI = 0° might represent an unmagnetised ideal ferrite. And a PHI = 45° would represent a perfect Faraday Rotator. The PHI = 125° has also been attenuated by 3dB's ($\alpha=0.5$). As can be seen from the graphs mentioned, the (X+Y) curve locates the angle of rotation at a power maximum.

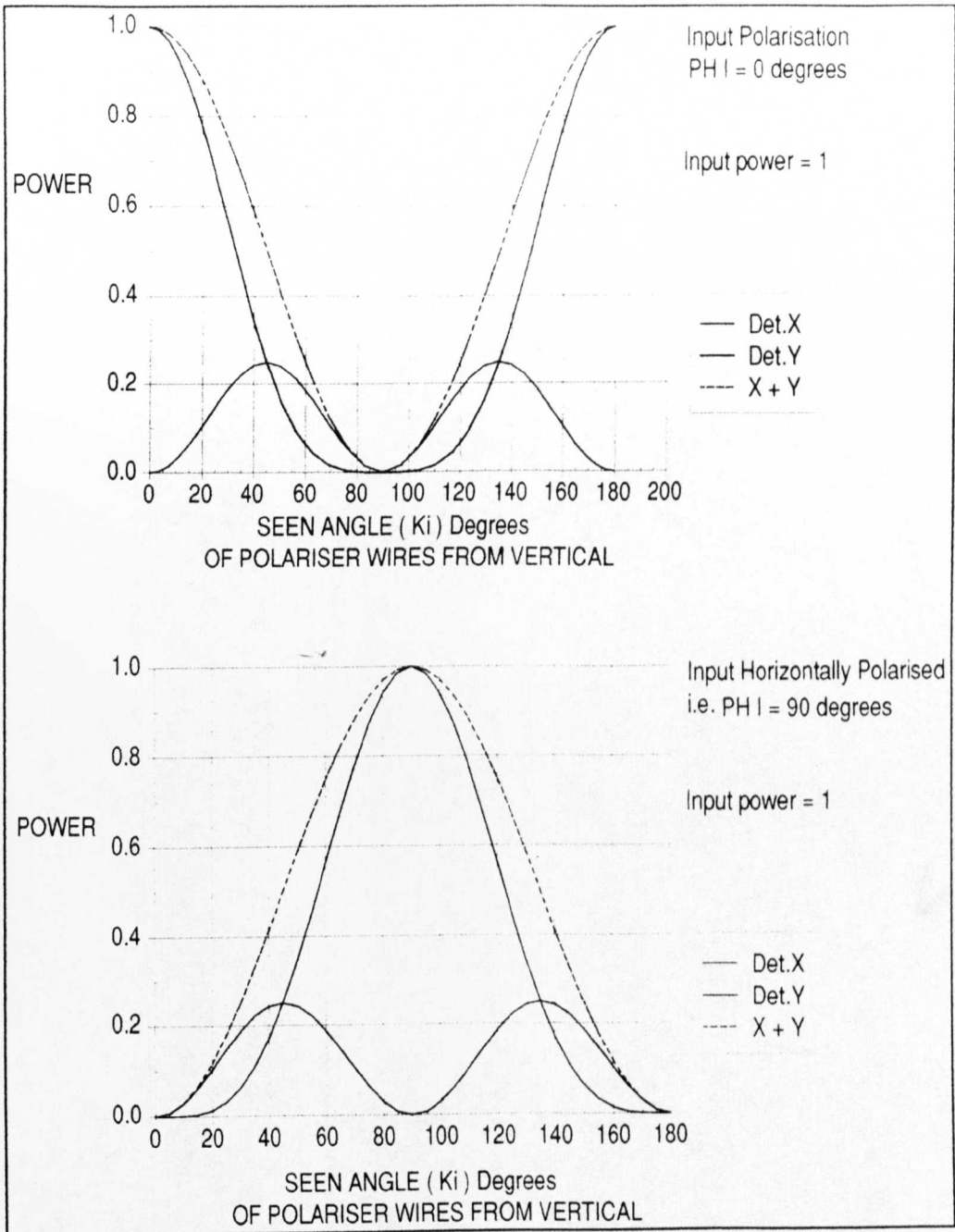


Figure 8.7

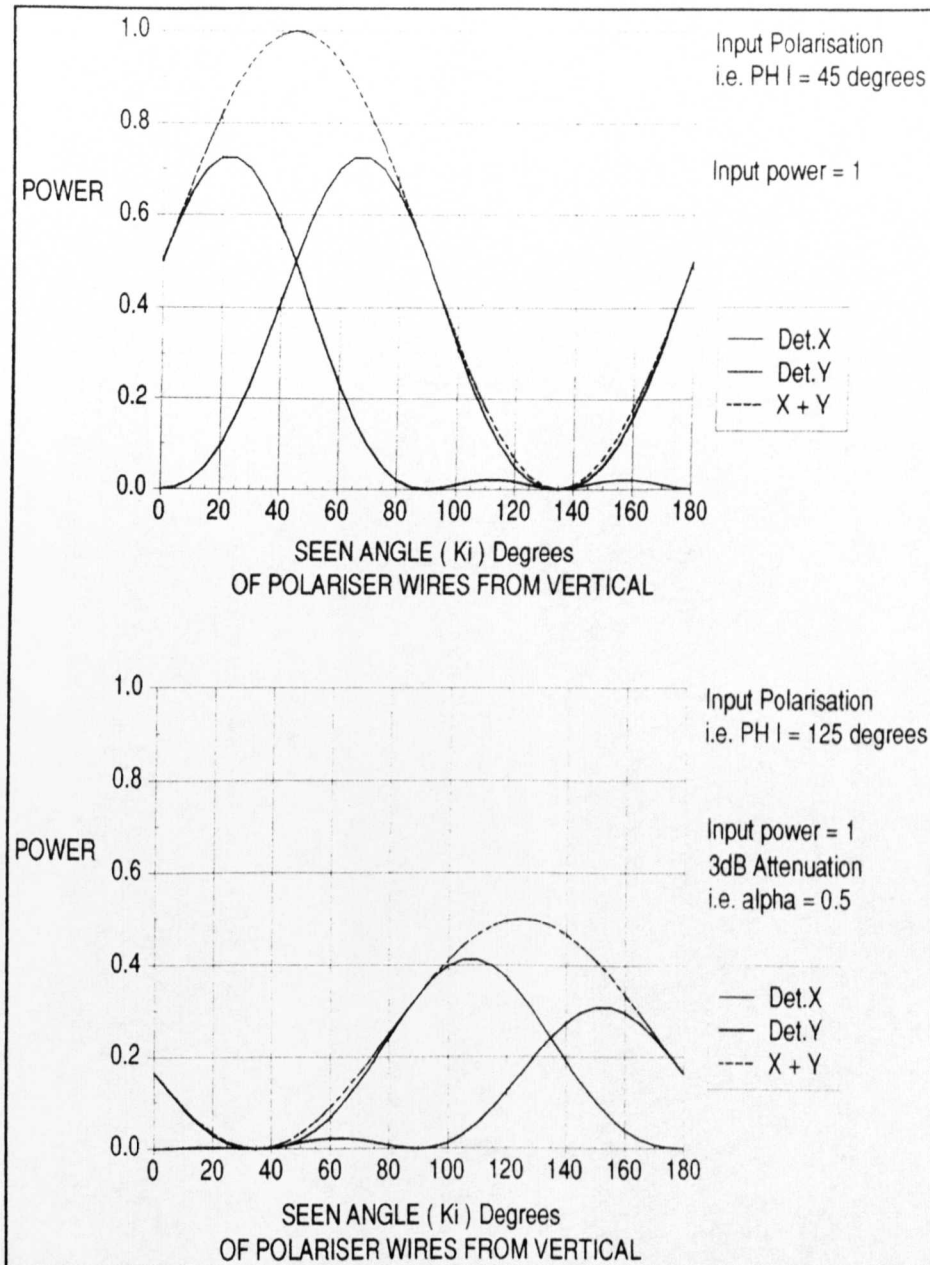


Figure 8.8

Now the ideal ferrite placed at position (A) in the experimental setup, does not alter the input beam in any way, except to rotate it. Therefore in experiment, one does not need to have an isotropic, lossless, perfectly matched ferrite in position (A) at all, but only a means of simulating the output from the ideal ferrite. Thus a rotated beam can be simulated by simply angling the source to the vertical. The experimental results in comparison to those predicted can be seen in Figures (8.9) & (8.10).

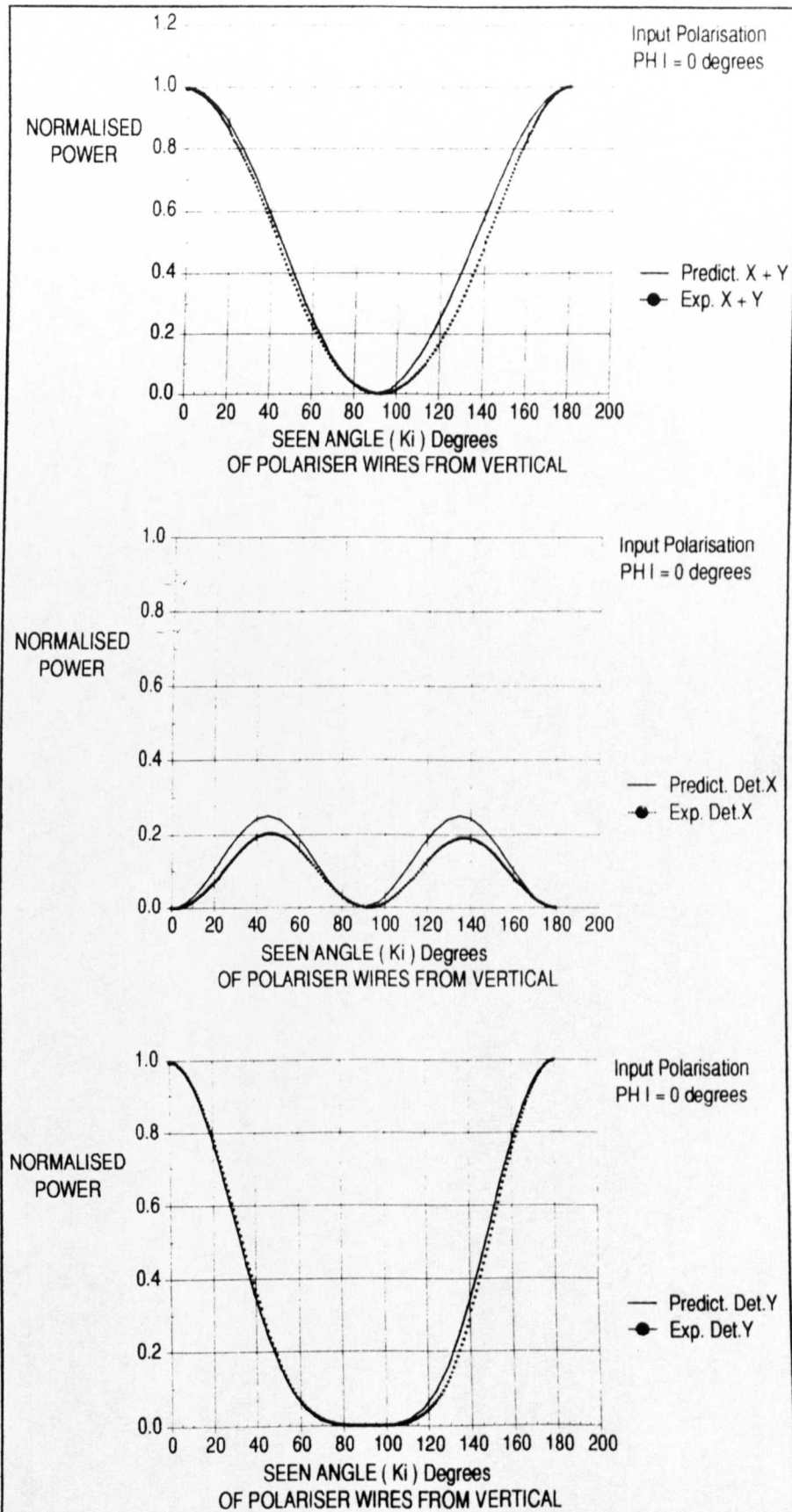


Figure 8.9

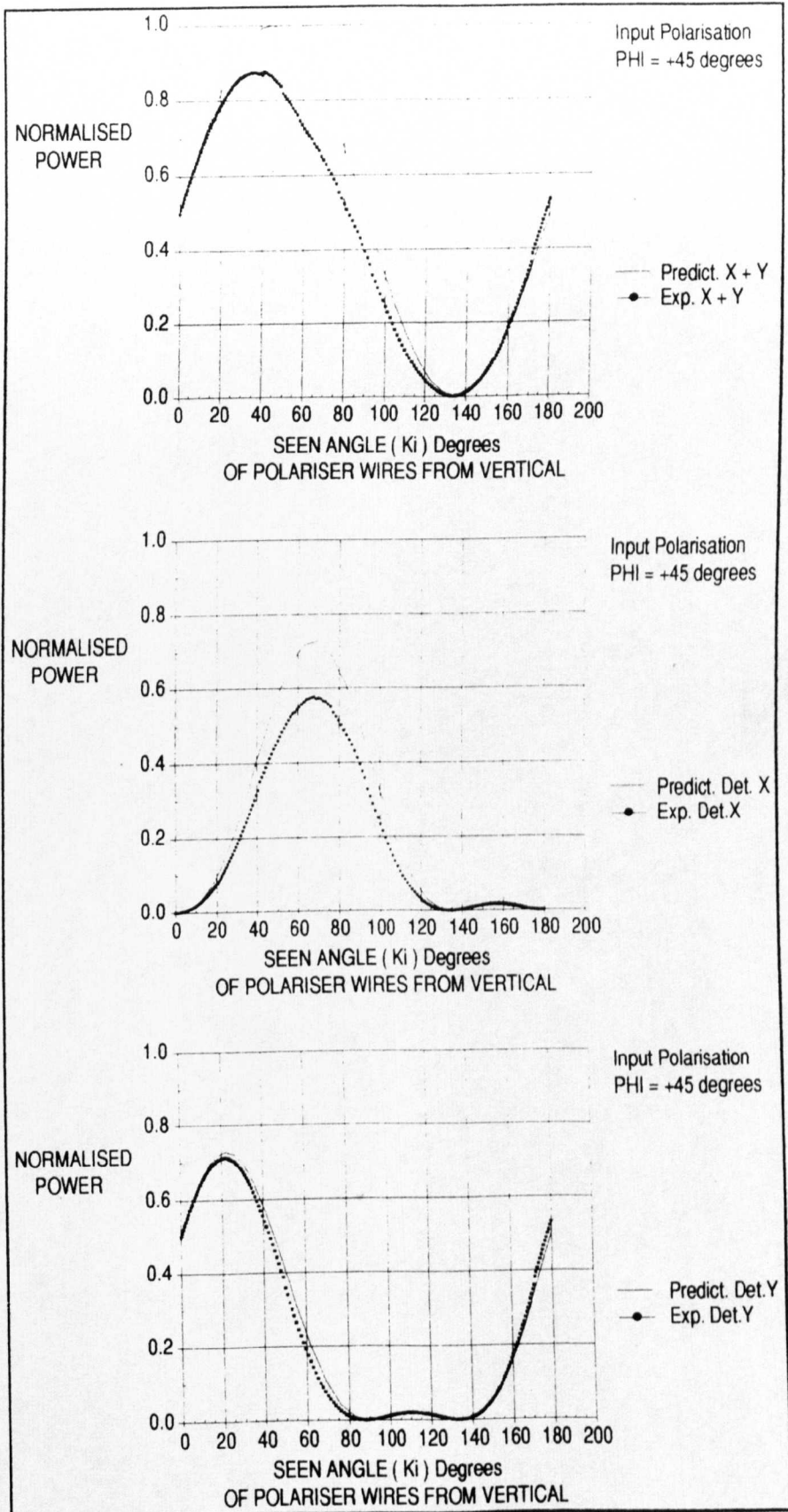


Figure 8.10

(8.2.1.2) Interpretation Of Results For Linear Polarisation

From the experimental results, one can see a good correlation with theory for the (y) detectors, shown in Figures (8.9 & 8.10). However, there is loss associated with the (x) detectors. In addition, the loss can be seen to increase proportionally with the detected power and also for the $\text{PHI}=45^\circ$ experiment the angle determined was less than 45° . This can be traced back to the way the experiment was performed and shown to lie in the coupling of the beam to the (x) detector.

Although the rotary polariser setup (A), in Figure(8.5), shows two detectors, we only have one detector with which to perform the measurements. The way the (y) measurements were performed is as follows. Firstly, the detector was oriented in the (y) position to receive vertical polarisation. With the rotary polariser wires initially in the vertical sense, a maximum power from the source could be recorded before the experiment began. The rotary polariser would then proceed to complete a run. After the run was completed and the rotary polariser wires had returned to the vertical another measurement of the maximum power was recorded. The average of the two maximum powers could then be used to normalise the data to. The error lies in the way the (x) measurements were performed. Since, we have only one detector an initial measurement of the power of the source was taken with the detector still in the (x) position and the rotary polariser wires in the vertical sense, for normalisation purposes. Then the detector was rotated through 90° to receive horizontal polarisation. In addition, the horizontal polariser half-cube was exchanged for a vertical polariser half-cube before a run proceeded. Two probable errors arise from this. Firstly, a coupling error with the horn can arise since one can never be certain that the horn was relocated at the same distance from the lens. Secondly, the lens in the vertical polariser was 0.5mm thicker than that in the horizontal polariser. Therefore, when the horizontal polariser was exchanged for a vertical polariser the beam would not

be focussed in exactly the same place and introduce a further coupling error. This loss due to coupling would also increase proportionally with power detected, which was one of the features observed from experiment. The other observation made earlier was that the angle detected for the $\text{PHI}=45^{\circ}$ experiment was less than 45° . If the error in angle determined does lie in the coupling with the (x) detector, then by simply attenuating the (x) detector in the computer model, mentioned in section(2.2.1), one should be able to see how the (x+y) plot changes. The computer model can be seen in Figures(8.11 & 8.12).

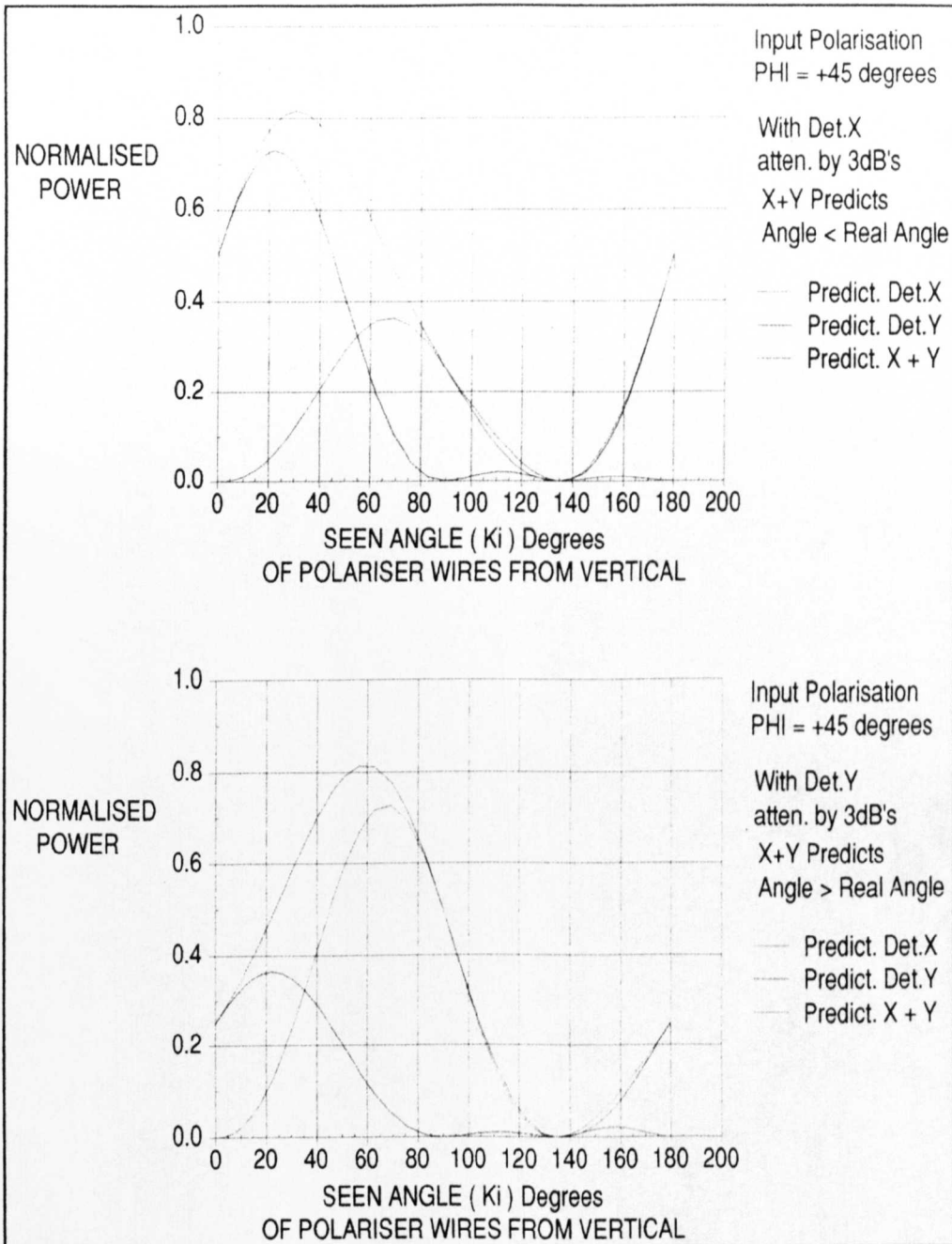


Figure 8.11

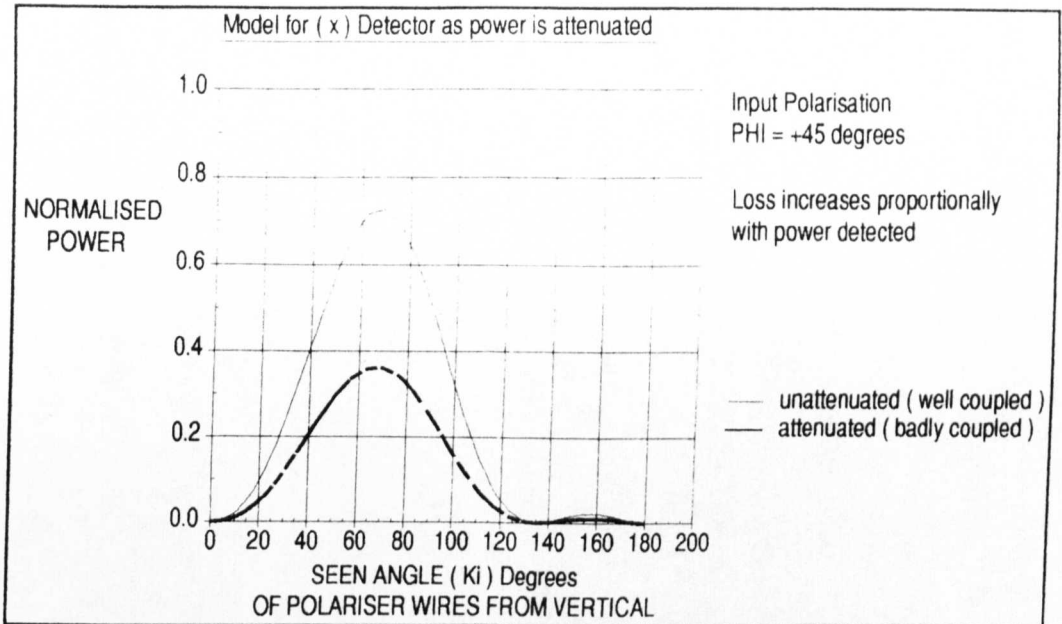


Figure 8.12

As one can see from Figure(8.11), if the (x) detector is attenuated the angle determined is actually less than the real angle. Also if the (y) detector is attenuated the angle determined is greater than the real angle. Also Figure(8.12) shows too that for an attenuated beam, the loss does in fact increase proportionally with power detected. Therefore, it is reasonable to say that the error in angle determined and the power loss in the (x) detector is indeed due to bad coupling. From this, an insight can be gained from the fact that the coupling for both detectors is critical for angle determination. This is one of the main reasons for using the T.K powermeter as will be described in Chapter 9.

In conclusion to this test case, we can say that a plot of power of (x+y) vs. angle will locate the rotated angle at a power maximum. However, if using (x) and (y) detectors the coupling is critical for correct angle determination. If the ferrite were perfectly matched then the difference between the maximum value of the (x+y) curve to the normalised power of one would represent the the attenuation (α) of the ferrite.

(8.2.2) Case Two : Elliptical Polarisation

The more complicated case of a general elliptical beam propagating through the experimental setup, is the next thing to look at. One could imagine the elliptical polarised beam as being the output produced by an Anisotropic, lossless perfectly matched ferrite placed at position (A) in the experimental setup. Again one does not need to have an anisotropic ferrite placed in position (A), but only a means of creating elliptically polarised light. This can be achieved by including the MPI in the original experimental setup to give a new "Rotary Polariser Setup (B)" as shown in Figure(8.13)

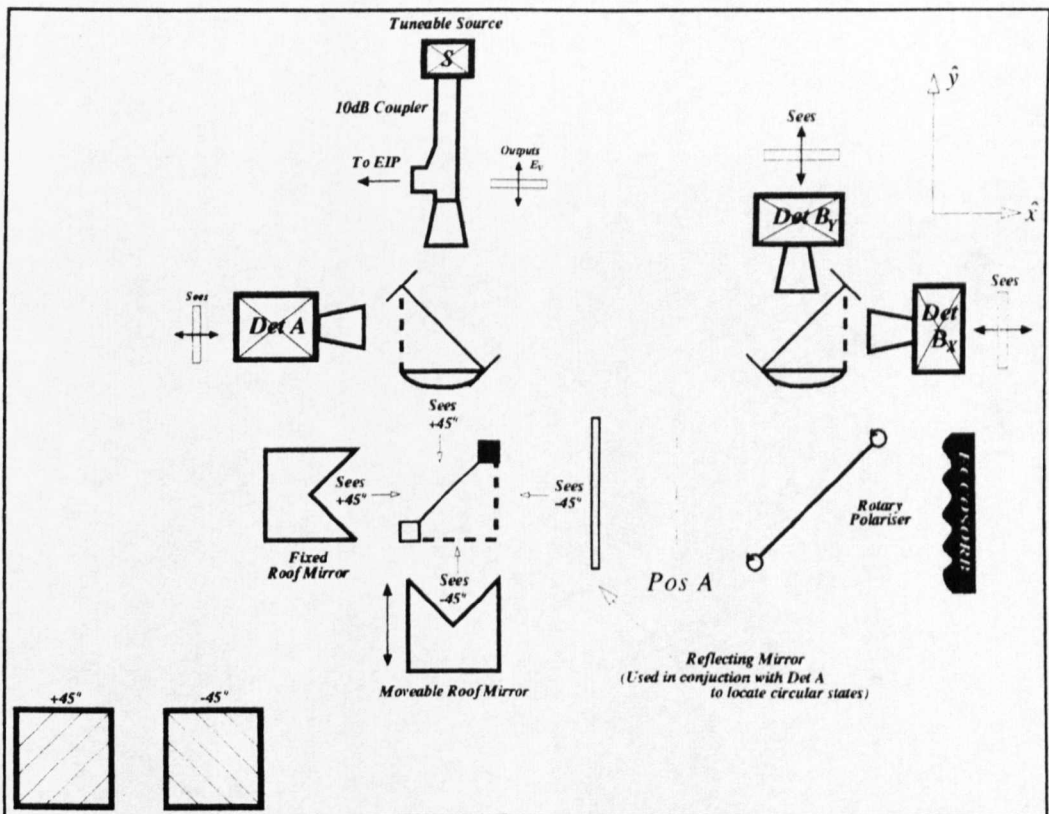


Figure 8.13

By using the Jones matrices for quasi-optical circuits² one can again predict what the detectors (B_x) and (B_y) will see for different (θ) values of the rotary polariser and also different path differences (d)

² A complete list of the matrices for quasi-optical circuits can be found in Appendix Two of Millimetre-Wave Optics, Devices & Systems, J. Lesurf, Adam Hilgar Publishers, 1990.

of the moveable roof mirror.

The (E) fields detected by the (x) and (y) detectors in setup (B) can be shown to be :

$$E_{BX} = \frac{-E_V}{2} \cos\theta \sin\theta \{ [2d] + 1 \} - \frac{E_V}{2} \sin^2\theta \{ [2d] - 1 \} \dots (8.14)$$

$$E_{BY} = \frac{E_V}{2} \cos^2\theta \{ [2d] + 1 \} + \frac{E_V}{2} \cos\theta \sin\theta \{ [2d] - 1 \} \dots (8.15)$$

Where, $[2d] = e^{i\varphi}$ and $\varphi = \left(\frac{2\pi}{\lambda}\right) \cdot 2d$

Where [2d] corresponds to the total path difference between the movable and fixed roof mirrors. The experimental results for the setup (B) can be seen in the following Figure (8.14) which represent a variety of elliptical polarisations.

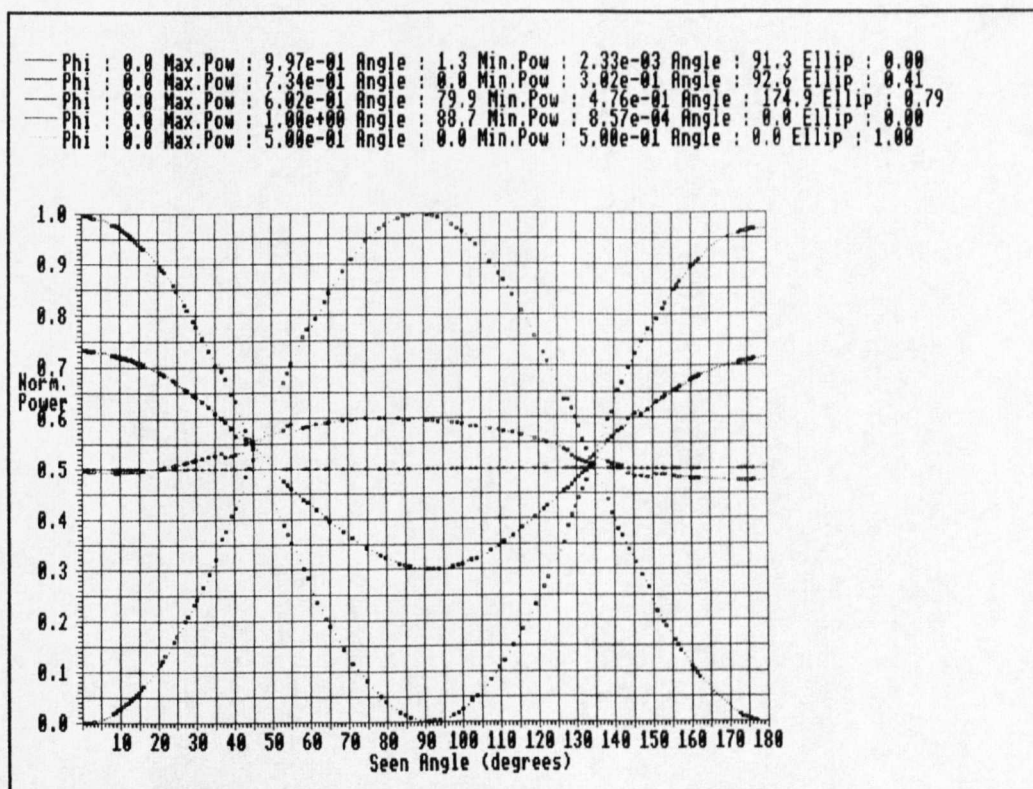


Figure 8.14

Again the amount of rotation can be determined by the location of

The angle of rotation of the linear polarised beam and also that of the major axis of an elliptically polarised beam can be located at the power maximum of their plot. However, if the beam emerging from a ferrite happens to be circularly polarised then nothing can be said immediately about the rotation imposed upon the radiation.

(8.3) Example - Predicted Rotation of Isolator IA1

As a test to the classifications described in the previous two cases one can look at a known isolator. I decided to look at the isolator (IA1) which was made from Anisotropic plastroferrite, discussed in section(6.12.2). The performance of the isolator can be seen in Figure (8.15).

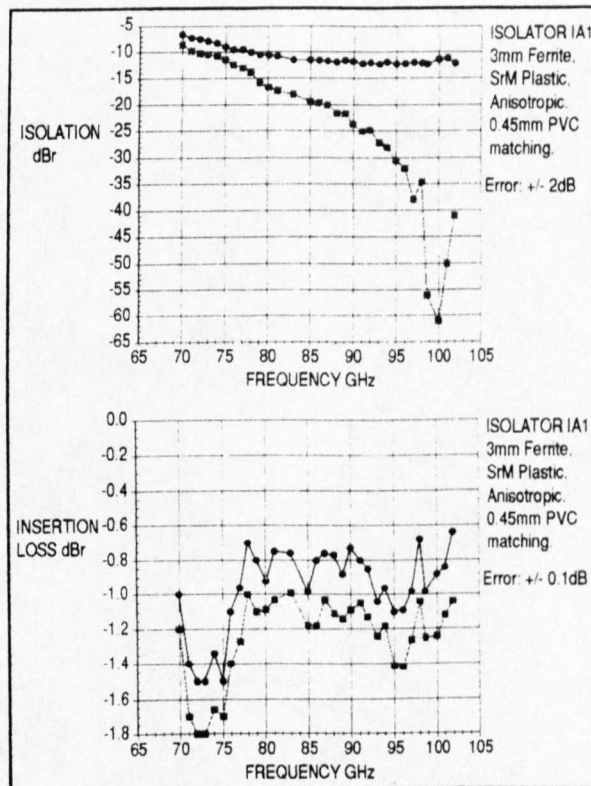


Figure 8.15

As one can see from the isolation results, the best isolation occurs at ≈ 100 GHz. (i.e. 45° rotation occurs here). Therefore, by placing the ferrite in setup(A) (Shown in Figure 8.5) one should expect to see $\approx 45^\circ$ rotation at 100 GHz.

The experiment was performed at 100.09 GHz and the results can be seen in Figure(8.16).

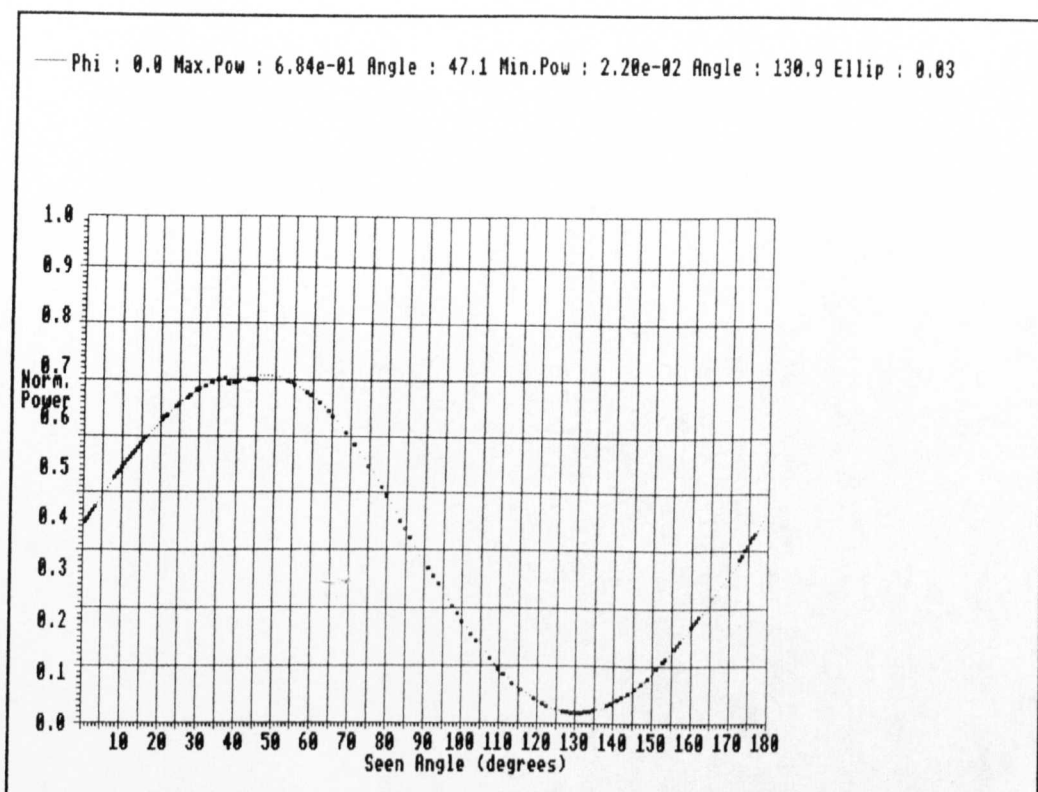


Figure 8.16

From the plot one can see a maxima at 47.11° and a minima at 130.9° . The difference between the maxima and minima should be 90° , however, it is 83.79° . The best estimate of the rotation can be made by subtracting 90° from the minimum angle and averaging this with the maximum angle. This gives a predicted rotation of 44° . There was some ellipticity associated to the resultant beam $ELLIP = 0.03$, however, this is very little.

(8.4) The Computer Data Plotting Program

What now follows is a brief description of the computer data plotting program which I developed. The program allows one to plot the data which is obtained from the files generated by the STEPrec program. The STEPrec program is the data acquisition program described in Chapter(7). As a quick recap, the STEPrec

program was developed to step the rotary polariser and record the power-meter measurements in a datafile in the RAMdisc of the computer.

There are two versions of the data plotting program. The programs are written in 'C '. The first version "Readdraw6" is for use with two separate (x) & (y) detectors. The second version "Readdraw7" is for use with the T.K Freespace power meter. The program first asks the user to input the number of datasets that are to be plotted. A dataset consists of two files, one file for each of the detectors (x) and (y) in the first version. In the second version a dataset consists of a single file. Up to seven different datasets can be plotted. The names of the datasets which are stored in the RAMdisc are then entered into the computer. An option to input the names of the calibration files then follows. The monitored power output values of the source are stored in the calibration files and each file within a dataset can have a complementary calibration file. The calibration files are used to normalise the detected powers of their corresponding datafiles. If no calibration files are recorded then the user has the option to input the power they require to normalise the dataset to. After all the dataset names have been input, the user is requested to enter whether a sprite file of the final plot should be saved to RAMdisc.

The computer program then proceeds to take each dataset in turn from RAMdisc and normalise it to its corresponding calibration file or the normalization power input from the user. These normalised values are plotted against the seen angle(χ) described in section(8.1.3). The maximum and minimum normalised power for each plot with its corresponding angle are located. And a measure of the ellipticity, described in section(8.2.2), is calculated. All the above mentioned values are displayed on the legend of the plot. Finally, a sprite file of the final plot is saved to RAMdisc if previously requested by the user.

(8.5) Experimental Work Performed For The D.R.A

Whilst here at St.Andrews, I performed a series of experiments using the the above mentioned system to assess the performance of four ferrite samples at W-band for the Defence Research Agency (D.R.A.). The batch of ferrite samples were all of the Sintered BaM Hexaferrite type. One sample was made up from pure Sintered BaM Hexaferrite and had a resonance frequency of 45GHz. The other three samples were sintered BaM samples into which different percentages of Cobalt/Titanium were substituted. This had the effect of reducing the resonant frequency of the sample. These other three 'doped' samples were quoted to have resonant frequencies of 26GHz, 13GHz and 4GHz. I shall refer to all five samples by their resonant frequency. All five samples were prepared and manufactured by Portsmouth University. As will be shown, all the 'doped' samples produced none, or very little rotation across W-band. The 45GHz 'undoped' sample did show rotation and from the results of the system one could see good signs of the 'Faraday Angle Resonance' phenomena. From using the maximum and minimum Faraday angles one could also predict the amount of rotation per single pass of the 45GHz sample and also provide an estimate of the optimum thickness that one should use to produce 45⁰ rotation. The results for all four samples now follow.

(8.5.1) The 26GHz Resonant Frequency Sample

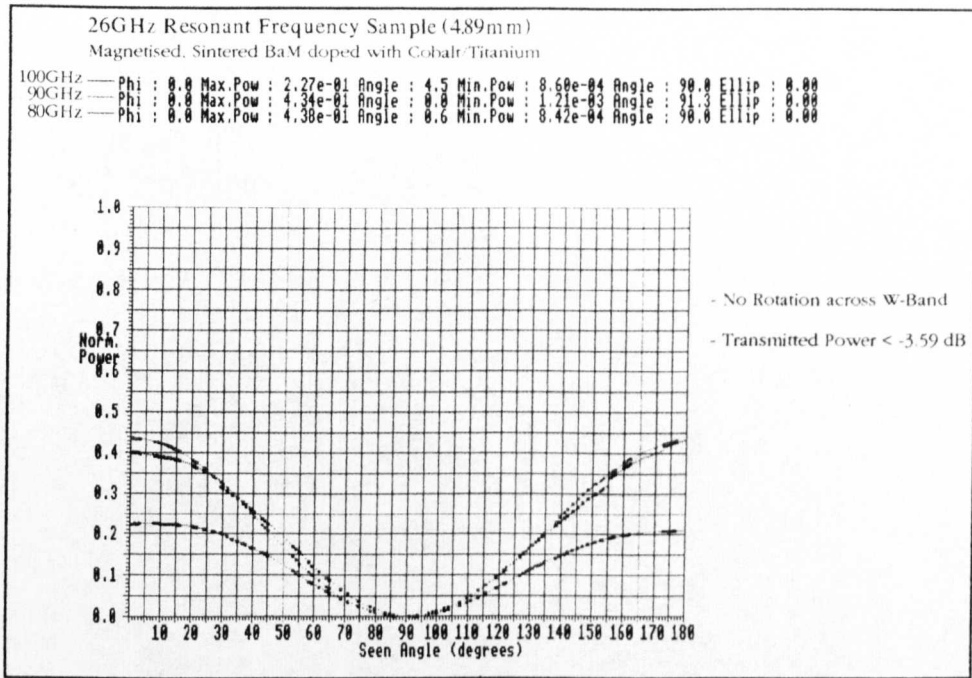


Figure (8.17)

(8.5.2) The 13GHz Resonant Sample

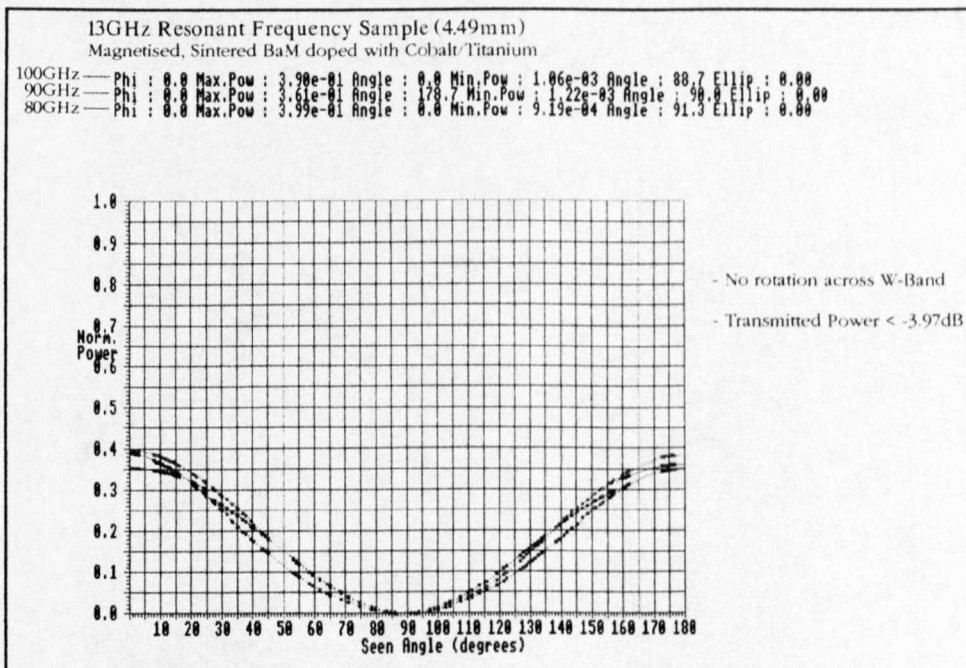


Figure (8.18)

(8.5.3) The 4GHz Resonant Sample

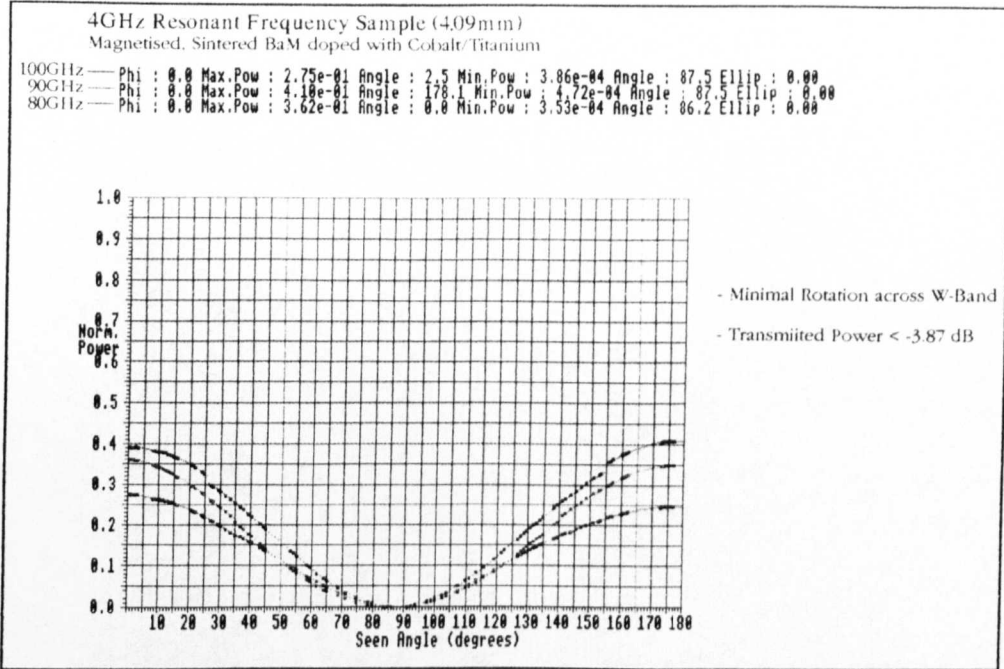


Figure (8.19)

The results for the doped 26GHz, 13GHz and 4GHz samples showed minimal or no rotation at the spot frequencies covering W-band. This suggests that the the doped samples did not retain a remnant internal magnetic field after saturation. This was attributed to the manufacturing process which led to high porosity(29%) of the ferrite material, as described by Kang³.

(8.5.4) The 45GHz Resonant Frequency Sample

For the undoped 45GHz sample, one set of experiments was performed on the unmagnetised sample. This was followed by a series of spot measurements across W-band that highlight the variation in rotation with frequency of the sample. The section is closed with the graphed result of the rotation variation with frequency which exhibits a strong feature of a 'Faraday Angle Resonance' profile.

³ DRA Report On Quasi-Optical Isolators In The 10-20GHz Region, S. Kang, May 1996

(8.5.4.1) 45GHz Unmagnetised Results

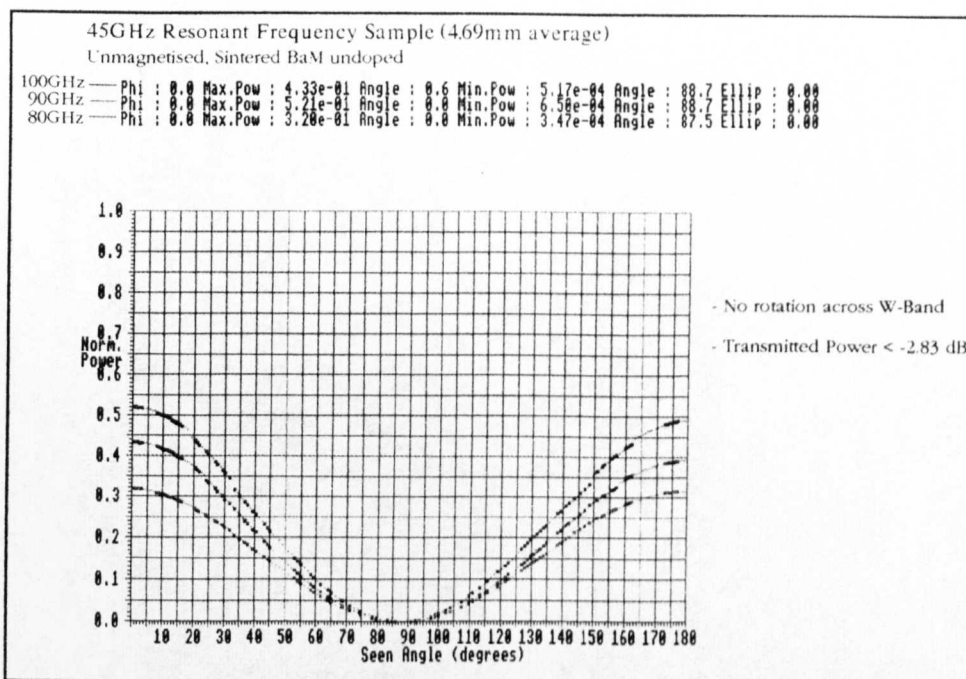


Figure (8.20)

(8.5.4.2) 45GHz Magnetised Results

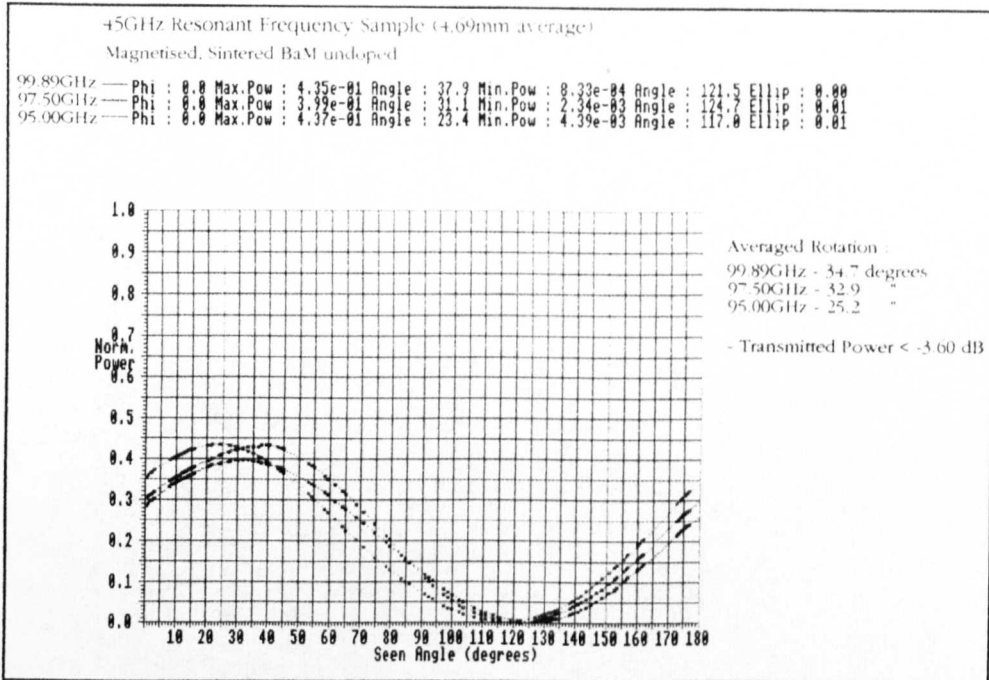


Figure (8.21)

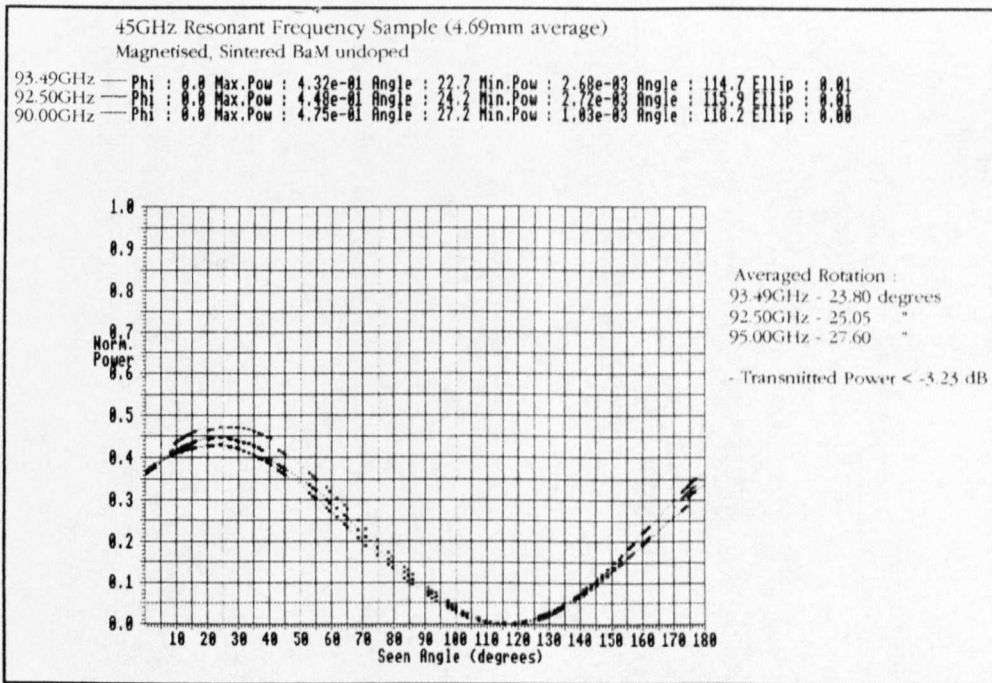


Figure (8.22)

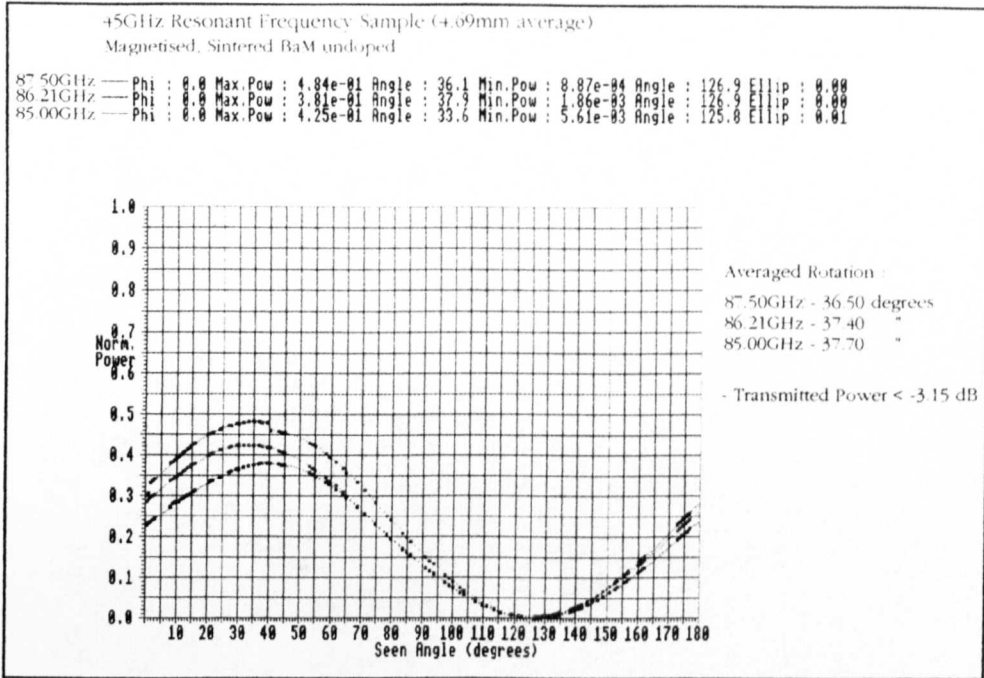


Figure (8.23)

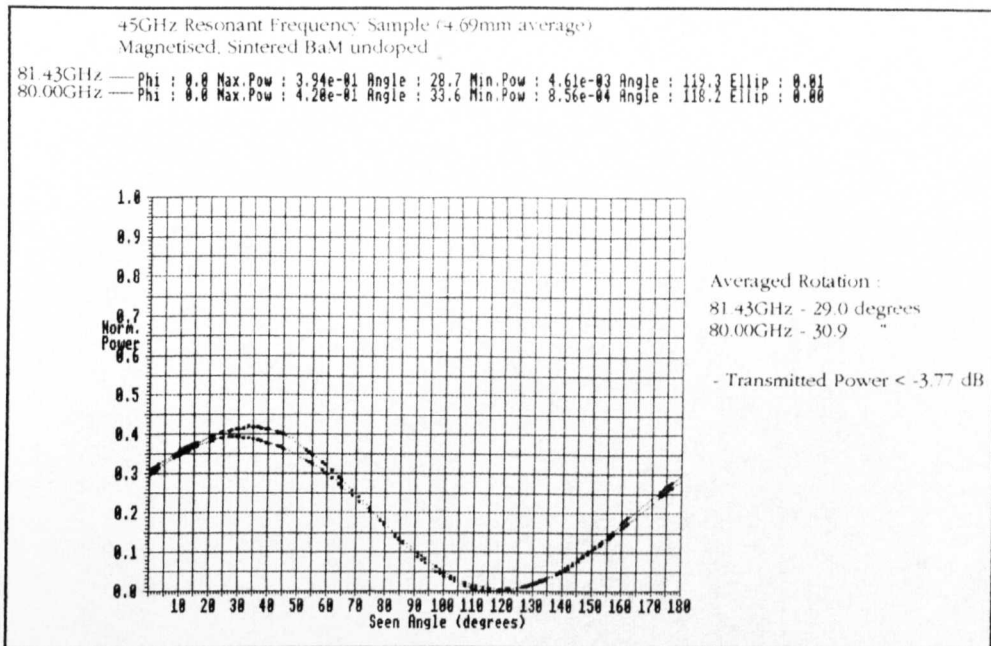
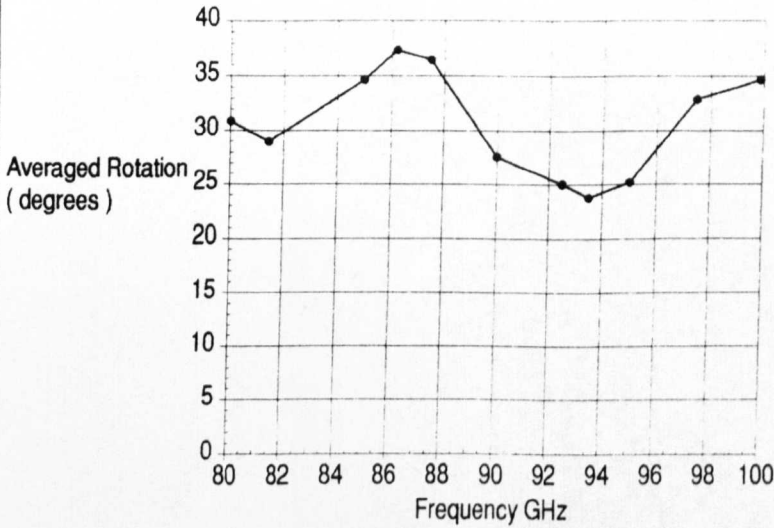


Figure (8.24)

As can be seen from figure(8.25), a rotation of 30⁰8 degrees/single pass could be estimated from the 'Faraday Angle Resonance' profile of the data. This leads to an optimum thickness of 7mm to achieve 45⁰ rotation across the frequency range specified. Furthermore, the 'Rotary Polariser Optical System' allows one to observe the ellipticity of the beam. It is evident that ellipticity effects are negligible and the linearity of the beam is preserved upon propagation through the sample.

45GHz Resonant Frequency Sample (4.69mm average)
Magnetised, Sintered BaM undoped

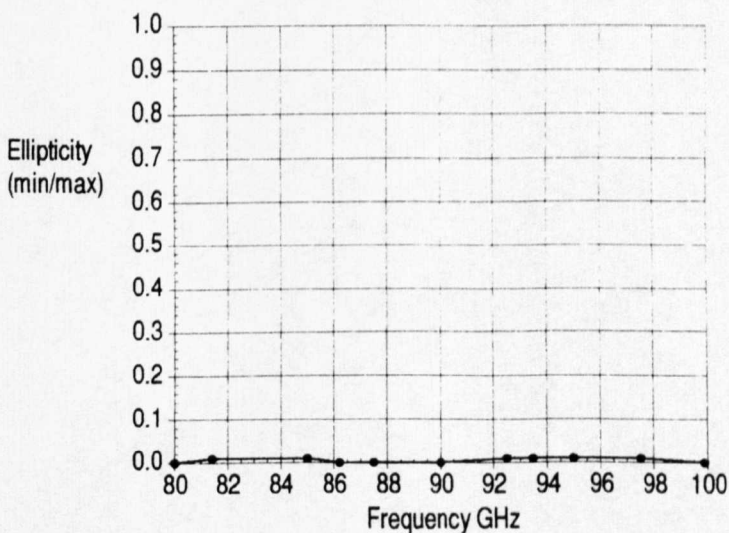
- Faraday Angle Resonance Observed



Maximum Angle : 37.40 degrees @ 86.21GHz

Minimum Angle : 23.80 degrees @ 93.49GHz

Theory predicts : $30^{\circ} 8'$ rotation per pass
: 7mm Optimal Thickness



- Linear Polarised Beam Output From Ferrite
(i.e. No distortion on input beam)

Figure (8.25)

Chapter 9

A Fully Automated Millimetric Rotary Polariser Quasi-Optical System

Introduction

This chapter details the 'Final Version' of the 'Rotary Polariser Quasi-Optical System'. The final system is a completely automated version of the system presented in Chapter Eight. The main difference of the new system is the detector that was employed. As mentioned in section(2.2.3), since the laboratory owns only one Boonton detector, measurements in the (x) and (y) directions had to be performed separately. This led to a coupling problem and hence an inaccurate measurement of the Faraday angle. The new system employs a Thomas Keating (T.K.) Freespace Power Meter which will be described shortly. By employing the T.K. off the Brewster Angle, the detector becomes polarisation insensitive. This offers the perfect opportunity to detect an arbitrary oriented polarisation state that is reflected from the Rotary Polariser using only the one T.K detector. The chapter begins by describing the operation of the T.K. power meter and how it can be used for polarisation insensitive detection. The computer routines developed to calibrate the T.K.'s output voltage to actual detected power are detailed and results are presented. From the results it will be shown that the calibration was unreliable. Although the calibration to determine the actual power was unsuccessful, it will be described how the voltages from the T.K. could still be used to determine the Faraday angle and give a measure of the ellipticity of the beam. The chapter continues with a description of how a 'Tracking' procedure was successfully

developed to reduce experimental time. Further sections describe the sources of noise that were present in the system. The sections suggest a specific experimental arrangement that can be used to combat standing waves. In addition, a 'Least Squares Parabolic Fit' routine was developed which successfully cuts through the noise floor and improves accuracy of measurement. The final sections demonstrate how the 'Fully Automated System' can be used to make 'Faraday Angle Resonance' measurements. This is in order to assess the suitability of magnetic materials for use as 'Freespace Faraday Rotators'. Also attention is given to highlight the difference in results expected from a material which is operating in the 'Frequency Dependent' region of its 'Rotation versus Frequency' curve. Further results are also given which highlight how the system can be used to give a deeper insight into the operation of Faraday Rotators. This is by the direct measurement of the Rotation and ellipticity of their output beam. The chapter is closed by describing two additional uses of the system. It will be demonstrated that the system can be employed for the characterisation of quasi-optical quarter-wave plates, by example of a 'Millimetric Fresnel Rhomb' that was developed. And also how the the system can used to locate the principle axes of a birefringent material, in particular that of an unmagnetised ferrite, by ellipticity measurement.

(9.1) The Thomas Keating (T.K.) Freespace Power Meter¹

The Thomas Keating or T.K. Freespace Power Meter consists of a closed air filled cell. A thin metal film of an area 30mm×30mm is located within the closed cell. When an amplitude modulated signal falls upon the cell, approximately 50% of the radiation is absorbed by the thin metal film. The other 50% is either reflected from or transmitted through the cell. The power absorbed heats the metal film and changes the air pressure within the closed cell. The pressure change of the cell is closely proportional to the power of

¹ All figures quoted are with reference to the T.K. Submillimeter Power Meter PM104 Operating Manual.

the incident beam. A pressure transducer is used to monitor the changes in pressure of the cell due to the amplitude modulated beam. Hence an A.C. voltage is output from the power meter which can be used to determine the amount of power in the incident beam.

(9.1.1) Positioning Of The T.K. Power Meter

The amount of reflection from and transmission through the cell is dependent on the orientation of the T.K. with respect to the incident radiation. When the T.K. meter is oriented at 55° , known as the Brewster Angle, to the incident radiation there is no reflection from the cell. Instead the radiation which is not absorbed, is transmitted through the cell. At the Brewster angle the T.K. calibration curve, of voltage output to power input, is frequency independent. However, at the Brewster angle the T.K. is sensitive only to a vertically polarised input. At angles other than the Brewster angle the T.K. becomes insensitive to the polarisation of the radiation. However, the T.K. calibration curve is frequency dependent and a separate calibration curve must be determined for different operational frequencies. Therefore, a classic tradeoff has to be made. As mentioned in the introduction, since the rotary polariser will be reflecting arbitrary polarisations toward the T.K., the T.K. should be oriented off the Brewster angle. At near normal incidence the T.K. should be sensitive equally to all polarisations. It was found that orienting the T.K. at 5° to the incident beam was sufficient for detection of arbitrary polarisations whilst allowing any frequency dependent reflections from the cell to be diverted such that standing waves could be reduced. The T.K. was positioned at this angle and at a distance of 87mm from the 2nd lens. This was the calculated in section(2.4.4) as the optimum distance that gave a beamwidth of no greater than 5.83mm over W-band at the detector's face. With the T.K. angled at 5° , an elliptical shaped beam with major axis 5.85mm and minor axis of 5.83mm is projected onto the T.K.'s face. This is

easily contained within the effective 30mm×29.8mm area of the T.K.

(9.1.2) Amplitude Modulation Of The Incident Beam

As mentioned previously, in order for the T.K. to operate correctly it is necessary for the incident beam to be modulated in amplitude. This was achieved by placing a rotary bladed shutter, or mechanical chopper, in the path of the propagating beam. The chopper consisted of three blades of the same area made from aluminium and coated with Eccosorb, a form of radar absorbent material (R.A.M.). The blades were separated from each other by an area of freespace equal to the area of a blade. Therefore, as the chopper rotated the continuous wave signal from the source, would not be allowed to propagate through the system when an blade was in front of the source. Similarly, the continuous wave signal would propagate when no blade was present in front of the source. In this way the T.K. would receive an mechanically 'chopped' signal which was amplitude modulated. A small light tachometer attached to the chopper and connected to a small electronics unit was used to output a reference voltage. The reference voltage corresponded to the rate at which the source was being chopped. The square wave modulation that occurred could be seen by connecting the output voltage to an oscilloscope. The modulation rate could then be adjusted by altering the voltage supplied to the motor of the chopper. A modulation rate of 20-40Hz is suggested in the operating manual of the T.K., as a maximum signal-to-noise ratio is obtained in this range. A modulation rate of 30Hz was chosen. Finally the mechanical chopper was located directly in front of the feedhorn of the source.

(9.1.3) Interfacing of the T.K. to the computer

A GPIB compatible EG&G Princeton Applied Research 5210 Lockin Amplifier was employed to interface the T.K. to the computer. As well as interfacing the T.K. to the computer the Lockin Amplifier

also gave one the opportunity to perform phase sensitive detection on the input signal. Phase sensitive detection could be achieved by connecting the a.c. output from the T.K. to the signal channel of the Lockin and connecting the a.c. reference voltage from the mechanical chopper to the Lockin's reference channel. In this manner, d.c drift can be eliminated and a high rejection of frequencies outside the chopping frequency of the source can be attained. This is achieved by increasing the time constant of the Lockin², to be discussed shortly.

(9.1.4) Computer Procedures Developed For The Lockin Amplifier

Just as for the Boonton Power Meter, it was necessary to create a variety of procedures for the Lockin Amplifier in order to control its operation.

Since the Lockin was GPIB compatible, transmitting and receiving information could be performed with PROCadrandoutput and FNadrandinput respectively together with the appropriate device specific commands.

The structure of a GPIB command for use with the Lockin is as follows. Each command consists of three parameters. The first two parameters are the same for both the PROCadrandoutput and FNadrandinput commands. The first parameter '0' tells the computer, if it is receiving information, to receive information until a termination character is sent. If the computer is sending information then to append the data with a termination character. The termination character was set to <CRLF> which is a carriage return followed by a linefeed. The second parameter '4' is the device address of the Lockin. Finally, the third command for FNadrandinput is '255' and represents the amount of data to take in a single measurement. For PROCadrandinput the third parameter is enclosed in quotes and consists of two parts. The first part consists of the actual command. Only the first part is sent if one wants to read

² All figures quoted are with reference to the EG&G Princeton Applied Research Model 5210 Lockin-Amplifier Instruction Manual.

information from the instrument. The second part is included if one wants to change a setting of the Lockin and it specifies what the setting will be.

For example,

```
PROCadrandoutput(0,4,"GP")  
result$ = FNadrandinput(0,4,255)
```

Will request the Lockin to return its GPIB address which will then be stored in result\$

Whereas,

```
PROCadrandoutput(0,4,"GP 4")
```

Will set the GPIB address to '4'.

Hence, combining both PROCadrandoutput and FNadrandinput one can send and receive information from the Lockin.

What now follows is a discussion of the main procedures developed in order to control the Lockin Amplifier.

PROCsetup_lockin

Before measurements could be taken with the Lockin, a series of initial commands had to be sent to setup the Lockin for accurate data retrieval. Fourteen initialisation commands were set. The most important commands will now be described.

Filter Commands

```
PROCadrandoutput(0,4,"F2F 0") -
```

Tells the computer that the reference channel (namely the frequency of the chopper) will be used as the reference frequency.

```
PROCadrandoutput(0,4,"ATC 1") -
```

Sets tuning filter to TRACK mode. The Lockin will track the

reference frequency within a certain range determined by parameters given with commands FLT3 and FF.

PROCadrandoutput(0,4,"FLT 3") -
Sets tuning filter to Bandpass mode.

PROCadrandoutput(0,4,"FF 300;2") -
Bandpass is set from 10 to 120 Hz. Tunes filter around 30Hz (The frequency of reference signal).

Amplification Commands

PROCadrandoutput(0,4,"G 0;0") -
Turns gain OFF
PROCadrandoutput(0,4,"EX 0") -
Turns Expand OFF, which is another amplification feature.

Time Constant Command

PROCadrandoutput(0,4,"TC 5") -
Sets the Time constant to code 5 = 300ms
Obviously a large time constant, of say 3secs, would give a very high rejection of frequencies and suppress noise well. However, this would mean that at least a 3 second delay would be necessary every time the input signal changed significantly. The input signal could be expected to change significantly every time the stepper moved through one step. Also it is good practice to allow for at least 3 time constants to pass before taking a measurement. Therefore, for 200 steps in half a revolution, a time of around 30 mins would be necessary. This is assuming that we are only taking a single measurement per step and no other instrument is being read and not allowing for the polariser to settle properly. I decided on a time constant of 3ms which would give the order of ≈ 1 second before measurements were taken. This is short enough as not to lengthen experimental time whilst also allowing for approximately 3 time

constants to pass and hence adequately suppressing noise.

Autosensitivity Command

PROCdrandoutput(0,4,"AS") -

This command causes an AUTOSENSITIVITY routine to commence. This involves the Lockin scanning its sensitivity ranges and determining the range in which measured voltage falls between 30% of a maximum full scale deflection. This command will be discussed again later in the section.

PROCpoll

This is a separate procedure which is called after every PROCdrandoutput command sent to the Lockin. It causes the Lockin to execute a serial poll. The procedure is exited when the Lockin responds with a '1' which corresponds to a 'Command has been executed - Ready to continue' status.

PROCrun_poll

This a more sophisticated version of the above PROCpoll procedure. It is used in conjunction with the PROCsample_lockin procedure, to be explained shortly, and was written to deal mainly with an 'Overload' situation which can occur with the Lockin, as will now be described. The start of the procedure firstly requests the Lockin to perform a serial poll. It then looks to see if the status value returned corresponds to either an 'Overload' status = '16', a 'System Request' = '64' or a 'Ready to continue' = '1'. When an 'Overload' is encountered then the measured voltage does not fall within the particular voltage sensitivity range. Therefore, in order to take an accurate reading, the correct sensitivity range must be found. This is achieved by calling PROCautosens which in turn calls PROCdrandoutput(0,4,"AS"), described earlier. A call to PROCpoll is then used to determine when the autosensitivity command has been executed. If a "System Request" has occurred then a fault has

occurred and maybe something needs to be manually altered on the Lockin. The computer then requests the user to press space when it is safe to continue. Finally, if a 'Ready to Continue' status is returned then the procedure is exited.

PROCread_lockin

This procedure is used to determine the correct output voltage measured from the Lockin. Although one can easily read the magnitude of the voltage in a display window and the units of magnitude, i.e. V, mV, μ V ... etc. from the sensitivity indicators, the instrument does not have the facility to send the absolute voltage to a computer. Instead the magnitude and a sensitivity code have to be separately read from the Lockin and then the absolute voltage can be determined via an equation supplied in the operating manual. The procedure determines the absolute magnitude of the voltage by firstly requesting the Lockin for its sensitivity code using PROCadrandoutput(0,4,"SEN"). The returned value which is an integer between 0-15 is stored in the variable 'sensitivity%'. A similar request is then made for the magnitude of the measured voltage which is stored in the variable 'magnitude%'. The absolute voltage can then be determined using the equation :

$$volts = \left(\frac{magnitude\%}{10000} \right) \times scale \quad \dots (9.1)$$

where,

$$scale = 10^{\left(\left(\frac{sensitivity\%}{2} - 7 \right) + (Log(6) \times (sensitivity\%MOD2)) \right)}$$

PROCsample_lockin

This calculates what I term as the 'corrected voltage'. This is the voltage from the Lockin divided by the output power from the source, as determined by the Boonton power meter. This correction on the volatge is necessary due to possible drift of the oscillators power. The units of this calculation are in (volts/mW). The procedure makes use of PROCrun_poll, PROCread_lockin

procedures, mentioned recently. It starts by firstly calling PROCpoll to determine if an autosensitivity is necessary. This is followed by five separate measurements being taken alternatively from the Boonton and Lockin. Every time the Boonton is sampled the measurement is multiplied by a factor of 10. This is because the Boonton is located on the arm of the 10dB coupler and the actual power propagating into the system is one order of magnitude greater than that detected. Both sets of measurements are then averaged and the corrected voltage is determined by dividing the average Lockin voltage by the average Boonton power. A typical experimental run consisting of a half revolution can be seen in figure(9.1).

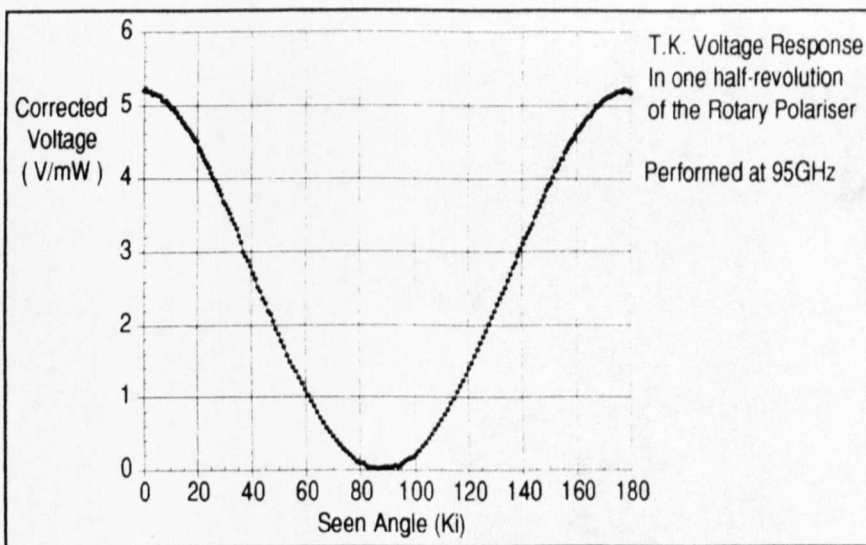


Figure (9.1)

(9.1.5) Calibration Of T.K. Power Meter Over W-Band

Although the T.K. is only sensitive to the vertical polarisation state when at the Brewster angle, the voltage output for various power input remains the same for all frequencies. One can say its calibration curve, or Detectivity (D^*), is frequency independent. When one angles the T.K. away from the Brewster angle, it becomes receptive to arbitrary polarised inputs. However, differing amounts of reflection occur at the faces of the cell of the T.K. for different

frequencies. This leads to a voltage output to power input, calibration curves or detectivity (D^*) that differs for different frequencies. Hence, separate calibration curves would need to be determined for each discrete frequency within this frequency dependent region. The following sections will describe by theory and experiment, the efforts made to calibrate the T.K. over W-band. Although, theoretically the T.K. can be calibrated, it was found experimentally that the calibration curves determined were unsatisfactory for practical use. It will be shown that the calibration curves determined were very reliable for some frequencies within the region of interest but were very unreliable for others. The method used to calibrate the T.K. will now be described.

(9.1.6) Method Of Calibration

As will be shown each calibration curve is linear in its profile. The difference lies in its gradient and intercept. As mentioned in the previous section, a different calibration curve would be needed ideally for each frequency. Ofcourse, this would be an impossible task. The way around this, would be to determine a calibration curve for the T.K. for a number of discrete frequencies. Therefore, knowing the gradient and intercept for each of these discrete frequencies, one could then simply interpolate the gradient and intercept for a different frequency and hence determine its calibration curve. Obviously, the closer the discrete frequencies are, the more accurate the interpolation of the gradient and intercept for the new frequency would be. To complicate matters even further two calibration curves would be necessary for each frequency. This is in order to predict the power for an arbitrary angled linearly polarised beam which would be reflected from the rotary polariser. By having one calibration curve for a horizontally polarised input and another calibration curve was for a vertically polarised input, one would be able to determine the power in both the (x) and (y) directions. As will be shown, since the angle of the reflected the

radiation toward the T.K. is known³, one can with the (x) and (y) powers known, deduce the power for an arbitrary angled reflected beam.

(9.1.7) Computer Program 'T_DLinReg' Developed For T.K. Calibration

A separate program had to be developed in order to calibrate the T.K.. This program was titled 'T_DLinReg' and performed the following task.

The program would start by moving the frequency tuner to the 100GHz position. The position of maximum power would then be located by traversing the backshort tuner. Depending upon the position of the backshort tuner relative to the critical limits allowed by crit_bs_up and crit_bs_down, it moves five discrete increments. The time interval per increment is two seconds. Five of these two second increments is sufficient for the majority of the backshort range to be traversed. Furthermore, this will allow one to attain a broad range of voltages and power outputs that occur for this particular frequency. At each increment, the power output from the Boonton and voltage output from the Lockin is sampled alternately, as described by PROCsample_lockin. After each increment the average T.K. voltage and average power output is stored in an array. When the backshort has completed its five discrete steps, a line of best fit is calculated from the data obtained from the five discrete positions. From the line of best fit, parameters necessary to describe the line, such as m, xbar and ybar which will be discussed shortly, are calculated. These parameters are then stored in separate columns of an array, the frequency tuner is incremented and the process repeats. When the frequency tuner has reached the 80GHz position, the program terminates by saving the frequency, (m),

³ The seen angle reflected from the rotary polariser is not the same as that detected at the T.K. This is due to the T.K. being inclined at 5° to the incoming radiation. The actual angle detected at the T.K. is to be known as the 'detected angle' and this correction is explained later.

\bar{x} and \bar{y} parameters in separate files which can be used later for interpolation. The experiment has to be repeated twice. Once with a vertical polarised beam and secondly with a horizontal polarised beam. Again another set of similar parameters are calculated but for the orthogonal polarisation state. The linear relationship that exists between the T.K. output voltage and the source output is evident from figures(9.2). A similar program, called 'LINregres', was run for the spot frequencies 99.75GHz, 89.98GHz & 80GHz. It was designed specifically to highlight this linear relationship. The only difference in program 'LINregres' to the program 'T_DLINreg', is that 30 samples are taken for one specific spot frequency.

Chapter Nine
A Fully Automated Millimetric Rotary Polariser Quasi-Optical System

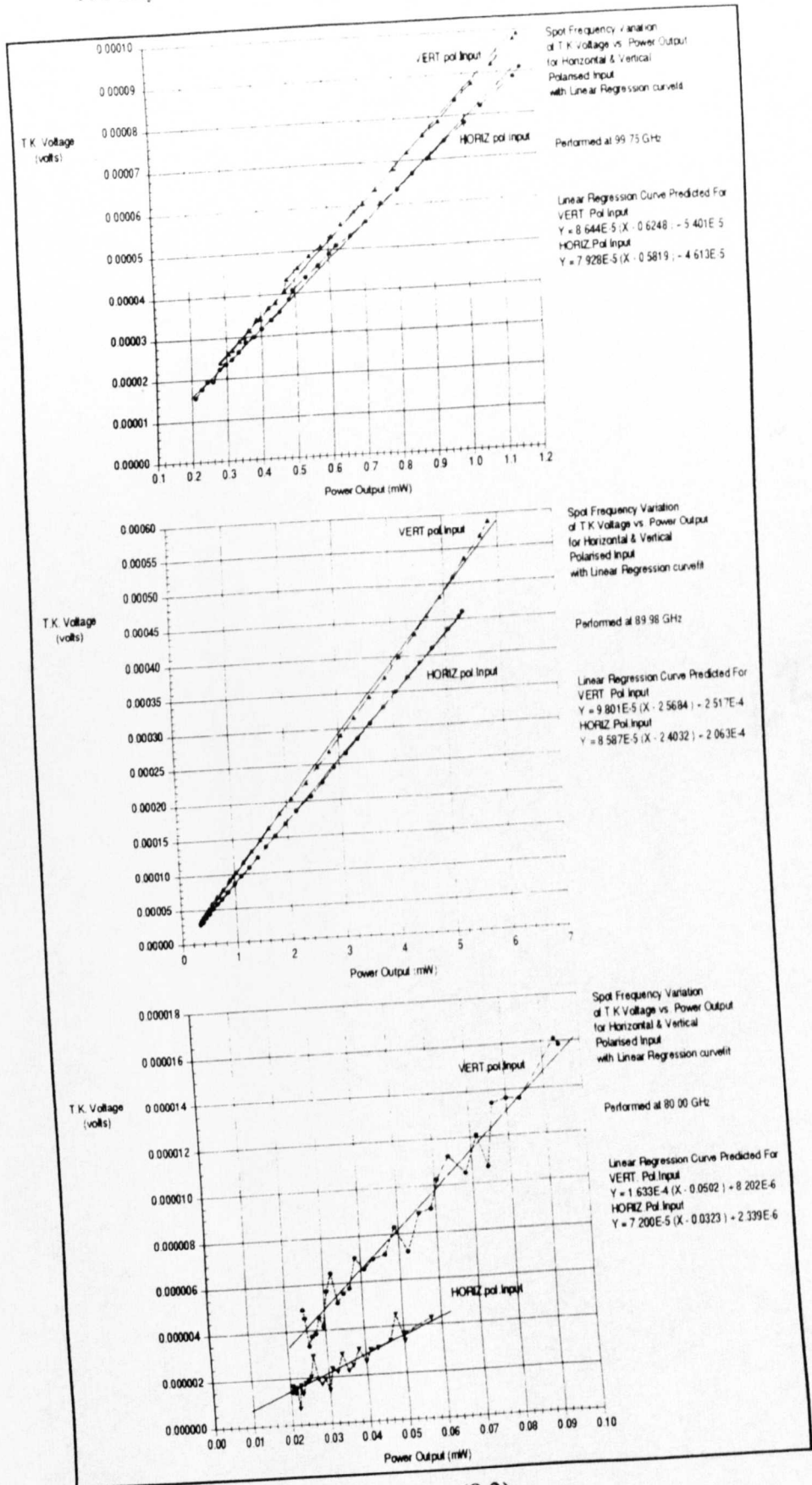


Figure (9.2)

The way in which the linear regression was performed is as follows. If one has (n) pairs of observations $(x_1, y_1), (x_2, y_2), \dots, (x_n, y_n)$. Then a line of best fit exists such that it can be described by the relationship.⁴

$$Y - \bar{y} = m(X - \bar{x}) \quad \dots (9.2)$$

Where, (\bar{x}) & (\bar{y}) represent the means of the (x_i) and (y_i) respectively, and

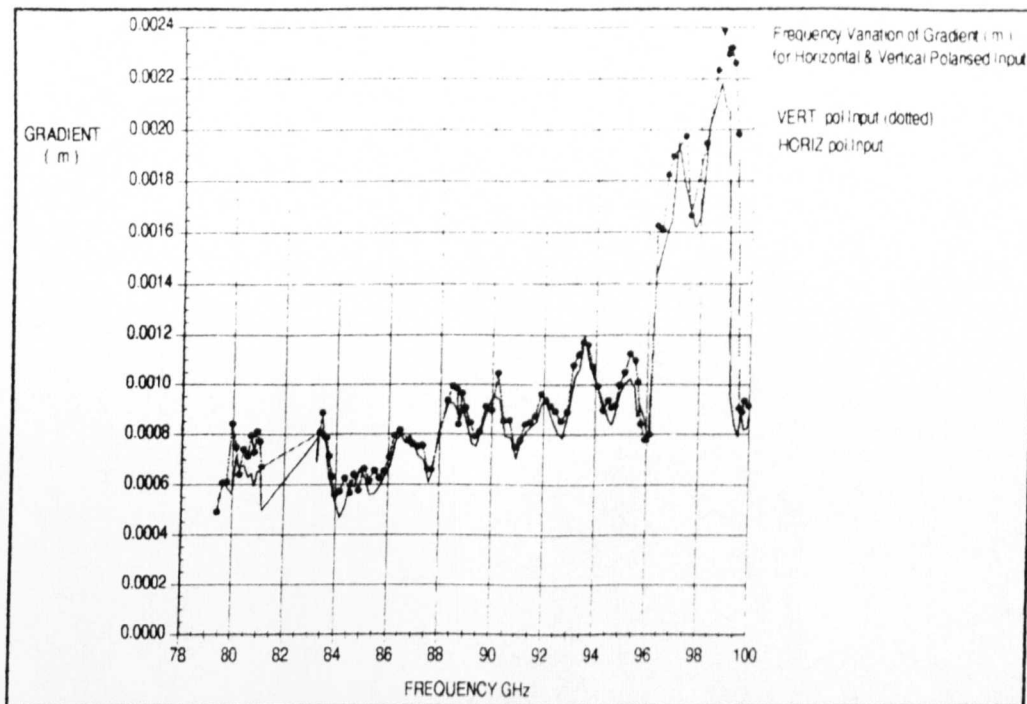
$$m = \frac{\sum_{i=1}^n x_i y_i - n \bar{x} \bar{y}}{\sum_{i=1}^n x_i^2 - n \bar{x}^2} \quad \dots (9.3)$$

A procedure known as PROClinear_reg performs the calculation given by equation(9.2) in order to determine the line of best fit. As can be seen from figure(9.2), the amount of scatter of the data can be very linear, as in the 99.75 and 89.98GHz plots. Hence, a least squares fit can provide a very good estimate of the voltage/power output behaviour at at these frequencies. However, some fits as in the 80GHz plot have data that is slightly more scattered. Therefore, a less accurate estimate of the power output for T.K.voltage could result from the least squares fit.

(9.1.8) Results obtained from program 'T_DLINreg'

As described earlier, program 'T_DLINreg' determines the parameters (m), (\bar{x}) and (\bar{y}) which are necessary to reconstruct the frequency dependent, linear voltage vs. power output profiles of the original data. The variation in (m), (\bar{x}) and (\bar{y}) over W-band for both vertical and horizontal input polarisations as determined by program 'T_DLINreg' can be seen in figures(9.4-9.6) below.

⁴ Jeffrey, A., *Mathematics For Engineers & Scientists (3rd Ed.)*, Van Nostrand Reinhold (UK) Co. Ltd., Chapter 18.5 pgs.772-773.



Figure(9.4)

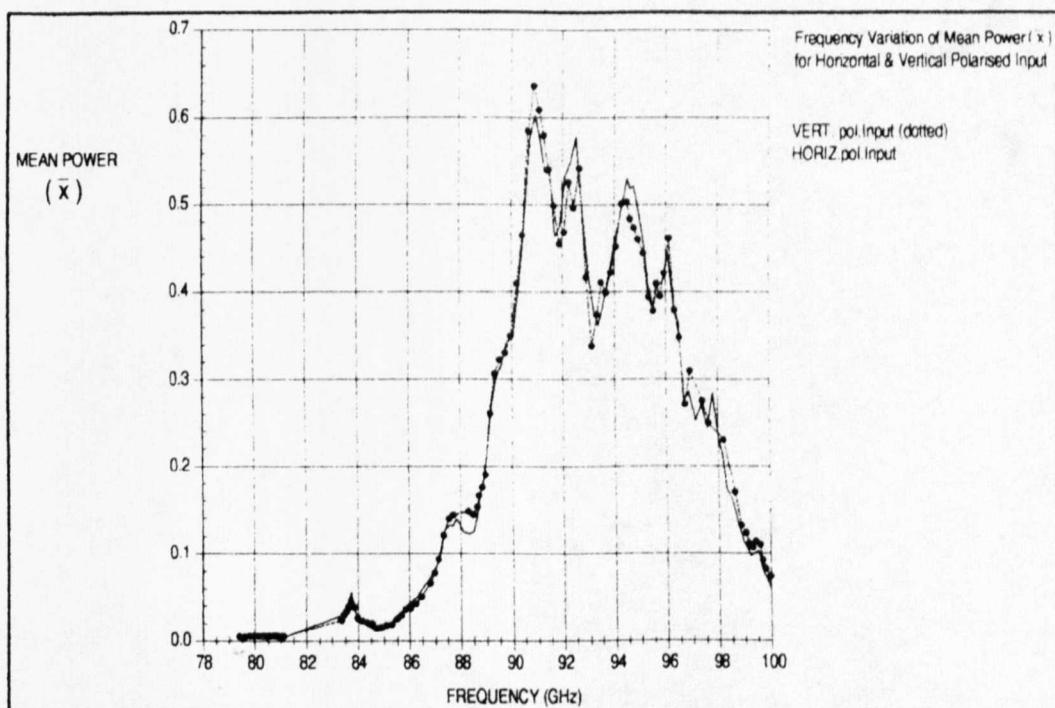


Figure (9.5)

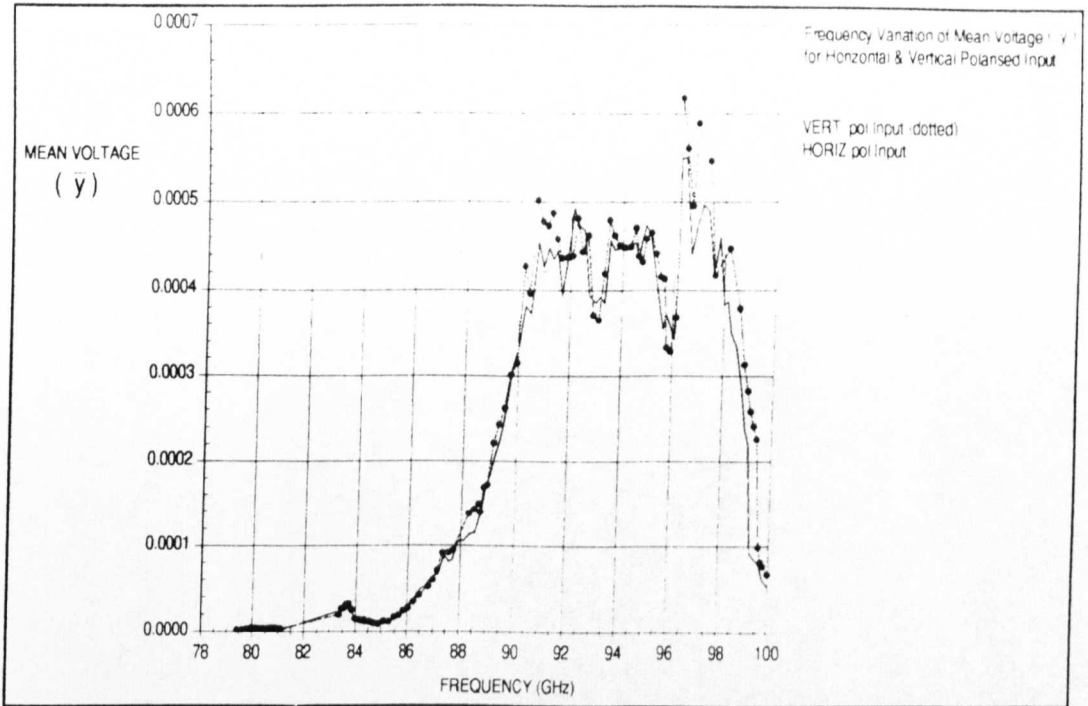


Figure (9.6)

As can be seen from figures(9.4 - 9.6), the vertical and horizontal polarisation for each of the (m) , (\bar{x}) and (\bar{y}) plots have an almost identical profile for some frequencies but differ slightly for others. This is as expected, determined from program 'LINregres'. The above three figures represent graphically the data that was used to interpolate calibration curves for the intermediate frequencies which can occur. The data for each curve shown, for both horizontal and vertical polarisations, were stored in separate files. The horizontal polarised input files for frequency, (m) , (\bar{x}) and (\bar{y}) were named corr_hfreq, corr_hgrad, corr_hpow and corr_hvolt respectively. Similarly the vertical polarised input files were named corr_vfreq, corr_vgrad, corr_vpow and corr_vvolt respectively. The eight files mentioned were located in a directory called 'LOOKUP' which was placed in RAMdisc. This directory would then be accessed by the interpolation routine which will now be described.

(9.1.9) Interpolation Of Datafiles For An Arbitrary Frequency

After the 'LOOKUP' directory had been created from the program

'T_DLINreg', it was now necessary to create some new routines for the main program that could be used to access the 'LOOKUP' directory, determine the particular calibration curve for a given frequency and then determine the actual power detected by the T.K. for a particular voltage and incident angle. The next section will describe the routines designed.

'PROCinterpolate' was designed to access the datafiles within the 'LOOKUP' directory and hence deduce the calibration curve for a specified frequency.

The procedure executes in the following manner. Firstly, it scans through the 'corr_hfreq' file. Recapping, this file contains all the frequencies encountered during a 'T_DLINreg' run for a horizontally polarised input. This 'scan' is performed by a secondary procedure called 'PROCscan_file(name\$)'. Its function is to scan a file in the 'LOOKUP' directory which is specified by "name\$", where 'name\$' in this case is 'corr_hfreq'. It compares every entry in the specified file to the frequency variable, obtained during procedure PROCgo_eip_go. At the end of the scan two adjacent frequencies will have been found in the file in which the frequency variable falls between. The frequency larger of the two frequencies is assigned to the variable 'top_freq' and the smaller is assigned to 'bot_freq'. Also the difference between 'top_freq' and 'bot_freq' is stored in the variable 'difference' and the position of the 'top_freq' in the datafile is stored in 'top_pos'. The percentage distance that the frequency variable is away from the 'top_freq' is finally determined and stored in the variable 'perc_away_from_top'. This variable will be used in the interpolation stage which will now be described. The first file to be interpolated over is specified by "name_two\$" and is 'corr_hgrad'. A secondary procedure, PROCdo_inter(name_two\$) takes the file 'corr_hgrad' and moves down the required amount of rows specified by 'top_pos'. This is the gradient associated to the 'top_freq' value and is thus stored in the variable 'read_grad_one'. The row below this holds the gradient associated with 'bot_freq' and

is similarly stored in a variable 'read_grad_two'. From these two values the difference between the gradients is determined and stored in the variable 'grad_diff'. The interpolated gradient, called 'inter_grad' can now be calculated using the following:

```
IF ( read_grad_one > read_grad_two) THEN
inter_grad = read_grad_one - (grad_diff*perc_away_from_top)
ELSE
inter_grad = read_grad_one + (grad_diff*perc_away_from_top)
ENDIF
```

Hence, in this manner the gradient can be interpolated for any frequency that is specified. After the interpolated gradient has been determined it is finally assigned to the more specific variable 'horiz_grad'. Similarly, the procedure PROCdo_interp(name_two\$) can be recalled, but with a different filename specified for the variable 'name_two\$', as shown below.

```
name_two$ = "corr_hpow" :REM determines file for interpolation
PROCdo_interp(name_two$) : REM Performs interpolation & stores result in
                           'inter_grad'
horiz_pow = inter_grad :REM inter_grad is reassigned to a more specific
                           variable
```

In this fashion, the other horizontal polarised input datafiles can be interpolated.

Furthermore, the vertical polarised input datafiles can also be interpolated in the same manner. However, since the vertical polarised input data was obtained from a separate experiment, it is necessary to scan the file 'corr_vfreq'. This holds the vertical polarised frequencies and must be scanned to determine a new 'top_freq' and 'bot_freq'. This can be accomplished by just reassigning name\$ in the following way.

```
name$ = "corr_vfreq"  
PROCscan_file(name$)
```

Once the PROCinterpolate is completed the calibration curves for a horizontal and vertical polarised input can be expressed respectively as:

$$Y - \text{horiz_volt} = \text{horiz_grad}(X - \text{horiz_pow})$$
$$Y - \text{vert_volt} = \text{vert_grad}(X - \text{vert_pow})$$

After the calibration curves have been determined for a specific frequency, one should be in a position to predict the power that has fallen on the T.K. detector from an arbitrary angled polarised linear input, just from the voltage that is output. The way this was determined shall be discussed in the following section.

(9.1.10) Determination Of Power From The Output Voltage Of The T.K.

In order to determine the power that has fallen on the T.K. from an arbitrary oriented linear polarised beam one needs to examine the (E) fields falling on the T.K.'s surface.

If one considers a typical linear polarised electric field (E), of a magnitude $|E_0|$ that has been reflected from the rotary polariser at some arbitrary angle (θ) from the (y-axis) and is falling onto the T.K. detector as shown in figure(9.7).

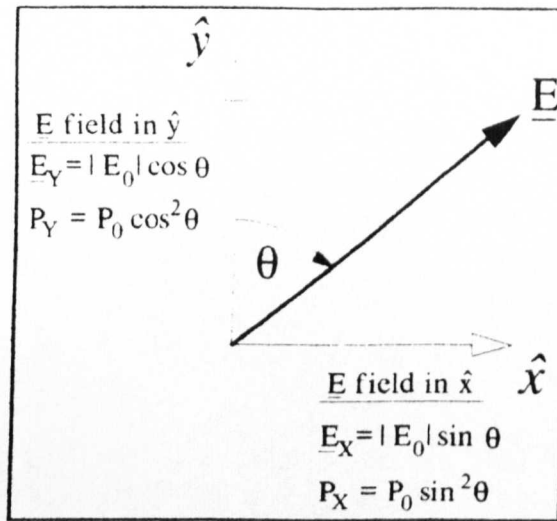


Figure (9.7)

Then the component (E_Y) of the (E) field resolved on the y-axis can be given as:

$$E_Y = |E_0| \cos \theta \quad \dots (9.4)$$

Furthermore, the power (P_Y) contained in the component field is given by :

$$\begin{aligned} P_Y &= |E_0|^2 \cos^2 \theta \\ &= P_0 \cos^2 \theta \end{aligned} \quad \dots (9.5)$$

Where, ($P_0 = |E_0|^2$) and is the power contained in (E)

Similarly, the resolved component of (E) in the x-axis (E_X) and its corresponding power (P_X) is given by :

$$E_X = |E_0| \sin \theta \quad \dots (9.6)$$

$$P_X = P_0 \sin^2 \theta \quad \dots (9.7)$$

Now power is conserved, such that :

$$P_0 = P_X + P_Y = P_0 \sin^2 \theta + P_0 \cos^2 \theta \quad \dots (9.8)$$

Furthermore, the voltage output from the T.K. detector (V_{OUT}), can be described as being proportional to the total power falling on it. As we have determined the power associated to the (x) and (y) axes, so too one can associate voltages (V_X) and (V_Y) to the respective axis. Therefore, it follows :

$$V_{OUT} = V_X + V_Y \quad \dots (9.9)$$

Now the voltages (V_X) and (V_Y) can be expressed from the calibration curves determined in the previous section (9.1.8), shown below.

$$Y = \text{horiz_grad}(X - \text{horiz_pow}) + \text{horiz_volt}$$

$$Y = \text{vert_grad}(X - \text{vert_pow}) + \text{vert_volt}$$

Re-writing using a more convenient notation, the respective equations become :

$$V_X = V_{GX}(P_X - \bar{P}_X) + \bar{V}_X \quad \dots (9.10)$$

$$V_Y = V_{GY}(P_Y - \bar{P}_Y) + \bar{V}_Y \quad \dots (9.11)$$

Substituting these equations into (9.9), gives :

$$V_{OUT} = V_X + V_Y = V_{GX}(P_X - \bar{P}_X) + \bar{V}_X + V_{GY}(P_Y - \bar{P}_Y) + \bar{V}_Y \quad \dots (9.12)$$

$$\Rightarrow V_{OUT} + V_{GX}\bar{P}_X + V_{GY}\bar{P}_Y - \bar{V}_X - \bar{V}_Y = V_{GY}P_Y + V_{GX}P_X \quad \dots (9.13)$$

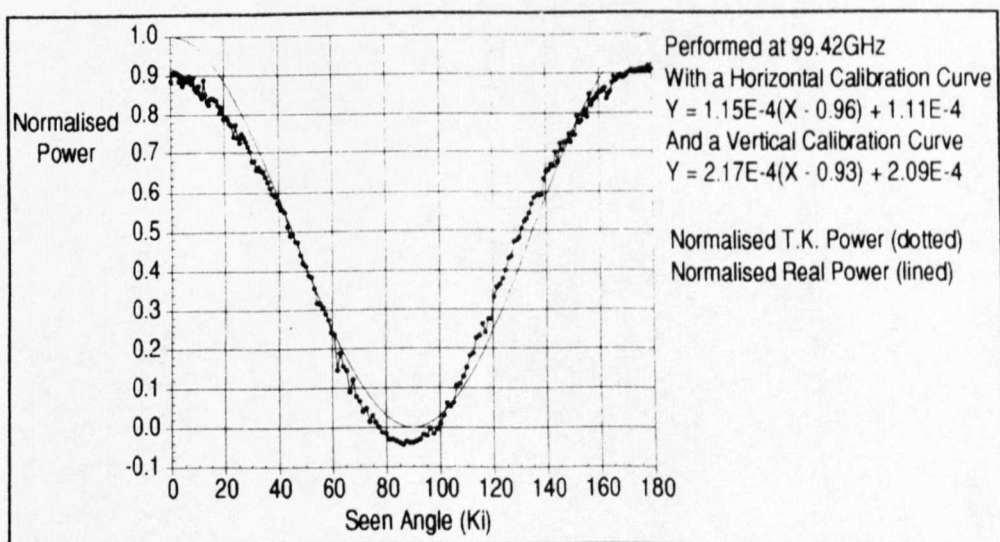
Substituting from (9.5) & (9.7) into (9.13) one gets :

$$V_{OUT} + V_{GY}\bar{P}_Y + V_{GX}\bar{P}_X - \bar{V}_X - \bar{V}_Y = P_0(V_{GY}\cos^2\theta + V_{GX}\sin^2\theta) \quad \dots (9.14)$$

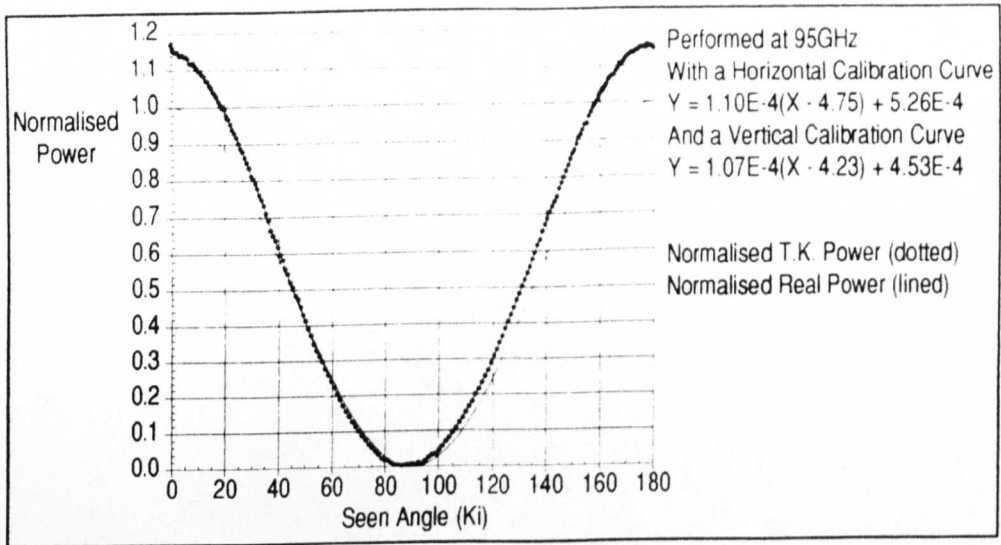
Rearranging the above equation, to make (P_0) the subject \Rightarrow

$$P_0 = \left\{ \frac{V_{OIT} + V_{GY}\bar{P}_Y + V_{GX}\bar{P}_X - \bar{V}_X - \bar{V}_Y}{(V_{GY}\cos^2\theta + V_{GX}\sin^2\theta)} \right\} \dots (9.15)$$

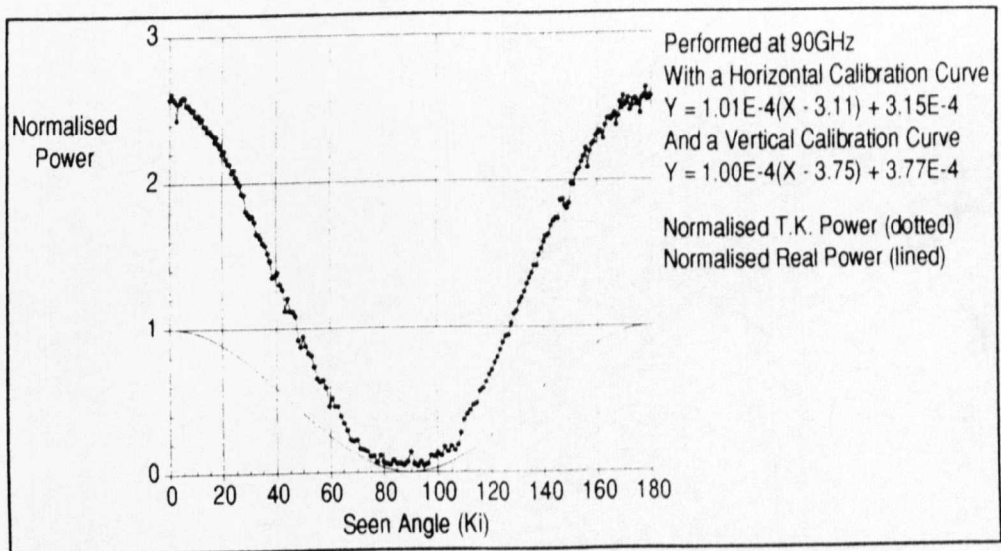
Hence, with this derived equation, one should be able to predict the power that is falling on the T.K. detector from the interpolated data of the calibration curves, the angle of the rotary polariser and the T.K. output voltage. This equation was incorporated into the first version of the complete program. The program was entitled "FarAngRes". The equation was located in a procedure known as PROCdetermine_tk_pow. When called the procedure would calculate the normalised power at the T.K.. One slight modification to the angle had to be made. The angle (θ) represented in the equation describes the angle of the radiation as seen by the T.K. Since the T.K. was inclined at 5° this had to be taken into account. The angle seen by the T.K. had to be recalculated. This was performed by another procedure known as PROCcalc_det_angle. It returned the angle as seen by the T.K. in the variable 'det_angle'. The results of the normalised calculated power compared to the normalised real power can be seen in figures(9.8 - 9.12). The results were obtained for several spot frequencies across W-band.



Figure(9.8)



Figure(9.9)



Figure(9.10)

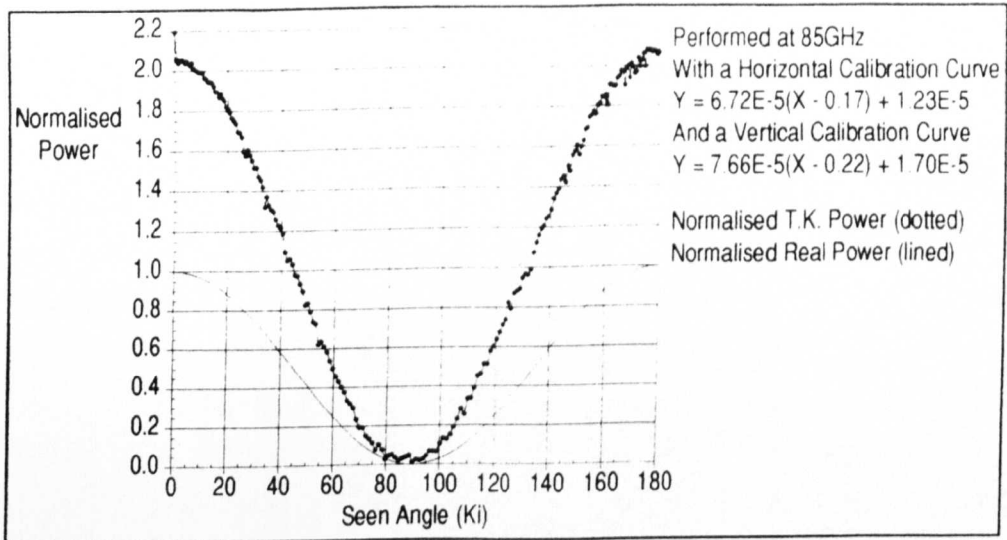


Figure (9.11)

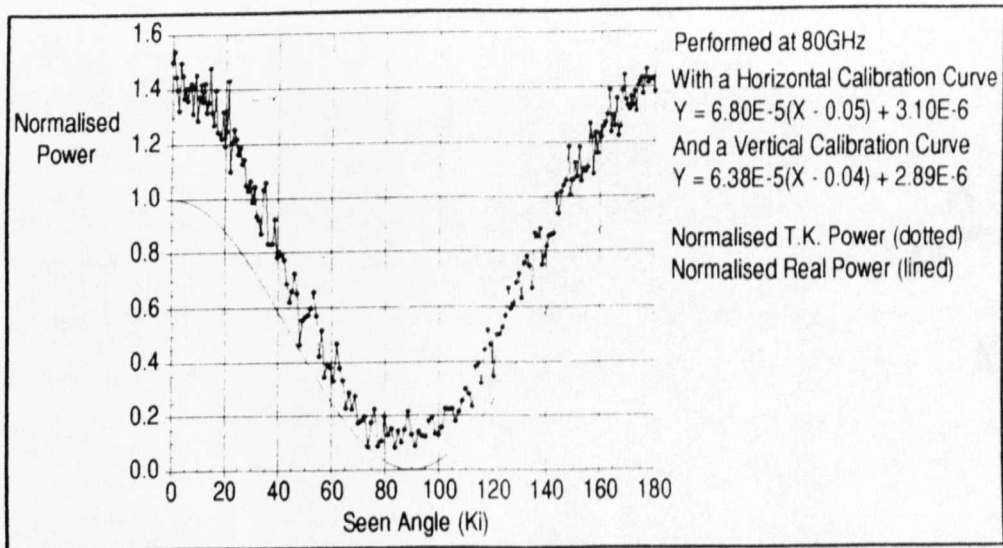


Figure (9.12)

As one can see from the results, sometimes the powers predicted were extremely accurate and other times the predictions were extremely inaccurate. Hence, I concluded from these results that the voltage conversion of the T.K. to detected power was too unreliable to be used to characterise real samples. Inaccuracies in the predicted power could well have been due to the number of samples (i.e. five samples) taken to determine a calibration curve. The reason only five samples were taken per frequency is to do with the time it took to run an experiment. The time it took to perform an experiment

with 5 samples per frequency and with frequency increments of 100MHz was 2hrs. Furthermore, two experimental runs were necessary, one for a horizontal polarised input and another for the vertical polarised input. Hence, the total time taken was 4 hrs. In order to perform 30 samples per frequency, as in the spot measurements shown before could have taken 7- 8 hrs. per run !

However, though one cannot predict the true power from the T.K. voltage, it is still possible to use the voltages directly from the T.K. to determine accurately the Faraday Angle. Although the power cannot be determined the voltages output from the T.K. for specific frequencies will all be relative to one another and proportional to the power. Hence, the largest voltage obtained will represent the largest power output. Therefore, when a sample is present and the rotary polariser is oriented such to give a maximum voltage, this maximum voltage corresponds to the position at which the Faraday Angle occurs. If the beam had become distorted from its linear polarised state to some elliptically polarised state, then the maximum voltage would represent the proportion of power in the major axis of the beam. Similarly, a minimum voltage would represent the proportion of power in the minor axis of the beam. This minimum voltage should also occur 90° away from the Faraday Angle. Therefore, by observing the maximum and minimum voltages one can determine the ellipticity of the beam. From here, I shall refer to the maximum voltage position as the 'Major Faraday Angle' and shall refer to the minimum voltage position as the 'Minor Faraday Angle'. Thus, it was important to locate both the Major and Minor Faraday Angles and also to measure the voltage at each of these locations to determine the ellipticity of the beam. Therefore, during an experiment the system would have to perform these measurements for every frequency. Experimental time now starts to play an important role. If it takes approximately 10 mins. to perform measurements for a full half-revolution which consists of 200 discrete steps. Then to execute a full half-revolution for every

discrete frequency, namely with frequency increments of 100MHz, would take a staggering 33+ hrs !!! Obviously, one does not want to wait nearly a day and a half to attain the results for a single sample. The following sections describe how I developed what will be known as a 'Tracking' feature to reduce experimental time to an acceptable level.

(9.2) Reducing Experimental Time by Introducing 'PROTrack'

As mentioned earlier, the experimental time needed to be reduced significantly. The way in which I tackled this problem was to firstly acknowledge that the information attained from a full half-revolution is only needed initially at the beginning of the experiment to establish the positions of the major and minor Faraday angle. Once the major and minor Faraday angles have been determined it would be more efficient to track about their known positions as the frequency is incremented. Since the frequency increment will be small, 100-200MHz, the change in the Faraday angle will also be small. Therefore, by tracking ± 10 degrees, (± 10 discrete steps) either side of the known major and minor Faraday angles one should easily encounter the new position of the major/minor Faraday angle. This would give an experimental time of roughly 6hrs. which is a great improvement. Furthermore, if smaller frequency increments were used, say 50MHz steps, then so too the change in Faraday angle would be less. Therefore, one could effectively track over a smaller range, i.e. $\pm 5^\circ$. Thus, although it would take slightly longer to increment the frequency tuner, the experimental time would effectively be reduced due to a shortened tracking range. The following procedure, PROTrack, was developed to reduce the experimental time to an acceptable level. The procedure was developed to be used in conjunction with the PROCstep_and_record procedure that performed a full half-revolution. Initially at the beginning of the new program 'FarAngRes2' the computer called PROCstep_and_record which performs a full half-revolution

consisting of 200 discrete steps. Once the major and minor Faraday angles, stepper positions and corresponding voltages together with the ellipticity had been determined they were stored in appropriate 'working variables' shown below.

<u>Parameter</u>	<u>Working Variable Used</u>
Major & Minor Faraday Angle	major_far_ang & minor_far_ang
Major & Minor Voltage	major_pow & minor_pow
Major & Minor Stepper Position	major_pow_pos & minor_pow_pos
Ellipticity	ellip

Table (9.1)

Once the working variables have been assigned in the first run, the computer decides whether to perform another full half_revolution or to track around the desired Faraday angles. The reason why one cannot simply track immediately, is due to the ellipticity of the beam that exited the sample. When the beam that exits the sample is elliptical then a major and minor axis exists and therefore one can track around the desired major and minor Faraday angles. However, in the case of the beam being circular, every voltage that is output from the T.K. would be the same. This is because no major or minor axis exists for a circular state. Hence, if no major or minor axis can be located then one cannot track around it ! This also implies that for a circular state nothing can be said about the amount of rotation that has been incurred on the beam by the sample. The only thing that can be measured, is the beam's ellipticity which will be unity from my previous definition. Realistically, due to noise effects described shortly, the ellipticity will most likely be very close to unity for a circular state. Therefore, as to not risk tracking around a fictitious Faraday angle when a circular state occurs I decided to make the computer evoke a full half-revolution when the ellipticity value is between 0.8-1. Therefore, at any ellipticity below this range,

one can safely say that the major and minor axis can be measured and it is safe to proceed with PROCtrack. This routine is performed for each run after the first and its main features are shown below.

```
IF( old_ellip > 0.8 ) THEN
  PRINT"Ellipticity > 0.8 --> Hence, Shall FULSTEP"
  PROCstep_and_record
ELSE
  PRINT"Ellipticity < 0.8 --> Shall TRACK"
  variable = old_major_pow_pos : PRINT" Tracking MAJOR faraday angle"
  PROCtrack
  variable = old_minor_pow_pos : PRINT" Tracking MINOR faraday angle"
  PROCtrack
ENDIF
```

The variables `old_ellip`, `old_major_pow_pos` and `old_minor_pow_pos` are used at the end of a run to assign the working variables `ellip`, `major_pow_pos` and `minor_pow_pos` to. This reassignment is performed by the procedure `PROCdisplay_params`. The old variables are only updated at the end of a run. They hold the information from the previous run to the run that is actually commencing. They are referenced during the run in order to determine whether to track or not and if tracking is to occur, then which major and minor positions to track around. The working variables described in Table(9.1) are reset to default values at the beginning of each run and are constantly overwritten during a run.

As can be seen from the code above, when the ellipticity is less than 0.8 then the procedure `PROCtrack` is evoked. Firstly, the major Faraday angle determined from the previous run is tracked and then the minor Faraday angle is tracked. Depending which Faraday angle is being tracked a variable called 'variable' is set to the stepper position of the appropriate Faraday angle. The stepper positions

determined from the previous run are held in the variables 'old_major_pow_pos' and 'old_minor_pow_pos', as mentioned earlier. The variable named 'variable' once set appropriately is then used in the procedure PROCtrack as will now be described.

(9.2.1) Dissection Of Procedure 'PROCtrack'

Although, the procedure PROCtrack should be very simple to design, there are a few subtleties involving how information should be passed to the stepper that add to the complexity of the routine.

The first piece of code in PROCtrack is as follows:

```
FOR LLL = 0 TO 2*tracksteps
  trackpos = variable - tracksteps + LLL : REM defines position of tracker
  testarray(0,LLL) = trackpos
```

The variable 'tracksteps' defines the number of discrete steps to be moved by the stepper either side of the desired Faraday angle. Therefore, the total number of discrete steps moved by the stepper will be twice the number of tracksteps. The variable 'tracksteps' is specified by the user at the beginning of the program. I set this variable to '10' which will give me a $\pm 10^\circ$ margin either side of the desired Faraday angle.

The variable 'trackpos' specifies the stepper position relative to the wires vertical position. It is influenced by the variables 'variable', tracksteps and 'LLL'. As 'LLL' is incremented the range of values that 'trackpos' takes will be from -10 steps behind the desired Faraday angle to +10 steps in front of it. Once 'trackpos' has been determined it is stored in the zeroth column of the array called 'testarray'. The range of values which 'trackpos' can take can lie between (-10 to +410). One of the subtleties lies in the fact that the stepper will return an error if it is passed values outside a (0 to 400) range. Therefore, it is necessary to have some kind of correction for this outcome. The next lines of code alleviate this problem.

```
IF (trackpos < 0 ) THEN
  wave = 0 :REM used to stop taking readings when stepper is moving
  zip_pos = (trackpos + 200)*size_of_move%
  L = trackpos + 200           : REM gives +ve (L) value so calc_seen_angle
  PRINT" trackpos < 0 : Shall move to ";L
  PROCcalc_seen_ang           : REM can be determined correctly
  seen_angle = seen_angle - 180 : REM Adjusts seen_angle to -ve value
  PRINT"Adjusted seen_angle = ";seen_angle

testarray(1,LLL) = seen_angle :REM stores seen_angle here
```

Also the values sent to the procedure PROCcalc_seen_ang, when determining the seen-angle, must be in a certain range. The range being within (0-200). The variables 'zip_pos', 'wave' and 'L' facilitate this.

Examining the first 'IF' statement were 'trackpos < 0'. If the stepper was asked to move to this negative position an error would result. The variable 'zip_pos' corrects for this. If the value of 'trackpos' is negative, then the stepper should be moved the corresponding number of steps to the left of the wires vertical⁵ position. An equivalent position exists which is +180 degrees or +200 steps to the right of the negative position. Hence, by adding +200 steps to the 'trackpos' value and assigning this to 'zip_pos' will locate the polariser in an equivalent position and also be an acceptable value for the stepper. Normally during a PROCstep_and_record procedure the stepper position is passed as the value 'L' to PROCcalc_seen_ang in order to determine the seen angle. Therefore, PROCcalc_seen_ang requires a value within the range (0-200). If 'trackpos' is negative then one could firstly add +200 steps to 'trackpos' and pass the value to PROCcalc_seen_ang. This would result in PROCcalc_seen_ang calculating the variable 'seen_angle' to be +180⁰ away from the angle we want. One can then reassign

⁵ As a recap the wires vertical position corresponds to a 'trackpos' value of zero.

seen_angle = seen_angle -180. I decided to let 'seen_angle' be negative since this would provide a continuity in the graphed results. The values calculated for the 'seen_angle' are stored in the first column of the array called 'testarray'. The other two 'IF' statements provide similar corrections to the 'seen_angle' and 'zip_pos' depending on the value of 'trackpos'.

The significance of the variable 'wave' will now be described. The 'wave' variable is an integer value between (0-2). It identifies which region the rotary polariser is in. This is the another subtlety of PROCtrack. The best way to explain its operation is by way of example. Say for example that the previous Major Faraday angle occurred at 0° (i.e. old_major_far_ang = 0) and the ellip < 0.8. This would mean that PROCtrack would be executed for the next run. During the next run, as 'LLL' is incremented from (0 to 2*tracksteps), 'trackpos' would take values from (-10 to +10) with the 'old_major_far_ang' occurring at its centre. For values of 'trackpos' < 0 the first 'IF' statement would be evoked. Since 'trackpos' is negative then the stepper would be moved to an equivalent position which is +200 steps away from the true position. Therefore, for 'trackpos' values (-10 to -1) the stepper would actually be at the stepper positions (+190 to +199) and 'wave'= 0. When the value of 'trackpos' is (0 to +10) it can be directly passed to the stepper and the stepper position will be in the range (0 to +10) and 'wave'=2. Therefore, during the complete track the stepper can be considered to be in two different regions which can be differentiated by their different 'wave' values. A new procedure called PROCcalc_wave is called at each new step position to compare the 'wave' values. If the 'wave' values are the same then the stepper is in the same region and the computer can automatically proceed to acquire data from the Boonton and T.K.'s Lockin, using PROCsample_lockin. However, if the PROCtrack is on its first move, i.e. LLL = 0, or the 'wave' values are different then one cannot automatically take data since the stepper will take a finite amount of time to get to the new region.

PROCcalc_wave allows a 5 sec. delay for these cases which is ample time for the stepper to move to a new region. After PROCcalc_wave has been called the data acquisition follows using PROCsend_string, described in section(7.5.4).

The only other feature of PROCTrack is to perform curvefits to the data acquired. The curvefits will be described in section(9.3.2.1).

In experiment the 'tracking' feature was found to perform well and hence saved valuable time in the laboratory.

(9.3) Sources of Noise

The following section identifies the sources of noise that the system was open to. It describes what measures were taken to alleviate the noise problem and verifies experimentally how successful the measures were when implemented.

The only instrument to be radically effected by noise was the detector in the system. The T.K. offers highly sensitive wideband detection. Ironically, this means it is also sensitive to a wideband of noise. I have defined two categories in which noise effects creep into the system and affect the T.K. meter. The first category will describe how one can reduce the amount of standing waves within the system that serve to affect a measurement. The second category will describe how one can predict a measurement even though it is swamped by random thermal and vibrational fluctuations by means of applying curvefits to the data.

(9.3.1) Standing Waves

The superposition of two harmonic waves of the same frequency travelling in opposite directions generates what is termed as a 'Standing Wave'. The resultant wave does not propagate through space but instead appears as a 'Stationary wave' which it is also sometimes referred to. A standing wave obviously contains energy in its very existence. Therefore, the presence of standing waves within a system serve to remove energy from a propagating beam

and hence reduce power throughput of the system. Reflections from any optical component within the system whose plane is perpendicular to the direction of propagation of the radiation can create a standing wave. By careful planning in the design of the optical system, standing waves can be greatly reduced or eliminated. By angling the ferrite samples and the T.K. power meter and by employing planar convex lenses and waveguide isolators, standing waves were minimised, as shown in the optical arrangement below.

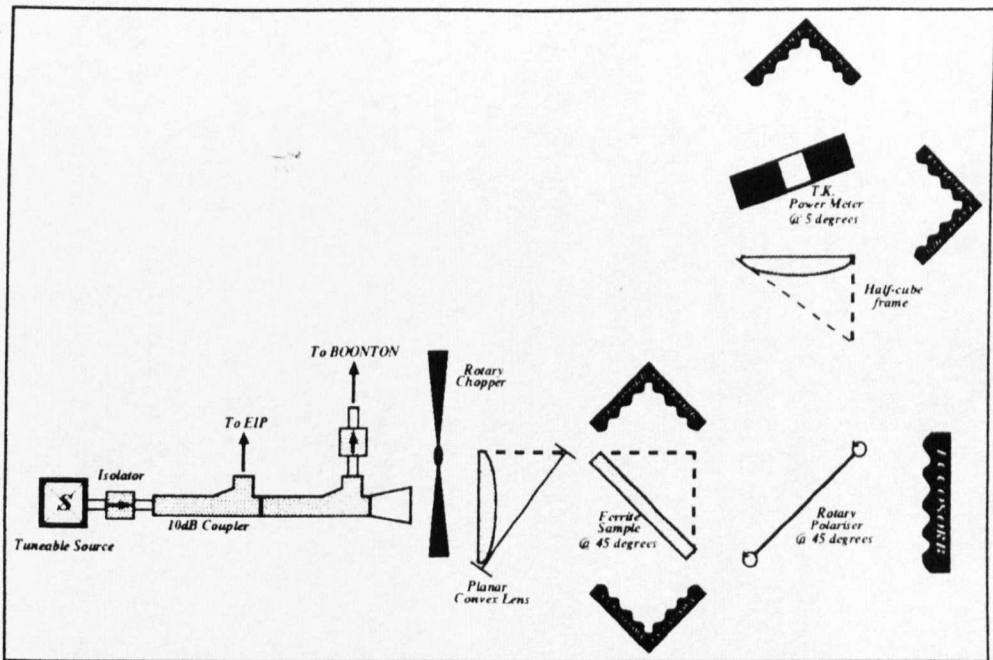


Figure (9.13)

Reflections were minimised in the following way :

The implementation of planar convex lenses into a system as shown in figure(9.13) can serve to reduce standing waves. If one considers the rapidly expanding gaussian beam that propagates from the source feedhorn toward the planar side of the lens. Any reflection from the planar face will not be channelled back into the feed, as would be the case with a simple convex lens, but instead would be diffracted in a very different manner out of the system, described by Harvey⁶. Reflections from the rotary chopper blades back to the

⁶ Harvey, A.R., Thesis, A Millimetric Wave, Quasi-Optical Complex Impedance Bridge, pgs.46-49.

source are dealt with the waveguide isolator. Similarly, reflections from the Boonton sensor are also dissipated with a waveguide isolator. As the gaussian beam propagates toward the unmatched ferrite sample reflections will occur. Angling the sample at 45° will divert any reflection from the sample toward the R.A.M. and out of the system. Similarly, if the beam propagates through the sample, but is then reflected from the convex face of the 2nd lens back toward the ferrite, it too is diverted to the R.A.M and absorbed. By angling the T.K. meter at 5° to the incoming radiation reflections are diverted whilst preserving the polarisation insensitivity necessary to detect an arbitrary polarisation reflected from the rotary polariser. Although the blazing of the lenses should minimise reflections from the lens surfaces, reflections between the convex surfaces of the lenses and the rotary polariser wires can also exist. Standing waves created from these reflections cannot be avoided. It follows that the most accurate measurements obtainable from the system should occur when all the radiation is transmitted through the rotary polariser wires, namely at a null measurement. It is for this reason, that tracking the minimum faraday angle is probably the more preferable method of achieving the most accurate results.

(9.3.2) Accurate Prediction of Major & Minor Faraday Angles over thermal and accoustic/vibrational noise fluctuations.

As described earlier, the T.K. is so sensitive that it will detect changes in temperature and accoustic/vibrational effects. Detection of these effects creates noise on a measurement. Some method of accurately locating the major and minor Faraday angles over these noise effects was necessary. Furthermore, an accurate prediction of the T.K. voltage for each of the major and minor Faraday angles was also necessary for an accurate ellipticity determination. It will be shown that by performing a 'Least Squares Parabola Fit' on a set of data points that describe the T.K. voltage with angle, accurate predictions can be achieved for the major/minor Faraday angle and

the ellipticity. These results will be contrasted against measurements where no fit was employed and just the maximum/minimum voltage measured was taken to be the location for the major/minor faraday angle.

(9.3.2.1) The Least Squares Parabola Fit

As mentioned above, it is only the major and minor Faraday angles and the voltage in each which needs to be predicted accurately. Simply looking for a maximum or minimum voltage from the T.K. should locate the major/minor Faraday angle. However, because of thermal and accoustic/vibrational noise fluctuations that occur randomly ontop of the true reading, the major/minor Faraday angle can be wrongly located, as shown in schematic Figure(9.14). The effect of using the maximum and minimum T.K. voltage to locate the major and minor Faraday angles together with standing waves can be seen from the results of an the experiment performed on Sample 5. Sample 5 was a thin Anisotropic sample of Plastroferrite inclined with its plane perpendicular to the incident radiation.

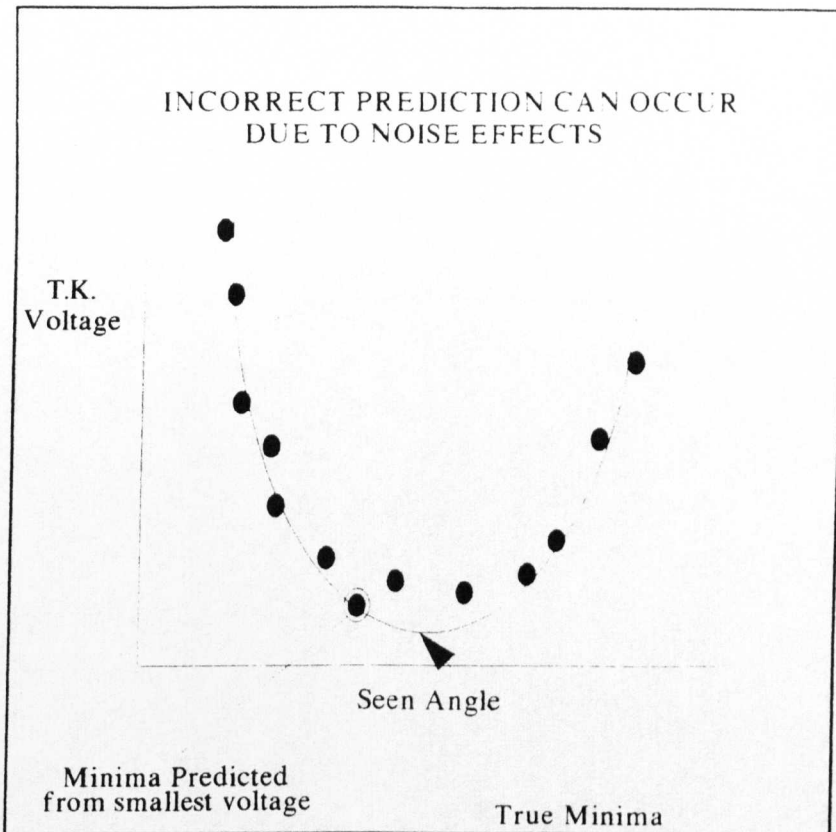


Figure (9.14)

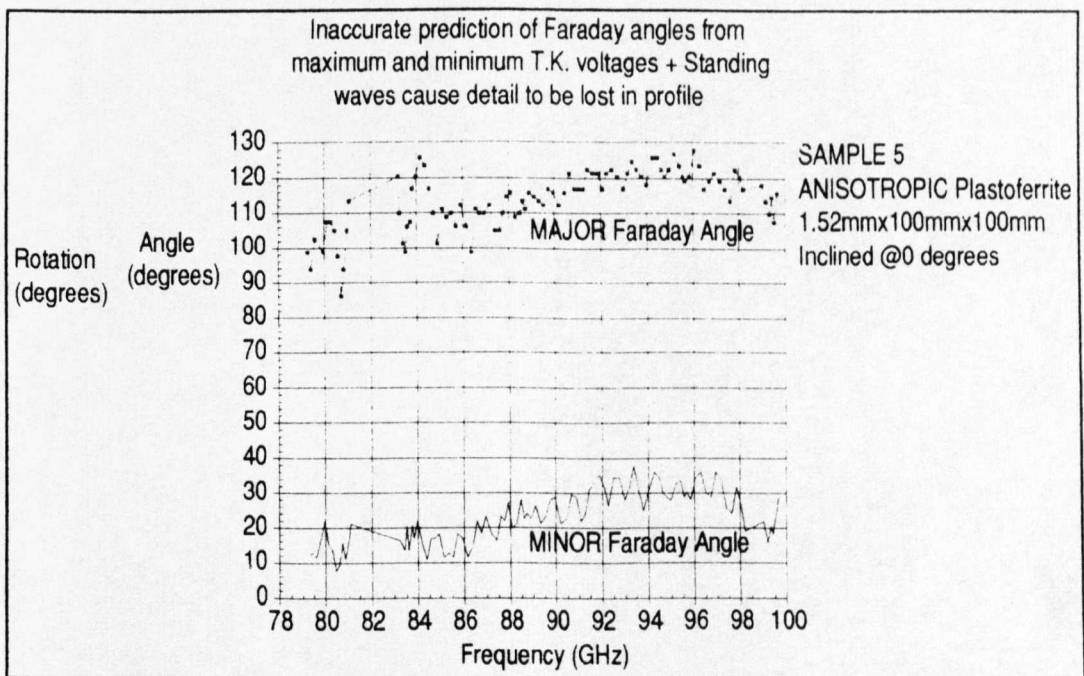


Figure (9.15)

It is clear that some sort of fit to the data is necessary to cut through the noise floor and accurately predict the major and minor Faraday angles together with their corresponding true voltage. This was achieved by acknowledging that the distribution of data points around the areas of interest, namely the major/minor Faraday angles, are parabolic in shape. Therefore, by fitting a least squares parabola around the area of interest one should be able to determine the major and minor Faraday angles accurately and also determine the true T.K. voltage which describes the relative amount of power in the major and minor axis of the beam.

A least squares parabola can be fitted to a set of data upon solving its normal equations, given below :

$$\begin{aligned} \Sigma y &= a_0 n + a_1 \Sigma x + a_2 \Sigma x^2 \\ \Sigma xy &= a_0 \Sigma x + a_1 \Sigma x^2 + a_2 \Sigma x^3 \\ \Sigma x^2 y &= a_0 \Sigma x^2 + a_1 \Sigma x^3 + a_2 \Sigma x^4 \end{aligned} \quad \dots (9.16)$$

The values for the constants a_0 , a_1 & a_2 was computed to be :

$$\begin{aligned} a_0 &= \frac{(\Sigma x^2)^2 (\Sigma x^2 y) - \Sigma x \Sigma x^3 \Sigma x^2 y - \Sigma x^2 \Sigma x^3 \Sigma x y + \Sigma x \Sigma x^4 \Sigma x y + (\Sigma x^3)^2 \Sigma y - \Sigma x^2 \Sigma x^4 \Sigma y}{(\Sigma x^2)^3 - 2 \Sigma x \Sigma x^2 \Sigma x^3 + n (\Sigma x^3)^2 + (\Sigma x)^2 \Sigma x^4 - n \Sigma x^2 \Sigma x^4} \\ a_1 &= \frac{\Sigma x \Sigma x^2 \Sigma x^2 y - n \Sigma x^3 \Sigma x^2 y - (\Sigma x^2)^2 \Sigma x y + n \Sigma x^4 \Sigma x y + \Sigma x^2 \Sigma x^3 \Sigma y - \Sigma x \Sigma x^4 \Sigma y}{-(\Sigma x^2)^3 + 2 \Sigma x \Sigma x^2 \Sigma x^3 - n (\Sigma x^3)^2 - (\Sigma x)^2 \Sigma x^4 + n \Sigma x^2 \Sigma x^4} \\ a_2 &= \frac{(\Sigma x)^2 \Sigma x^2 y - n \Sigma x^2 \Sigma x^2 y - \Sigma x \Sigma x^2 \Sigma x y + n \Sigma x^3 \Sigma x y + (\Sigma x^2)^2 \Sigma y - \Sigma x \Sigma x^3 \Sigma y}{(\Sigma x^2)^3 - 2 \Sigma x \Sigma x^2 \Sigma x^3 + n (\Sigma x^3)^2 + (\Sigma x)^2 \Sigma x^4 - n \Sigma x^2 \Sigma x^4} \end{aligned}$$

Where (n) represents the total amount of data samples in the dataset.

In calculating the turning point of the first of the normal equations, the exact location of the minima/maxima can be determined from the (x) coordinate. And the best estimation of the true T.K. voltage that is associated to the major/minor axis of the beam is given by the (y) coordinate. The turning point co-ordinates can be expressed in terms of the constants a_0 , a_1 , a_2 & n and are given below.

$$(X, Y)_{TURNING\ PT} = \left(\left(\frac{-a_1}{2a_2} \right), a_0n + a_1 \left(\frac{-a_1}{2a_2} \right) + a_2 \left(\frac{-a_1}{2a_2} \right)^2 \right) \dots (9.17)$$

The 'least squares parabolic fit' was performed by the procedure PROCdet_centre on a dataset of twenty one data points. The dataset of interest was placed in three separate columns of an array defined as 'testarray'. The zeroth column held the stepper position numbers. The first column held the calculated seen angle for the corresponding stepper position. And the second column held the T.K. voltage + noise measurement which corresponded to the stepper position and calculated seen angle. Two curvefits were actually performed. The first curvefit was performed with the stepper position number on the x-axis and the T.K. voltage on the y-axis. Hence locating the stepper position that was closest to the turning point. This was stored in the variable 'pos_inter%'. The second curvefit was calculated with the seen angle as the x-axis and the T.K. voltage as the y-axis. This resulted in accurately determining the seen angle that corresponded to the major or minor Faraday angle which was stored in the variable 'ang_inter'. Furthermore, the best estimate of the true T.K. voltage is calculated on this second run and stored in the variable 'volts_inter'. A small routine within the procedure then follows which determines whether the major or minor Faraday angle is being calculated. This is determined by looking if the variable 'variable' is equal to the variable 'old_major_pow_pos' or 'old_minor_pow_pos'. If 'variable' is equal to 'old_major_pow_pos' then the major Faraday angle has been calculated and variable 'volts_inter' is assigned to the new variable 'major_volts'. Similarly, if 'variable' is equal to 'old_minor_pow_pos' then the minor faraday angle is being calculated and 'volts_inter' is assigned to the new variable 'minor_volts'. The assignment only takes place if the calculated stepper position falls within the range of stepper positions stored in the zeroth column of the array 'testarray'. When the calculated stepper position falls within the range of the stepper positions

stored in the zeroth column, it signifies that the calculated stepper position is a good calculation and is within $\pm 10^0$ of the previously calculated stepper position. It also signifies that the calculated true T.K. voltage is a good estimate. This is displayed to the user as a 'GOOD MAJOR/MINOR PREDICTION' and a marker called 'major_marker' or 'minor_marker' which is used later to signify a good prediction is set to unity. If the calculated stepper position does not occur within the zeroth column of the array 'testarray' then the calculated position is outside the $\pm 10^0$ range of the previous measurement and the markers remain at the default value of zero. There are two possible outcomes for an out of range result. Either the calculated position is just outside the $\pm 10^0$ range, say within a $\pm 20^0$ range which is acceptable or the position has been miscalculated due to an excess of noise or a near circular polarisation state being created⁷. The procedures PROCdisplay_params and PROCsort_out deal with these outcomes. PROCdisplay_params checks the major and minor markers described earlier. If they are both set to unity then both of the major and minor position calculations were good and the ellipticity can be calculated. If either of the markers is zero then the calculated position is outside the $\pm 10^0$ limit and PROCsort_out is called. To avoid a bad ellipticity calculation the ellipticity is set to zero which will represent an uncalculated ellipticity. In addition, a comment is placed in the string variable "COM\$". This is 'WR' and represents that the angle is within a $\pm 20^0$ range. Both the 'major_pow_pos' and 'minor_pow_pos' variables are checked against the 'old_major_pow_pos' and the 'old_minor_pow_pos' variables respectively. This to see if they are $\pm 20^0$ greater or less than their old values. If they are then a bad estimate has occurred and the ellipticity is set to unity which will force the procedure PROCstep_and_record to execute in the next run rather than

⁷ A near circular state would lead to the T.K. voltage for every datapoint in the dataset being almost identical. Hence, it would be very hard to locate the turning point and a bad calculation could result.

PROCtrack. An appropriate comment is placed into 'COMS' which depends whether the major or minor angle was mis-predicted. 'MX' represents a bad major prediction whilst 'mX' represents a bad minor prediction. With the above two mentioned procedures, bad predictions can be identified and suitable measures are taken to avoid tracking around a miscalculated position. Furthermore, the procedure PROCdet_center performs a chi-square test and measures the sum of the deviations of the datapoints from their calculated parabola of best fit.

Figure(9.15) shows the major and minor Faraday angle predictions for a typical set of data obtained from a fullstep of the rotary polariser. During a fullstep there is no knowledge of where the major or minor Faraday angles are. Therefore, a rough estimate of the major and minor location is determined by looking for the maximum and minimum T.K. voltage. Then 10 datapoints either side of the rough estimate are placed in the array 'testarray', giving a total of 21 datapoints. From this dataset the best prediction is calculated using the procedures mentioned. During the track mode of the rotary polariser, the old_major_pow_pos and old_minor_pow_pos are known. Therefore, the rotary polariser moves through 21 positions, where the central position is the old major or minor Faraday angle. It is these 21 datapoints that are placed directly into the array 'testarray'. As can be seen from Figure(9.15), although there is a lot of noise around the turning points the major and minor Faraday angles are predicted accurately and are shown to be 89.81° apart. A perfect prediction would displace the major and minor Faraday angles by 90° .

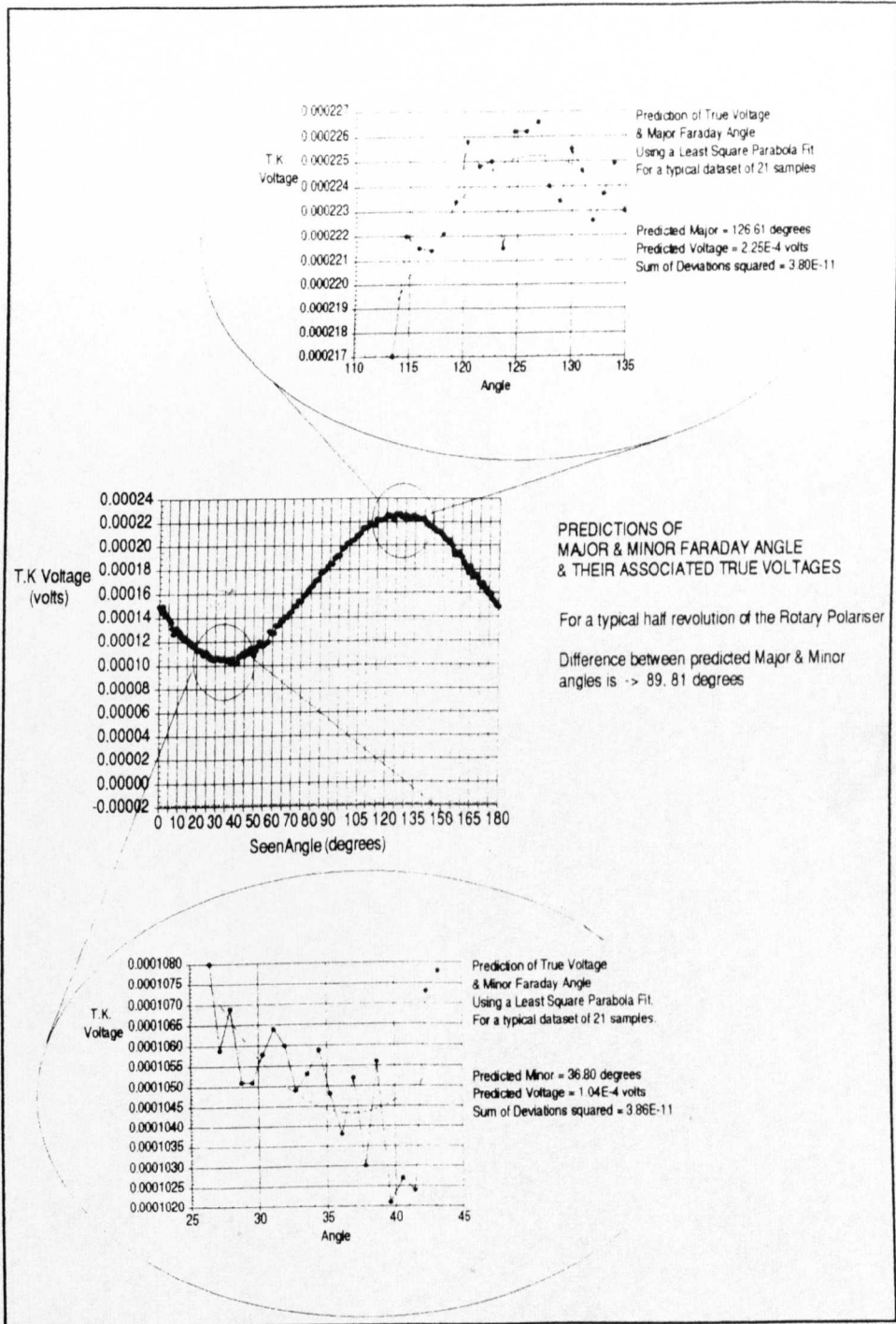


Figure (9.15)

Therefore, the above result gives a 99.8% accuracy of prediction. Figure (9.16) contrasts the results of two experimental runs. The first run calculated the major/minor Faraday angles directly from the maximum/minimum T.K. voltages. The second run employed the 'least square parabola fit' to predict the major and minor Faraday

angles. It is obvious from the results that the least squares parabola fit can be used successfully to suppress the thermal and acoustic/vibrational noise effects that occur randomly on top of the measurements. As one can see from the dotted profile, resolution is enhanced using the parabolic fit to the noisy data.

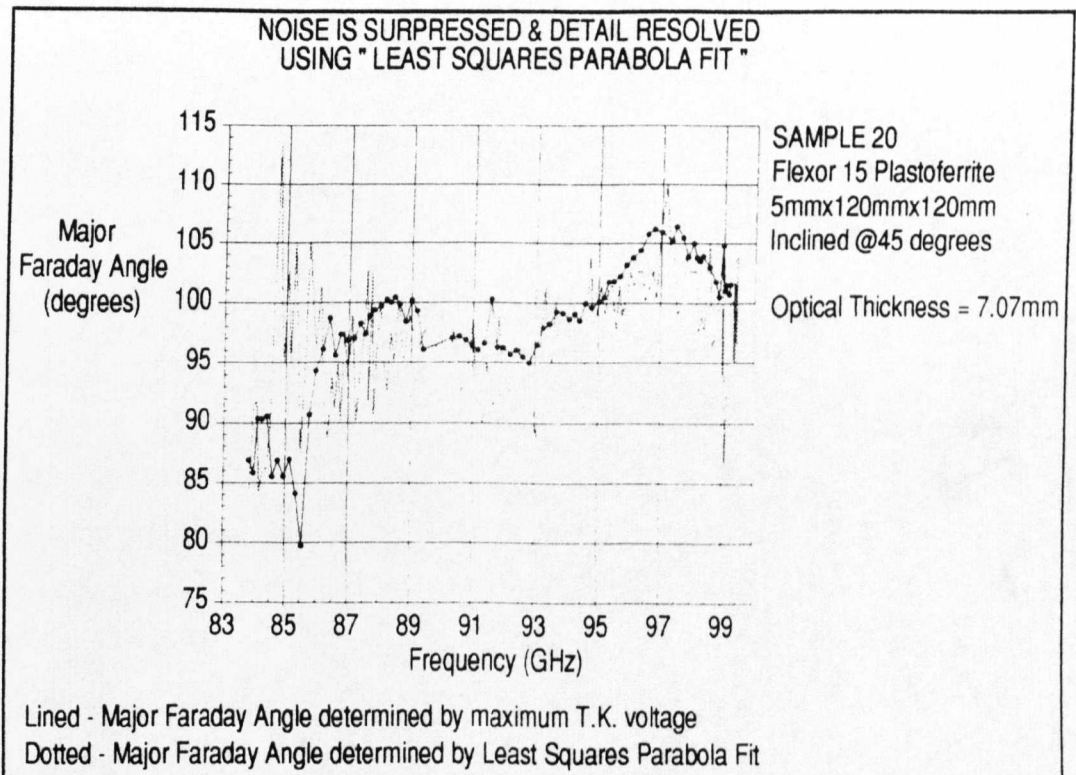


Figure (9.16)

With the aid of the parabolic curve fit, one is now in a position to make measurements on samples. The next section will describe how I used the system to demonstrate the 'Faraday Angle Resonance' Phenomenon at millimeter wavelengths. In addition, the section will show how one could use the same system in order to investigate Faraday Rotator's performance.

(9.4) Experimental Results Using the Fully Automated System.

The next few sections present results obtained from the 'Fully Automated Millimetric Rotary Polariser Quasi-Optical System'. The

first part, highlights the 'Faraday Angle Resonance' results performed at W-band. The second part demonstrates how Faraday Rotators can be examined using the system. It will be shown from the Faraday Angle Resonance results, that there a slope is encountered in the plotted graph of the Ceramic 8 material. This suggests the material is operating in its frequency dependent region as predicted from Chapter 5. Furthermore, the results from Faraday Rotators (IA1), (I9) and (IC81) will show that it is possible for the rotation and ellipticity of a Faraday Rotator to be measured directly using the new system which gives a further insight into how these devices actually behave during operation.

(9.5) Faraday Angle Resonance Results

Faraday Angle Resonance experiments were performed on two samples. In both experiments the samples were angled at 45° degrees to the incident radiation. This was in order to reduce standing waves within the system as described in section(9.3.1). In addition, an increase in the optical thickness of the sample leads to more 'peaks' and 'troughs' occurring in the data which is desirable from the profile analysis point of view. However, as will be described in the analysis section this also serves to incline the c-axis of the samples by 45° to the incident radiation. Therefore, the results will only apply to a Faraday Rotator made from the materials studied if it is inclined in this manner.

(9.5.1) Results For Sample 11.

Sample 11 consisted of two pieces of the SrM Semi-Anisotropic plastoferrite that were affixed together. The material had be cut at 22.5° to the magnetic flux lines described in Chapter(6). The total thickness of the sample was 3.05mm. Inclining the sample at 45° to the incident radiation would therefore give it an optical thickness of 4.31mm. The results obtained using the fully automated system are shown below in figure(9.17). The upper plot is a plot of the Major

Faraday Angle with frequency. The middle plot is a plot of the Minor Faraday angle versus frequency and the lower plot is that of the ellipticity variation with frequency. All the plots were performed over the 80-100GHz region using 100MHz frequency increments. Due to an oscillator frequency jump no information was available between ≈ 81 -83GHz.

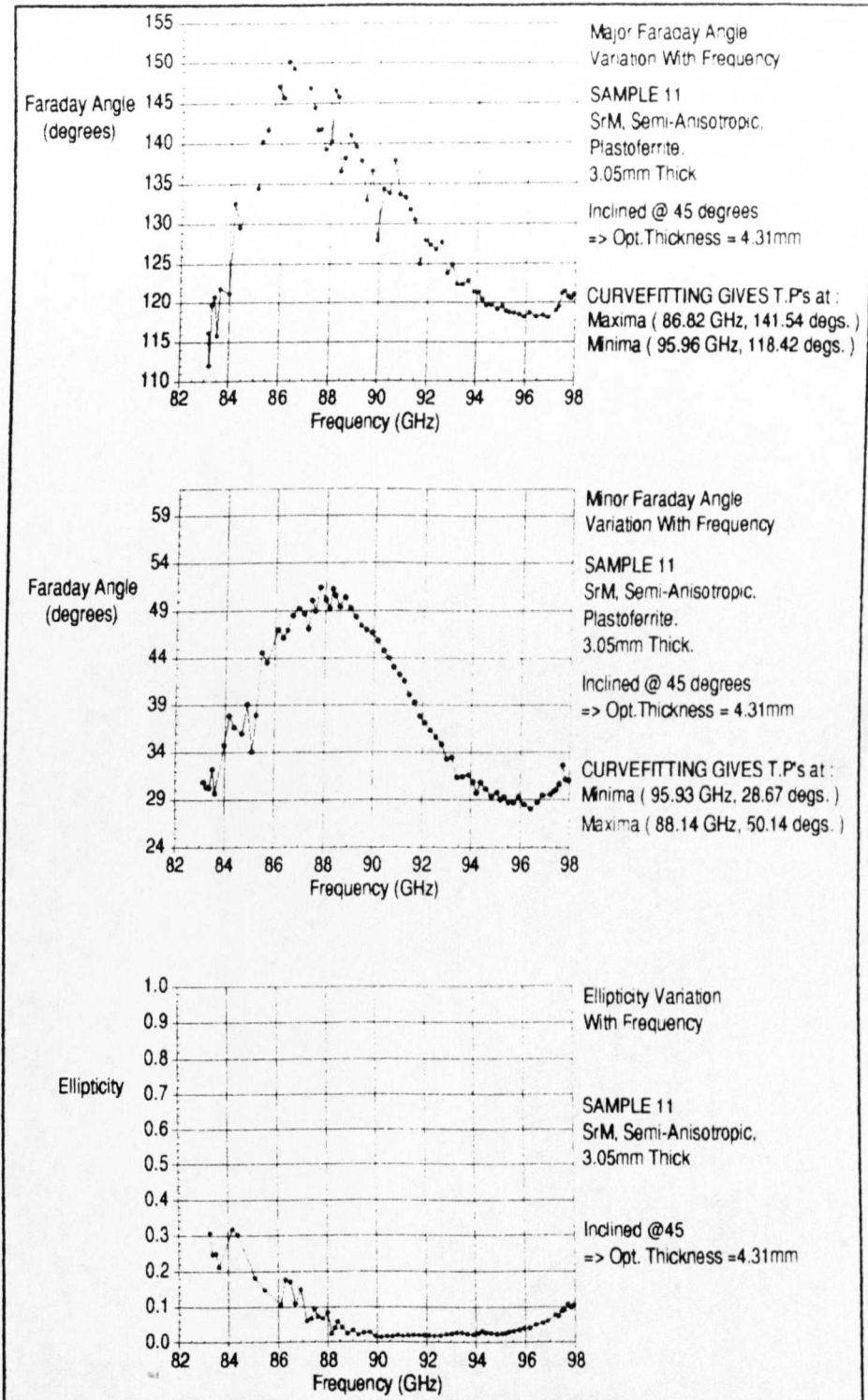
(9.5.1.1) Results Analysis For Sample 11

From the results the 'Faraday Angle Resonance' trait is evident. As can be seen from the results, the Minor Faraday Angle plot is much smoother than the Major Faraday Angle plot. This was expected since the Minor Faraday Angle contains very little power compared to the Major Faraday Angle. This can be seen from the ellipticity values. Therefore, the Minor Faraday Angle is effectively a null measurement. The erratic nature of the Major Faraday Angle plot is also likely to be heightened since the sample consisted of two pieces. With the Major Faraday Angle containing a very large portion of the power there is a greater likelihood of multiple reflections occurring between each of the two pieces of ferrite and introducing further rotational effects.

The parabolic curvefit, described in section(9.3.2.1), was then applied to a range of points around the maxima and minima features of both plots. Using this method it is possible to locate very accurately their true positions. The results from the curvefit are tabulated in table(9.2).

Type Of Turning Point	Major Faraday Angle	Minor Faraday Angle
Maxima T.P.	(86.82 GHz, 141.54 ^o)	(88.14 GHz, 50.14 ^o)
Minima T.P.	(95.96 GHz, 118.42 ^o)	(95.93 GHz, 28.67 ^o)

Table (9.2)



Figure(9.18)

The maxima turning points of both the major and minor Faraday angles should be located at the same frequency and should also occur 90° apart. From the curvefitted results this is almost exact with

$\approx 2\%$ error. Similarly, this should be true for the minima turning points with a $< 1\%$ deviation. An accurate value for the Major Faraday Angle and its corresponding frequency is necessary to make a good prediction of $(\Delta\varphi)$ which is the rotation/single pass, as described in section(5.8.2). By averaging the maxima turning points of the major and minor Faraday angle and similarly for the minima turning points, even better estimate of the turning points can be made for the maxima and minima of the Major Faraday Angle plots. The averages shown in table(9.3) were calculated to be :

Type of Turning Point	Major Faraday Angle
Averaged Maxima ($\Delta\varphi_{MAX}$)	(87.48 GHz, 140.84 ^o)
Averaged Minima ($\Delta\varphi_{MIN}$)	(95.95 GHz, 118.55 ^o)

Table (9.3)

Substituting for $(\Delta\varphi_{MAX})$ and $(\Delta\varphi_{MIN})$ in equation(5.18) the amount of rotation incurred upon a single pass through an optical thickness of 4.31mm of Sample 11 was found to be :

$$\begin{aligned}\Delta\phi &= 50^{\circ} 44' / \text{single pass} \\ &= 11^{\circ} 46' / \text{mm}\end{aligned}$$

Therefore, for 45^o rotation over the region (87.48 - 95.95GHz) a sample of optical thickness 3.82mm is required. Translating this back to the actual thickness required gives 2.70mm. However, this is for a sample inclined at 45^o. From the previous predictions made in section(6.11) a thickness of $\approx 2.75\text{mm}$ is necessary which is for a sample that has its plane perpendicular to the incident radiation. Hence, its optical thickness is also 2.75mm. Therefore, the figure determined here is an overestimate. The main reason for the overestimate is due to the actual angling of the ferrite by 45^o. Although, this will prevent standing waves in the experimental

setup, it also angles the c-axis and thus the internal biasing field of the sample by 45° . Now the incident radiation will see an effective component of the anisotropy field which is a factor $\sqrt{2}$ smaller in magnitude. The smaller field will serve to rotate the incident radiation less and hence a larger thickness is to be expected to attain 45° rotation. In addition, there will also exist a field component which is perpendicular to the direction of propagation of the beam. This will also affect the incident beam in a way described by the Cotton-Mouton Effect⁸. This effect is related to the Faraday Effect, but the rotation incurred upon the beam is smaller in comparison. Hence, the angling of the ferrite serves to reduce the rotation incurred upon the beam. In addition, the sample seems to have become demagnetised during storage. This is evident also in the Faraday Rotator results that will appear in the following sections. All the samples were stored together which could have resulted in a reduction in their magnetisation.

From relative permittivity (ϵ_R) can also be calculated from equation(5.21) and was found for this orientation to be 3.42 and can be considered as an 'effective permittivity' for a sample oriented at 45° to the incident radiation. The value calculated in section(6.9) for a semi-anisotropic sample with its plane perpendicular to the incident radiation was 10.43.

(9.5.2) Results For Sample 32

Sample 32 consisted of a single piece of a SrM polycrystalline ferrite known as Ceramic 8. The supplier of the material was 'Magnetic Developments'. The thickness of the sample was 4.97mm. Since the material was inclined at 45° to the incident radiation it has an optical thickness of 7.03mm. The results obtained using the fully automated system are shown below in figure(9.18). Only a plot of the Minor Faraday angle versus frequency and a plot of the ellipticity variation with frequency is given. This is because a lot of miscalculations of

⁸ Introduction To Magnetism & Magnetic Materials, D.Jiles, Chapman & Hall, pg 57.
297

the Major Faraday Angle resulted which were highlighted in the 'comment' part of the results array, described in section(9.3.2.1). Therefore, not enough points were available to plot. Also the plot only covers a (88-98GHz) region. This was due to the oscillator becoming erratic for frequencies below the 88GHz. However, there are sufficient information in the results which highlights exactly the prediction made in section(5.8.2) for the 'Frequency Dependent' region that one expects to occur at W-band. This serves to compliment Raum's results performed in the Terahertz region and also gives a further insight into the Faraday Angle Resonance phenomena at millimetric frequencies. The results obtained for Sample 32 are shown in figure(9.18).

(9.5.2.1) Results Analysis For Sample 32

As is evident from the minimas of the plot, there is a definite slope to the curve. As described in section(5.8.2), this implies that the material is operating in its 'frequency dependent' region. Namely, the rotation is varying with frequency. Performing the parabolic curvefits as described earlier resulted in the following location of the turning points, shown in table(9.4).

Type Of Turning Point	Minor Faraday Angle
1st Minima ($\Delta\varphi_{1st.MIN}$)	(90.85 GHz, 69.94 ^o)
Maxima ($\Delta\varphi_{MAX}$)	(93.25 GHz, 78.67 ^o)
2nd Minima ($\Delta\varphi_{2nd.MIN}$)	(96.77 GHz, 59.32 ^o)

Table (9.4)

As demonstrated earlier from the results of Sample11, the corresponding Major Faraday Angles occur 90^o apart. For example, the first minima would occur at (90.85 GHz, -20.06^o) or (90.85 GHz, 159.94^o). As long as one is consistent in choice of whether the Faraday angle is $\pm 90^0$, this will not alter the results. By taking the

first minima and the maxima, one can calculate the ($\Delta\varphi$) associated to the (90.85-93.25GHz) frequency region. Similarly, by taking the second minima and the maxima, one can calculate the ($\Delta\varphi$) associated to the (93.25-96.77GHz) frequency region. In addition, one can make an estimate of (ϵ_R) for these frequency regions.

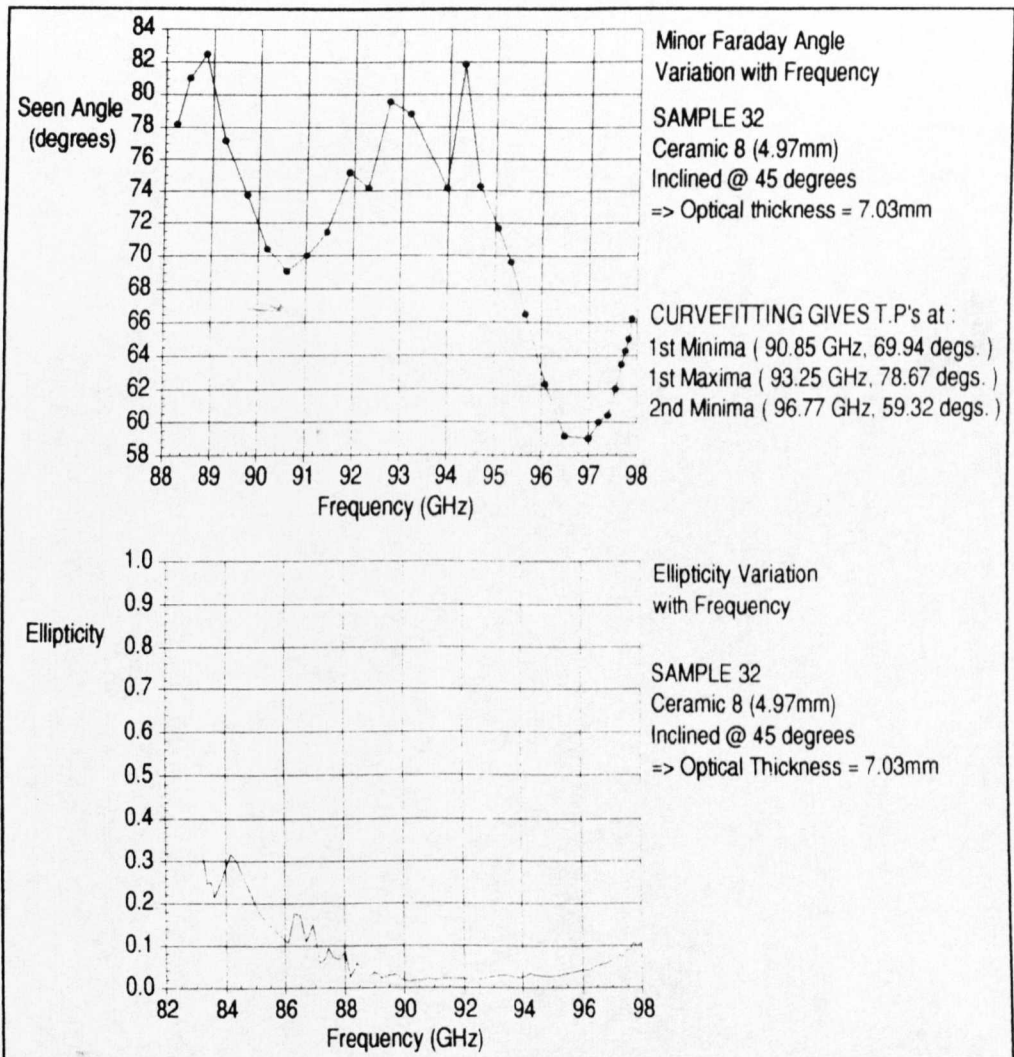


Figure (9.18)

The tabulated results for ($\Delta\varphi$) and (ϵ_R) for the frequency regions described is given in table(9.5).

Frequency Region	$\Delta\varphi$ /single pass	Rotation/mm	Eff.Rel.Permittivity
(90.85-93.25GHz)	76.86 ⁰	10.64 ⁰	19.76
(93.25-96.77GHz)	70.97 ⁰	10.09 ⁰	9.18

Table (9.5)

From the Rotation/mm figures an optical thickness of 4.22mm would be necessary for 45⁰ in the (90.85-93.25GHz) region. This translates to a sample of thickness of 2.98mm inclined at 45⁰ to the incident radiation. Similarly, in the (93.25-96.77GHz) region an optical thickness of 4.46mm would be required for 45⁰ rotation. This translates to a sample of thickness 3.15mm inclined at 45⁰ to the incident beam. As described in section(5.1.1), concerning Sample 11, because of the angling of the sample and hence its c-axis one would expect the smaller thickness to be required if the sample were oriented perpendicular to the incident beam. The effective relative permittivity for a sample of this type inclined in this manner ranged from 9.18-19.76. Typical manufacturers (ϵ_R 's) measured at (≈ 10 GHz)^{9,10} for polycrystalline ferrites of this type range from (9-25). We would expect the SrM polycrystalline sample to have an (ϵ_R) value at the high end of this scale if the ferrite were inclined perpendicular to the radiation. Also more investigation is necessary to determine (ϵ_R) for the frequency dependent region, since the calculation may not be as straight forward as in the frequency independent region. In addition, the sample could have demagnetised in storage which could serve to effect the results.

(9.6) Faraday Rotator Assessment

This section details the measurements made on the Freespace Faraday Rotator (I9). The materials used are described in section(6.12.3). The Faraday Rotator has been thought to have demagnetised significantly. This was suspected from the manual

⁹ Microwave Materials-A Technical Supplement, Trans.Tech Inc., Rev.3, Publication Number 50010080, February 1992.

¹⁰ Quasi-Optical Measurement Of Ferrite Parameters At Terahertz Frequencies By A New Method - Faraday Angle Resonance, M.Raum, International Journal Of Infrared & Millimeter Waves, Vol.15, No.7, 1994.

isolation results obtained for the rotator compared to those measured in section(6.14.3).

(9.6.1) Results For Faraday Rotator (I9)

The Faraday Rotator (I9)'s isolation was firstly remeasured. This was performed manually using the experimental setup as described in section(5.9). Recapping, the rotator was cut at 22.5° in order to maximise the isolation in the forward direction. This allowed it to be placed in the system without having to incline it to the vertical. The Rotator was placed in the system at a slight angle of $\approx 5^{\circ}$ to the incident radiation. This was to reduce the standing waves within the system. System measurements were performed and a plot of the Major and Minor Faraday Angle Variation with frequency together with a plot of the ellipticity variation with frequency was obtained. Both the manual and system measurements obtained for both sides of the isolator are shown in figure(9.19) and figure(9.20).

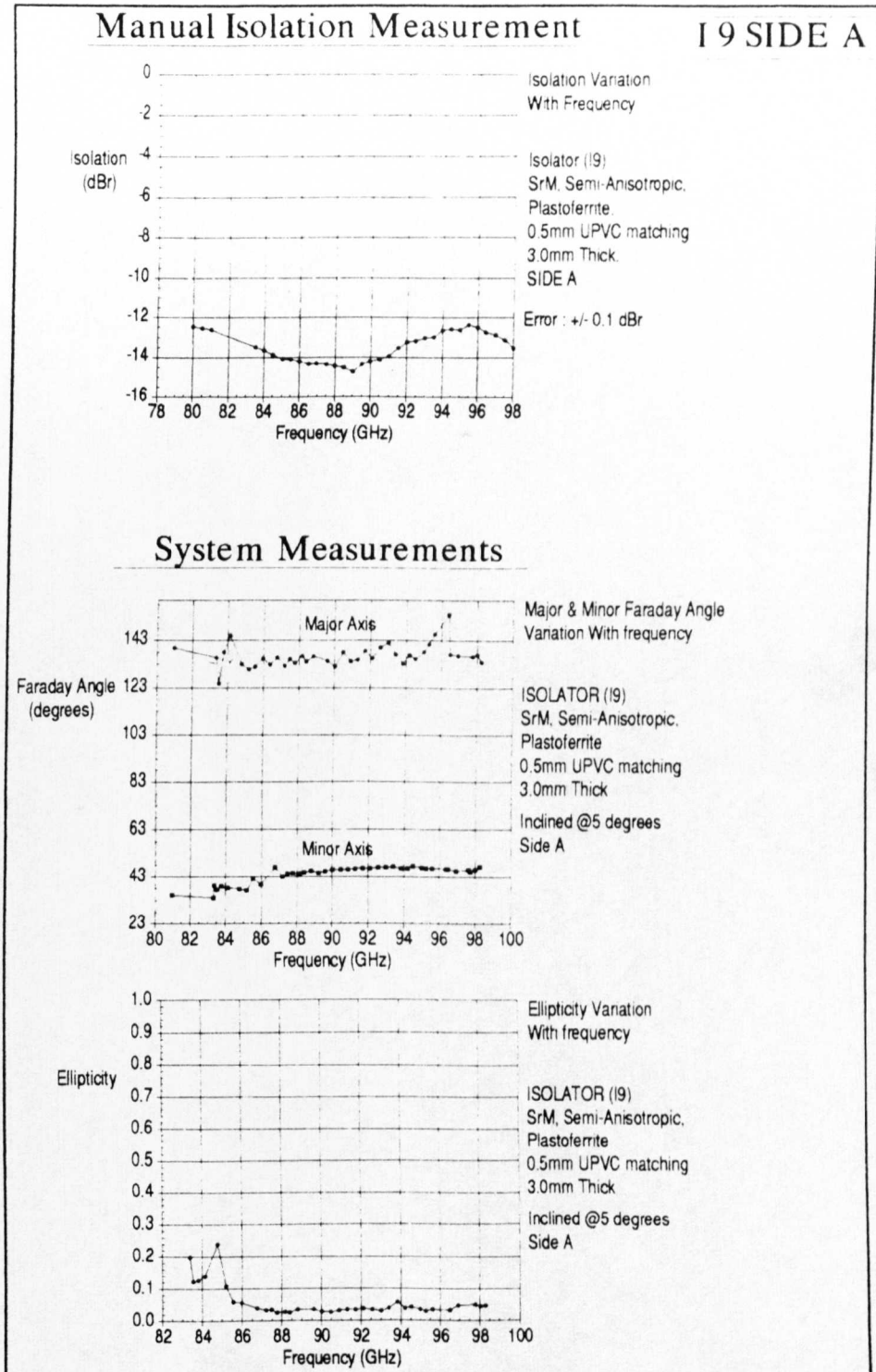


Figure (9.19)

As can be seen from the isolation results, the performance of (I9) is reduced in comparison to its performance measured in section(6.14.3). Recapping, the previous results showed an isolation of >-20dB's over 80-100GHz. The isolation progressively increased

from $\approx 20\text{dB}$'s

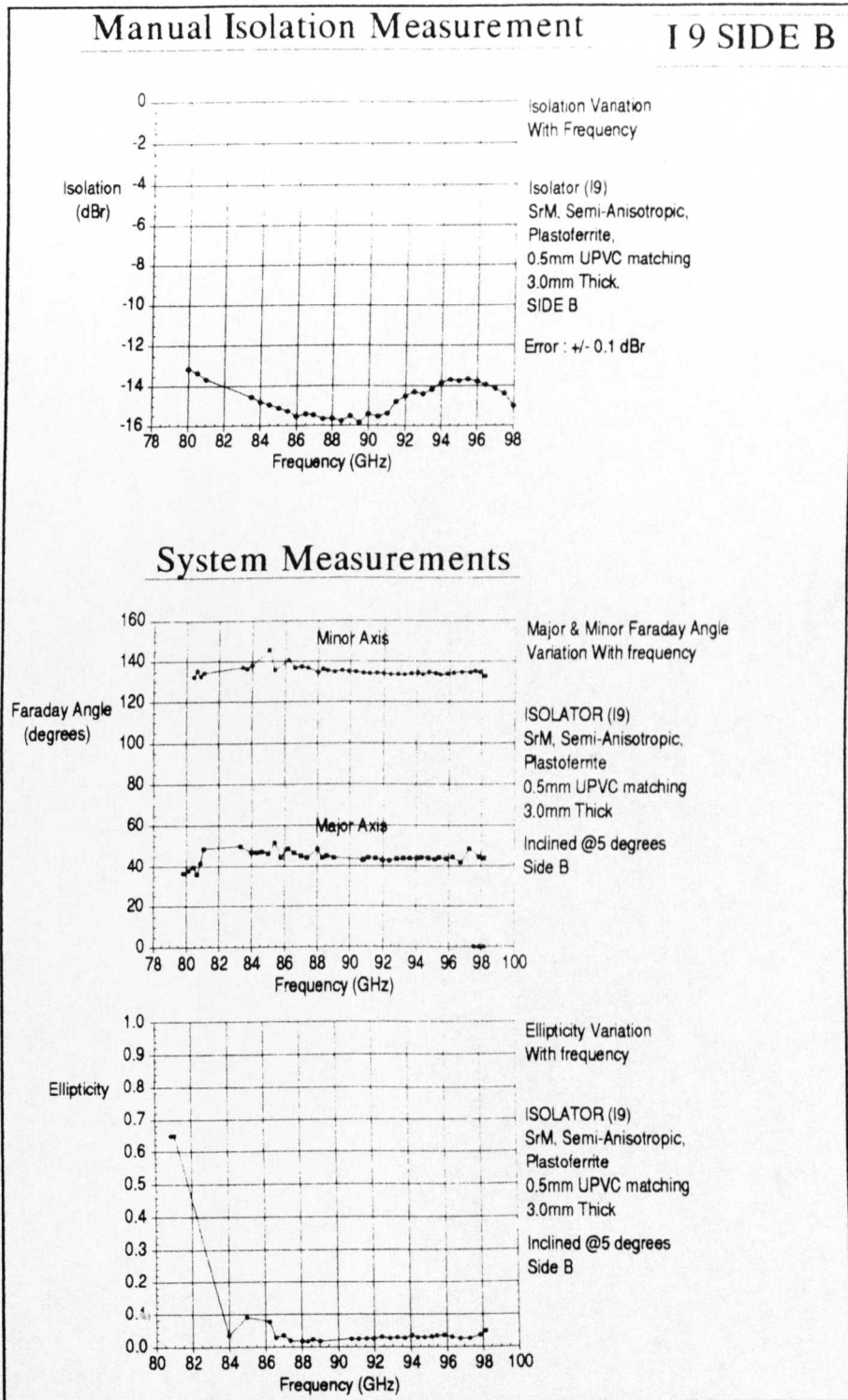


Figure (9.20)

at 80GHz up to $\approx 35\text{dB}$'s at 97GHz. After remeasuring the isolation for the same side it was found that isolation had been reduced by

≈50% to ≤ -15dB's with the largest isolation occurring at 89GHz. This is also true in the reverse direction where an isolation of no greater than 16dB's was recorded which is actually greater than the -14dB level obtained previously. This kind of equalisation of the isolation in both directions, leads me to believe that the magnetisation within the sample has been reduced.

As mentioned at the beginning of the results section, all the samples and Rotators were stored together which could have over time reduced their magnetisation. Also the original set of measurements were performed a year apart from the new set. Over this time scale, with the samples being in close proximity to one another, they will be exposed to each others demagnetisation fields, described in section(2.13). This will cause some of the dipoles to realign in different orientations to reduce the magnetostatic energy of the sample. This could even continue to the extent that the domains within the sample reorient themselves. As can be seen from the system results a rotation of 45° also seems to occur about 88GHz and also the lowest ellipticity occurs at the same position. The system results also tell us that the low isolation that occurs below 88GHz is due to the rotator actually rotating less and the beam becoming more elliptical. Whereas above 88GHz the isolation is reduced because rotation is actually larger than 45°.

In the reverse direction the best isolation occurs at roughly the same frequency of 88GHz. Either side of this frequency, the isolation degrades slightly. From the system results, the rotation remains very close to the 45° but either side of this figure the ellipticity seems to be responsible for the drop in isolation.

In both sets of results presented here the Minor Faraday Angle again proves to give the smoothest profile. As mentioned in section(9.5.1.1) for sample 11, multiple reflections between pieces of ferrite will introduce additional rotational effects which would be apparent in the Major Faraday Angle plot as it holds significantly more power than that in the Minor Faraday Angle. During both

experiments the results showed erratic behaviour of the oscillator occurring around the 84GHz region and below. Thus any results given below this frequency are probably inaccurate, as can be seen in the ellipticity measurement of side(B) of (I9). Points that the frequency could not be determined were interpolated. However, some caution should be made with the figures determined for the ellipticity values around this area.

(9.7) Additional Functions Of The 'Rotary Polariser Quasi-Optical System'.

The following sections, detail two experiments performed which highlight two other useful areas in which the 'Rotary Polariser Quasi-Optical System' can be employed.

(9.7.1) Design & Testing Of A Millimetric Fresnel Rhomb

An additional piece of work I accomplished, was the development of a 'Fresnel Rhomb Quarter-Wave Plate' for use at W-Band. The following section will explain how this device was developed and also highlight how the 'Rotary Polariser Quasi-Optical System' could be used to analyse the performance of the device.

Near the completion of the Fully Automated Rotary Polariser Quasi-Optical System I thought of a way one could fully automate a transmissive version of the Reflection Setup described in the section(5.8.1). Recapping, the reflection setup previously described required a polarising version of the 'Martin Puplett Interferometer' to create circular light. The circular states created were then used to interrogate magnetic samples in order to determine their suitability as isolators. Ofcourse, this proved a very laborious and time consuming task since the interferometer had to be adjusted manually at every frequency in order to create the desired circular state. The whole crux of the experiment relies on creating a circular state. The same effect could be accomplished by replacing the interferometer by a quarter wave plate, as will now be described.

(9.7.1.1) Quarter Wave Plates

A quarter wave plate can be considered as some type of construct that serves to retard one component of an incident electric field by a phase 90° ($1/4$ of a wavelength) relative to its orthogonal component. This amount of retardation occurs when the incident electric field has propagated through the device and results in a circularly polarised field. Therefore, a device that creates a circularly polarised state from a linear polarised state is termed as a quarter-wave plate. There are a whole myriad of quarter-wave plate designs¹¹ which utilise different methods to retard one orthogonal component. However, all the designs except for one suffer from being bandlimited. It is the physical dimensions of the quarter-wave plate that create this band limitation problem. Hence, these type of devices have a specific design frequency at which they create circular light. Deviations from this design frequency which occur outside the designated band lead to inefficient performance and result in elliptically polarised light. The bandwidth for a typical band limited quarter-wave plate is approximately 12.9%. Therefore, a fully automated transmissive system which would take measurements across the whole of W-band would also become bandlimited due to the quarter-wave plate. The only quarter-wave plate that does not suffer from band limitation is the 'Fresnel Rhomb'¹². The circular light created is theoretically independent of a frequency contribution which plagues all the other designs, as demonstrated in equation (9.18).

$$\tan\left(\frac{\delta}{2}\right) = \frac{\cos\theta\sqrt{\sin^2\theta - n^2}}{\sin^2\theta} \quad \dots (9.18)$$

(δ) is the amount of phase retardation that occurs at each reflection.
(θ) is the slant angle of the rhomb and (n) its refractive index as

¹¹ Quarter-Wave Plates for Submillimeter Wavelengths, International Journal of Infrared & Millimeter Waves, Vol.2, No. 3, pgs 67-79, 1981.

¹² Polarisation Interferometer Applications In Microscopy & Macroscopy, M.Francon, S.Mallick, Institut d'Optique, Paris, Wiley-Interscience, sect. (1.8).

shown in figure(9.20)

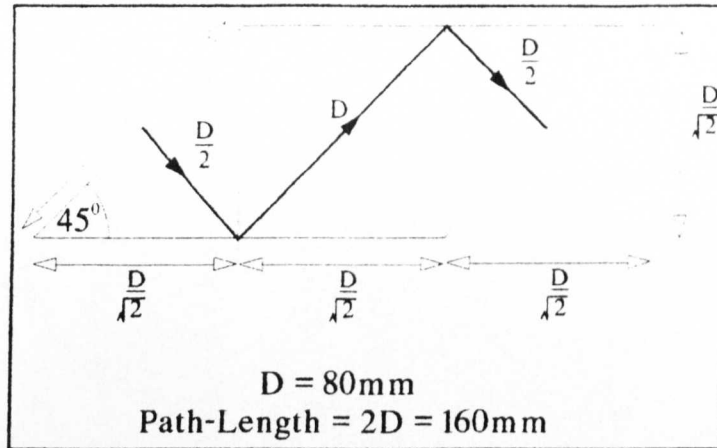


Figure (9.20)

The way in which the Fresnel Rhomb creates circular light, is due to the two total internal reflections that the electric field is forced to undergo as it propagates through the device. At each total internal reflection one of the orthogonal components of the electric field is shifted by (δ) degrees of phase relative to the other orthogonal component. In order to create a circular state (δ) is set to 45° . As one can see from equation (9.18), the amount of phase shift incurred on the component can be altered by choice of the slant angle(θ) and refractive index(n) of the rhomb.

For a Fresnel Rhomb to conform to the geometry of the quasi-optics used here at St.Andrews its slant angle(θ) would have to be 45° . Setting (δ) to 45° in order to create circular light therefore defines a value for what the refractive index must be. By substitution of these values into equation (9.18) one discovers the refractive index must be 1.55. As well as the refractive index conforming to this value, the medium must also be suitably transparent (low loss) at millimeter wave frequencies. As fortune would have it, the refractive index of High Density Polyethylene (H.D.P.E) is 1.524. This is the same material as is used in the manufacture of our low loss quasi-optic lenses and has a loss at 100GHz of :

$$\text{loss} = 0.91(\text{loss tangent})(n)(f_{\text{GHz}}) \quad \dots (9.19)$$

$$\begin{aligned}
 &= 0.91 (0.3 \times 10^3) (1.524) (100) \\
 &= 0.4 \text{ dB/cm}
 \end{aligned}$$

From some simple geometry the pathlength traversed through the Fresnel Rhomb, if the slant length is (D), is 2D. In order that the rhomb fit within the existing optics, (D) had to be a multiple of 40mm. For this reason, (D) was chosen to be 80mm. Hence, the largest loss which would occur at 100GHz is 0.64dB.

In order to avoid unwanted surface reflections at the front and back surfaces of the rhomb, two blazed H.D.P.E. plates were made. These were designed with a blazing depth of 0.67mm, groove width of 0.42mm and a mark to space ratio of one. This would allow them to operate effectively at 90GHz which was at the centre of the desired band I wished to operate at. The matching plates were affixed to the rhomb by vacuum grease. A small aluminium base was also manufactured to mount the optics.

After the construction of the Fresnel Rhomb¹³ it needed to be characterised. Its efficiency as a quarter-wave plate would depend upon how circular the light was. The amount of ellipticity could be conveniently determined by placing it in the 'Rotary Polariser Quasi-Optical System' as shown in figure(9.21)

¹³ Many thanks to Andy Barman, who skilfully manufactured the Fresnel Rhomb and the Lenses for my system.

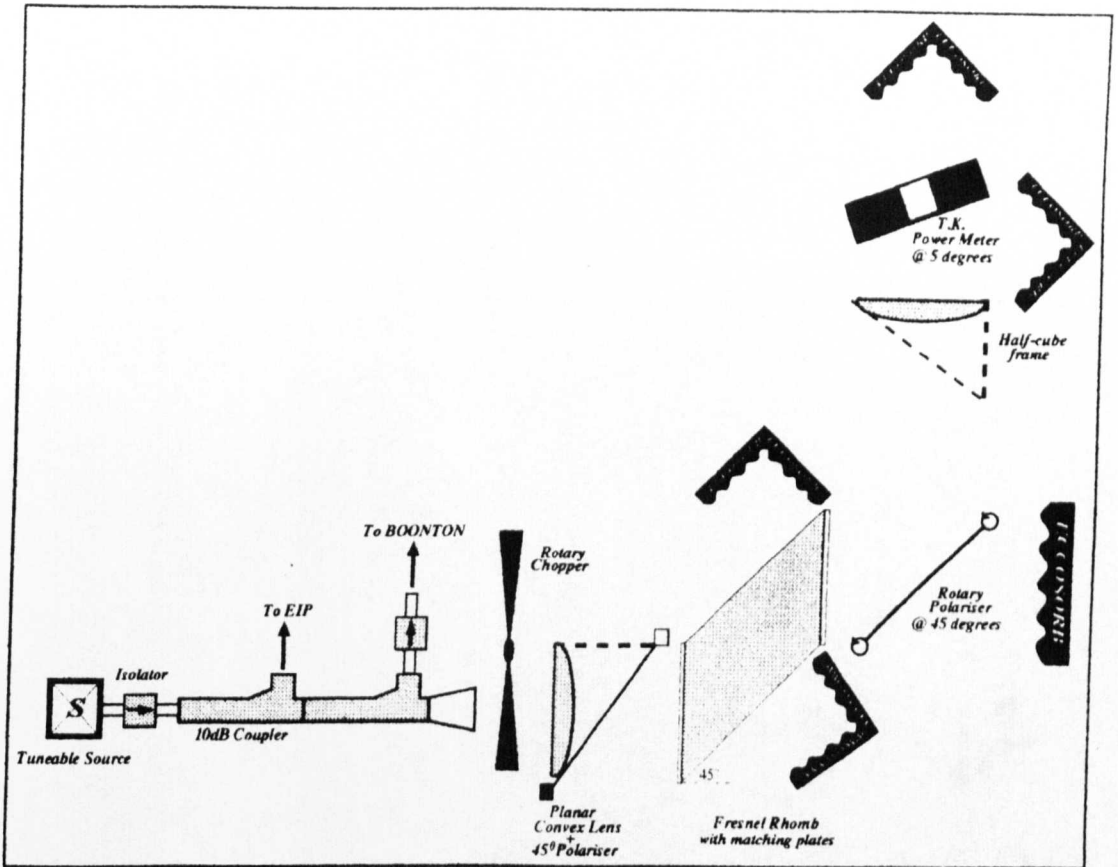


Figure (9.21)

An ellipticity of unity would render a circular state. The best ellipticity one could hope for would be 0.91. This is due to the refractive index of H.D.P.E not being exactly 1.55. This would cause a 41° phase shift to result at each dielectric-air interface, i.e. an 82° total phase shift would occur.

The results obtained over W-band by the Rotary Polariser Optical are shown below in figures(9.22-9.23).

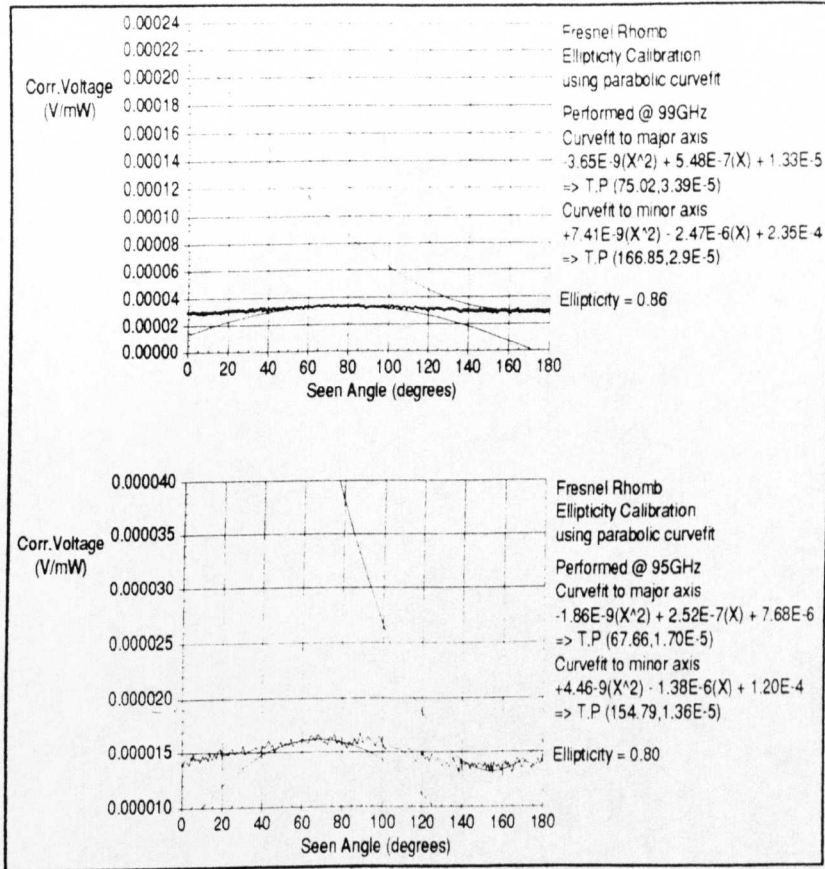
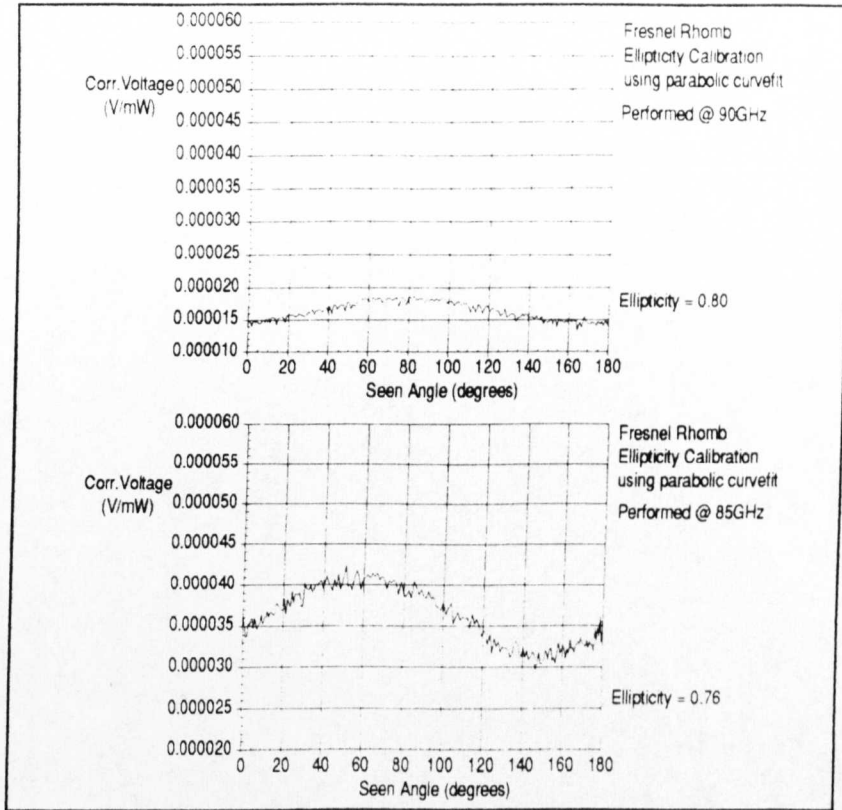


Figure (9.22)



Figure(9.23)

Taking the maximum theoretical ellipticity of 0.91 that could be achieved by an ideal Rhomb of these dimensions, one can now determine the efficiency of the Rhomb over W-band. The way in which the Rhomb's efficiency varies over W-band is shown in figure(9.24).

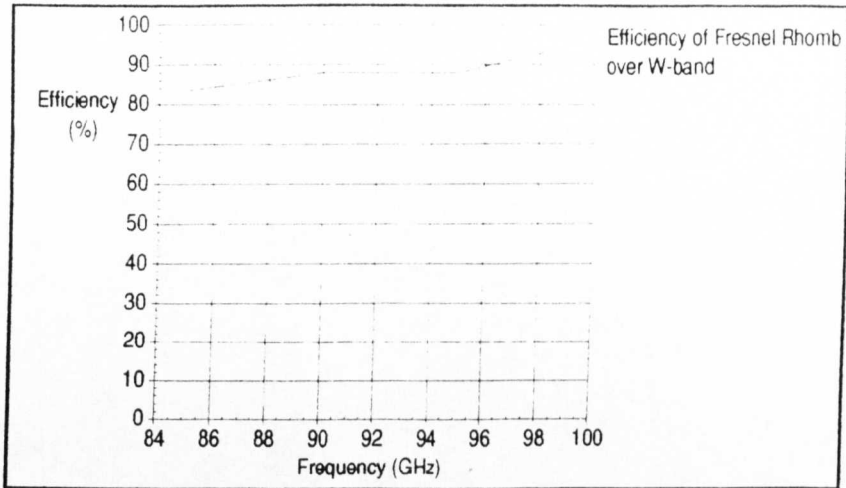


Figure (9.24)

From the results shown, it is evident that the 'Rotary polariser quasi-optical system' has alternative uses and can prove very effective in assessing the performance of a quarter-wave plate. With respect to the theoretical value of the ellipticity, the Fresnel Rhomb operates very efficiently. Any degradation in the ellipticity of the beam can probably be associated to the matching plates that were affixed to the Rhomb with vacuum grease. The small separation that could exist between the matching plate and the Rhomb could impose phase distortions upon beam. Furthermore, multiple reflections could be set up within the Rhomb which could also reduce its performance. In retrospect, the performance of the Rhomb could be improved by directly blazing its faces. However, any type of matching serves to bandlimit a device.

(9.7.2) Location Of The Principle Axes Associated To A Birefringent Material

A novel use of the 'Rotary Polariser Quasi-Optical System' is to locate the principal axes of a birefringent material. It will be demonstrated that by examination of the ellipticity of the beam, one can determine the orientation of these axes.

A material can said to exhibit birefringence¹⁴ if two orthogonal axes

¹⁴ Optics (2nd Ed.), E. Hecht, Addison-Wesley Publishing Co., Chapter 8, pgs. 282-292.

exist which have different indices of refraction. These materials are sometimes referred to as being 'Optically Anisotropic'. Hence, the path-length traversed by a beam or the amount of refraction that is incurred upon it, is dependent on its orientation to these axes. The birefringence phenomena has been exploited in the design of quarter-wave plate devices¹⁰. This is where it is arranged for the incident linear polarised wave to bisect the two orthogonal principle axes such that one of its orthogonal components propagates along one principle axis and the other along the the second principle axis. The length of the material is arranged such that one of the orthogonal components of the (E) vector travels ($\pi/2$) radians further. Hence, the beam exits circularly polarised.

Magnetic materials can also be birefringent. However, Birefringence can sometimes serve to hinder the performance of a non-reciprocal magnetic device such as an isolator. The birefringent nature of the material can incur some ellipticity upon the beam and hence reduce the isolation of the device. The reverse isolation of the device can also be reduced, since the amount of rotation is dependent upon the orientation of the beam.

If one can determine the location of the principle axes, it can be arranged to machine the material such that the input beam rotates through one of the principle planes. This serves to minimise the ellipticity on the beam in the forward direction and hence maximise the device's isolation. However, the tradeoff comes when the beam passes through in the reverse direction and suffers maximum ellipticity¹⁵. Most of the magnetic materials we employ to make Faraday Rotators are all of the Barium or Strontium Hexaferrite type. These are all hexagonal in structure and thus are anisotropic and hence birefringent in nature. Therefore, such a test to locate the principle axes would prove very beneficial in optimising a Faraday Rotator's performance.

¹⁵ Microwave, Millimeter Wave & Sub-Millimeter Wave Freespace Faraday Rotators, IEEE MTT-S 1995 International Microwave Conference Proceedings (Orlando), G.M. Smith, S. Kang, C. Unsworth, E. Puplett, D. Franklin, J.C.G. Lesurf.

The way in which one can locate the principle axes of a birefringent material is as follows.

If one considers a material to be birefringent, then it possesses two principle axes (P_1) and (P_2) with respective indices of refraction (n_1) and (n_2). These principle axes are orthogonal to one another. If one inputs a linear polarised beam (E) along one of the two principle axes then its orthogonal components (E_1) and (E_2) will be inclined at 45° to both (P_1) and (P_2). This will result in (E_1) and (E_2) traversing the same relative path-length. Hence, the beam will remain linear upon exiting the material. Furthermore, a power meter will detect the loss associated to the particular principle axis. Now if the (E) vector is inclined at some arbitrary angle (θ) to say the principle axis (P_1), then the path-lengths traversed by each of the orthogonal components (E_1) and (E_2) will be proportional to the sum of the component resolved along both axes. This will result in the orthogonal components traversing different path-lengths and hence an ellipticity being imposed on the beam. When the (E) vector is input such that it bisects (P_1) and (P_2) the ellipticity measured as $(\frac{min}{maj})$ will be largest and also a ratio of the refractive indices of (P_1) and (P_2).

Therefore,

- Ellipticity = 0 \Rightarrow A Principle Axes
- The Largest Ellipticity \Rightarrow The ratio of the refractive indices of (P_1) and (P_2)

Since, the principle axes are fixed due to the intrinsic structure of a material it is possible to use an unmagnetised sample to locate them and hence avoid the rotation effects of the magnetised sample. The experiments undertaken, were performed using the 'Prototype Rotary Polariser Quasi-Optical System', detailed in Chapter 8. The only change to the main setup was the incorporation of a manual rotary polariser instead of the horizontal polariser in the first half-cube. This was employed to create arbitrary angled inputs for the interrogation of the sample. All measurements were performed at 99.9GHz. Sample 12 was investigated which was an Anisotropic,

Unmagnetised Plastroferrite of thickness 3.73mm. The results of which are shown in figure (9.24) below.

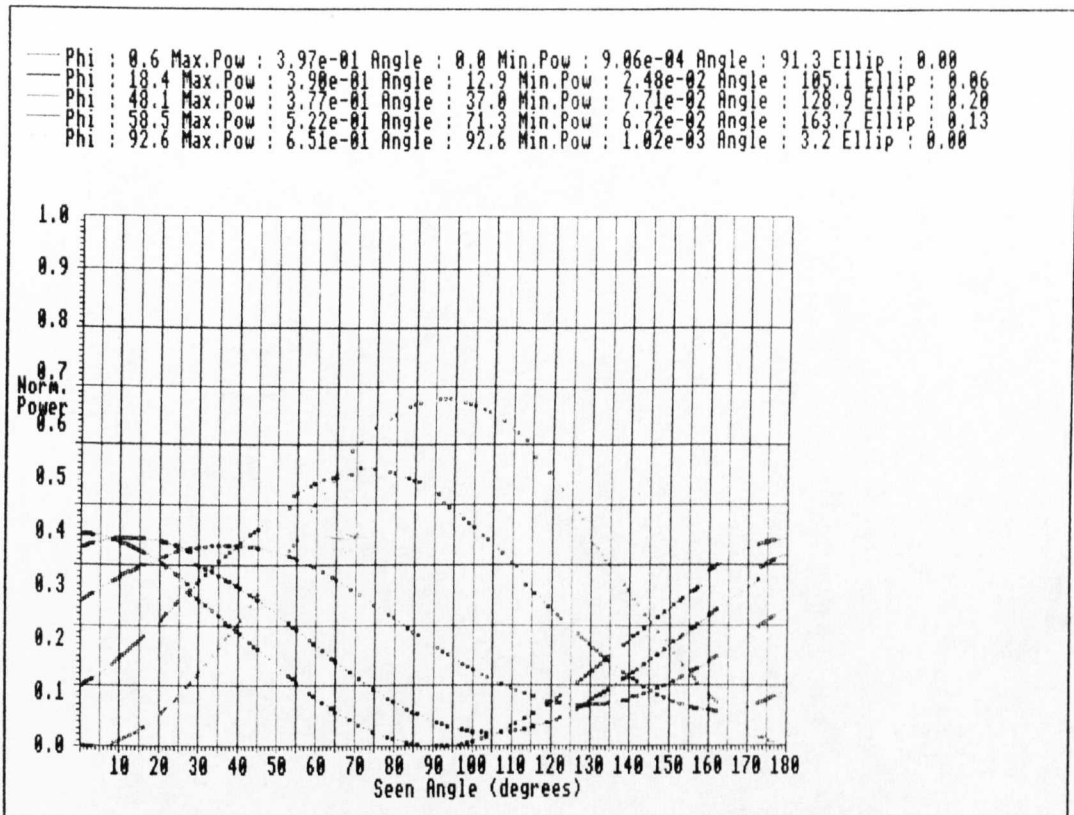


Figure (9.24)

The Phi value is the measured angle of the manual rotary polariser wires from the vertical position. The results clearly show that the principle axis for Sample 12 were located in the horizontal and vertical axes of the ferrite. Furthermore, the horizontal and vertical axes of the ferrite are also square to the horizontal and vertical sides of the sheet of material that the ferrite was cut from. Hence, the principle axes are roughly parallel to the sides of the manufactured sheets of material. The measurement at 48° which is very close to the angle that bisects the principle axis (namely 45°) gives one a feel for the ratio of the refractive indices of the principle axes which is roughly 1 : 5. A point to note from the graph is that the major Faraday angle calculated should be the same as the input angle (phi) of the radiation. However, the slight rotation detected suggests

that there is some intrinsic remnant field in the unmagnetised sample. This remnant field can usually be attributed to the type of manufacturing process, see chapter(5). The collated results from the above figure(9.24) can be seen in figure(9.25).

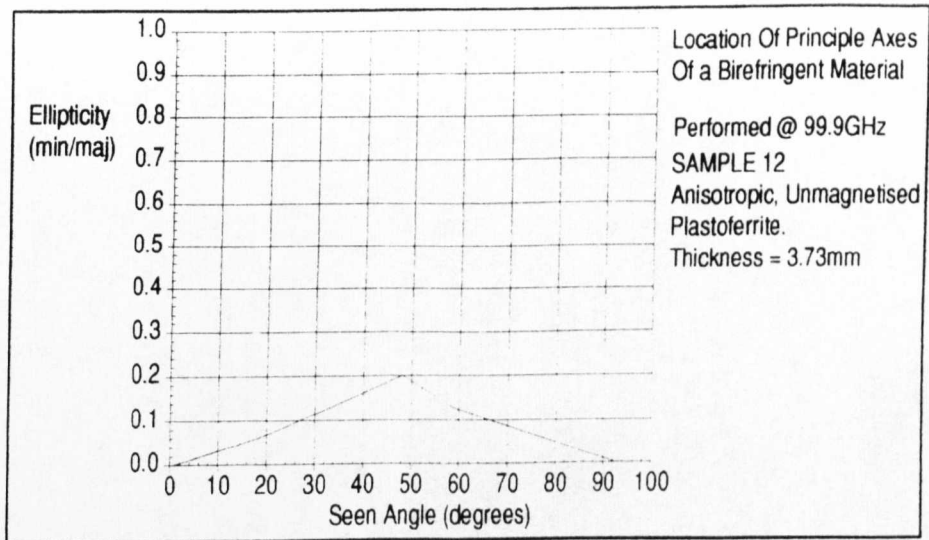


Figure (9.25)

Therefore, with reference to the discussion at the beginning of this section, it would be advisable to arrange for one of the principle axis to be oriented such that a vertically input polarised (E) vector would pass through it as it rotates through a full 45° upon propagation through the sample. As described in our paper¹³, this would suggest machining the ferrite such that the principle axis was inclined at 22.5° to the vertical. Results can be seen for this type of material in section(6.14) of the Plastroferrite work. The isolator was cut at 22.5° to the manufactured sheet of material. As predicted the isolation is maximised in one direction and reduced in the other direction.

Another way to highlight the effect of orientating the principle axes, was to create an isolator and to examine the spatial variation of the isolation as the isolator was angled to the vertical. I investigated this spatial variation of isolation well before the Rotary polariser system was conceived. The results from the experiments compliment those performed here. So it is worth while briefly describing them. The

ferrite material used was also a plastoferrite material except it was supplied in a rolled form, as opposed to the sheet form described above. This implies that the material was calendered. As well as calendering, the material was also exposed to a magnetic field at some stage of its manufacture. This was evident by a remnant field that could be clearly seen in the plane of the surface, when iron filings were sprinkled over the surface of a 100mm×100mm sample. The sample was cut such that the lines of flux ran parallel to one of the sides. Although I was unaware of the material being birefringent at the time, the lines of flux actually served to locate one of the principle axes of material. The other being orthogonal to it. An isolator (I6) was made from two pieces of the material. Both pieces were bonded together such that the flux lines of the remnant fields were parallel. The isolation was measured using the experimental setup described in section(5.9) at a spot frequency of 99.9GHz. The variation of the isolation was noted for different orientations of the isolator with reference to the vertical. This also implies the angle which one of the principle axes is inclined to the vertical. The results obtained are shown in figure(9.26) below.

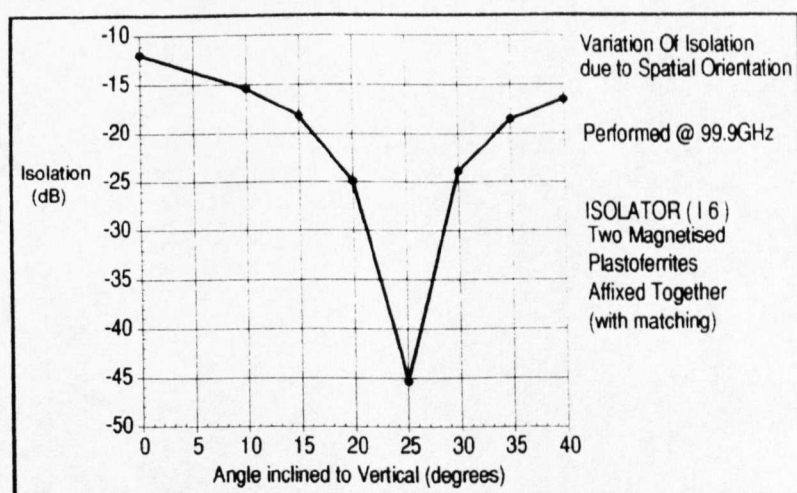


Figure (9.26)

As one can see the isolation is maximised when the isolator, and therefore one its principle axes, was inclined at 25° to the vertical. The experiment was performed manually so there could be a few

degrees error on the results. However, this also gives weight to the results and predictions made previously and shows that a 22.5° would be a good angle at which to machine the ferrite to attain a maximum isolation in one direction.

(9.3) Conclusions & Final Remarks

The chapter has guided us through the whole development of the 'Fully Automated Rotary Polariser Quasi-Optical System'. A tracking routine was developed which led to a significant reduction in the time required to perform an experiment. Also the use of a parabolic curvefit proved very successful. This allowed one to cut through the noise floor in order to make accurate predictions of the Major and Minor Faraday Angles as well as the ellipticity of the beam. Faraday Angle Resonance experiments were then performed on two samples. The results from the experiment highlighted the phenomena well in both cases. The result from Sample 32 proved of particular interest as it verified the prediction made in section(5.8.2) of how the 'Faraday Angle Resonance' curves behave in the 'Frequency Dependent' region of the ferrite. This serves to compliment the work performed by Raum and give an extra insight into Faraday Angle Resonance at millimetric frequencies. Measurements were also performed on a Faraday Rotator (19) which demonstrated how the system can be used to measure the rotation and ellipticity of a Faraday Rotator directly. In addition, two extra sections were included which highlighted two different ways in which the system can be employed. A 'Millimetric Fresnel Rhomb' was developed in the first of these sections. The system was used to then determine how efficient the Rhomb operated as a quarter-wave plate. This was achieved by analysing the ellipticity of the Rhomb's output over W-band. The final section describes how one can use the system to locate the principle axes of a birefringent material by examining the ellipticity of beam upon output from the sample. In addition, the ratio of the refractive indices of the principle axes can

be determined. Knowledge of the orientations of the principle axes of a magnetic sample proved useful when optimising the performance of a Faraday Rotator made from a hexagonal ferrite.

Chapter 10

Final Summary & Scope For Further Work

The thesis presented has focussed upon the development of a 'Fully Automated Rotary Polariser Quasi-Optical System' for use at millimetric frequencies. Particular interest in such a system arose because it gave one the opportunity to investigate new ferrite materials quickly and accurately and to determine their suitability for application in Freespace Faraday Rotators/Isolators.

In Chapter One, a general background to millimeter-waves is presented and also the important characteristics of wave propagation at millimeter-wave frequencies is highlighted. In addition, a short review of how the characterising features of millimeter-wave technology is exploited, is given.

Chapter Two, explained the essential attributes of Gaussian Beams, which are necessary to understand the freespace propagation of millimeter-waves. A description of Gaussian Beam mode theory and lens design is included together with a practical example of how two planar/convex dielectric lenses were designed and expected to perform for the final system.

Chapter three, is concerned with the Gunn oscillator. A full description of how the Gunn oscillator operates is given. In addition, a description of how one constructs the coaxial cavity, resonant cap oscillators, used here at St.Andrews is presented with performance results. The last part of the chapter, describes the successful development of an 'Automatic Oscillator Tuning System'. The system allows one to generally tune the frequency and backshort tuners of an oscillator in any manner which is governed by a computer control program. Particular attention was given to the development of an 'oscillator characterisation' control program. With

the system, it was demonstrated that an oscillator could be characterised across W-band in 100MHz steps within half an hour.

Chapter Four, links the behaviour of magnetic materials to the proximity of the neighbouring atoms. Special attention is given to the 'Exchange Interaction' which accounts for a magnetic material being able to establish and retain its own internal magnetic field after magnetisation. The concepts of Domains and Bloch Wall formation are also discussed together with the temperature dependence of a magnetic material on its Curie point.

Chapter Five, documents the 'Faraday Effect' and how its non-reciprocal nature is exploited by Faraday Rotators. Preceding sections, detail how one can construct a Freespace Faraday Rotator and Quasi-Optical Isolator. In addition, a description of the types of ferrite materials used in this study is given together with the processes required in their manufacture. Later sections, describe the two experimental methods I used to determine the suitability of new magnetic materials for use in Freespace Faraday Rotators and Isolators. The chapter is drawn to a close by listing the advantages a Freespace Faraday Rotator/Isolator has over a conventional waveguide isolator.

Chapter Six, investigated experimentally the suitability of three different types of plastroferrite for use as Freespace Faraday Rotators. The materials were investigated using the Reflectance method. The refractive index variation of the (+ve) and (-ve) circular states with frequency is determined for the three types. In addition, the 'Ideal thickness' required for 45° rotation is determined. The chapter also documents how three Freespace Faraday Rotators were constructed from the same materials and characterised. It was found that the error in the predicted thickness from the experimental results was no greater 4.4%. All the rotators were found to have spot isolations $\gt -56\text{dB}$'s and a -20dB operation over a band of (22GHz+) and up to (-0.6dB) insertion loss was recorded. In conclusion, the Semi-Anisotropic Plastroferrite was identified as the best material for a

general purpose Faraday Rotator Isolator.

Chapter Seven, documents the instrument design, construction and interfacing of a 'Quasi-Optical Rotary Polariser' which was the most important feature of the final system.

Chapter Eight, details the experimental results obtained from the first prototype version of the 'Rotary Polariser Quasi-Optical System'. Through experiment it is demonstrated how the 'Rotary Polariser' can be corrected for skew, misalignment and offset. Thus, readying the system for accurate measurement retrieval. The chapter also demonstrates how the system can identify linear, elliptical and circular polarisation uniquely and give a measure of the Faraday rotation and ellipticity of the beam directly. The results of which are displayed by computer program that was also developed to display the data retrieved from experiment. Results are included on Rotator performance and also ferrite measurements that performed for the Defence Research Agency (D.R.A.). The ferrite measurements for the D.R.A. confirmed measurements performed at 15-18GHz that the 'doped' magnetic samples had not been manufactured correctly. This was associated to the high porosity of the materials. The 'undoped' sample proved to rotate the plane of polarisation across W-band. The results of which exhibited strong signs of the 'Faraday Angle Resonance' phenomenon. It was calculated from 'Faraday Angle Resonance' theory that the undoped material produced 30^{08} rotation/pass and that a 7mm piece of material would be required for 45^0 optimal rotation across W-Band.

Chapter Nine, details the final 'Fully Automated' version of the 'Rotary Polariser Quasi-Optical System' using the AOTS and a single T.K. Freespace Power Meter. Although, theoretically one should be able to calculate the actual power that falls upon the T.K. meter from the voltage it outputs when inclined off the Brewster Angle, it was demonstrated that in practice the calibration was unreliable. However, it was demonstrated that one could still use the T.K. meter voltages to determine the Faraday Angle and ellipticity of a

beam.

The chapter also describes how a 'Tracking' feature was successfully developed to reduce experimental time. In addition, the noise effects which can affect the T.K. were tackled. From this an optimum experimental arrangement was devised to reduce standing waves and also a successful 'Parabolic Curvefit' routine was implemented in real time on the data to cut through the noise floor and to improve accuracy of measurement.

The later sections, depict the 'Faraday Angle Resonance' results that were performed with the system on two samples. Both samples were inclined at 45° to the incident radiation, thus the thicknesses predicted were only for a sample inclined in the same manner. Sample 11, showed $11^{\circ}46'$ /mm rotation giving an optimum thickness of 2.7mm. Sample 32 depicted the 'Frequency Dependent' rotational behaviour expected at millimetric wavelengths. This served to complement the original work performed by Raum and to give an extra insight into the Faraday Angle Resonance phenomenon.

In addition, results were presented for Faraday Rotator (19). However, the device was shown to have demagnetised significantly from previous results. The results confirmed, however, that the final system can be used to measure the Faraday angle and ellipticity of a Rotator and provide an extra insight into how the device operates.

In all the experimental cases, it was apparent that the minor Faraday angle gave a smooth profile with frequency. This was due to less power being available in the minor axis which served to reduce the amount of multiple reflections that could be set up within the ferrite and distort a measurement for a many layered sample.

The last sections of the chapter, describe the other two alternative uses for the system. The first was to assess the performance of quarter-wave plates. This was verified experimentally in the assessment of a 'Millimetric Fresnel Rhomb' that was developed for an 'Automated Fresnel Rhomb Transmission System'. In experiment

it was found to operate with an efficiency between 83%-96% across W-band. The degradation in ellipticity was associated to the matching plates of the device which served to introduce multiple reflections and phase distortion.

The other use of the system, was to locate the 'Principle Axes' of a birefringent material by examination of the ellipticity of the output beam. This was demonstrated in an unmagnetised version of a plastroferrite sample. It was shown that when a linear polarised beam passes through a sample and parallel to a principle axis that it exits undistorted. Any other orientation of the beam to the principle axis causes a ellipticity to be evoked upon the beam. Also when the linear polarised beam bisects both the principle axes a measure of the ratio of the refractive indices can be obtained. From the experimental results, it was deduced that to maximise the performance of a birefringent Faraday Rotator, the device should be inclined with one of its principle axes at 22.5° to the incident radiation. This was also predicted from spatial angling measurements of a Faraday Rotator which are also given.

Overall, the final 'Fully Automated System' demonstrated that it could be used successfully and accurately for 'Faraday Angle Resonance' measurements at W-band. This proved a quick and easy method to assess new magnetic materials and determine their suitability for use in Freespace Faraday Rotators/Isolators over the Reflectance Method. In addition, the system offers one the opportunity to investigate the ellipticity of a gaussian beam. Three possible uses were given whereby the measurement of the ellipticity of the beam could be used to successfully investigate the operation of Faraday Rotators and the performance of Quarter-wave plates and location of the principle axes of a birefringent material. However, the amount of applications, where one may want to investigate how a beam has become distorted or effected by a material, device or component is endless.

it was found to operate with an efficiency between 83%-96% across W-band. The degradation in ellipticity was associated to the matching plates of the device which served to introduce multiple reflections and phase distortion.

The other use of the system, was to locate the 'Principle Axes' of a birefringent material by examination of the ellipticity of the output beam. This was demonstrated in an unmagnetised version of a plastoferrite sample. It was shown that when a linear polarised beam passes through a sample and parallel to a principle axis that it exits undistorted. Any other orientation of the beam to the principle axis causes a ellipticity to be evoked upon the beam. Also when the linear polarised beam bisects both the principle axes a measure of the ratio of the refractive indices can be obtained. From the experimental results, it was deduced that to maximise the performance of a birefringent Faraday Rotator, the device should be inclined with one of its principle axes at 22.5° to the incident radiation. This was also predicted from spatial angling measurements of a Faraday Rotator which are also given.

Overall, the final 'Fully Automated System' demonstrated that it could be used successfully and accurately for 'Faraday Angle Resonance' measurements at W-band. This proved a quick and easy method to assess new magnetic materials and determine their suitability for use in Freespace Faraday Rotators/Isolators over the Reflectance Method. In addition, the system offers one the opportunity to investigate the ellipticity of a gaussian beam. Three possible uses were given whereby the measurement of the ellipticity of the beam could be used to successfully investigate the operation of Faraday Rotators and the performance of Quarter-wave plates and location of the principle axes of a birefringent material. However, the amount of applications, where one may want to investigate how a beam has become distorted or effected by a material, device or component is endless.

(10.1) Improving Design & Scope For Further Work

Additional tasks one could perform to improve accuracy with the T.K. as a detector, would be to measure the 'polariser leakage' of the wires. Due to the polariser wires being of finite width, some reflection of power could occur even when a linear polarised state is orthogonal to the wires. Although a polarised detector, such as the Boonton Power Meter would not pick this reflection up, the T.K. could detect such a reflection which could serve to affect an ellipticity measurement.

Although the T.K. was originally a good idea due to limited resources, in an ideal world two Boonton detectors would be best suited for detection. They would provide accurate measurements of absolute power. In addition, this would enable one to accurately characterise a Faraday Rotator in one experiment. Namely, its isolation and insertion loss could be measured and in addition the amount of power lost due to over/under rotation and ellipticity could be measured separately.

The oscillator power supply, although stable could be prone to drift and hence adjust the frequency slightly. Ideally, development of a computer controlled power supply which could set the voltage, constantly monitor and correct the bias would maintain stability in the frequency of oscillation by elimination of the d.c. drift. Furthermore the oscillator could be tuned accurately in even smaller frequency increments via a combination of mechanical and bias tuning over W-band.

Although the ministepper is very precise, the rotary polariser could be improved by investment in 'absolute rotary encoder feedback' which would eliminate any error due to mis-stepping.

Finally, if extra time were invested in the system, 'curvefitting algorithms' could be added to the final computer program to fit the data to theory and thus provide a greater accuracy of prediction.

APPENDIX A

Program ~ FarAngRes6

```

REM *****
REM                                     FarAngRes6
REM *****

REM ***** MAIN *****

ON ERROR PROCerr:END
watch = TIME
no_of_samples = 5 : REM ** no. of samples taken by Lockin to be averaged **

eip = 19 : REM GPIB Address of EIP Frequency Counter

REMelip = 0
minor_volt = 0
major_volt = 1
minor_marker = 0
major_marker = 0

REM ***** AOTS Initialisation Parameters *****
REM ***** Assign critical limiting parameters to frequency & backshort tuners *****

freq_step = 0.01 : REM **** The voltage difference in one step of the frequency tuner ****
REM                **** Can be as small as 0.010000. Approx voltage step.Used to ****
REM                **** dimension array ****

crit_ft_down = 4.38 : REM *** Corresponds to critical down voltage of ft cannot exceed = 4.34***
ft_start_pos = 4.20 : REM *** Start voltage for ft, should give 100GHz with BLOCK D4 = 4.28 ***
crit_ft_up = 3.00 : REM *** Critical up voltage of ft.= 3.00
REM                Also corresponds to finish voltage gives 80GHz with BLOCK D4 ***

crit_bs_up = 4.46 : REM *** Critical bs up voltage. Cannot exceed ***
crit_bs_down = 4.29 : REM *** Critical bs down voltage. Cannot exceed ***

wait = 1.2 : REM waiting period for ft step ...wait =2.3 should give approx 0.02 voltage step
REM                ...wait =1.2 " " " 0.01 " "
REM                ...wait =0.7 " " " 0.005 " "
REM *****

REM ***** STEPPER Parameters Initialisation *****

divisions% = 200 : REM will be 200
steps_res% = 2000
big_steps% = steps_res%/divisions%
size_of_move% = big_steps%
home_pos% = 0
major_pow = -1000 : REM Used to locate maximum power value
minor_pow = 1000 : REM Used to locate minimum power value
degree_step = 0.9 : REM number of degrees in one step i.e 180 degs./200 steps = 0.9
power = 0
DIM results(10, divisions%)
root_two = SQR(2) : REM Constant used in Seen Angle Calc
cos_eta = 0.996194698 : REM Constant for det_angle - at 5 degrees
conv_factor = 0 : REM originally put in to find T.K power, will use supersede this

tracksteps = 10 : REM No.of steps to track either side of max/min far angles
REM DIM track(10,tracksteps*2+20)
REM PRINT "track array dimensioned to track(10,;tracksteps*2+20;)"

tsamps = 2*tracksteps : REM Used in PROCdet_centre
DIM testarray(4,30) : REM Used to put (N=21) data samples in
DIM diff(4,tsamps) : REM Used to put (N-2) difference samples in

```

```

REM *****
PROCFlush_Buffers
PROCEnable_Input
PROCstartupGPIB
PROCsetup_boonton
PROCsetup_lockin
PROCinitialise
REM ***** Assigns velocity, acceleration etc. to stepper *****

one$ = CHR$(13)+"8MN"+CHR$(13)+"8PZ"+CHR$(13)+"8MPA"+CHR$(13)+"FSB0"+CHR$(13)+"8A180"+CHR$(13)+
"8V0.15"+CHR$(13)+"8PR"+CHR$(13)

PROCSend_String(one$) : REM Sets UP Mode Absolute
PROCvalues_returned
PRINT:PRINT "Stepper Ready To Go !! "
REM *****

PROCstop
PROCposition_ft

PROCscan_bs
PRINT"Press space when ready "
x$ = GET$
PROCgo_eip_go

REM PROCInterpolate :REM Calcs.horiz&vert grads, mean powers(xbars) & mean voltages(ybars) for
REM frequency obtained from EIP
COM$ = "F," :REM comment placed in array comment$ F = Fine , no prob with measurement
lap=0
PROCstep_and_record

PROCdisplay_params :REM Assigns major_pow_pos to old_major_pow_pos etc..
array(0,lap) = 1 :REM needed because no step_ft routine
array(1,lap) = nft_value :REM voltage of frequency tuner
array(2,lap) = frequency :REM frequency determined by EIP
REM array(3,lap) = a :REM max power of boonton
REM array(4,lap) = average :REM Sampled lockin voltage
array(11,lap) = major_chi :REM chi value for major faraday angle
array(12,lap) = minor_chi :REM chi value for minor faraday angle
array(7,lap) = major_far_ang :REM major faraday angle
array(8,lap) = minor_pow :REM power in minor axis
array(9,lap) = minor_far_ang :REM minor faraday angle
array(10,lap) = ellip :REM ellipticity (minor power/major power)
REM array(11,lap) = horiz_grad :REM Interpolated horiz_grad for particular frequency
REM array(12,lap) = horiz_pow :REM Interpolated horiz_pow (horiz xbar)
REM array(13,lap) = horiz_volt :REM Interpolated horiz_volt (horiz ybar)
REM array(14,lap) = vert_grad :REM Interpolated vert_grad for particular frequency
REM array(15,lap) = vert_pow :REM Interpolated vert_pow (vert xbar)
REM array(16,lap) = vert_volt :REM Interpolated vert_volt (vert ybar)
REMPROCDisplay_params :REM Assigns major_pow_pos to old_major_pow_pos etc..
comment$(0,lap) = COM$

REMPRINT" Press SPACE to continue "
REMX$ = GET$

PRINT:PRINT:PRINT

lap=0

REM lap=0
REPEAT
COM$ = "F," :REM Reassign comment to okay for next run F = Fine , no prob with measurement
PRINT " COM$ reset to : ";COM$
major_pow = -1000 :REM Have to reassign after ever revolution
minor_pow = 1000 :REM Have to reassign after ever revolution
minor_marker = 0
major_marker = 0
lap=lap+1
PROCstep_ft
PROCscan_bs
REMPRINT" Press SPACE to continue "

```

```

REMx$ = GET$
PROCgo_eip_go
REMPROCinterpolate
REMPROCstep_and_record

IF (old_ellip > 0.8) THEN
  PRINT"Ellipticity > 0.8 --> Hence, shall FULLSTEP"
  PROCstep_and_record
ELSE
  PRINT"Ellipticity < 0.8 --> Shall TRACK"
  variable = old_major_pow_pos : PRINT " Tracking MAJOR faraday angle "
  PROCTrack
  PRINT:PRINT
  variable = old_minor_pow_pos : PRINT " Tracking MINOR faraday angle "
  PROCTrack
ENDIF

PROCdisplay_params      :REM Prints results far_ang, ellip etc..
array(0,lap) = lap+1
array(1,lap) = nft_value :REM voltage of frequency tuner
array(2,lap) = frequency :REM frequency determined by EIP
REM array(3,lap) = a      :REM max power of boonton
REM array(4,lap) = average :REM Sampled lockin voltage
REM array(5,lap) = power_av :REM Sampled Output power (=Boonton x10)
array(6,lap) = major_pow  :REM power in major axis
array(7,lap) = major_far_ang :REM major faraday angle
array(8,lap) = minor_pow  :REM power in minor axis
array(9,lap) = minor_far_ang :REM minor faraday angle
array(10,lap) = ellip     :REM ellipticity (minor power/major power)
array(11,lap) = major_chi :REM chi value for major faraday angle
array(12,lap) = minor_chi :REM chi value for minor faraday angle
REMarray(13,lap) = horiz_volt :REM Interpolated horiz_volt (horiz ybar)
REMarray(14,lap) = vert_grad :REM Interpolated vert_grad for particular frequency
REMarray(15,lap) = vert_pow  :REM Interpolated vert_pow (vert xbar)
REMarray(16,lap) = vert_volt :REM Interpolated vert_volt (vert ybar)
REMPROCdisplay_params    :REM Prints results far_ang, ellip etc..
comment$(0,lap) = COM$

      PRINT:PRINT:PRINT
      PRINT " new tracking centers are : "
      PRINT " Major center : ";old_major_pow_pos
      PRINT " Minor center : ";old_minor_pow_pos
UNTIL FNreadft_pot <= crit_ft_up

VDU7:VDU7
CLS
run_time = (TIME - watch)/6000
PRINT" Experiment Time : ";run_time
PRINT " Press space to continue "
x$ = GET$
PROCfile_results      :REM Prints all results to files in RAM

END

REM ***** TRACKING ROUTINES *****

DEF PROCfillarray(which_one)
REM *** Routine needed for FULLSTEP since only have data for positions 0-200 ***

IF (which_one - tracksteps < 0) THEN
  counter = 0 :REM 1st Sample to put in testarray
  PRINT"Angle of interest is between 0-10 degrees"
  PRINT"Shall put samples 0-20 in testarray"
  PROCdelay(10)
ENDIF
IF (which_one + tracksteps > 200) THEN
  counter = 179 :REM 1st Sample to put in testarray
  PRINT"Angle of interest is between 170-180 degrees"
  PRINT"Shall put samples 179-200 in testarray"
  PROCdelay(10)
ENDIF

IF (which_one - tracksteps > 0 AND which_one + tracksteps < 200) THEN
  counter = which_one - tracksteps :REM 1st Sample to put in testarray

```

```

PRINT "Angle of interest is within limits"
PRINT "Shall put samples ";which_one - tracksteps;" - ";which_one + tracksteps;" in testarray"
PROCdelay(10)
ENDIF

FOR W = 0 TO tsamps
testarray(0,W) = (counter+W) :REM Position stored here
testarray(1,W) = results(0,(counter+W)) :REM angle stored here
testarray(2,W) = results(3,(counter+W)) :REM corr_voltage stored here
NEXT W
PRINT "Test arrays full"

ENDPROC

DEF PROCdet_centre

REM total samples in testarray = 21 = (tsamps+1)
REM ** Two runs firstly position vs.voltage & secondly angle vs. voltage **
REM ***** Firstly calcs. £x,£y,£xy,£(x^2) of (N-2) pts. in difference array ***** £=sum *****

FOR x_axis = 0 TO 1
REM ***** corr_voltage sums *****
vx = 0 :REM £x for corr_voltage
vx sqr = 0 :REM £(x^2) for corr_voltage
vx cube = 0 :REM £(x^3) for corr_voltage
vx four = 0 :REM £(x^4) for corr_voltage
vy = 0 :REM £y for corr_voltage
vxy = 0 :REM £xy for corr_voltage
vx sqry = 0 :REM £x^2y for corr_voltage

REM testarray(0,1) - Actually my positions (Xi)
REM testarray(1,1) - Actually my angles (Xii)
REM testarray(2,1) - Actually my voltages (Y)

FOR J = 0 TO (tsamps)
REM ***** Calc. sums for corr_voltages *****

vx = vx + testarray(x_axis,J)

vx sqr = vx sqr + (testarray(x_axis,J)*testarray(x_axis,J))
vx cube = vx cube + (testarray(x_axis,J)*testarray(x_axis,J)*testarray(x_axis,J))
vx four = vx four + (testarray(x_axis,J)*testarray(x_axis,J)*testarray(x_axis,J)*testarray(x_axis,J))

vy = vy + testarray(2,J)
vxy = vxy + testarray(x_axis,J)*testarray(2,J)
vx sqry = vx sqry + (testarray(x_axis,J)*testarray(x_axis,J)*testarray(2,J))

NEXT J

REM ***** Secondly calcs. linear regression fit to (N) pts. of testarray *****
REM ** Equation of fit is : Y = v_azero + v_aone(X) + v_atwo(X^2) for corr_voltages *****

NN = (tsamps+1) :REM total number of samples in dataset

bot_part = (vx sqr^3)-(2*vx*vx sqr*vx cube)+(NN*vx cube*vx cube)+(vx*vx*vx four)-(NN*vx sqr*vx four)

v_azero = (vx sqr*vx sqr*vx sqry)-(vx*vx cube*vx sqry)-(vx sqr*vx cube*vxy)+(vx*vx four*vxy)
v_azero = (v_azero + (vx cube*vx cube*vy) - (vx sqr*vx four*vy))/ bot_part

v_aone = (vx*vx sqr*vx sqry)-(NN*vx cube*vx sqry)-(vx sqr*vx sqr*vxy)+(NN*vx four*vxy)+(vx sqr*vx cube*vy)
v_aone = (v_aone - (vx*vx four*vy))/(-1*bot_part)

v_atwo = (vx*vx*vx sqry)-(NN*vx sqr*vx sqry)-(vx*vx sqr*vxy)+(NN*vx cube*vxy)+(vx sqr*vx sqr*vy)
v_atwo = (v_atwo - (vx*vx cube*vy))/bot_part

REM ** Next 3 lines prevents division by zero occurring in ang_inter & pos_inter equations **
IF (v_atwo = 0) THEN
v_atwo = 1E-15
ENDIF

```

```

PRINT
PRINT" ***** Equation for corr_voltage prediction is *****"
PRINT" Y = ";v_atwo;"(X^2) + ";v_aone;"(X) + ";v_azero :PRINT

REM testarray(0,I) - Actually my positions (Xi)
REM testarray(1,I) - Actually my angles (Xii)
REM testarray(2,I) - Actually my voltages (Y)

FOR J=0 TO (tsamps)
REM *** Calc. Least Square voltages for known angles. store in testarray(4,J) for plot later ***
REM * Also testarray(5,J) holds differential of fitted equation. hence can determine turning pt *

testarray(4,J)=v_azero+(v_aone*testarray(x_axis,J))+(v_atwo*testarray(x_axis,J)*testarray(x_axis,J))
REMtestarray(5,J)= v_aone + (2*v_atwo*testarray(x_axis,J))

NEXT J

IF (x_axis = 0) THEN
pos_inter% = (-1*v_aone/(2*v_atwo)) :REM Calc. Minimum/Maximum Position
PRINT"Nearest Stepper Position is ---> ";pos_inter%

ELSE

ang_inter = (-1*v_aone/(2*v_atwo)) :REM Calc. Minimum/Maximum Faraday Angle
volts_inter = v_azero + (v_aone*ang_inter) + (v_atwo*ang_inter*ang_inter) :REM Min/Max Voltage

PRINT:PRINT"Turning point is (";ang_inter;"";volts_inter;"")"
ENDIF

REM *** Calc. Chi Square which gives estimate of how noisy the data samples were *****

chi = 0
FOR J = 0 TO (tsamps)
deviation = testarray(4,J) - testarray(2,J)
chi = chi + (deviation*deviation) :REM squared diff. of data from fitted line
NEXT J
PRINT" Chi value for sample is : ";chi
PRINT" Zero is a perfect fit ( No noise on data )"

NEXT x_axis

IF (variable = old_major_pow_pos) THEN
FOR J = 0 TO (tsamps)
IF (testarray(0,J) = pos_inter%) THEN
PRINT" GOOD MAJOR PREDICTION"
major_volts = volts_inter :REM Checks to see if position is within +-10degree range
major_marker = 1 :REM If it is, a flag "marker" is set to 1
ENDIF
NEXT J
ELSE

FOR J = 0 TO (tsamps)
IF (testarray(0,J) = pos_inter%) THEN
PRINT" GOOD MINOR PREDICTION"
minor_volts = volts_inter
minor_marker = 1
ENDIF
NEXT J
ENDIF

ENDPROC

DEF PROCtrack
FOR LLL = 0 TO 2*tracksteps
trackpos = variable - tracksteps + LLL : REM Defines position of tracker

```

```

testarray(0,LLL) = trackpos :REM stores track position number here

COLOUR 3 :REM Puts next line of text in red
PRINT "Track number : ";LLL
VDU 20 :REM Goes back to white on black text
PRINT" TRACKPOS = ";trackpos

IF (trackpos < 0 ) THEN
  wave = 0 :REM used to stop taking readings when stepper is moving
  zip_pos = (trackpos + 200)*size_of_move%
  L = trackpos + 200 :REM gives +ve (L) value so calc_seen_angle
  PRINT" trackpos < 0 : Shall move to ";L
  PROCcalc_seen_ang :REM can be determined correctly
  seen_angle = seen_angle - 180 :REM Adjusts seen_angle to -ve value
  PRINT" Adjusted seen_angle = ";seen_angle

testarray(1,LLL) = seen_angle :REM stores seen_angle here

ELSE
  wave = 1
  zip_pos = (trackpos*size_of_move%)
  IF (trackpos > 200) THEN
    L = trackpos - 200
    PRINT" trackpos > 200 : Shall move to ";L
    PROCcalc_seen_ang
    seen_angle = seen_angle + 180
    PRINT" Adjusted seen_angle = ";seen_angle

testarray(1,LLL) = seen_angle :REM stores seen_angle here

ELSE
  wave = 2
  L = trackpos
  PRINT" trackpos within normal range : Shall move to ";L
  PROCcalc_seen_ang
  seen_angle = seen_angle
  PRINT" Adjusted seen_angle = ";seen_angle

testarray(1,LLL) = seen_angle :REM stores seen_angle here

ENDIF
ENDIF

two$ = STR$(zip_pos)
three$ = CHR$(13)+"8D-"+two$+CHR$(13)+"8G"+CHR$(13)+"8PR"+CHR$(13)
PROCSend_String(three$)
PROCvalues_returned

IF (LLL=0 )THEN
  PRINT" wave is : ";wave
  PRINT"INITIAL MOVE delay 5secs until move completed"
  PROCdelay(5) :REM **** Let Polariser settle ****
  oldwave = wave
  ELSE
    PROCcalc_wave
  ENDIF

PROCsample_lockin :REM Takes 5 samples from Boonton & Lockin and returns corr_voltage (V/mW)

testarray(2,LLL) = corr_voltage :REM corr_voltage stored here

PRINT" Frequency : ";frequency;" GHz"
NEXT LLL
PROCdet_centre :REM calcs. true centre of data samples stored in testarray

PRINT:PRINT
IF(variable = old_major_pow_pos) THEN
  major_far_ang = ang_inter :REM true MAJOR faraday angle determined by PROCdet_centre
  major_pow_pos = pos_inter% :REM Nearest stepper position determined by PROCdet_centre
  major_pow = major_volts :REM Corresponding corr_pow for major_pow_pos
  major_chi = chi :REM Chi value for data set
  PRINT" TRUE MAJOR far angle = ";major_far_ang

```

```

PRINT" NEAREST stepper position = ":major_pow_pos
PRINT" Corresponding corr_voltage = ":major_pow
PRINT" Major chi value -> ":major_chi
ELSE
  minor_far_ang = ang_inter :REM true MINOR faraday angle determined by PROCdet_centre
  minor_pow_pos = pos_inter% :REM Nearest stepper position determined by PROCdet_centre
  minor_pow = minor_volts :REM Corresponding corr_pow for major_pow_pos
  minor_chi = chi :REM Chi value for data set
  PRINT" TRUE MINOR far angle = ":minor_far_ang
  PRINT" NEAREST stepper position = ":minor_pow_pos
  PRINT" Corresponding corr_voltage = ":minor_pow
  PRINT" Minor chi value -> ":minor_chi
ENDIF

REMPRINT" Press SPACE to continue "
REMX$ = GET$

REM ellip = (minor_pow/major_pow)

ENDPROC

DEF PROCcalc_wave
PRINT
PRINT" oldwave : ";oldwave
PRINT" wave : ";wave
PRINT
IF (oldwave = wave) THEN
  PRINT"Same region --> Just delay by 1 sec"
  PRINT
  PROCdelay(1)
  oldwave = wave
ELSE
  PRINT"Different region --> Delay by 5sec"
  PRINT
  PROCdelay(5)
  oldwave = wave
ENDIF

ENDPROC

REM ***** INTERPOLATION ROUTINES for BEST Linear Regression Fit to frequency *****

DEF PROCinterpolate

REM ***** Calcs. linear regres. params. for HORIZ *****

name$ = "corr_hfreq":REM *** get top_pos & perc_away_from_top ****
PROCscan_file(name$)

name_two$ = "corr_hgrad"
PROCdo_interp(name_two$)
horiz_grad = inter_grad

name_two$ = "corr_hpow"
PROCdo_interp(name_two$)
horiz_pow = inter_grad :REM xbar

name_two$ = "corr_hvolt"
PROCdo_interp(name_two$)
horiz_volt = inter_grad

PRINT"HORIZ Equation is : Y = ":horiz_grad;"(X - ":horiz_pow;") + ":horiz_volt

REM ***** Calcs. linear regres. params. for VERT *****

name$ = "corr_vfreq":REM *** get top_pos & perc_away_from_top ****
PROCscan_file(name$)

name_two$ = "corr_vgrad"
PROCdo_interp(name_two$)
vert_grad = inter_grad

```

```

name_two$ = "corr_vpow"
PROCdo_interp(name_two$)
vert_pow = inter_grad :REM xbar

name_two$ = "corr_vvolt"
PROCdo_interp(name_two$)
vert_volt = inter_grad

PRINT"VERT Equation is : Y = ";vert_grad;"(X - ";vert_pow;" ) + ";vert_volt

ENDPROC

DEF PROCscan_file(name$)

address$ = "RAM::RamDisc0.$LOOKUP."+name$

start_pos = 1000

channel = OPENIN(address$) :REM Opens for reading only
J = 1
REPEAT
  REMPRINT" J = ";J
  IF (J=1) THEN
    reading$ = GET$#channel
    read_freq_one = VAL(reading$) :REM First reading in file is assigned to 'read_freq_one'

  ENDIF

  REMPRINT"read_freq-one : ";read_freq_one
  reading$ = GET$#channel
  read_freq_two = VAL(reading$) :REM 2nd reading in file is assigned to 'read_freq_two'
  REMPRINT"read_freq_two : ";read_freq_two

  difference = (read_freq_one - frequency) :REM calcs difference between first reading and
              REM frequency looking for
  REMPRINT"Difference is : ";difference
  IF (difference < start_pos AND difference >= 0) THEN

    REM **** freq. file - Has max frequency as first reading and descends to lowest frequency ***

    start_pos = difference :REM Looks for smallest +ve difference between 'read_freq_one'
    top_pos = J :REM and EIP frequency
    top_freq = read_freq_one
    bot_freq = read_freq_two

  ENDIF

  read_freq_one = read_freq_two :REM Reassigns 2nd reading as first for next run
  J = (J+1) :REM Increments J for next run

  REMPRINT"Press space for next run "
  REM x$ = GET$

UNTIL EOF#channel
CLOSE# channel
perc_away_from_top = (start_pos/(top_freq - bot_freq))

ENDPROC

DEF PROCdo_interp(name_two$)

file$ = "RAM::RamDisc0.$LOOKUP."+name_two$
channel = OPENIN(file$)

PRINT " INTERPOLATION STAGE "

FOR I = 1 TO top_pos

  reading$ = GET$#channel
  REMPRINT"reading$ = ";reading$

  IF (I = top_pos) THEN
    read_grad_one = VAL(reading$) :REM
    reading$ = GET$#channel
    read_grad_two = VAL(reading$) :REM

```

```

    REMPRINT"read_grad_one :";read_grad_one
    REMPRINT"read_grad_two :";read_grad_two
  ENDIF
NEXT I
CLOSE# channel

grad_diff = ABS(read_grad_one - read_grad_two)

IF (read_grad_one > read_grad_two) THEN
  REMPRINT"Top grad is > than Bot grad "
  inter_grad = read_grad_one - grad_diff*perc_away_from_top
ELSE
  REMPRINT"Top grad is < than Bot grad "
  inter_grad = read_grad_one + (grad_diff*perc_away_from_top)
ENDIF

REM PRINT" Gradient difference ";grad_diff

REM PRINT" INTERPOLATED GRADIENT : ";inter_grad

ENDPROC

REM ***** Boonton Routines *****
DEF PROCsetup_boonton
PROCadrandoutput(0,3,"SS1") : REM *** Selects Sensor 1, W band Sensor
PROCadrandoutput(0,3,"PW") : REM *** Unit fixed to mW (pg.4-16, Boonton Manual )
PROCadrandoutput(0,3,"TM0") : REM *** Selects Talk Measurement Floating point, pg. 4-16
PRINT " Boonton Setup "
ENDPROC

DEF PROCread_boonton
IF ( frequency > 100 ) THEN
  freq_string$ = "FR100"
  PRINT"Frequency > 100GHz Cal Boonton to 100GHz"
ENDIF
IF ( frequency < 75 ) THEN
  freq_string$ = "FR75"
  PRINT"Frequency < 75GHz Cal Boonton to 75GHz"
ENDIF

PROCadrandoutput(0,3,freq_string$) : REM *** Sends frequency of EIP to Boonton in order to
REM          calibrate boonton reading ***

boon$ = FNadrandinput(0,3,255) : REM Takes calibrated reading from boonton
B$ = MID$(boon$,3)
power = VAL(B$)
PRINT" Power Output --> ";power;" mW"
ENDPROC

REM *****
REM ***** PRINT Routines *****

DEF PROCfile_results
REMPROCprint_array
PROCprint_array(1,"freq_volt") :REM array(1,lap) file freq_volt
PROCprint_array(2,"freq") :REM array(2,lap) " freq
REM PROCprint_array(3,"maxpow") :REM array(3,lap) " maxpow
REM PROCprint_array(4,"lockin") :REM array(4,lap) " lockin
PROCprint_array(5,"boonpow") :REM array(5,lap) " boonpow
PROCprint_array(6,"majorpow") :REM array(6,lap) file majorpow
PROCprint_array(7,"majfarang") :REM array(7,lap) " majfarang
PROCprint_array(8,"minorpow") :REM array(8,lap) " minorpow
PROCprint_array(9,"minfarang") :REM array(9,lap) " minfarang
PROCprint_array(10,"ellip") :REM array(10,lap) " ellip
PROCprint_array(11,"majchi") :REM array(11,lap) " major_chi
PROCprint_array(12,"minchi") :REM array(12,lap) " minor_chi
REM PROCprint_array(13,"hvolt") :REM array(13,lap) " hvolt - variable horiz_volt
REM PROCprint_array(14,"vgrad") :REM array(14,lap) " vgrad - variable vert_grad
REM PROCprint_array(15,"vpow") :REM array(15,lap) " vpow - variable vert_pow
REM PROCprint_array(16,"vvolt") :REM array(12,lap) " vvolt - variable vert_volt

REM ***** Used only for one run - Delete when doing full experiment *****

```

```

PROCprint_results(0,"results0") :REM results(0,L) - seenangle variable
PROCprint_results(1,"results1") :REM results(1,L) - average tk voltage
PROCprint_results(2,"results2") :REM results(2,L) - power_av of boonton
PROCprint_results(3,"results3") :REM results(3,L) - corr_voltage
REM PROCprint_results(4,"results4") :REM results(4,L) - real_pow
REM PROCprint_results(5,"results5") :REM results(5,L) - norm_tk_pow
REM PROCprint_results(6,"results6") :REM results(6,L) - norm_real_pow
PROCprint_comment(0,"comment") :REM comment$(0,L) - COM5

ENDPROC

DEF PROCprint_comment(column,name$)
address$ = "RAM::RamDisc0.$."+name$
channel = OPENOUT(address$)
PRINT"Saving to RAMdisc..."
FOR loop% = 0 TO freq_div

BPUT# channel, (comment$(column,loop%))

NEXT
CLOSE# channel
OSCLI("SETTYPE "+address$+" TEXT")
PRINT" .....Finished!"
ENDPROC

DEF PROCprint_track(column,name$)
address$ = "RAM::RamDisc0.$."+name$
channel = OPENOUT(address$)
PRINT"Saving to RAMdisc..."
FOR loop% = 0 TO (2*tracksteps+10)

BPUT# channel, STR$(track(column,loop%))

NEXT
CLOSE# channel
OSCLI("SETTYPE "+address$+" TEXT")
PRINT" .....Finished!"
ENDPROC

DEF PROCprint_array(column,name$)
address$ = "RAM::RamDisc0.$."+name$
channel = OPENOUT(address$)
PRINT"Saving to RAMdisc..."
FOR loop% = 0 TO freq_div

BPUT# channel, STR$(array(column,loop%))

NEXT
CLOSE# channel
OSCLI("SETTYPE "+address$+" TEXT")
PRINT" .....Finished!"
ENDPROC

DEF PROCprint_results(column,name$)
address$ = "RAM::RamDisc0.$."+name$
channel = OPENOUT(address$)
PRINT"Saving to RAMdisc..."
FOR loop% = 0 TO divisions%

BPUT# channel, STR$(results(column,loop%))

NEXT
CLOSE# channel
OSCLI("SETTYPE "+address$+" TEXT")
PRINT" .....Finished!"
ENDPROC

REM *****
REM ***** PROCEDURES *****

```

```

DEFPROCinitialise

MODE 21

PRINT "Initialising "

PROCeip_start
PROCdelay(2)

Limit%=1024      :REM Sets the data set size
DIM Buffer% Limit%*4 :REM Assigns memory area called Buffer% - 4 times
REM DIM ftBuffer% Limit%*4 :REM bigger because words returned are 4 bytes

REM ***** ADC card Assignments *****
REM ***** Work out size of array to store results in *****

freq_div = (( ft_start_pos - crit_ft_up)/freq_step ) + 500

DIM array(20,freq_div)
DIM comment$(2,freq_div)
PRINT"Array dimensioned to (20, ",freq_div,")"
REM *****

REM=====REM
REM By converting the SWI names into numbers we save time REM
REM in critical routines later.          REM
REM=====REM

SYS "OS_SWINumberFromString",,"WVAIO_ViaWrite" TO ViaWrite%
SYS "OS_SWINumberFromString",,"WVAIO_ViaRead" TO ViaRead%
SYS "OS_SWINumberFromString",,"WVAIO_Channel" TO Channel%
SYS "OS_SWINumberFromString",,"WVAIO_ADC" TO ADC%
SYS "OS_SWINumberFromString",,"WVAIO_Clock" TO Clock%

SYS Clock%.160000 :REM Maximum sampling rate (167kHz)

REM=====REM
REM Here the VIA register numbers are stored in integer REM
REM variables for readability and to reduce the risk of REM
REM mistakes from misplacing digits through typos. REM
REM=====REM

IORegisterB% = &0
Dat_Dir_Reg% = &2

REM=====REM
REM Setup Port B according to the table above. A line REM
REM which is to be used for writing is indicated by REM
REM setting the corresponding bit in the Data Direction REM
REM Register of the VIA chip. Also we set PB1 and PB2 to REM
REM be high along with PB7 so that the middle pulse can REM
REM be read although its current state is undefined. REM
REM=====REM

SYS ViaWrite%,Dat_Dir_Reg%,%00111100
SYS ViaWrite%,IORegisterB%,%00000000

ENDPROC

REM ***** PROCS for MOVING TUNERS *****

DEFPROCmovebs_up :REM moves backshort up
PRINT "bs_up "
SYS ViaWrite%,IORegisterB%,%00010000
ENDPROC

DEFPROCmovebs_down :REM moves backshort down
PRINT "bs_down "
SYS ViaWrite%,IORegisterB%,%00100000
ENDPROC

```

```

DEFPROCmoveft_up           :REM moves frequency tuner up
PRINT "ft_up "
SYS ViaWrite%,IORegisterB%,%0000100
ENDPROC

DEFPROCmoveft_down        :REM moves frequency tuner down
PRINT "ft_down "
SYS ViaWrite%,IORegisterB%,%00001000
ENDPROC

DEFPROCstop                :REM STOP
PRINT "PROCstop "
SYS ViaWrite%,IORegisterB%,%00000000
ENDPROC

DEFPROCposition_ft
PRINT "!! Positioning_ft !!"
PROCmoveft_down
REPEAT
UNTIL FNreadft_pot >= crit_ft_down
PROCstop
PROCmoveft_up
REPEAT
UNTIL FNreadft_pot <= ft_start_pos
PROCstop
PROCdelay(2)
nft_value = FNreadft_pot
PRINT "ft start voltage : ";nft_value
PRINT" Positioning Completed "
ENDPROC

REM *****
REM ***** PROCS for 5210 LOCK-IN-AMPLIFIER *****
DEF PROCsetup_lockin
PRINT" in PROCstart_lia"
PROCadrandoutput(0,4,"DD 59") : REM
PRINT" adr done"
PROCpoll
PRINT"DD done"
PROCadrandoutput(0,4,"GP 4;2") : REM Set lockin address to 4 ans <cr.If> terminator
PROCpoll
PRINT"GP done"
PROCadrandoutput(0,4,"IE 0") : REM Read external reference frequency
PROCpoll
PRINT"IE done"
PROCadrandoutput(0,4,"D1 5") : REM Set Display1 to DISP - shows MAG value
PROCpoll
PRINT"D1 done"
PROCadrandoutput(0,4,"D2 2") : REM Set Display2 to MAG/phase - shows phase value
PROCpoll
PRINT"D2 done"
PROCadrandoutput(0,4,"TC 5") : REM Set Time Constant to 300ms = code 5
PROCpoll
PRINT"TC done"
PROCadrandoutput(0,4,"ATC 1") : REM Set tuning filter mode to TRACK ref. freq.
PROCpoll
PRINT"ATC done"
PROCadrandoutput(0,4,"F2F 0") : REM Set Ref. freq mode to 'F'
PROCpoll
PRINT"F2F done"
PROCadrandoutput(0,4,"FLT 3") : REM Set Filter to Bandpass
PROCpoll
PRINT"FLT done"
PROCadrandoutput(0,4,"FF 300;2") : REM Track around 30Hz=300, BP 10-120Hz
PROCpoll
PRINT"FF done"
PROCadrandoutput(0,4,"G 0;0") : REM Turn gain OFF
PROCpoll
PRINT"G done"
PROCadrandoutput(0,4,"EX 0") : REM Set expand to OFF
PROCpoll
PRINT"EX done"
PROCadrandoutput(0,4,"AS") : REM Perform AUTOSENSITIVITY
PROCpoll
PRINT"AS done"

```

```

ENDPROC

DEF PROCpoll
REPEAT
number% = FNserial_poll(4)
UNTIL (number% AND %0001) = %0001
ENDPROC

DEF FNserial_poll(tad%)
LOCAL d0%,d1%,stb%
SYS &40340,&00,&2B.&00,tad% TO d0%,d1%,stb%
=stb%

DEF PROCrun_poll
REPEAT
number% = FNserial_poll(4)
IF (number% AND 16) =16 THEN
PRINT"!!! OVERLOAD !!!"
PROCAutosens
ENDIF
IF (number% AND 64) =64 THEN
PRINT" !!! SYS REQUEST !!!"
PRINT " Press a key to continue"
x$= GET$
ENDIF
UNTIL (number% AND %0001) = %0001
ENDPROC

DEF PROCAutosens
PROCArandoutput(0,4,"AS")
PRINT " Performing autosensitivity "
PROCpoll
ENDPROC

DEF PROCread_lockin
PROCArandoutput(0,4,"SEN") : REM determine SENSITIVITY CODE
zap$ = FNadrandinput(0,4,255)
sensitivity% = VAL(zap$)
PROCpoll
REMPRINT " Sensitivity code : ";sensitivity%
alpha% = sensitivity%/2

PROCArandoutput(0,4,"MAG") : REM determine MAGNITUDE
zap$ = FNadrandinput(0,4,255)
magnitude% = VAL(zap$)
PROCpoll
REMPRINT " Magnitude value : ";magnitude%

REM PROCArandoutput(0,4,"NN") : REM determine NOISE
REM zap$ = FNadrandinput(0,4,255)
REM noise% = VAL(zap$)
REM PROCpoll
REM PRINT " Noise value : ";noise%

scale = 10^(alpha%-7) + (LOG(6)*(sensitivity%MOD2)) )
volts = (magnitude%/10000)*scale

REMPRINT:PRINT"f.s.d is : ";scale;" volts"
REMPRINT"voltage : ";volts;" volts"
REMPRINT"recified output noise : ";rec_noise;" volts"
ENDPROC

DEF PROCsample_lockin
PROCrun_poll
sum = 0
add = 0
REM fuzz= 0
FOR I = 1 TO no_of_samples
PROCread_lockin
sum = sum + volts
PROCAread_boonton :REM boonton sampled also in same routine
add = add + power*10
REM fuzz = fuzz + rec_noise

```

```

NEXT I
average = (sum/no_of_samples)
power_av = (add/no_of_samples)
corr_voltage = (average/power_av)
PRINT " Average Lockin Voltage : ";average;" volts"
PRINT " Average Boonton Power : ";power_av;" mW"
PRINT " CORR_VOLTAGE -----> ";corr_voltage;" volts:mW"
REM av_fuzz = (fuzz/no_of_samples)
ENDPROC

REM *****

REM ***** STEPPER ROUTINES *****

DEF PROCstep_and_record

REM ***** Made twice as fast by just stepping over half of a revolution *****

T% = TIME : REM **** Calculates the time taken to determine home position ****
L = 0

FOR K% = 0 TO steps_res% STEP size_of_move% :REM *** steps 0,10,20,...,2000 **

COLOUR 3 :REM Puts next line of text in red
PRINT "Step number : ";L
VDU 20 :REM Goes back to white on black text

PROCcalc_seen_ang :REM calculates seen angle

IF K% = 0 THEN
  REM **** DO NOTHING *****
  PROCdelay(5)
ELSE
  two$ = STR$(K%)
  three$ = CHR$(13)+"8D-"+two$+CHR$(13)+"8G"+CHR$(13)+"8PR"+CHR$(13)
  PROCsend_string(three$)
ENDIF

PROCdelay(1) :REM **** Let Polariser settle *****
PROCsample_lockin :REM Takes 5 samples from lockin,in 'average' and in Boonton in 'power_av'
REM PROCdetermine_tk_pow :REM Calcs. gradient + normalised tk power + norm error above and below

REM ***** Can remove for full run *****
results(0,L) = seen_angle :REM Angle at which radiation is reflected to detector
results(1,L) = average :REM This line is to put average voltage of lockin in array
results(2,L) = power_av :REM Power output from feed (=Boonton x10)
results(3,L) = corr_voltage :REM Corrected Voltage (average/power_av)
REM results(4,L) = real_pow :REM Calc. fraction of output power from polariser to detector
REM results(5,L) = norm_tk_pow :REM Normalised T.K power between 0 & 1
REM results(6,L) = norm_real_pow :REM Normalised real power between 0 & 1
REM *****

PROCcalc_max_and_min :REM ** returns major and minor_pow_pos's which are a rough estimate ***
REM ** of the whereabouts of the major and minor positions *****
PROCvalues_returned
PRINT " FREQUENCY : ";frequency;" GHz"

REM PRINT " NORM TK power -----> ";norm_tk_pow
REM PRINT " Normalised Real Power : ";norm_real_pow
L = L + 1
PRINT

NEXT K%

REM ***** NEXT TWO PARAGRAPHS LOCATE TRUE Major/Minor Pos's, Angles and corr_voltages
PROCfillarray(major_pow_pos) :REM fills testarray with 21 samples around major_pow_pos

old_major_pow_pos = major_pow_pos :REM Assignments required for PROCdetcentre
variable = old_major_pow_pos

PROCdet_centre :REM determines TRUE MAJOR position, angle

```

```

major_far_ang = ang_inter :REM true MAJOR faraday angle determined by PROCdet_centre
major_pow_pos = pos_inter% :REM Nearest stepper position determined by PROCdet_centre
major_pow = major_volts :REM Corresponding corr_pow for major_pow_pos
major_chi = chi :REM Major chi value
PRINT " TRUE MAJOR far angle = ";major_far_ang
PRINT " NEAREST stepper position = ";major_pow_pos
PRINT " Corresponding corr_voltage = ";major_pow
PRINT " Major chi value -> ";major_chi
PROCdelay(15)
PROCfillarray(minor_pow_pos) :REM fills testarray with 21 samples around minor_pow_pos

old_minor_pow_pos = minor_pow_pos :REM Assignments required for PROCdetcentre
variable = old_minor_pow_pos

PROCdet_centre :REM determines TRUE MINOR position, angle
minor_far_ang = ang_inter :REM true MINOR faraday angle determined by PROCdet_centre
minor_pow_pos = pos_inter% :REM Nearest stepper position determined by PROCdet_centre
minor_pow = minor_volts :REM Corresponding corr_pow for minor_pow_pos
minor_chi = chi :REM Minor chi value
PRINT " TRUE MINOR far angle = ";minor_far_ang
PRINT " NEAREST stepper position = ";minor_pow_pos
PRINT " Corresponding corr_voltage = ";minor_pow
PRINT " Minor chi value -> ";minor_chi

REM *****

REM ellip = (minor_pow/major_pow)

time_taken% = (TIME - T% )/6000
PRINT " Time taken for half revolution : ";time_taken%; " mins"

PRINT "Moving to HOME POSITION" :REM remove for full run

three$ = CHR$(13)+"8D-0"+CHR$(13)+"8G"+CHR$(13)+"8PR"+CHR$(13) :REM goes back to home position
PROCSend_String(three$)
PROCvalues_returned

PRINT"! Back in home position. Full step completed !"
ENDPROC

DEF PROCvalues_returned
REM PRINT "VALUES RETURNED":PRINT
REPEAT
PROCGet_Byte
REM IF message% = 13 THEN

REM PRINT "ASCII returned: ";message%; " --> "; "Return";" cflag: ";
REM ELSE
REM answer$ = CHR$(message%)
REM PRINT "ASCII returned: ";message%; " --> ";answer$;" cflag: ";
REM ENDIF

SYS "OS_Byte",152,1 TO Z,ZZ,ZZZ;Cflag% : REM looks to see if buffer empty
REM PRINT Cflag%

REMUNTIL ZZZ = 0
UNTIL (Cflag% AND %0110) = %0110
SYS "OS_Byte",152,1 TO Z,ZZ,ZZZ;Cflag% : REM looks to see if buffer empty
REM PRINT Z,ZZ,ZZZ,Cflag%
ENDPROC

DEF PROCEnable_Input
SYS "OS_Byte",2,2
ENDPROC

DEF PROCGet_Byte
SYS "OS_SerialOp",4 TO ,message%;newflags%

ENDPROC

```

```

DEF PROC Send_String(data$)
LOCAL i%
REM PRINT "Values sent ":PRINT
FOR i% = 1 TO LEN(data$)
w$ = MID$(data$,i%,1)
w% = ASC(w$)
REM PRINT "ASCII value sent: ";w%;" --> ";w$
PROCSend(w%)

NEXT i%
ENDPROC

DEF PROC Send(byte%)
REM *** Send Carriage return to serial output ***
LOCAL flags%
REPEAT
SYS "OS_SerialOp",3,byte% TO ;flags%
UNTIL (flags% AND %0010) = %0000
ENDPROC

DEF PROC Flush_Buffers
SYS "OS_Byte",21,1
SYS "OS_Byte",21,2
ENDPROC

DEF PROC calc_seen_ang
theta = (L*degree_step) : REM Actual Angle in rads
PRINT "theta is :";theta
eins = TAN(RAD(theta))
zwei = eins/root_two

IF (theta < 90) THEN

seen_angle = DEG(ATN(zwei)) : REM for theta < 90 degrees
PRINT " theta is less than 90 degrees "
PRINT " Seen Angle is :";seen_angle
REM PROCcalc_det_angle
PRINT

ELSE
IF (theta = 90) THEN
seen_angle = theta
PRINT " theta is equal to 90 degrees "
PRINT " Seen Angle is :";seen_angle
REM PROCcalc_det_angle
PRINT

ELSE
IF (theta > 90) THEN
seen_angle = DEG(ATN(zwei)) + 180 : REM for theta >= 90 degrees
PRINT " theta is greater than 90 degrees "
PRINT " Seen Angle is :";seen_angle
REM PROCcalc_det_angle
PRINT

ENDIF
ENDIF
ENDIF
ENDPROC

DEF PROC calc_det_angle
REM ***** DETECTED ANGLE *****

drei = TAN(RAD(seen_angle))
vier = (drei/cos_eta)

IF (seen_angle < 90) THEN

det_angle = DEG(ATN(vier)) : REM for theta < 90 degrees
PRINT " Seenangle is less than 90 degrees "
PRINT " Detected Angle is :";det_angle

PRINT

```

```

ELSE
  IF (seen_angle = 90) THEN
    det_angle = seen_angle
    PRINT " Seen_angle is equal to 90 degrees "
    PRINT " Detected Angle is : ";det_angle

  PRINT

ELSE
  IF (seen_angle > 90) THEN
    det_angle = DEG(ATN(vier)) + 180 : REM for seen_angle > 90 degrees need to add PI
    PRINT " Seen angle is greater than 90 degrees "
    PRINT " Detected Angle is : ";det_angle

  PRINT
ENDIF
ENDIF
ENDIF

ENDPROC

DEFPROCcalc_max_and_min

IF (results(3,L) > major_pow) THEN
  REM ** Initially max_power = 0
  major_pow = results(3,L) :REM determines normalised power of beam in major axis
  major_pow_pos = L :REM max_power step position held here
  major_far_ang = results(0,L) :REM max faraday angle stored here

ENDIF
IF (results(3,L) < minor_pow) THEN
  REM ** Initially min_power = 1
  minor_pow = results(3,L) :REM determines normalised power of beam in minor axis
  minor_pow_pos = L :REM min_power step position held here
  minor_far_ang = results(0,L) :REM min faraday angle stored here

ENDIF
ENDPROC

DEF PROCsort_out
REM ** When this Proc. is called, either the major or minor or both predictions are out of
REM the 10 degree track range either side. **
REM ** If the prediction is within a 20 degree range either side result is still feasible.
REM but can't predict the ellipticity, since no voltages known outside 10 degree range.
REM ** If prediction is out of the 20 degree range then a bad calculation has resulted.
REM Shall put ellip equal to 1 so that FULLstep occurs next round trip
PRINT" In PROCsort_out"
ellip = 0 :REM Represents Uncalculated ellipticity
major_volts = 1
minor_volts = 0
COM$ = COM$ + "WR," :REM WR= Within +-20 degree range of previous angle

IF (major_pow_pos > (old_major_pow_pos + 20) OR major_pow_pos < (old_major_pow_pos - 20)) THEN
  PRINT:PRINT" Bad estimate of MAJOR position - Fullstep next time"
  ellip = 1
  COM$ = COM$ + "MX," :REM MX= Bad prediction on Major Angle/Position
ENDIF

IF (minor_pow_pos > (old_minor_pow_pos + 20) OR minor_pow_pos < (old_minor_pow_pos - 20)) THEN
  PRINT:PRINT" Bad estimate of MINOR position - Fullstep next time"
  ellip = 1
  COM$ = COM$ + "mX," :REM mX= Bad prediction on Minor Angle/Position
ENDIF

old_ellip = ellip
REM Leave old_minor and major_pow_pos's as ones determined in previous run

ENDPROC

DEFPROCdisplay_params
IF (major_marker = 1 AND minor_marker = 1) THEN
  PRINT:PRINT" Estimates of positions are GOOD"

```

```

ellip = (minor_pow/major_pow)
old_ellip = ellip : REM Used to determine whether to track or fullstep
old_minor_pow_pos = minor_pow_pos : REM Used for determining start of Track for min
old_major_pow_pos = major_pow_pos : REM Used for determining start of Track for max

ELSE
PRINT:PRINT " Estimates are out of range "
PROCsort_out
ENDIF

PRINT:PRINT "***** FINAL PARAMETERS *****"
PRINT " major_far_angle : ";major_far_ang
PRINT " Power in major axis : ";major_pow
PRINT
PRINT " minor_far_angle : ";minor_far_ang
PRINT " Power in minor axis : ";minor_pow
PRINT
PRINT " Ellipticity : ";ellip
PRINT
ENDPROC

DEF PROCdetermine_tk_pow
real_pow = power_av*((COS(RAD(2*seen_angle))+1)/2) : REM Power expected from Boonton

upper = average + (vert_pow*vert_grad) + (horiz_pow*horiz_grad) - (vert_volt + horiz_volt)
lower = (vert_grad*((COS(RAD(det_angle)))^2)) + (horiz_grad*((SIN(RAD(det_angle)))^2))

REMct = ((COS(RAD(det_angle)))^2)
REMst = ((SIN(RAD(det_angle)))^2)

calc_power = (upper/lower)

nom_tk_pow = calc_power/power_av : REM Normalised T.K Power
nom_real_pow = real_pow/power_av : REM Normalised expected power from boonton
ENDPROC

REM *****

REM ***** READ POTS *****

DEF FNreadbs_pot
SYS Channel%,1 : REM reads voltage of backshort pot from channel 1 of breakout box to ADC
SYS ADC%,10,1,Buffer% : REM takes 10 samples from channel 1
total%=0
FOR I% = 0 TO 9*4 STEP 4
total% = total% + !(Buffer%+I%)
NEXT I%
av = total%/10
bsp = (((av)-2048)/2048)*5
=bsp

DEF FNreadft_pot
SYS Channel%,2 : REM reads voltage of frequency pot from channel 2 of breakout box to ADC
SYS ADC%,20,2,Buffer% : REM takes 20 samples from channel 2
total%=0
FOR I% = 0 TO 19*4 STEP 4
total% = total% + !(Buffer%+I%)
NEXT I%
av = total%/20
ftp = (((av)-2048)/2048)*5
=ftp

DEF FNreadft_pot_two
REM **** This is Used to read ft_pot accurately after stepping ft_tuner ****
SYS Channel%,2 : REM reads voltage of frequency pot from channel 2 of breakout box to ADC
SYS ADC%,1000,2,Buffer% : REM takes 1000 samples from channel 2
total%=0
FOR I% = 0 TO 999*4 STEP 4
total% = total% + !(Buffer%+I%)
NEXT I%
av = total%/1000
ftp = (((av)-2048)/2048)*5
=ftp

```

```

REM ***** STEP & SCAN POTS *****

DEFPROCstep_ft
PRINT "!! Stepping frequency tuner !!";
oldft_value = FNreadft_pot_two : REM steps frequency tuner one division
PRINT " Old value : ";oldft_value

PROCmoveft_up
PROCdelay(wait)
PROCstop
PROCdelay(2) : REM allows for backlash and settling of tuner
nft_value = FNreadft_pot_two
PRINT " New value : ";nft_value
PRINT " Diff = ";oldft_value - nft_value
PRINT " Step Completed"

ENDPROC

DEFPROCcrr
REPORT:PRINT" at line ";ERL
PROCstop
REMCLOSE# channel
PROCfile_results
ENDPROC

DEFPROCscan_bs
PRINT"!! Scanning backshort !!"
bs_pot = FNreadbs_pot
IF (bs_pot < crit_bs_up) THEN
  PROCmovebs_up
  REPEAT
  UNTIL FNreadbs_pot >= crit_bs_up
  PROCstop
ENDIF

PRINT" Starting bs_voltage : ";FNreadbs_pot
PROCadrandoutput(0,3,"TM0") : REM sets Boonton to Talk Mode 0
A$ = FNadrandinput(0,3,255)
B$ = MID$(A$,3)
a = VAL(B$)

PROCmovebs_down

REPEAT
C$ = FNadrandinput(0,3,255)
D$ = MID$(C$,3)
b = VAL(D$)

IF b > a THEN
  a = b
  bs_pot = FNreadbs_pot
ENDIF
UNTIL FNreadbs_pot <= crit_bs_down

PROCstop

PRINT " MAX POWER = ";a;" voltage = ";bs_pot
PRINT "Moving to area of max.power "
PROCmovebs_up :REM moves backshort,back to last place of max.power
REPEAT
UNTIL FNreadbs_pot >= bs_pot
PROCstop

PRINT "voltage at max power = ";FNreadbs_pot
PRINT " Scan Completed"
ENDPROC

REM ***** GPIB PROCEDURES *****

DEFPROCstartupGPIB
PRINT "Startup_gpiB"
PROCinit :REM INITIALISES HARDWARE

```

```

ENDPROC

REM ***** NEW EIP PROC'S . that really work !!! *****

DEFPROCeip_start
PRINT " In PROCeip_start "
PROCadrandoutput(0,eip,"PFP") :REM Resets Coarse Tune to +5V
PROCeip_ready
PRINT "EIP ready "
PROCdelay(2)
PROCadrandoutput(0,eip,"ES") :REM Scientific Notation
BAND$ = "B44"
PROCband
PRINT " In BAND 44 "
ENDPROC

DEFPROCeip_ready
REM *****This PROC is only used in eip_start *****
PROCadrandoutput(0,eip,"RS") :REM Resets EIP
PROCadrandoutput(0,eip,"SR01") :REM Measurement available?
REPEAT
state% = FNservice_requested :REM Waits until count completed.
UNTIL state% = TRUE
ENDPROC

DEF PROCchange_band
IF BAND$ = "B44" AND lockflag$ = "U" THEN
BAND$ = "B43" : PROCband
PROCrun_poll_eip
ELSE IF BAND$ = "B43" AND lockflag$ = "U" THEN
BAND$ = "B44" : PROCband
PROCrun_poll_eip
ENDIF
ENDIF
ENDPROC

DEF PROCgo_eip_go
PRINT "!! Trying to locate Frequency !!"
PROCrun_poll_eip
IF lockflag$ = "U" THEN
PROCchange_band : REM changes to other band
ENDIF

IF lockflag$ = "U" THEN
PROCchange_band : REM changes back to original band
ENDIF

IF lockflag$ = "U" THEN
PRINT " Have tried three times -> Shall move on "
frequency = 0
COM$ = COM$ + "BF." :REM Represents Bad frequency Measurement
PRINT "Frequency stored as : ";frequency
ENDIF

ENDPROC

DEFPROCband
PRINT "CHANGE TO BAND : ";BAND$
PROCadrandoutput(0,eip,BAND$) :REM changes Band of EIP.Use B43 or B44
PROCdelay(2)
PROCadrandoutput(0,eip,"RS") : PRINT " Resetting" :REM Resets EIP
PROCdelay(10) : REM gives eip time to reply
ENDPROC

DEF FNserial_poll(tad%)
LOCAL d0%,d1%,stb%
SYS &40340,&00.&2B.&00,tad% TO d0%,d1%,stb%
=stb%

DEF PROCrun_poll_eip
quartz = TIME
circuit% = 0
REPEAT
number% = FNserial_poll(eip)

```